1991

A Study of the Metal Clusters in the Nitrogenase Proteins of Azotobacter Vinelandii.

Melinda Ehrlich Oliver
Louisiana State University and Agricultural & Mechanical College

INFORMATION TO USERS

This manuscript has been reproduced from the microfilm master. UMI films the text directly from the original or copy submitted. Thus, some thesis and dissertation copies are in typewriter face, while others may be from any type of computer printer.

The quality of this reproduction is dependent upon the quality of the copy submitted. Broken or indistinct print, colored or poor quality illustrations and photographs, print bleedthrough, substandard margins, and improper alignment can adversely affect reproduction.

In the unlikely event that the author did not send UMI a complete manuscript and there are missing pages, these will be noted. Also, if unauthorized copyright material had to be removed, a note will indicate the deletion.

Oversize materials (e.g., maps, drawings, charts) are reproduced by sectioning the original, beginning at the upper left-hand corner and continuing from left to right in equal sections with small overlaps. Each original is also photographed in one exposure and is included in reduced form at the back of the book.

Photographs included in the original manuscript have been reproduced xerographically in this copy. Higher quality 6" x 9" black and white photographic prints are available for any photographs or illustrations appearing in this copy for an additional charge. Contact UMI directly to order.

U·M·I

University Microfilms International
A Bell & Howell Information Company
300 North Zeeb Road, Ann Arbor, MI 48106-1346 USA
313/761-4700 800/521-0600

Order Number 9200080

A study of the metal clusters in the nitrogenase proteins of *Azotobacter vinelandii*

Oliver, Melinda Ehrlich, Ph.D.

The Louisiana State University and Agricultural and Mechanical Col., 1991

U·M·I
300 N. Zeeb Rd.
Ann Arbor, MI 48106

A STUDY OF THE METAL CLUSTERS IN THE NITROGENASE PROTEINS OF *Azotobacter vinelandii*

A Dissertation

Submitted to the Graduate Faculty of the
Louisiana State University and
Agricultural and Mechanical College
in partial fulfillment of the
requirements for the degree of
Doctor of Philosophy

in

The Department of Chemistry

by
Melinda Ehrlich Oliver
B.S., Louisiana State University, 1982
May 1991

ACKNOWLEDGEMENTS

I would like to thank my advisor, mentor, and most of all, my friend, Brian J. Hales, for his guidance, support, and friendship during the course of my research. His help has meant more to my success than any other factor. I would also like to thank him for really teaching his students.

To my father for his belief in me, and to my mother for her everlasting influence on my life even though it was brief.

To group members past and present for their help, guidance, and camaraderie. Special thanks to Yvonne Onate for her support and friendship.

To the Pennington Biomedical Research Center for allowing me to use their EPR facility. A special thanks to Kerrie Munson and Richard Tulley for their help during my work there.

To Mary Jane Peters and her office staff for all the help they have given me in my work. An extra special thanks to Mary Jane because her help involved both the professional and personal sides of my life.

To Dave Fritze, Don Patterson, and Tom Pentecost for their friendship and support during my time here. My daily coffee breaks with Dave and Don got me through graduate school. Tom provided technical and shoulder assistance.

To my husband, Mike, for his support, and to my daughter, Lauren, for coming into my life during this work, she is my greatest inspiration.

To J.B. for pointing out: "Answers are the easy part, its questions that raise doubts."

Finally, and they deserve to be last, thanks to The Library group for the afternoon sessions that capped the week. A special thanks to Susan Finley for listening to me.

TABLE OF CONTENTS

LIST OF TABLES

LIST OF FIGURES

LIST OF ABBREVIATIONS

ADP	Adenosine diphosphate
Av1	Conventional MoFe protein from *Azotobacter vinelandii*
Av2	Conventional Fe Protein from *A. vinelandii*
Av1'	Alternative VFe Protein from *A. vinelandii*
Av2'	Alternative Fe Protein from *A. vinelandii*
Bipy	Bipyridyl
Cp1	MoFe Protein from *Clostridium pasteurianum*
Cp2	Fe Protein from *C. pasteurianum*
DEAE	Diethylaminoethyl
DMF	Dimethylformamide
DRAG	Dinitrogenase-reductase-activating glycohydrolase
DRAT	Dinitrogenase reductase ADP-ribosyltransferase
DTN	Dithionite or sodium hydrosulfite
EDC	1-ethyl-3-(3-Dimethylaminopropyl)carbodiimide
EDTA	Ethylenediaminetetraacetate
EPR	Electron Paramagnetic Resonance
ENDOR	Electron Nuclear Double Resonance
EXAFS	X-Ray Absorption Fine Structure
FeMoco	FeMo cofactor from MoFe Protein
ICP	Inductively Coupled Plasma
KpB-	Apo-MoFe Protein from *Klebsiella pneumoniae*
MCD	Magnetic Circular Dichroism
MgATP	Magnesium Adenosine triphosphate
Nif	Nitrogen Fixation Genes
NMF	N-methylformamide
PAGE	Polyacrylamide Gel Electrophoresis
T_1	Spin-lattice Relaxation time
T_2	Spin-spin Relaxation time
TBD	Tetrabutylammonium dithionite
TES	N-tris[Hydroxymethyl]methyl-2-aminoethanesulfonic acid
TRIS	Tris(hydroxymethyl)aminomethane
XANES	X-Ray Absorption Near Edge Structure
XAS	X-Ray Absorption

ABSTRACT

Electron Paramagnetic Resonance (EPR) spectroscopy was used to examine the paramagnetism of the clusters in nitrogenase from *Azotobacter vinelandii*. The EPR spectrum of nitrogenase (Av1 and Av2) was examined in the presence of an extrinsic paramagnet, DyEDTA, at different concentrations of NaCl, during thionine oxidation (Av1), and in the presence of MgATP (Av2). Cross combinations of Av1 and Av2 were also investigated in the presence and absence of the chemical cross-linker, EDC as well as with the nitrogenase components from *Clostridium pasteurianum*.

From relaxation enhancement measurements, the distance of closest approach of DyEDTA to the intrinsic metal clusters in Av1 and Av2 was calculated. For Av2, the distance was calculated to be 5 Å. The calculated distance for Av1, however, put the M center practically on the surface of the protein. One reason for this (probably) spurious result may be that the distance calculation is derived for a model with total spin S=1/2. The M center in Av1 is a faster-relaxing S=3/2 system which will affect the different terms of the dipolar Hamiltonian in ways different from an S=1/2 system.

The results of the thionine oxidation of Av1 provided evidence of dipolar interactions between paramagnetic P clusters and the paramagnetic M centers. These results were fitted to a model for the interaction and arrangement of the P clusters relative to the M centers.

The paramagnetism of the metal clusters of Av1' (the alternative nitrogenase from *Azotobacter vinelandii*) was investigated as a function of (1) enzymatic turnover; (2) thionine oxidation of Av1'; (3) the effects of pH on Av1', and (4) isolation of the cofactor. The S=1/2 signal was completely quenched upon completion of turnover, while the S=3/2 signal decreased only slightly in intensity. Thionine oxidation of Av1'

produced analogous results in which the S=1/2 signal was oxidized with one-half equivalent of thionine. The S=3/2 signal required almost four equivalents before decreasing significantly in amplitude. Increasing the pH of Av1' shifted the S=3/2 signal and the S=1/2 signal increased in amplitude. Finally, FeVco, the cofactor or M center of Av1', was successfully extracted into DMF but not into NMF.

BACKGROUND

1.1 NITROGEN FIXATION

It has long been known that nitrogen fixation occurs in legumes via a symbiotic relationship with bacteria. In 1884 this symbiotic relationship was discovered (1.1), followed in 1888 by the isolation and cultivation of the responsible bacteria (1.2). The symbiosis appeared to be necessary for nitrogen fixation, as the isolated bacteria did not exhibit nitrogen fixation activity. It was not until the 1970's when conditions were established such as a low partial pressure of oxygen that enabled the bacteria to fix nitrogen independent of the root nodules where they reside on legumes. During this evolution, it had also become apparent that other free-living bacteria could fix nitrogen such as observed in *Clostridium pasteurianum* (1.3) in 1893. A few years later, in 1901 the aerobic bacteria *Azotobacter chroococcum* and *Azotobacter agilis* were also shown to be able to fix nitrogen (1.4). It wasn't until 1949 that it was recognized that most photosynthetic bacteria were capable of fixing nitrogen. At the same time it was recognized that (members of) purple sulfur and green sulfur bacteria fixed nitrogen as well (1.5). In Southeast Asia the combination of the water fern *Azolla* with the cyanobacterium *Anabaena azollae* had been used in practical agriculture because the combination fixes nitrogen vigorously. In addition, some of the methanogenic bacteria and the cellulose digesting organisms have proved to be nitrogen fixers. The biochemistry of nitrogen fixation was first studied in 1928 using *A. chroococcum* (1.6). The influence of the partial pressure of oxygen and nitrogen on nitrogen fixation were examined. By the late 1930's Harold Urey had found a way of concentrating ^{15}N so it could be used as a tracer. In 1951 it was found that under specific conditions *Clostridium pasteurianum* would excrete ammonia (1.7). When the ammonia from *C. pasteurianum* was recovered from cultures supplied with $^{15}N_2$, it had a far higher ^{15}N

concentration than any other compound isolated previously. This was the most direct and specific evidence for the role of ammonia in the nitrogen fixation process.

It now became important that nitrogen fixation be achieved outside the cell. In 1960, the first consistent cell-free nitrogen fixation from *C. pasteurianum* was reported (1.8). This was the first technique to give consistent repeatable cell-free nitrogen fixation. Requirements such as anaerobicity had prevented researchers from reaching this goal earlier. Following the success achieved with *C. pasteurianum*, cell-free preparations for nitrogen fixation were extended to other organisms such as *Rhodospirillum rubrum*, blue-green algae, azotobacter, and *Klebsiella pneumoniae.*

In 1965 Mortenson showed that nitrogenase, the nitrogen-fixing enzyme, consists of two different proteins (1.9). The larger of the two (called the molybdenum-iron protein) contains molybdenum and iron; the smaller (called the iron protein) contains only iron. The molybdenum-iron protein has a molecular weight between 220,000 and 240,000, while the iron protein has a molecular weight of about 60,000. Depending on which species nitrogenase is isolated from, its secondary structure varies somewhat as does the molecular weight of each protein. (Table 1.1 outlines these differences between the species.) Because the molybdenum-iron (MoFe) protein elutes from a gel filtration column first, it is also called component 1, while the iron (Fe) protein elutes second and is therefore called component 2. Abbreviated labels (1.10) for these different proteins have been used where the name of the organism they are isolated from is incorporated: Av1 for component 1 from *Azotobacter vinelandii* and Ac2 for component 2 from *A. chroococcum*, for example. Nitrogenase requires MgATP for nitrogen fixation (1.11); in fact, two moles of MgATP are required for each electron donated (1.12). Bui and Mortenson in 1968 (1.13) discovered that the Fe protein donates electrons to the MoFe protein and that MgATP binds specifically to the Fe protein. The ATP is hydrolyzed to ADP where the latter was found to be inhibitory,

TABLE 1.1

Properties of Component 1 From the Different Nitrogenase Enzymes

Property\Enzyme	Mo-N_2ase	V-N_2ase		Fe-N_2ase[a]	
		Av	*Ac*	Av^F	Av^S
Subunits	$\alpha_2\beta_2$	$\alpha_2\beta_2\delta_2$	$\alpha_2\beta_2\delta_2$	$\alpha\beta_2\delta_2$	$\alpha_2\beta_2\delta_2$
Subunit Weights					
α	59,438[b]	55kD[c,d]	55kD[d,e]	58,391[f]	58,391[f]
β	55,267[b]	52kD[c,d]	50kD[d,e]	51,157[f]	51,157[f]
δ		n.d.	13,275[g]	15,324[f]	15,324[f]
Metals (Atoms)					
Mo	2	0.064[c]	0.05[e]	0.016[h]	0.126[h]
V	-	0.7[c]	2.0[e]	0.032[h]	0.010[h]
Fe	30-33	9.32[c]	20.8[e]	11.0[h]	24.2[h]
Zn	0.7[i]	1.1[i]	n.d.	0.402[h]	0.409[h]

[a]Av^F and Av^S represent component 1 proteins from Fe-nitrogenase that migrate fast and slow, respectively, on native polyacrylamide gels (1.58).
[b]Ref. 1.87
[c]Ref. 1.88
[d]Estimated from SDS polyacrylamide gels.
[e]Ref. 1.56
[f]Ref. 1.61
[g]Ref. 1.89
[h]Ref. 1.58
[i]From ICP emission spectroscopy (Hales, unpublished results)
Table taken from Ref. 1.82.

i.e., MgADP binds to one of the MgATP-binding sites on the Fe protein (1.14). Earlier studies had suggested ferredoxin to be the in vivo electron donor for the nitrogenase from *C. pasteurianum*. In 1965, Bulen (1.15) discovered that $Na_2S_2O_4$ (dithionite or sodium hydrosulfite) could be used as an in vitro electron donor, thus greatly facilitating the in vitro study of nitrogenase.

ferredoxin

flavodoxin ----e'--> Fe protein + MgATP ----e'--> MoFe protein

$Na_2S_2O_4$

Scheme 1: Order of Electron Transfer in Nitrogenase

After the two nitrogenase proteins were successfully purified, it became necessary to probe the sequence of events during electron transfer (see Scheme 1, above). It was observed that the EPR spectrum of the proteins changes during catalytic turnover. From these studies it became quite clear that only one electron is transferred at a time to the MoFe protein from the Fe protein (1.16). In 1954, it was discovered that several compounds other than dinitrogen could also be reduced by nitrogenase. At that time it was demonstrated that nitrous oxide was reduced by nitrogenase forming N_2 and H_2O (1.17). Soon after that, protons, acetylene, and azide were shown to be reduced as well (1.18,1.19). Cyanide, methyl isocyanide, and cyclopropene were later added to the growing list of substrates (1.20,1.21). Because these various substrates all compete for electrons from reduced MoFe protein, there are numerous interactions among them. Therefore, a basic question is: if more than one substrate is present at a time, where do the electrons go first? In 1980, it was demonstrated that the allocation of electrons to various substrates depends on the electron flux through the MoFe protein (1.22). If the

electron flux is low and protons, acetylene, and dinitrogen are all present, then production of H_2 and reduction of acetylene will be favored over the reduction of nitrogen. If the electron flux is high, however, nitrogen will be preferentially reduced while H_2 and ethylene formation will decrease.

Nitrogenase not only has many substrates but also several inhibitors, such as cyanide, MgADP, and carbon monoxide. What is the nature of the interactions between them, and how might the numerous binding sites be identified? These questions have been explored (1.23) and modeled extensively by Thorneley and Lowe (1.24-1.28). If it is assumed that all substrate reductions occur at the MoFe protein after it has been reduced by the Fe protein, then any blockage of electron transport that occurred before electrons reached the MoFe protein should block all substrate reduction by nitrogenase. A partial reduction in electron flow would affect substrate reduction differentially. The fact that the presence of one substrate affects the reduction rate of another substrate supports the concept that all substrates are bound to the reduced MoFe protein (1.29-1.32). For example, N_2 reduction is affected by the presence of protons which are reduced to H_2 at the same time. As a substrate, H^+ is unique in that it is the only substrate whose reduction by nitrogenase is not inhibited by carbon monoxide, which has been shown to inhibit all other substrate reductions. Furthermore, none of the other inhibitors (or substrates acting as inhibitors) are as potent as CO.

The competition between H_2 production and N_2 reduction became better understood from the following discovery: If D_2 is added to the nitrogenase system, HD is produced in an N_2-dependent reaction (1.33). Unlike H_2 production, HD formation is inhibited by CO. This inhibition by CO is observed by all the other reactions of nitrogenase which require a fully reduced form of the MoFe protein. Therefore, H_2 production occurs in two distinct steps, one which occurs early (when CO cannot

inhibit) and another later step (HD formation--inhibited by CO) when the MoFe protein is more fully reduced. HD formation occurs through an ordered sequential reaction. If D_2 binds before N_2 (1.34), two electrons are added to generate 2HD and N_2 is released unchanged. If N_2 binds before D_2 (H_2), no HD (H_2) is formed and N_2 is reduced normally. Thus, the HD-generating reaction demonstrates how H_2 is a competitive inhibitor of nitrogenase.

In 1936, it was shown that nitrogenase could be expressed in Mo-deficient environments if vanadium is present (1.35). This phenomenon became known as the "vanadium effect". Vanadium appeared to be able to substitute for molybdenum and thereby stimulate growth only in selected species of aerobic nitrogen-fixing organisms: *A. vinelandii, A. chroococcum,* and *Mycobacterium flavum* (1.36). If one compares the Mo-grown cell-free extracts to those grown on vanadium, a lower acetylene binding constant is observed for the V-grown organisms (1.37), different Michaelis-Menten constants (K_m) for acetylene, and higher ratios of H_2 evolution to substrate reduction (1.38). The incorporation of V into nitrogenase appeared to affect both specific activity and substrate binding. Many problems were encountered due to Mo contamination in the vanadium preparations, resulting in expression of the conventional nitrogenase in trace amounts. Attempts to purify the V-containing nitrogenase into its specific components resulted in loss of both activity and metal content (1.39). Addition of purified MoFe protein to the V-grown *A. vinelandii* crude extracts showed the presence of an iron protein, indicating that the lower activities are not due to an inhibition of nitrogenase biosynthesis in the V system.

Mutant strains of *A. vinelandii* that are unable to grow by nitrogen fixation (Nif-) were isolated, analyzed genetically, and characterized with respect to electron paramagnetic resonance signals and activities (1.40-1.42). In 1980, Bishop and

coworkers demonstrated that if these mutant strains were grown under conditions of Mo-deficiency, a phenotypic reversal to Nif$^+$ occurred (1.43). On the other hand, extracts of these N_2-grown cells from two different strains lacked significant amounts of the conventional Mo-nitrogenase protein subunits. Furthermore, these pseudorevertants were not able to grow on molybdenum, but were able to grow in the presence of tungsten, i.e., the strains used were tungsten-tolerant. The origin of this tungsten resistance is still unknown today, but tungsten has been observed to be a potent inhibitor for the Mo-containing wild-type strains (1.44-1.46).

Using two-dimensional gel electrophoresis, Bishop and coworkers observed four new proteins in extracts of these pseudorevertants expressed under conditions of molybdenum deficiency, thus exhibiting the first evidence of an alternative N_2-fixation system (1.43). Because of the aforementioned vanadium effect (1.36-1.39) as well as the observation of a possible rhenium effect (1.47), it was postulated that vanadium or rhenium might be involved in the alternative N_2 fixation system (1.48). When cells were grown under N_2-fixing conditions in Mo-deficient media plus 5 μM V_2O_5, two new proteins were observed that did not correspond to the proteins of conventional nitrogenase or to the four proteins described above. Cells grown in the presence of Re (without Mo) showed both the four-protein pattern and the new two-protein pattern. Proteins corresponding to the iron protein were found in cells cultured under Mo-deficient conditions whether or not V or Re were present. The Nif$^-$ mutant strains would not grow, however, in the absence of an N source in the presence of Mo. The relationship between the two-protein pattern and the four-protein pattern was unknown except that the two proteins were observed in wild-type cells grown in N-free Mo-deficient media containing V and in Nif$^-$ mutant cells cultured in N-free Mo-deficient media regardless of the phase of growth. (Table 1.2 outlines the differences between

the appearance of the different proteins under different growing conditions.) The four proteins are observed in the late exponential growth phase in the presence of V or Re but not at all in the Nif- mutants grown in the absence of Mo or V regardless of growing conditions. Therefore, Bishop and coworkers labeled the two patterns N_2ase B_1 (V-induced) and N_2aseB_2 (Mo-deficient). Furthermore, unless the conventional nitrogenase is expressed, no detectable EPR signal at g = 3.65 (indicative of the MoFe protein) was observed for any of the cells containing either the two- or four-proteins. Other researchers presented results that corraborated the results of Bishop, showing that *A. vinelandii* synthesized ammonia and Mo-repressible proteins (1.49) from the similar Nif- mutants as well as the appearance of W-resistant mutants that did not contain the conventional enzyme proteins (1.50).

If nitrogenase was purified from V-grown cells and the amino acid sequence compared to that of the Mo-nitrogenase, several differences were observed, in addition to differences in the metal content between the Mo-nitrogenase and the V-nitrogenase (1.39). It had been speculated that V might merely replace the Mo in the conventional polypeptides, but it is hard to imagine that the mere presence of V would reverse the mutational lesion that gives rise to the Nif- mutants. Another interpretation was that V is incorporated into the two-protein pattern mentioned above (1.48).

It is important to realize that many thought that both V and W were merely substituting for Mo in the same polypeptides. In the case of tungsten, however, the so-called tungsten inhibition always yielded cells that had a residual amount of component 1 activity. The V-grown cells also had a residual amount of component 1 activity. The origin of this residual activity was discovered with the isolation of a W-grown *A. vinelandii* nitrogenase which contained equal amounts of both Mo and W in component one (1.51). Even though Mo was not added to the medium, trace amounts of Mo present were incorporated into one of the cofactors of component one while the other

cofactor contained Fe, W, and S. This W cofactor is inactive but the hybrid component one has activity attributable to the one Mo-containing cofactor which shows that the enzyme does not need two active cofactors to be active. In the case of the V-grown cells, it was also assumed that the trace Mo in the form of the conventional nitrogenase accounted for the residual activity.

Using two-dimensional gel electrophoresis, it was shown that the alternative component 2 was slightly more basic than the conventional component 2 (1.52). The presence of trace quantities of Mo did not seem to affect the production of the alternative Fe protein by the Nif- mutant strains. The presence of V or W affected the production of the alternative Fe protein differently; V did not alter its expression but W did. (Table 1.3 outlines the conditions under which the Fe protein is expressed.) These results suggest that both the conventional and alternative Fe proteins are encoded by different genes and are under different regulatory controls (1.52).

Before any more of the background on the alternative system is presented, it might be helpful to describe the genetic structure controlling nitrogenase expression. This has become the most rapidly growing area in nitrogen fixation, perhaps because it is so extremely complex and offers a formidable challenge to those in and out of the field. The most complete picture of the genetics of nitrogen fixation comes from the species *Klebsiella pneumoniae,* a species close in nature to *Escherichia coli* in its genetics. One unanticipated fact is that there are no alternative nitrogenases in *K. pneumoniae.* Most of the genetics of alternative nitrogenases has come from *A. vinelandii.*

In *K. pneumoniae* there are 20 contiguous genes accounting for over 20kb of DNA, all of which are arranged on eight transcriptional units. The functions of the products of all of the genes are not understood; however, several of the gene products are well-characterized (in Table 1.4).

TABLE 1.2

Expression of Wild Type and Nif⁻ Mutants by Nitrogen Fixation

	N-free Mo-Free	+V	+Mo	+Re	+W
Wild Type	low growth	+	÷	-	-
Nif⁻ Mutants (pseudorevertants)	÷ *	÷ *L #	-	÷ *L #	÷

÷ diazotrophic growth - no growth

*four-protein pattern: N_2ase B_2 (Mo-deficient)

#two-protein pattern: N_2ase B_1 (V-induced)

*L: appears only in late phase of growth

TABLE 1.3

Expression of Wild Type and Nif⁻ Mutant Fe Proteins

	+Mo	-Mo	+V	+W
Nif⁻ Mutant (pseudorevertants)	+	+	+	-
Wild Type	+	-	+	-*

*expressed but inactive

\+ diazotrophic growth

\- no growth

TABLE 1.4

***Klebsiella pneumoniae Nif* Gene Products**

Gene(s)	Product Description
J, F	Electron Transport Components
H	Component 2 Subunit
D, K	Component 1 α and β Subunits; respectively
E, N, V, B, Q	FeMo Cofactor Biosynthesis
M	Component 2 Maturation
L	Negative Regulatory Element
A	Positive Regulatory Element
T, Y, X, U, S, W, Z	Unknown Function

(1.82)

Because most of the mutations had been chemically induced, one might argue that the expression of the so-called alternative system occurred because of an increased "leakiness" of the mutant phenotypes. If, however, there were deletions made in the structural genes for nitrogenase (*nif* HDK), it would be easier to distinguish between

"leaky phenotypes" and those that can be attributed to alternative system expression (1.53).

All of *nif* HKD was cut from purified *A. vinelandii* DNA and incorporated into a plasmid. Subsequently, a major section of this gene cluster was removed, leaving only a small piece of both *nif* H and *nif* K with no *nif* D. This plasmid was then transformed into whole cells where the ends of the HK region of the plasmid complemented the edges of the HDK cluster on the chromosome. Exchange (i. e., recombination) occurred between the "sticky" ends of the plasmid and the corresponding regions on HDK. The chromosome now has only pieces of *nif* H and *nif* K and, therefore, is unable to express the structural genes for the conventional Mo-containing nitrogenase (1.53). Two different groups isolated deletion strains from *A. vinelandii* and demonstrated that these could still fix nitrogen in the absence of Mo-nitrogenase (1.54,1.55). In 1986, the alternative nitrogenases from *A. chroococcum* (1.56) and *A. vinelandii* (1.57) were isolated and purified and shown to contain vanadium instead of Mo. These vanadium nitrogenases would be N_2ase B_1 in the Bishop system of nomenclature; what became of N_2ase B_2? The second alternative nitrogenase was isolated only recently from *A. vinelandii* (1.58) and has been suggested to contain only Fe. Re has been shown to induce the production of this third nitrogenase but is obviously not incorporated into the enzyme (1.59). *A. vinelandii* seems to stand alone so far in its ability to synthesize three different enzymes, while *A. chroococcum* has been shown to produce two: the vanadium and the molybdenum nitrogenases.

How do the alternative nitrogenases compare to the Mo-nitrogenase in polypeptide structure? As already mentioned, the component 2 from the alternative vanadium system is very close in structure and amino acid sequence to that of the Mo-nitrogenase. Component 2 is always a γ_2 dimer and contains one [4Fe-4S] cluster that

is most likely held between the two protein subunits by highly conserved cysteines (1.60). When comparing the polypeptide structures for component 1, however, a very different situation exists.

The Mo-nitrogenase component 1 consists of an $\alpha_2\beta_2$ structure with a combined MW of about 220,000 daltons. The V-nitrogenase component 1 from *A. vinelandii* and *A. chroococcum* (1.56) consists of an $\alpha_2\beta_2\delta_2$ structure where the δ subunit (13kD in *A. chroococcum* and 15kD in *A. vinelandii*) is considerably smaller than the α or β subunits, both of which are relatively similar in MW to those for the Mo-nitrogenase. The second alternative nitrogenase (or third nitrogenase) from *A. vinelandii* appears to have two different polypeptide compositions: either an $\alpha_2\beta_2\delta_2$ or an $\alpha\beta_2\delta_2$ structure. The reason for this discrepancy is unknown, although the Re-induced third nitrogenase exhibits only the $\alpha_2\beta_2\delta_2$ structure. The iron in component 1 of the third nitrogenase appears to reside in the α subunit, as the $\alpha\beta_2\delta_2$ structure has half the iron (11 atoms per mole) as the $\alpha_2\beta_2\delta_2$ structure (24 atoms per mole) (1.61). The properties of the different component 1 proteins are outlined in Table 1.1.

1.2 METAL CLUSTERS

Having discussed the protein structure of nitrogenase and compared Mo-nitrogenase to the alternative nitrogenases, what follows is a more thorough description of the metal clusters thought to be involved in electron transfer. The Fe protein contains one [4Fe-4S] cluster per dimer and has been characterized by both EPR and Magnetic

Circular Dichroism (MCD). The charge on [4Fe-4S] can be either 1+ or 2+ and, therefore, appears to be very similar to a typical ferredoxin. However, this is where the similarity ends. First of all, component 2 does not show the typical complementation of reserved cysteines necessary to bind the [4Fe-4S] center (1.62). Furthermore, its g = 2 EPR spectrum does not quantitate to one full spin per molecule. However, recently a combined EPR, Mössbauer and magnetic susceptometric study (1.63) of component 2 showed that the low S = 1/2 spin quantitation arose from the fact that the cluster can exist in either an S = 1/2 or S = 3/2 spin state, the ratio of the two depending on the solvent environment. For example, in buffer, about 20% of the clusters are in the S = 1/2 state, while in ethylene glycol this value is about 95%, and in the presence of 4 M urea it is about 5%.

Component 1 is more complex in protein structure and in metal composition than component 2. For the MoFe protein there are 2 Mo, 30 to 33 Fe, and 28 to 30 atoms of S per molecule. These metal atoms are arranged into at least two different types of clusters as observed by Mössbauer spectroscopy (1.64, 1.65): M clusters, also referred to as the cofactor or FeMo-co, and P clusters. Each protein molecule most likely contains two cofactors and four P clusters. Each may exist in at least two different oxidation states as outlined in Table 1.5. The P clusters are believed to be similar to [4Fe-4S] clusters in composition (1.65) as determined by core extrusion and Mössbauer studies (1.66) but are different in their spectroscopic properties from conventional [4Fe-4S] clusters. Recent Mössbauer evidence (1.67) indicates that there are at least two different subclasses of P clusters, with the possibility that all four might be electronically different. The unusual oxidation state of the P clusters upon oxidation by thionine has been confirmed by Mossbauer and MCD studies (1.68) as well as magnetic susceptibility measurements. However, unlike what might be expected for the observed half-integer spin states, the P clusters are EPR silent when oxidized.

TABLE 1.5

DIFFERENT SPIN STATES OF THE MOLYBDENUM-IRON PROTEIN METAL CLUSTERS[a]

Cluster	As-isolated[b] (Reduced)	Thionine[c] (Oxidized)
P Cluster	S = 0	S = 5/2 or 7/2
M Cluster	S = 3/2	S = 0

[a]Spin state determined by a combination of EPR and Mössbauer spectroscopies(64,65)

[b]In the presence of 2 mM dithionite

[c]Addition of six equivalents to one-electron oxidize the four P clusters and the two M clusters.

(1.82)

The M clusters are also unique in many ways. The metal composition of Mo:Fe:S exists in a ratio of 1:6-7:8-9 (1.70,1.71). There are two M clusters per protein molecule which are paramagnetic in the as-isolated state with a S = 3/2 spin state. Both become diamagnetic upon oxidation with thionine, as shown in Table 1.5. EPR spectroscopy, followed by Mössbauer (1.65) and MCD spectroscopies, confirmed the paramagnetism of the M clusters as well as a positive zero-field splitting energy and near-axial symmetry. Like the P clusters, the M clusters also exhibit an unusual MCD spectrum, which indicates that their electronic structure is quite unique. The most information about the electronic and magnetic interactions in the M cluster has come

from electron nuclear double resonance (ENDOR) spectroscopy (1.71-1.74). In ^{57}Fe-enriched samples, it has been shown that there are five different iron hyperfine interactions indicating that at least five of the iron atoms are in unique environments. Proton ENDOR was done as well as deuterium-enriched ENDOR, indicating that there is at least one exchangeable proton associated with the cluster. There are also two inorganic sulfur atoms interacting with the cluster, as observed with ^{33}S ENDOR. In ^{95}Mo-enriched samples, there is a weak hyperfine interaction, also indicating that Mo is involved in the paramagnetism of the cluster and that its oxidation state may be Mo(IV). EPR shows, however, that ^{95}Mo does not broaden the EPR spectrum of the M cluster (64). If Mo is involved in spin-coupling, however, there should not be any observable hyperfine splittings under the conditions used in a typical EPR experiment. Because it has always been assumed that the molybdenum atom was at or near the site of substrate reduction in the M cluster, a lot of attention has been focused on the properties of this metal. The most detailed information concerning the electronic properties and coordination sphere around Mo has come from x-ray absorption studies (XAS) (1.75-1.78). These studies include the near edge of the absorption spectrum (XANES) and the absorption fine structure just beyond the edge (EXAFS). The XANES studies show the oxidation state of Mo to be between 3+ and 5+, which is in agreement with the 4+ assignment from ENDOR. The EXAFS studies show that the coordination sphere around Mo contains Fe, S and O (or N). Recent XAS studies on model compounds corroborate the assignment of either O or N as an unusual ligand for this type of cluster. Furthermore, recent electron spin echo (ESE) experiments (1.79) have shown N coordination to the M centers, which is absent from the same spectrum when the M center is extracted from the protein. The extracted form of the M cluster is usually referred to as the FeMo-cofactor or FeMoco.

1.3 METAL CLUSTERS AND SPECTROSCOPY OF ALTERNATIVE NITROGENASE

The alternative nitrogenases are always compared to the more familiar conventional nitrogenase when comparing metal clusters and corresponding spectroscopy. Figure 1.1 is a comparison of the EPR spectra of the M clusters from the three different nitrogenases from *A. vinelandii*. As in Mo-nitrogenase, there appear to be four P clusters in the vanadium system which are EPR-silent and two M clusters which are paramagnetic. It is easy to see that the EPR spectra are different in g-value and in the spin system. While the Mo-nitrogenase has an M cluster which is near axial in symmetry and a spin of S = 3/2 with a positive zero-field splitting, the EPR spectrum of the V-nitrogenase is more complex (1.56, 1.80, 1.81), consisting of three major paramagnetic components, S1, S2, and S3. S1 is axial with g-values of 2.04 and 1.95 and is most probably due to a reduced Fe/S cluster. The S2 inflections at g = 5.80 and 5.40 represent only two of a possible six inflections for a rhombic S = 3/2 spin system. The temperature dependence of the S2 signal allows the determination of the zero-field splitting (-0.74 cm^{-1}). The rhombicity (E/D) for any system can vary between 0 and 1/3 with 0 corresponding to a purely axial system and 1/3 to a purely rhombic system. Figure 1.2 shows how the rhombicity or λ correlates with g-values for S = 3/2 in Mo- and V-nitrogenases. The g-values for the inflections observed for S2 in V-nitrogenase correspond to a λ of 0.26, while those of Mo-nitrogenase occur at a λ of 0.053. From the rhombicity, it is possible to predict all six g-values for this signal. However, the reason why the other four inflections are not observed under normal conditions is not known but may be due to g-strain broadening (1.82).

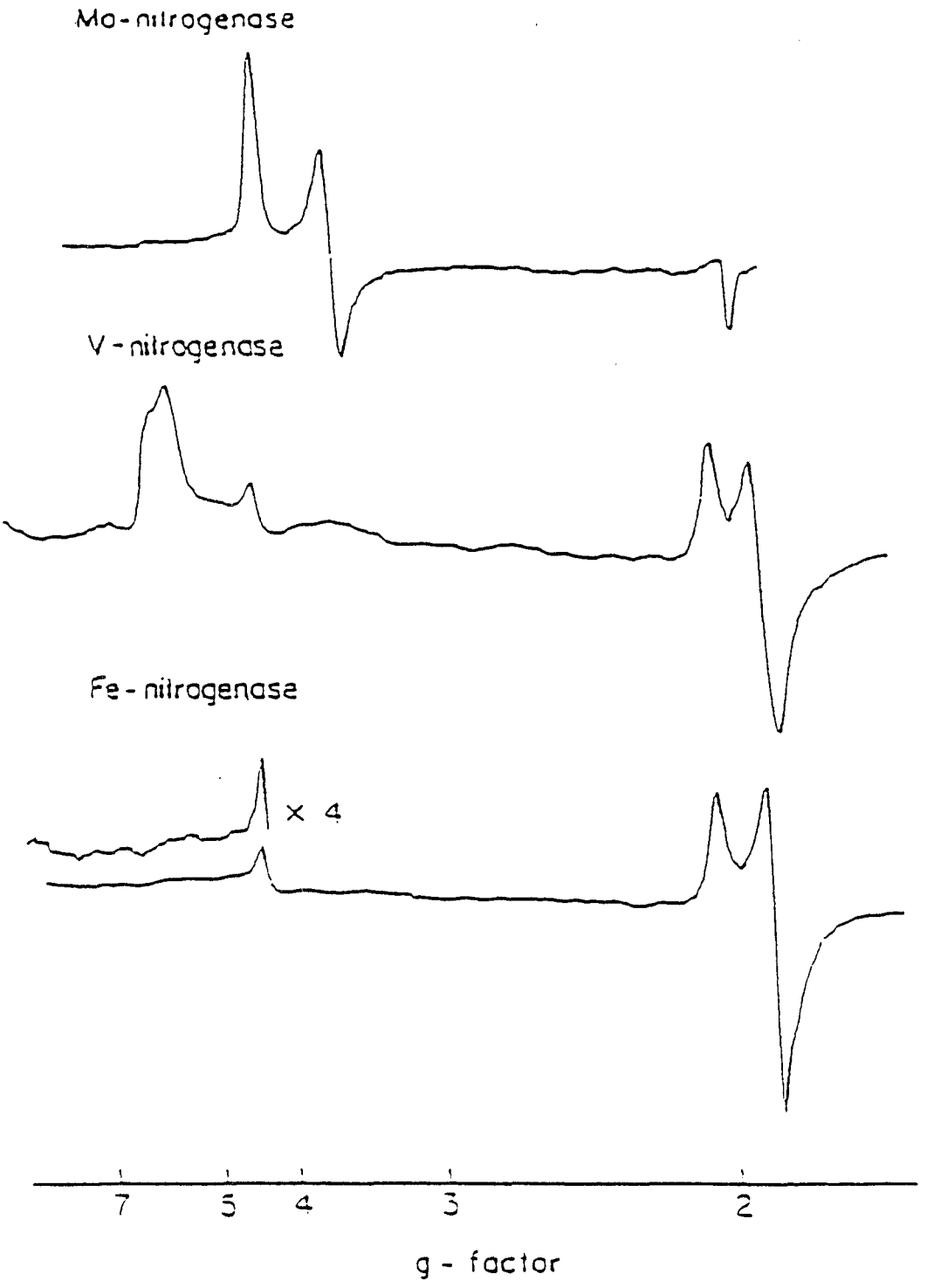

Figure 1.1. EPR spectra of the component 1 proteins from the three different nitrogenases of *A. vinelandii.* The spectrum of Mo-nitrogenase arises from the ground state of a single S = 3/2 species. The spectra of both the V- and Fe-nitrogenase contain an axial S = 1/2 species with $g_{av} < 2$ while the V nitrogenase also exhibits a rhombic S = 3/2 species in the g = 5.5 region. Conditions: temperature, 12 K; microwave power, 20 mW. Figure taken from ref. 1.82.

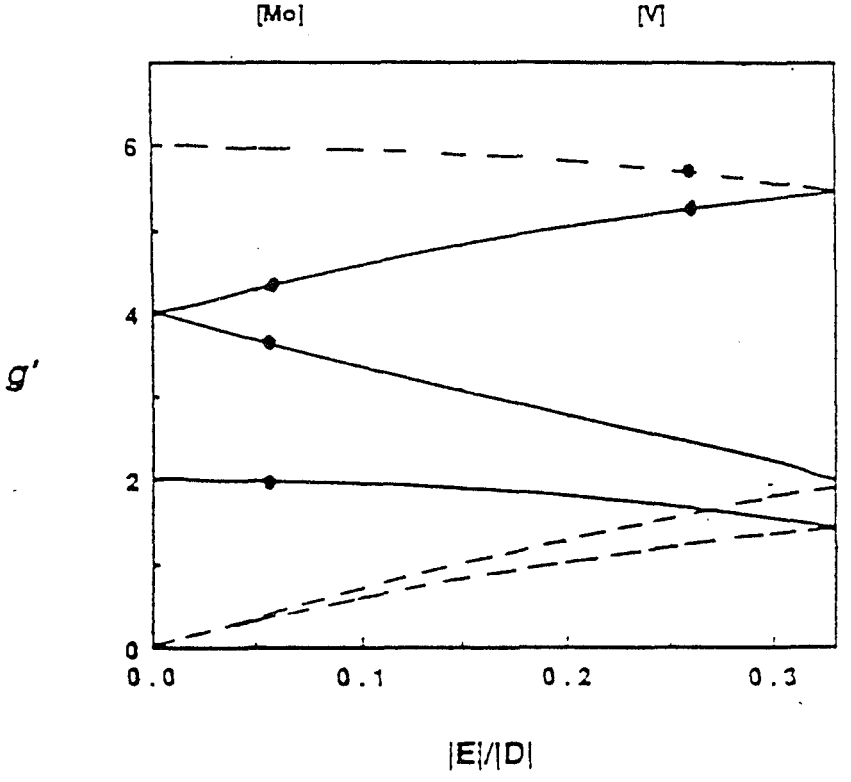

Figure 1.2. Plot of the apparent g factors (g') for the two Kramers doublets of an S = 3/2 spin system having zero-field splitting greater than the Zeeman splitting. For an axial system with positive zero-field splitting, the ground state (solid line) will have g' factors at 4, 4, and 2 while the excited state (dashed line) will be at 6, 0 and 0 (and will be unobservable). The observed resonances for component 1 from Mo-nitrogenase and V-nitrogenase are marked with circles at |E|/|D| = 0.053 and 0.26, respectively. Figure taken from ref. 1.82.

The S3 signal for the VFe protein is not observable in the absorption mode but may be seen in the dispersion mode under conditions of rapid passage (1.81) (Figure 1.3). The reason this signal is not observable in the derivative mode is that, unlike other EPR signals, it has ill-defined shoulders that are not easily detectable in the derivative representation. This has been observed in other metalloproteins which have spin-coupled centers.

The EPR spectrum of the second alternative nitrogenase conspicuously lacks the characteristic S = 3/2 center present in both the Mo- and V-nitrogenases. In the Mo system, the S = 3/2 signal is attributed to the M center and is inferred to be the same in the V system. The lack of this signal in the EPR spectrum of the second alternative nitrogenase raises questions concerning the presence, if any, of a cofactor in this system. Otherwise the EPR spectrum looks more like that of the V system than that of the Mo system.

MCD spectroscopy is very successful in elucidation of the different forms of Fe/S clusters present in metalloproteins (1.83). As shown with the M centers of Mo-nitrogenase, two different types of clusters (M and P) can be monitored just by changing the redox conditions on the protein. In the as-isolated state the M centers are paramagnetic while the P clusters are diamagnetic. Oxidation by thionine reverses this condition and, therefore, each type of cluster may be observed independent of the other. Because ^{57}Fe-enriched samples, which are needed for Mössbauer studies, of the VFe protein are still forthcoming, it is MCD spectroscopy that has identified the presence of P-like clusters in the VFe protein (1.83). Figure 1.4 gives a comparison of the thionine-oxidized MoFe and VFe MCD spectra. These spectra show some differences. Specifically the band at 800 nm in the MoFe protein has shifted to 760 nm in the VFe protein, while the band centered at 380 nm is resolved into two components at 390 and 340 nm. Magnetization curves plotted from this data are similar for both proteins and

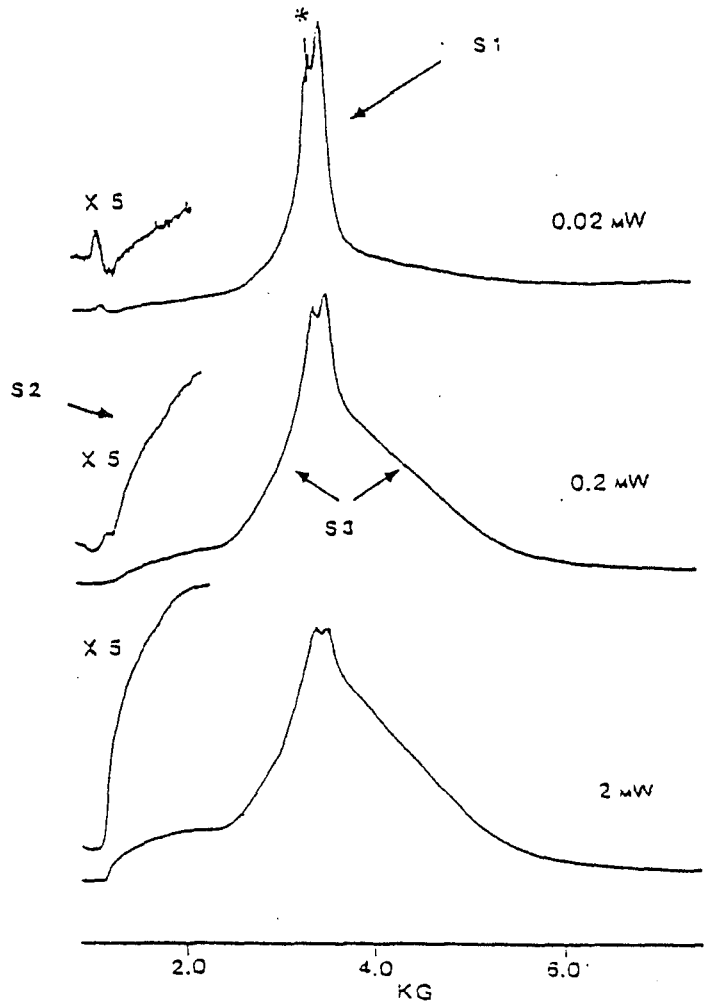

Figure 1.3. Dispersion spectra of component 1 of V-nitrogenase at 2.0 K showing the effect of power. S1 in the top spectrum is due to the S = 1/2 species (S1) while signal S2 originates from the S = 3/2 species. The broad signal between ~ 2800 G and ~ 5500 G is due to S3. The * marks a cavity impurity. Figure taken from ref 1.82.

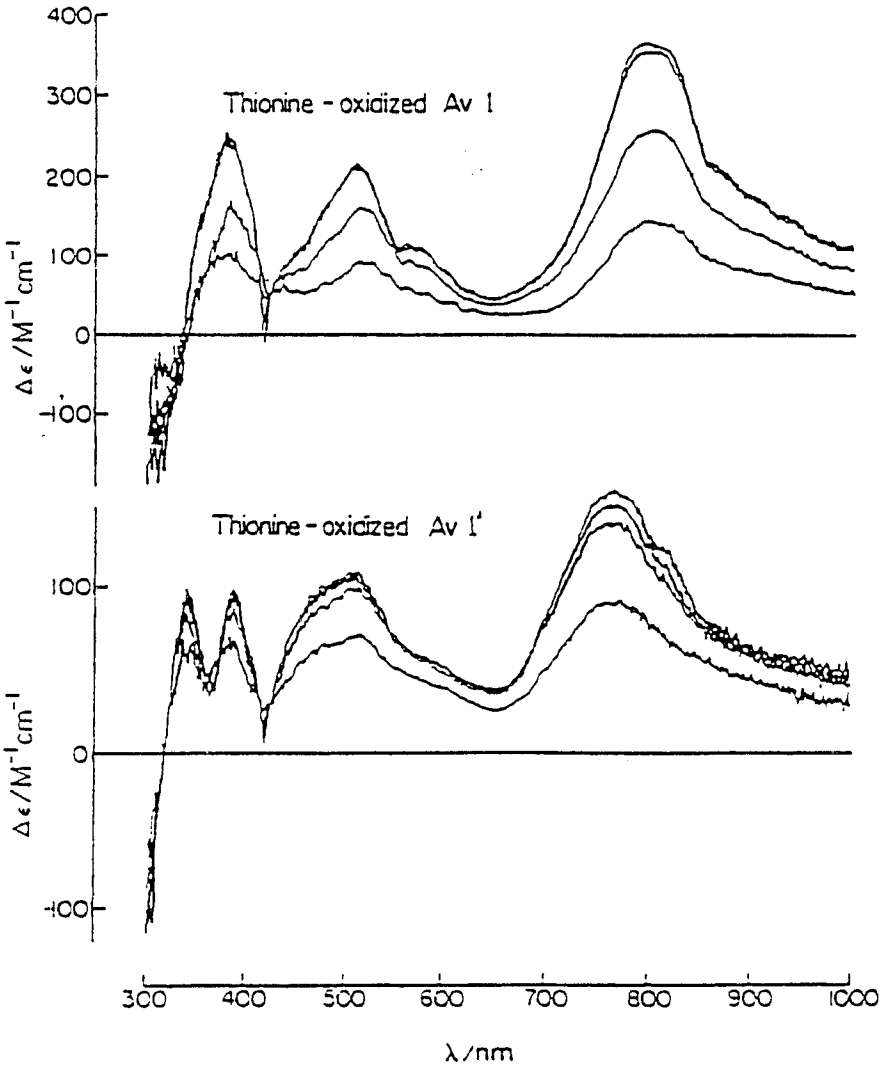

Figure 1.4. Low-temperature MCD spectra of thionine-oxidized component 1 from Mo-nitrogenase (Av1) and from V-nitrogenase (Av1'). Conditions: temperature (top to bottom), 1.57, 4.22, 18.0 and 30.0 K (Av1) and 1.58, 4.22, 7.6 and 20.0 K (Av1'); magnetic field, 4.5 T. Figure taken from ref. 1.83.

can be interpreted as being representative of an S = 5/2 to 7/2 spin system with near-axial symmetry and a large negative zero-field splitting energy. This energy picture would place EPR-silent levels as the ground state, which may account for the inability to observe an EPR spectrum for paramagnetic P clusters.

The MCD spectrum for the as-isolated or dithionite-reduced VFe protein is compared to that for the MoFe protein in Figure 1.5 (1.83). Because of the complexity of the VFe EPR spectrum, it is not known which paramagnetic signals (S1, S2, or S3) are contributing to this MCD spectrum. However, the magnetization curves for the VFe protein differ from those for the MoFe protein but may be simulated as arising from predominantly an S = 3/2 spin system, which infers that the MCD specta arise from the M centers in both proteins.

The vanadium K-edge X-ray absorption spectrum for the VFe protein from *A. vinelandii* (1.84) as well as the XANES (1.85) has been reported. The XANES spectrum is very similar to that of a cubane-like VFe_3S_4 model compound where a 1s $\rightarrow$ 3d transition is seen in both, which indicates a tetrahedral environement for V as well as an oxidation state between 2+ and 4+. The EXAFS of the VFe protein can be simulated by three components in the first coordination sphere around V: three S (or Cl), three O (or N), and 3 Fe for which the M-Fe distance in VFe is longer than that in MoFe.

Recently the K-edge Fe EXAFS of the cofactor from the V-nitrogenase of *Azotobacter chroococcum* was published (1.86). They found that the V cofactor is very similar to FeMo-co. They also found the Fe-Fe distance to be quite long (0.369 nm) as compared to that for FeMo-co (0.365 nm). The data is best simulated by including 3S and 2Fe in the first coordination sphere, and a mixed iron/vanadium second shell.

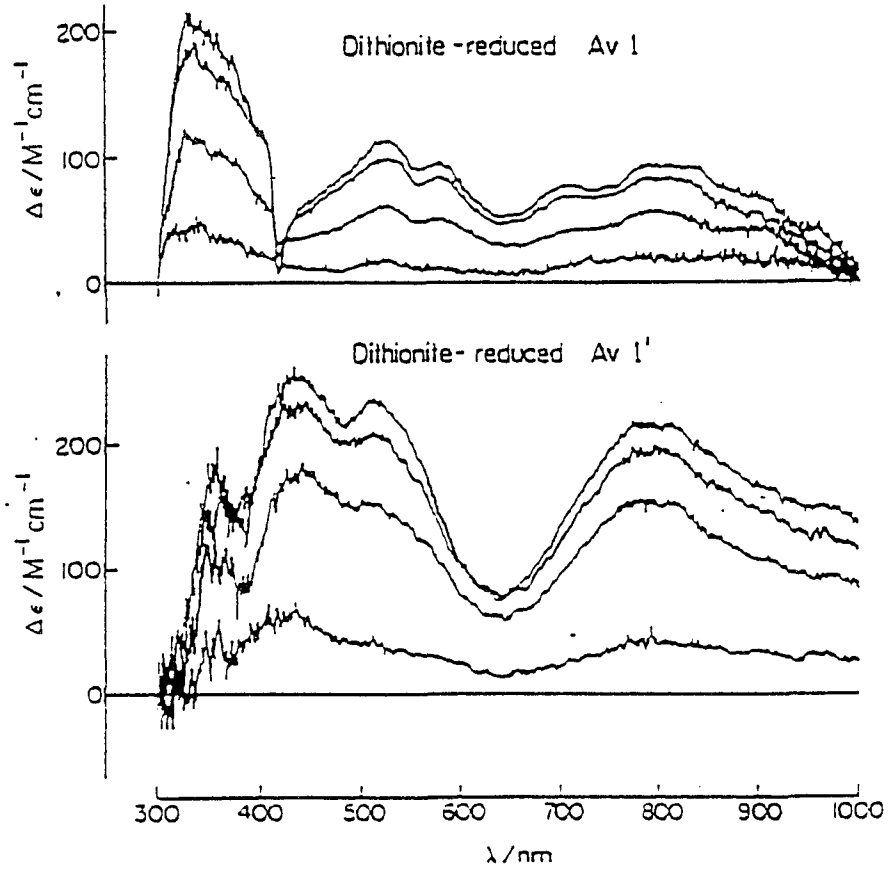

Figure 1.5. Low-temperature MCD spectra of dithionite-reduced component 1 of Mo-nitrogenase (Av1) and V-nitrogenase (Av1'). Conditions: temperature (top to bottom), 1.64, 4.22, 15.0 and 120 K (Av1) and 1.64, 4.22, 9.5 and 60 K (Av1'); magnetic field, 4.5 T. Figure taken from ref. 1.83.

REFERENCES

1.1. Schindler, F. (1885) Jour. Landw. **33**, 325-336

1.2 Beyerinck, M. W. (1888) Bot. Ztg. **46**, 725-735, 741-750, 757-790

1.3. Winogradsky, S. (1893) Comp. Rend. Acad. Sci. **116**, 1385-1388

1.4. Beijerinck, M. W. (1901) Zentr. Bakteriol. Parasitenk, Abt. II, **7**, 561-582

1.5. Kamen, M. D. and Gest, H. (1949) Science, **109**, 560

1.6. Meyerof, O. and Burk, D. (1928) Zeit. Physik. Chem., A, **139**, 117-142

1.7. Zelitch, I., Rosenblum, E. D., Burris, R. H. and Wilson, P. W. (1951), J. Biol. Chem. **191**, 295-298

1.8. Carnahan, J. E., Mortenson, L. E., Mower, H. F. and Castle, J. E. (1960), Biochim. Biophys. Acta **38**, 188-189

1.9. Mortenson, L. E., (1965) Non-heme iron proteins: role in energy conversion, 243-259, San Pietro, A. ed., Antioch Press, Yellow Springs, Ohio

1.10. Eady, R. R., Smith, B. E., Cook, K. A., and Postgate, J. R. (1972) Biochem. J. **128**, 655

1.11. McNary, J. E. and Burris, R. H. (1962) J. Bacteriol. **84**, 598-599

1.12. Winter, H. C. and Burris, R. H. (1968), J. Biol. Chem. **243**, 940-944

1.13. Bui, P. T. and Mortenson, L. E. (1968), Proc. Natl. Acad. Sci., U. S. A. **61**, 1021-1027

1.14. Tso, M-Y. W., and Burris, R. H. (1973) Biochim. Biophys. Acta **309**, 263

1.15. Bulen, W. A., Burns, R. C. and LeCompte, J. R. (1965) Proc. Natl. Acad. Sci., U. S. A. **53**, 532-539

1.16. Ljones, T. and Burris, R. H. (1978) Biochem. Biophys. Res. Comm., **80**, 22-25

1.17. Mozen, M. M. and Burris, R. H. (1954) Biochim. Biophys. Acta **14**, 577-578

1.18. Dilworth, M. J. (1966) Biochim. Biophys. Acta **127**, 285-294

1.19. Schollhorn, R. and Burris R. H. (1966) Fed. Proc. **25**, 710

1.20. Hardy, R. W. F., Burns, R. C. and Parshall, G. W. (1971) Advan. Chem. Ser. **100**, 219-247

1.21. McKenna, C. E. and Huang, C. W. (1979) Nature **280**, 609-611

1.22. Hageman, R. V. and Burris, R. H. (1980) Biochim. Biophys. Acta **591**, 63-75

1.23. River-Ortiz, J. M. and Burris, R. H. (1975) J. Bacteriol. **123**, 537-545

1.24. Lowe, D. J., Thorneley, R. N. F. (1984) Biochem. J. **224**, 877-86

1.25. Lowe, D. J., Thorneley, R. N. F. (1984) Biochem. J. **224**, 903-9

1.26. Thorneley, R. N. F., Lowe, D. J. (1983) Biochem. J. **215**, 393-403

1.27. Thorneley, R. N. F., Lowe, D. J. (1984) Metal Ions in Biology Vol. 7, Chap. 5, ed. T. Spiro, New York, Wiley

1.28. Thorneley, R. N. F., Lowe, D. J. (1984) Biochem J. **224**, 887-94

1.29. Hardy, R. W. F., and Knight, E. (1967) Biochim. Biophys. Acta **139**, 69-90

1.30. Hwang, J. C. and Burris, R. H. (1972) Biochim. Biophys. Acta **283**, 339-350

1.31. Hwang, J. C., Chen, C. H., and Burris, R. H. (1973) Biochim. Biophys. Acta **292**, 256-270

1.32. Lockshin, A., and Burris, R. H. (1965) Biochim. Biophys. Acta **111**, 1-10

1.33. Bulen, W. A. (1976) Proceedings of the First International Symposium on Nitrogen Fixation, 177-186. Newton, W. E. and Nyman, C. J., Ed's. Washington State Univ. Press.

1.34. Guth, J. H. and Burris, R. H. (1983) Biochemistry **22**, 5111-5122

1.35. Bortels, H. (1936) Zentr. Bakteriol. Parasitenk Abt. II **95**, 193-218

1.36. Benemann, J. R., McKenna, C. E., Lie, R. F., Traylor, T. G. and Kamen, M. D. (1972) Biochim. Biophys. Acta **264**, 25-38

1.37. McKenna, C. E., Benemann, J. R. and Traylor, T. G. (1970) Biochem. Biophys. Res. Commun. **41**, 1501

1.38. Burns, R. C., Holsten, R. D. and Hardy, R. W. F. (1970) Biochem. Biophys. Res. Commun. **39**, 90

1.39. Burns, R. C. and Hardy, R. W. F. (1971) Fed. Proc. **30**, 1291

1.40. Shah, V. K., Davis, L. C., Gordon, J. K., Orme-Johnson, W. H. and Brill, W. J. (1973) Biochim. Biophys. Acta **292**, 246-255

1.41. Shah, V. K., Davis, L. C., Stieghorst, M. and Brill, W. J. (1974) J. Bacteriol. **117**, 917-919

1.42. Bishop, P. E. and Brill, W. J. (1977) J. Bacteriol. **130**, 954-956

1.43. Bishop, P. E., Larlenski, D. M. L. and Hetherington, D. R. (1980) Proc. Natl. Acad. Sci. USA **77**, 7342-7346

1.44. Keeler, R. F., and Varvey, J. E., (1957) Arch. Biochem. Biophys. **70**, 585

1.45. Benemann, J. R., Smith, G. M., Kostel, P. J., and McKenna, C. E. (1973) *FEBS Lett.* **29**, 219

1.46. Nagatani, H. H., and Brill, W. J. (1974), Biochim. Biophys. Acta **362**, 160

1.47. Erdody, S. and Gehrke Jr., H. (1975) Proc. S. D. Acad. Sci. **54**, 246

1.48. Bishop, P. E., Jarlenski, D. M. L. and Hetherington, D. R. (1982) J. Bacteriol. **150**, 1244-1251

1.49. Page, W. J., and Collinson, S. K. (1982) J. Microbiol. **28**, 1173

1.50. Riddle, G. P., Simonson, J. G., Hales, B. J., and Braymer, H. D. (1982) J. Bacteriol. **152**, 72

1.51. Hales, B. J., and Case, E. E. (1987) J. Biol. Chem. **262**, 16205

1.52. Premakumar, R., Lemos, E. M. and Bishop, P. E. (1984) Biochim. Biophys. Acta **797**, 64-70

1.53. Bishop, P. E., Premakumar, R., Dean, D. R., Jacobson, M. R., Chisnell, J. R., Rizzo, T. M. and Kopczynski, J. (1986) Science **232**, 92-94

1.54. Hales, B. J., Case, E. E., and Langosch, D. J. (1985) in Nitrogen Fixation Research Progress; Evans, H. J., Bottomley, P. J., and Newton, W. E., Eds., Martinus Nijhoff Publishers, Dordrecht, The Netherlands, p. 612

1.55. Chisnell, J. R., and Bishop, P. E. (1985) in Nitrogen Fixation Research Progress; Evans, H. J., Bottomley, P. J., and Newton, W. E., Eds., Martinus Nijhoff Publishers, Dordrecht, The Netherlands, p. 623

1.56. Robson, R. L., Eady, R. R., Richardson, T. H., Miller, R. W., Hawkins, M., and Postgate, J. R. (1986) Nature **322**, 388

1.57. Hales, B. J., Langosch, D. L., and Case, E. E. (1986) J. Biol. Chem. **261**, 15301

1.58. Chisnell, J. R., Premakumar, R., Bishop, P. E. (1988) J. Bacteriol. **170**, 27

1.59. Scorsone, K. A., and Hales, B. J., manuscript in preparation

1.60. Pretorius, I-M., Rawlings, D. E., O'Neill, E. G., Jones, W. A., Kirby, R., and Woods, D. R. (1987) J. Bacteriol. **169**, 367-370

1.61. Joerger, R. D., Jacobson, M. R., Premakumar, R., Wolfinger, E. D., and Bishop, P. E. (1989) J. Bacteriol. **171**, 1075

1.62. Hausinger, R. P., and Howard, J. B. (1983) J. Biol. Chem. **258**, 13486

1.63. Lindahl, P. A., Gorelick, N. J., Münck, E., and Orme-Johnson, W. H. (1987) J. Biol. Chem. **262**, 14945

1.64. Münck, E., Rhodes, H., Orme-Johnson, W. H., Davis, L. C., Brill, W. J., and Shah, V. K. (1975) Biochim. Biophys. Acta **400**, 32

1.65. Zimmermnn, R., Münck, E., Brill, W. J., Shah, V. K., Henzl, M. T., Rawlings, J., and Orme-Johnson, W. H. (1978) Biochim. Biophys. Acta **537**, 185

1.66. Kurtz, D. M., McMillan, R. S., Burgess, B. K., Mortenson, L. E., and Holm, R. H. (1979) Proc. Natl. Acad. Sci. USA **76**, 4986

1.67. McLean, P. A., Papaefthymiou, V., Orme-Johnson, W. H., and Münck, E. (1987) J. Biol. Chem. **262**, 12900

1.68. Johnson, M. K., Thompson, A. J., Robinson, A. E., and Smith, B. E. (1981) Biochim. Biophys. Acta **671**, 61

1.69. Yang, S.-S., Pan, W.-H., Friesen, G.D., Burgess, B.K., Corbin, J.L., Stiefel, E.I., and Newton, W.E. (1982) J. Biol. Chem. **257**, 8042

1.70. Schultz, F.A., Gheller, S.F., Burgess, B.K., Lough, S., and Newton, W.E. (1985) J. Am. Chem. Soc. **107**, 5364

1.71. Hoffman, B. M., Roberts, J. E., and Orme-Johnson, W.H. (1982) J. Am. Chem. Soc. **104**, 4711

1.72. Hoffman, B. M., Venters, R. A., Roberts, J. E., Nelson, M. J., and Orme-Johnson, W. H. (1982) J. Am. Chem. Soc. **104**, 4711

1.73. Venters, R. A., Nelson, M. J., McLean, P. A., True, A. E., Levy, M., Hoffman, B. M., and Orme-Johnson, W. H. (1986) J. Am. Chem. Soc. **108**, 3487

1.74. True, A. E., Nelson, M. J., Venters, R. A., Orme-Johnson, W. H., and Hoffman, B. M. (1988) J. Am. Chem. Soc. **110**, 1935

1.75. Conradson, S. D., Burgess, B. K., Newton, W. E., Hodgson, K. O., McDonald, J. W., Rubinson, J. F., Gheller, S. F., Mortenson, L. E., Adams, M. W. W., Mascharak, P. K., Armstrong, W. A., and Holm, R. H. (1985) J. Am. Chem. Soc. **107**, 7935

1.76. Flank, A. M., Weininger, M., Mortenson, L. E., and Cramer, S. P. (1986) **108**, 1049

1.77. Conradson, S. D., Burgess, B. K., Newton, W. E., Mortenson, L. E., and Hodgson, K. O. (1987), J. Am. Chem. Soc. **109**, 7507

1.78. Hedman, B., Frank, P., Gheller, S. F., Roe, A. L., Newton, W. E., and Hodgson, K. O. (1988) J. Am. Chem. Soc. **110**, 3798

1.79. Thomann, H., Morgan, T. V., Jin, H., Burgmayer, S. J. N., Bare, R. E., and Stiefel, E. I. (1987) J. Am. Chem. Soc. **109**, 7913

1.80. Morningstar, J. E., and Hales, B. J. (1987) J. Am. Chem. Soc. **109**, 6854

1.81. Hales, B. J., True, A. E., and Hoffman, B. M. (1989) J. Am. Chem. Soc. **111**, 8519

1.82. Hales, B. J. (1990) Advances in Inorganic Biochemistry Vol. 8: Metal-Ion Induced Regulation of Gene Expression, Ch. 6, pp165-194, Ed., Eichhorn, G. L. and Marzilli, L. G., Elsevier, New York

1.83. Morningstar, J. E., Johnson, M. K., Case, E. E., and Hales, B. J. (1987) Biochemistry **26**, 1795

1.84. George, G. N., Coyle, C. L., Hales, B. J., and Cramer, S. P. (1988) J. Am. Chem. Soc. **110**, 4057

1.85. Kovacs, J. A., and Holm, R. H. (1986) J. Am. Chem. Soc. **108**, 340

1.86. Harvey, I., Arber, J. M., Eady, R. R., Smith, B. E., Garner, C. D., and Hasnain, S. S. (1990) Biochem. J. **266**, 929-931

1.87. Jacobson, M.R., Brigle, K.E., Bennett, L.T., Setterquist, R.A., Wilson, M.S., Cash, V.L., Beynon, J., Newton, W.E., and Dean, D.R. (1989) J. Bacteriol. **171**, 1017

1.88. Hales, B.J., Case, E.E., Morningstar, J.E., Dzeda, M.F., and Mauterer, L.A. (1986) Biochemistry **25**, 7251

1.89. Eady, R. R., Robson, R. L., Pau, R. N., Woodley, P., Lowe, D. J., Miller, R. W., Thorneley, R. N. F., Smith, B. E., Gormal, C., Fisher, K., Eldridge, M., and Bergstrom, J. (1988) Nitrogen Fixation: Hundred Years After, Bothe, H., de Bruijn, F. J., and Newton, W. E., Eds.; Gustav Fischer Verlag, Stuttgart, Federal Republic of Germany, p. 81

MATERIALS AND METHODS

2.1 Purification of the V-Nitrogenase from *Azotobacter vinelandii*

The V-nitrogenase of *Azotobacter vinelandii* was first isolated in 1986 (Hales et al, 2.1). This V-nitrogenase was purified from a strain called LS15, which is a resistant mutant of strain LS10 from *A. vinelandii*. LS15 cells were grown either at LSU or the University of Wisconsin, in which case they were frozen in liquid nitrogen and shipped as cell paste in dry ice. For protein purification, the cells were thawed and lysed by osmotic shock. Because of the oxygen sensitivity of the nitrogenase proteins, all procedures were conducted in an inert atmosphere glove box or under anaerobic reducing conditions outside the box.

The procedure for cell lysis was as follows: 300 g of frozen cell paste was weighed out in six 300 ml centrifuge bottles at 50 g each. The bottles with tops and inner lids were transferred into the glove box before the cells thawed, being careful to evacuate the insides of the centrifuge bottles to prevent oxygen from being transferred into the box along with the cells. The cells were allowed to thaw inside the box and then suspended in 250 ml 25 mM TRIS, pH 7.4 containing 4 M glycerol and 2 mM dithionite (sodium hydrosulfite). Dithionite was added to all solutions as follows: Degassed dithionite (0.2 g per ml of stock solution needed) and 25 mM NaOH were combined anaerobically and this 1 M stock solution was added in all our solutions to make the final concentration 2 mM. After 30 minutes, the mixture of cells and buffer was centrifuged at 13,300 x g for 15 min. The glycerol solution was discarded and the cell pellet resuspended in 25 mM buffer containing 10-20 mg each of DNase, RNase, and ligase. Following a second 30 min. period, the mixture was again centrifuged at 22,500 x g for one hour at 4°C. The resulting supernatant (about 250 ml) was concentrated to about one-fifth the original volume on a Minitan® ultrafiltration system (Millipore Corp.) containing PTTK 30,000 NMWL

filtration plates (Millipore Corp.). The cell extract was either frozen as pellets in liquid nitrogen for later use or loaded directly onto a DEAE column.

The second step in purification was an anion exchange column. The resin used was DEAE cellulose or Sephacel (Sigma Chemical). These columns were usually 42 mm in diameter and 20-25 cm in length (~300 ml bed volume) and were run inside or outside the glove box. The column was equilibrated with three to five bed volumes of 0.08 M NaCl in 25 mM TRIS, pH 7.4 with 2 mM dithionite, until it was reducing. Reducing conditions were tested with a piece of filter paper which had been dried in a 1% solution of methyl viologen. Dithionite reduces methyl viologen to give a characteristic blue color. Any oxygen on the column will react with the dithionite and the methyl viologen will test negative.

Cell extract was loaded onto the DEAE column and washed with two bed volumes of 0.1 M NaCl in 25 mM TRIS, pH 7.4 to remove loose-binding proteins. The column was then washed with a linear salt gradient prepared by combining equal volumes of 0.1 M NaCl in 25 mM TRIS and 0.3 mM NaCl in 25 mM TRIS, pH 7.4 as follows: The lower salt buffer was pumped onto the column at two times the rate at which the higher salt buffer was pumped into the reservoir of lower salt buffer. The total volume of the gradient was usually five bed volumes. The V-nitrogenase proteins tends to co-elute at a salt concentration between 0.15 and 0.25 M. Therefore, this first DEAE column was used mainly as a gross purification step and not for separation of the two nitrogenase proteins in the vanadium system. In contrast, the two component proteins of Mo-nitrogenase separate on the first DEAE column (2.2).

To separate the component proteins of V-nitrogenase after the DEAE column a sizing column (Sephacryl S-300, Sigma Chemicals) was used. This resin consists of polyacrylamide beads in which pore sizes vary thus enabling larger proteins to pass

through the column while smaller molecules are trapped and retarded. Because these beads are susceptible to packing, slower flow rates must be employed for longer columns. The columns used in this procedure were about 30 mm wide and 1.2 m long (~280 ml bed volume). The buffer used was 0.3 M NaCl in 25 mM TRIS, pH7.4. The protein samples applied to these columns were generally at or near the same salt concentration as the buffer. Again, the buffer was anaerobic containing dithionite, and the column is reducing before the protein is applied. In general, the concentration of the protein solution loaded was 70 mg/ml, and 5-7 ml of protein was loaded at this concentration.

Av1' with a 200,000 MW elutes first followed by Av2' at 60,000 MW, although there was often some overlap of the protein bands. Fractions of 5-10 ml were collected in large (30 ml) anaerobic serum bottles that had been capped with rubber septa in the glove box. Activity for each protein was tested using the acetylene assay, as described below. The active fractions for each protein were pooled and concentrated with an Amicon® ultrafiltration system (Millipore Corp.). This system uses membranes which contain pores with a molecular weight "cutoff". For instance, in concentrating Av2' with a molecular weight of 60,000, a membrane was used which allows proteins with a molecular weight less than 30,000 to pass through the membrane (YM30, Millipore). Similarly the membrane used for Av2' (200,000 MW) cuts off at 50,000 MW (XM50, Millipore). During the purification, polyacrylamide gel electrophoresis (PAGE) often was used to ascertain the degree of purity.

Av1' often required further purification. Recent results have indicated that a second DEAE column should be run employing a shallower gradient to further purify Av1'. In such a situation, the purified Av1' was loaded onto a DEAE cellulose column using the same procedure outlined above and a gradient was then run using 0.1 to 0.6 M salt in 25 mM TRIS, pH 7.4.

2.2 ACETYLENE ASSAY

The reduction of the substrate C_2H_2 to C_2H_4 is a convenient and almost universal assay for nitrogenase activity. The purified nitrogenase proteins have no intrinsic enzymatic activity by themselves and, therefore, require the presence of the complementary protein for activity. Measurement of the specific activity for each protein is slightly different with respect to component ratios. Maximal activity for component 1 was usually obtained when there was a 10- to 20-fold excess of component 2. Component 2 exhibited maximal activity when there was an optimal ratio of the two proteins; if this ratio was exceeded, inhibition of activity occured. In either type of assay, specific activity was measured as nmol of ethylene produced per mg of protein per min.

The acetylene assay was run as follows: One of the nitrogenase proteins was added to a vial (13.5 ml) containing 10% acetylene in argon and one ml of an ATP-regenerating solution. This solution contains 2.5 mM ATP, 30 mM phosphocreatine, 0.125 mg/ml creatine phosphokinase, 20 mM dithionite, and 5 mM $MgCl_2\,6H_2O$ in 38 mM Tes-KOH and has been degassed. After the first nitrogenase protein was added, the vial was incubated with shaking for a couple of minutes at 30° C. The assay was initiated upon addition of the complementary protein, timed for 15 minutes, and stopped by addition of 0.1 ml of 30% trichloroacetic acid which precipitated the proteins.

The amount of ethylene produced was measured using a Varian Model 3700 gas chromatograph fitted with a Porapak® column, an FID (Flame Ionization Detector), and connected to a strip chart recorder. A small amount of contaminating methane present in the 10% acetylene gas (or the acetylene itself) was used as an internal standard.

2.3 PROTEIN CONCENTRATION

Protein concentrations were determined using a biuret assay. Protein (typically 200 to 300 μg) was added to water to a final volume of 200 ml to which 1 ml of biuret reagent was added. The biuret reagent was made by dissolving 0.75 g $CuSO_4$ $5H_2O$, 0.5 g KI, and 3.0 g sodium potassium tartrate in 250 ml water to which 150 ml 10% NaOH was added. The biuret solution containing the protein was incubated at room temperature for 20-30 minutes and absorption of the solution was measured at 540 nm with a Varian Cary 219 spectrophotometer. Protein concentrations were determined from a standard curve using BSA (bovine serum albumin) in a range of 200 to 1000 μg.

2.4 EPR SAMPLE PREPARATION

EPR samples were prepared using the purest protein available in each case. Because there are many different types of samples used, individual differences in preparation will be outlined in the appropriate chapters to follow. In general, however, quartz EPR tubes were used to which approximately 0.3 ml of protein was added. All of the EPR samples were kept frozen in liquid nitrogen.

EPR spectra were recorded on a Bruker ER300D spectrometer interfaced to a Bruker 1600 computer for data handling and manipulation. Low temperatures were achieved using an Oxford Instruments ESR-9 flow cryostat (4.2 to 300 K) positioned in a TE_{102} cavity, resonating at X-band frequencies. Temperatures were read using an Oxford Instruments model ITC4 temperature controller with a digital readout.

EPR spectra were recorded as the first derivative of the absorption as a function of the magnetic field at a given microwave frequency. Spin quantitations were evaluated as described below. Power saturations were quantitated manually and then graphed using Cricket Graph software on a Macintosh PC.

2.5 QUANTITATION OF EPR SPECTRA

It is often instructive to measure the concentration of the paramagnetic species in a sample giving rise to the EPR signal. This is done by integrating the EPR spectrum to obtain the spin concentration. The area obtained from the double integration of the first derivative of the EPR absorption spectrum is directly proportional to the concentration of paramagnetic species giving rise to the signal, provided the signal is not power saturated. This integration may be performed either manually or with the computer software supplied with the EPR spectrometer, and using the method derived by Wyard (2.3). The area is corrected for g-value dependence according to the methods described by Aasa and Vanngard (2.4). A reference standard is run under the exact same conditions as the unknown where the spin concentration in the sample is related to that of the reference by the following equation

$$C_s = A_s/A_r \cdot G_r/G_s \cdot g_r/g_s \cdot C_r \qquad (2.1)$$

where the subscripts r and s refer to the reference and unknown sample, respectively, A represents the area under the absorption curve calculated by double integration, G is the spectrometer gain, C is the concentration, and g corresponds to the average g-factor. The area under the absorption curve is manually calculated according to

$$A = 1/2h^2 \sum (n-2i+1)\, Y_i \qquad (2.2)$$

where h is the magnetic field interval, n is the number of intervals, and Y_i is the intensity of the EPR signal for the i^{th} interval. The average g-value is given by

$$g = 2/3[1/3(g_x^2 + g_y^2 + g_z^2)]^{1/2} + 1/3[1/3(g_x + g_y + g_z)] \qquad (2.3)$$

Aasa and Vanngard (4) also devised a useful method for obtaining the total intensity of a EPR spectrum from a single, isolated absorption-shaped component of an anisotropic signal. The area, A, of the isolated band is evaluated as

$$A = h\sum Y_i \qquad (2.4)$$

and g is given by

$$g_x^2 + g_y^2 \qquad (2.5)$$

$$g = 2g_z B_{max}[(1 - p_x)(1 - p_y)]^{1/2} \qquad (2.5b)$$

where

$$p_{x,y} = \frac{g_{x,y}^2}{g_z^2} \qquad (2.5c)$$

and B_{max} corresponds to the magnetic field at which the maximum of the absorption band occurs. The concentration of the sample is then calculated from equation 2.1. This method is valid provided that the linewidth is smaller than the g-value anisotropy, and is useful for integrations of very broad spectra and from spectra arising from species whose signals overlap.

2.6 MAGNETISM

The magnetic effect seen in almost all substances arises from the result of the application of a magnetic field on the overall magnetic moment. Because the magnetic moment of an electron is about 10^3 times that of a proton, it is the electrons in a substance which give rise to magnetic effects. The extent of magnetization, M, brought about by a magnetic field of strength B is called the magnetic susceptibility, κ

$$M = \kappa B$$

Since κ is the volume magnetic susceptibility, it is related to the more commonly used χ, or mass magnetic susceptibility, by the density, ρ:

$$\chi = 1000\ \kappa/\rho(g/cm^3)$$

If the magnetization is opposed to the applied field then the value of χ is negative and these substances are *diamagnetic*. Diamagnetism arises in all systems from field-induced circulation of paired electrons and, therefore, all substances contain a diamagnetic contribution to their magnetic behavior. On the other hand, if the magnetization is aligned with the external field, χ is positive, and these substances are called *paramagnetic*.

Molecules possessing unpaired electrons have a permanent magnetic moment, and this can be extracted from the susceptibility by plotting χ vs. 1/T (see equation 4). The magnetization or magnetic dipole moment per unit volume is directly proportional to an external magnetic field aligning the dipoles and inversely proportional to the temperature; this is the so-called Curie law

$$M = C\ (B/T)$$

where B is the applied field and C is a constant. The magnetization is really the magnetic moment per unit volume, $M = \mu/V$. The Curie law states that the contribution of the permanent magnetic moment to the paramagnetic susceptibility vanishes at high temperatures because the thermal motions radomize the orientations of the individual spin magnetic moments and, therefore, the magnetization from this source is eliminated.

The contributions to the paramagnetism of a substance have different temperature dependences. The spin-only contribution from unpaired electrons is temperature-dependent and vanishes at high temperatures as already discussed. The so-called induced paramagnetsim from an applied field is temperature-independent however. This temperature-independent paramagnetism (t.i.p.) is a consequence of the stimulation of orbital motion in a molecule. In some cases, the t.i.p. is strong enough to make a molecule paramagnetic even though it has no unpaired electrons (2.5-2.8).

In describing the magnetic properties of systems with unpaired electrons, it is common to use a quantity called the effective magnetic moment, μ_{eff}, where

$$\mu_{eff} = 2.828\ (\chi T)^{1/2}$$

If spin is the only contribution to the magnetic behavior, then μeff becomes

$$\mu_{eff}\ (\text{spin-only}) = g[S(S + 1)]^{1/2}$$

Many systems exhibit experimental μeff very close to that calculated from the number of unpaired electrons. If this is not the case and the temperature dependence also varies, then other effects need to be considered. Spin-orbit coupling and crystal-field effects are two of the major contributions to a change in μeff from the spin-only value.

There are some important deviations from the Curie Law which need to be considered. Theoretically, a plot of χ vs. 1/T gives a straight line with a zero intercept. This type of behavior is not often seen experimentally. Straight line plots are common but with a non-zero intercept, and can be expressed as

$$\chi = C/(T-\theta)$$

where θ corrects the temperature for the non-zero intercept. This is called Curie-Weiss behavior. At low temperatures some paramagnetic substances exhibit a phase transition to a state where the spins are aligned in a parallel fashion. This parallel arrangement of spins gives rise to a strong magnetization of the sample known as *ferromagnetism.* The temperature at which this transition occurs is called the Curie temperature. Conversely, if the spins in the substance were to align themselves in an alternating manner, this would give rise to a low magnetization arrangement called *antiferromagnetism* . This transition occurs at the Neel temperature.

2.7 ELECTRON PARAMAGNETIC RESONANCE

2.7.1 BASIC THEORY

A spinning electron possesses a magnetic moment, μ_e, which is defined as

$$\mu e = -g\beta S$$

where hS is the spin angular momentum vector of the electron, g is the dimensionless constant called the electronic g factor and β is the electronic Bohr magneton. Electron Paramagnetic Resonance (EPR) involves the reorientation of the magnetic moment of an

electron in a strong magnetic field. This technique probes the environment of an unpaired electron by defining the size and shape of the magnetic moment and by characterizing any magnetic fields that might be produced by the parent molecule in the vicinity of the unpaired electron. The Pauli exclusion principle only allows us to reorient the spin of an electron if it is unpaired, therefore EPR is restricted to systems which contain an unpaired electron such as transition metal compounds and free radicals.

The interaction of the electron magnetic moment and an applied field **B** is represented by the Hamiltonian

$$H = -\mu e \cdot \mathbf{B}$$

which becomes

$$H = g\beta \mathbf{B} \cdot S$$

where S is the spin operator. This interaction is better known as the electronic Zeeman interaction. Because S = 1/2 for the electron, there are allowed two possible orientations of the spin, parallel or antiparallel to **B**. The lowest state is denoted by $m_s = -1/2$ and the upper state by $m_s = +1/2$ as shown in Figure 2.1. Application of an oscillating electromagnetic field perpendicular to **B** induces transitions (i.e., $\Delta m_s = \pm 1$) between these states provided that the frequency ν of oscillation satisfies the equation

$$h\nu = g\beta \mathbf{B}$$

Radiation which is typically used to induce transitions has a wavelength of approximately 1 cm and is, therefore, in the microwave region. From the above equation, it might seem that either the frequency of the microwave radiation and/or the applied magnetic field could be varied. But in practice it is the magnetic field that is varied while holding the frequency of the oscillating field constant. Two common frequencies employed are in the X-band

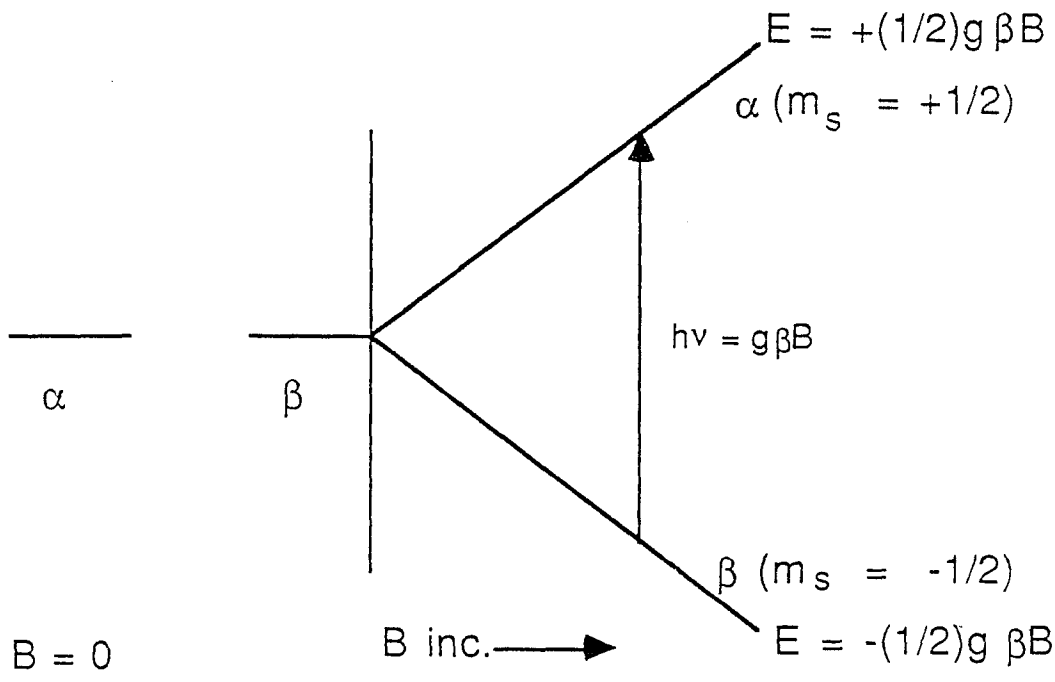

Figure 2.1. The removal of the degeneracy of the α and β electron spin states by a magnetic field.

frequency range (9.5 GHz), where a field strength of about 340 mT is employed or in the Q-band frequency range (35 GHz), where a field strength of about 1250 mT is used. The position of the resonance can be calculated in terms of g, which measures the ratio of the resonance frequency to the applied field. If ν is expressed in GHz and **B** is in mT, the numerical expression for the observed g-value is given by

$$g = 7144.5\nu/\mathbf{B}.$$

For a free electron, $h\nu = 2.00232\beta\mathbf{B}$. G-values for unpaired electrons will deviate from this value due to spin-orbit coupling. This effect is often negligible in free radicals but very pronounced in transition metal systems.

Resonance absorption can be detected only when there is a population difference between the two spin levels. The selection rule for transitions in EPR is $\Delta M_s = \pm 1$. There is an equal probability that transitions are produced from the lower state, β, to the upper state, α, and vice versa. At thermal equilibrium there is a slight excess of spins in the β state, which gives rise to a small temperature-dependent paramagnetism. The ratio of β to α spins is given by Boltzmann's equation

$$N_\alpha/N_\beta = e^{-g\beta B/kT}$$

and it follows that $N_\beta + N_\alpha = N$, the total number of spins.

There are many effects that further modify these electron energy states. Each effect will be treated alone as more complex systems are described. Usually these effects will change the value of g in the EPR experiment.

2.7.2 HYPERFINE STRUCTURE

In a free atom or ion, the resultant electronic angular momemtum, **J**, and nuclear spin, **I**, are generally coupled together through the magnetic interaction between the electronic and nuclear moments, the so-called electron-nuclear hyperfine interaction. For most systems this hyperfine interaction is at least an order of magnitude smaller than the Zeeman interaction. The hydrogen atom is an excellent example of a system where there is one unpaired electron and a nucleus with I = 1/2. Because of the spherical distribution of charge on this nucleus, there is no quadrupole moment, and, furthermore, due to the spherical symmetry of the hydrogen atom there is no anisotropy in the hyperfine structure. The EPR spectrum for the hydrogen atom is illustrated in Figure 2.2.

The appearance of the EPR spectrum is different from what might be expected in that it is presented as the first derivative of the absorption. To first order, the g-value would be measured midway between the absorption maxima which corresponds to the inflection points on the derivative curves. There are two transitions observed for the hydrogen atom as there will be 2I + 1 lines from the hyperfine interaction.

What would the effect be if the electron were delocalized over several equivalent nuclei? In a system such as the methyl radical, for example, there are four possible transitions because the selection rules are $\Delta m_s = \pm 1/2$ and $\Delta M_I = 0$. The transitions indicated in Figure 2.3 would have a ratio of 1:3:3:1 in observed relative intensities as there are three times as many ways to arrange nuclear spins to give $M_I = \pm 1/2$ as for $M_I = \pm 3/2$. In general, when the absorption spectrum is split by n equivalent nuclei of equal I, the number of lines is given by 2nI + 1. Similarly, if there are n equivalent nuclei with spin I_x and m equivalent nuclei with spin I_y, there will arise $(2nI_x + 1)(2mI_y + 1)$ lines with relative intensities corresponding to the coefficients.

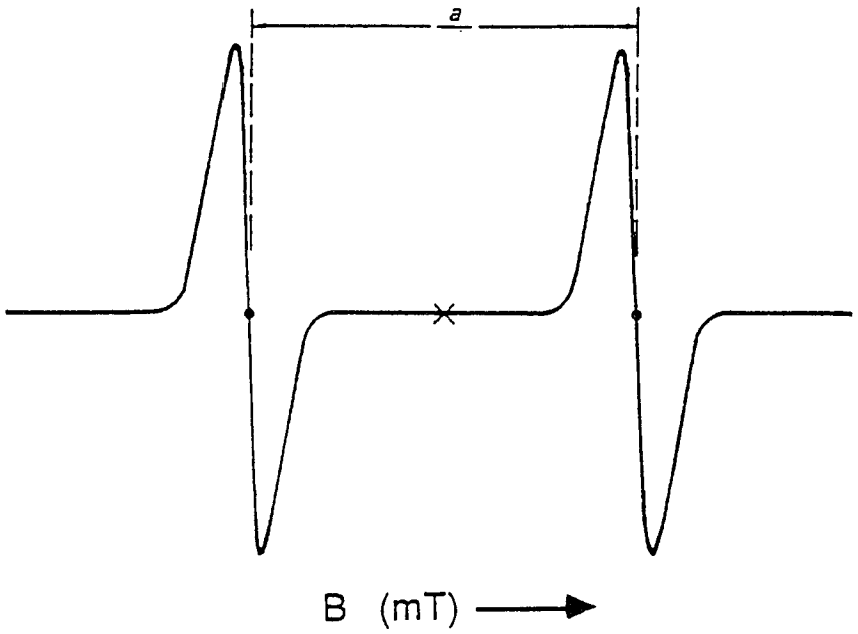

Figure 2.2. The EPR spectrum of a hydrogen atom.

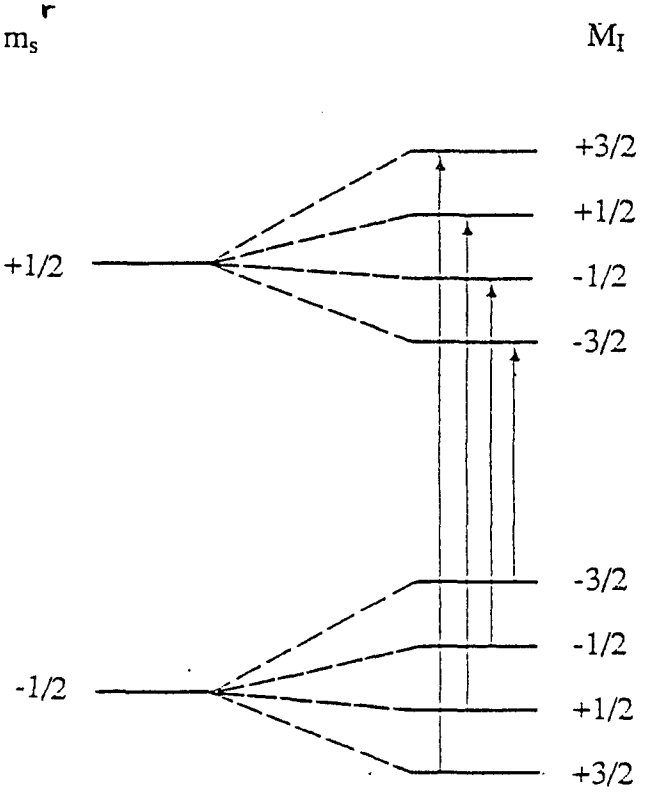

Figure 2.3. The four transitions that occur in the EPR spectrum of the methyl radical. (As with the H atom, the $+m_I$ state is lowest for $m_s = -1/2$ and the $-m_I$ state is lowest for $m_s = +1/2$)

2.7.3 ANISOTROPY

The hydrogen atom is an example of an isotropic system. Other radicals which fit this description are those possessing spherical or cubic symmetry like the hydrogen atom. For these sytems different orientations of the sample in the magnetic field do not affect the spectrum. For other systems with lower symmetry, anisotropic effects can be manifested in both the g-value and hyperfine coupling constants. These anisotropic effects are usually averaged out in solution due to rapid tumbling of the molecules, and the resulting spectrum appears isotropic.

Spin-orbit coupling contributions are small for most free radicals, because the unpaired electron is associated with parent atoms of low atomic number. Since electronic excited states are well removed from the ground state, contributions to the magnetic moment other than the electron spin are very small. Therefore, g-values for these systems rarely deviate greatly from that for the free electron.

As mentioned above, transition metal systems often have g-values which deviate strongly from that of the free electron due to large spin-orbit coupling and, therefore, may be strongly anisotropic. The magnitude of the effect of spin-orbit coupling is dependent on the symmetry of the paramagnet and the energy separation between the ground and excited states. Even when the ground state of a molecule has no orbital angular momentum associated with it, low-symmetry ligand fields can effectively "mix" a low-lying excited state possessing orbital angular momentum with the ground state leading to anisotropy in g. The spin-orbit Hamiltonian is given by

$$H_{so} = \lambda(S \cdot L)$$

where S and L are the spin and orbital angular momentum operators, respectively, and λ is the spin-orbit coupling constant. Because the tensors in EPR are symmetrical, they are

easily diagonalized via a rotation, and, therefore, a coordinate system can always be chosen such that the off-diagonal terms of the g-tensor can be eliminated and the system can be defined by the three diagonal, or principal, g-values g_{xx}, g_{yy}, and g_{zz}. In order for this to work experimentally, all the molecules in the unit cell must have the same orientation of their molecular axes relative to the crystal axes. Therefore, these measurements are often carried out in conjunction with a single crystal x-ray determination.

The dependence of g on orientation has a significant effect on the line shape of an EPR powder spectrum. Three basic types of symmetry exist -isotropic, axial, and rhombic (Figure 2.4). In isotropic systems, $g_x = g_y = g_z$ and a single resonant frequency is observed regardless of sample orientation. For axial systems, $g_x = g_y \neq g_z$ and the spectrum permits the determination of two principal g-values. These are designated as $g_{\parallel} = g_z$ and $g_{\perp} = g_x$ and g_y. Rhombic symmetry ($g_x \neq g_y \neq g_z$) gives rise to an even more complex absorption envelope where all three principal g-values must be evaluated. The EPR absorption spectra of these limiting cases are shown in Figure 2.4b. Because of the broadness of EPR absorption spectra (Figure 2.4b), the first derivative of the absorption spectrum is often plotted instead (Figure 2.4c).

2.7.4 THE TRIPLET STATE

Another complication in our ever increasingly complex picture is the presence of more than one unpaired electron. Additional anisotropy in this system arises from spin-spin interactions between electrons. The magnitude of this contribution to the EPR spectrum depends upon the extent of the interaction of the spins. This interaction can manifest itself in two forms: [1] the exchange interaction involving overlap of the electron wavefunctions; and [2] through space interactions via the dipole-dipole coupling. Information about two electrons can be deduced from their interactions with one another.

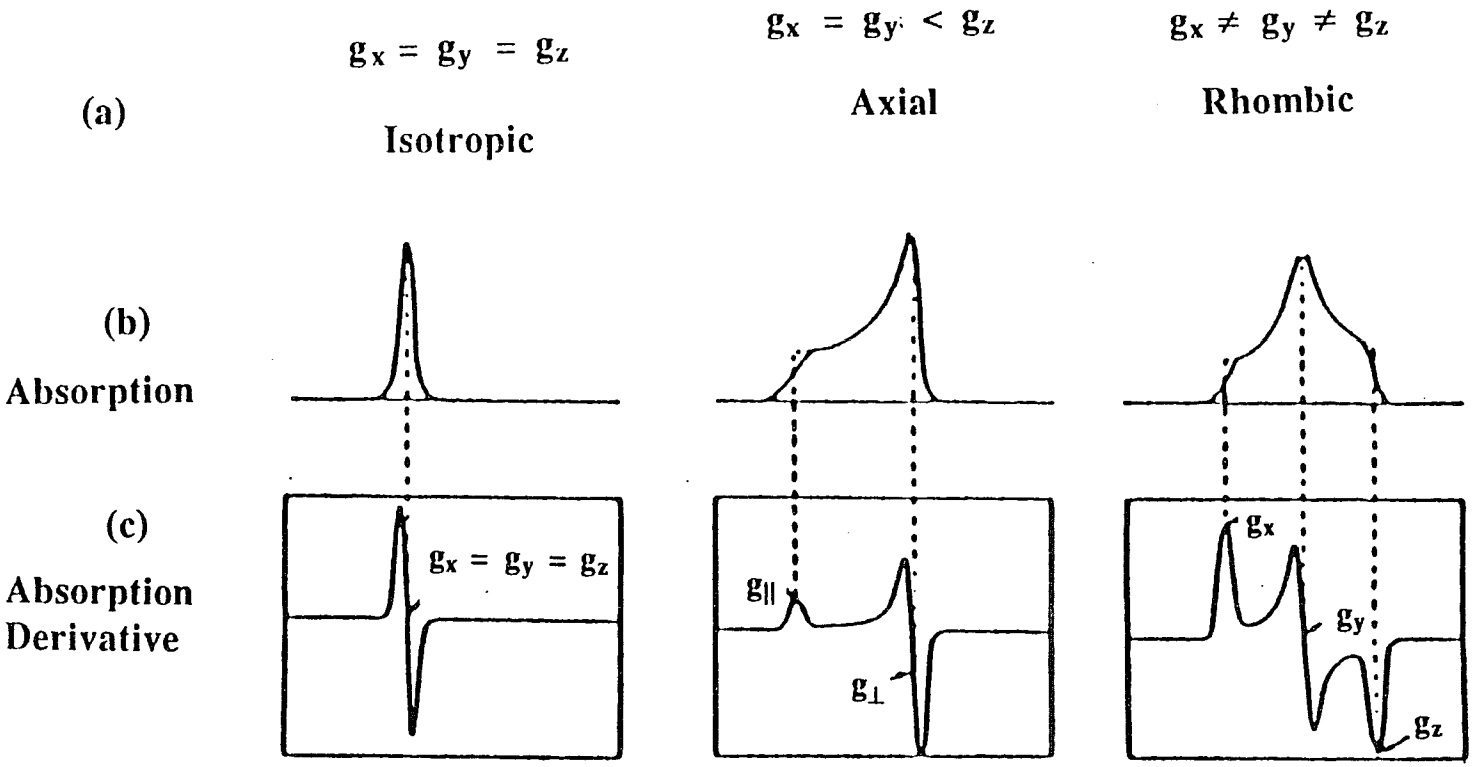

Figure 2.4. Schematic representation of the idealized powder EPR spectra for an isotropic, axial, and rhombic S = 1/2 system. (a) Relative g-values associated with isotropic, axial, and rhombic magnetic moments; (b) absorption curves with a finite linewidth; (c) EPR first derivative curves.

The dipolar interaction is especially useful in determining the distance between the two spins. Further discussion of this topic can be found in another chapter where lanthanide ions are used to perturb the relaxation of an intrinsic paramagnet.

When two spins are close enough for there to be some overlap of their wavefunctions, the unpaired electrons are coupled via exchange forces. The exchange energy takes the form

$$H = JS_1 \cdot S_2$$

Exchange coupling allows the electrons on neighboring sites to exchange spin states rapidly: this usually averages out both the hyperfine and fine structure so that only a single "exchange-narrowed" resonance line remains.

For a system where S = 1, the three spin levels (m_s = 1, 0, -1) would be degenerate in the absence of an external magnetic field if there is negligible dipole-dipole interaction between the two unpaired electrons. However, in the presence of such interaction, the degeneracy is removed even in the absence of an external field (Figure 2.5b). This removal of degeneracy in the absence of the field is called *zero-field splitting*. The dipolar interaction in free radicals is much larger in magnitude than any spin-orbit coupling that might occur in these systems. In contrast, in transition metals systems, it is spin-orbit coupling that produces zero-field splitting and not the weaker dipolar interaction. When the spin states are split by the external field, there exist two $\Delta m_s = \pm 1$ transitions. If the zero-field splitting is large (Figure 2.5c), the $\Delta m_s = \pm 1$ transitions become too large to be observed in the microwave region with magnetic fields normally used and no spectrum is observed (i.e., the system is EPR silent).

Transition metal complexes often exhibit large zero-field splittings due to the mixing of ground and excited states by spin-orbit coupling. The fact that many transition metal complexes also contain several unpaired electrons further makes these spectra

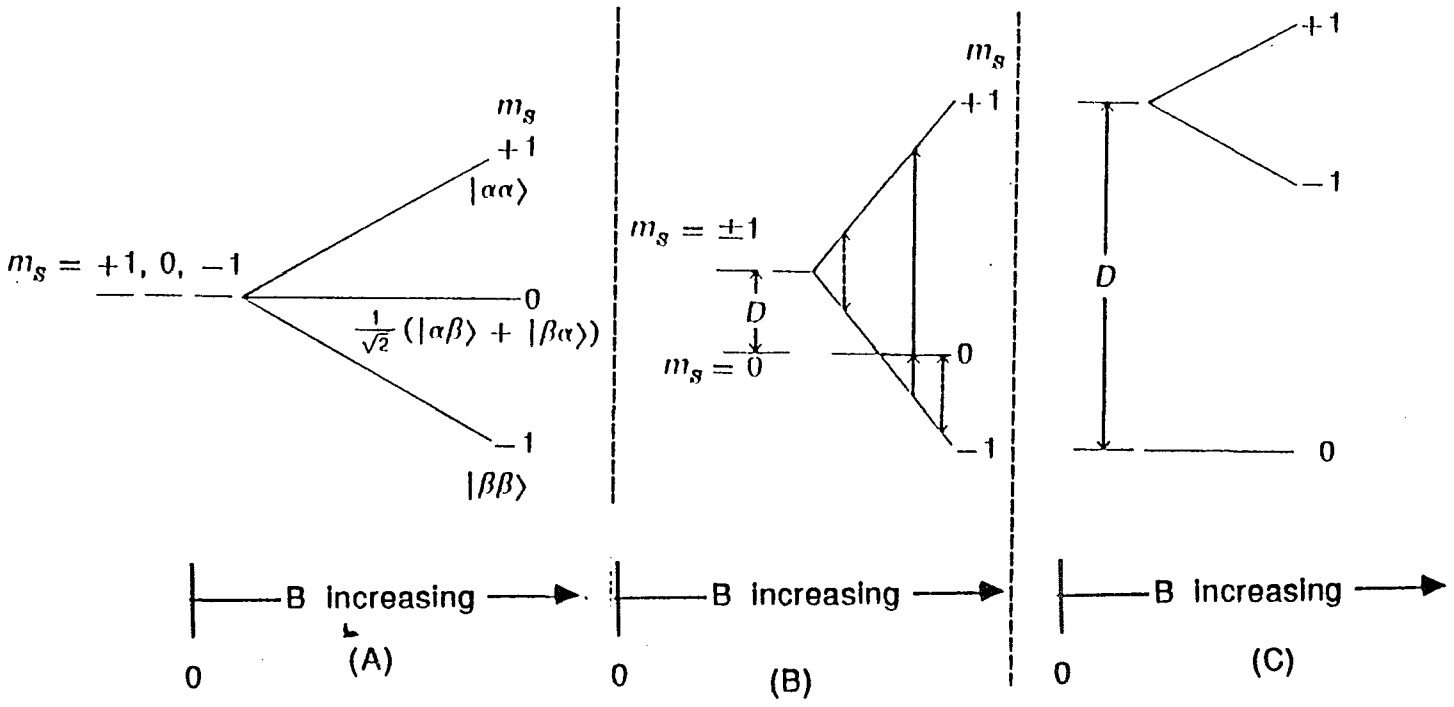

Figure 2.5. The effects of zero-field splitting on the expected EPR transitions. (A) No zero-field effects. (B) Moderate zero-field splittings. The dashed arrows show the fixed frequency result, and the solid arrows show the fixed field result. (C) Large zero-field effects. The magnetic field is assumed to be parallel to the dipolar axis in the molecule.

increasingly complex. An important theorem that summarizes the properties of multi-electron systems is *Kramers' Theorem.* This rule states that if an atom or ion has an odd number of electrons, the degeneracy of every level must remain at least two-fold degenerate in the absence of a magnetic field. In other words, a species with an odd number of electrons must always have as its lowest level at least a doublet, called a *Kramers doublet.* This degeneracy is removed by a magnetic field and an EPR spectrum is observed. On the other hand, if an ion contains an even number of electrons, the degeneracy can be removed by a low symmetry crystal field so that only singlet levels remain which may be separated by energies so large that no EPR transition will be observed in the microwave region (again, EPR silent).

In the case of an odd number of unpaired electrons, Kramers degeneracy leaves each level doubly degenerate. If the zero-field splitting is large, these doublets will be well-isolated from one another. Therefore, transitions will only be observed within each doublet which behave like the simpler systems having $S = 1/2$. These systems are said to have an *effective spin* $S' = 1/2$.

For many transition metal systems interactions of the paramagnetic ion with thermal vibrations of the lattice result in a broadening of the EPR line width. This process is called spin-lattice relaxation and can be so pronounced that the spectrum cannot be observed at room temperature. For this reason many transition metal systems must be cooled to liquid N_2 or He temperatures in order to take advantage of increasing lifetimes with decreasing temperature. This is especially true in metalloproteins where temperatures below 70 K often must be used to observe a spectrum. Many other factors affect the line width of an EPR spectrum including spin-spin interactions, and electron exchange and transfer.

2.7.5 LIGAND HYPERFINE STRUCTURE

In addition to metal hyperfine structure some metal complexes show extra splitting from ligand nuclei. This is called ligand hyperfine or superhyperfine structure. This type of structure is seen if the unpaired electron is delocalized onto the ligand from the parent metal atom. When this is the case, spin-orbit coupling is reduced and, therefore, so is the anisotropy in g. Metal hyperfine splittings will also be smaller in this situation. Interaction of the unpaired electron with ligand nuclei is strongly symmetry dependent in that the orbitals of the ligands and metal containing the unpaired electron should be similar in symmetry in order for interactions to occur.

2.7.6 RELAXATION

Our discussion so far has been limited to those factors affecting the degree of separation of the electron spin states so that an EPR spectrum may be observed. Whether or not a spectrum can be observed is also related to the lifetime that an electron spends in these spin states. The effects of spin-lattice relaxation on the lifetime of a spin state have already been mentioned. Ideally, the population difference, n, between the spin states if not at equilibrium will decay exponentially to equilibrium because of spin-lattice relaxation and the rate of change is given by

$$dn/dt = -n/T_1$$

The magnetic moment, M, is proportional to n and also decays to zero with a characteristic time T_1. In the absence of a field there is no distinction in direction for the magnetic moment. Upon application of an external field along the z axis, for instance, M_z no longer decays to zero but approaches a steady value M_o which is proportional to the static magnetic

susceptibility χ_o of all the N spins

$$M_o = \chi_o B_o$$

The relaxation of M_z now obeys the equation

$$dM_z/dt = -(M_z - M_o)/T_1$$

Although the transverse components of the magnetic vector still decay exponentially to zero, the decay time is different from T_1 and it is referred to as the transverse relaxation time T_2 where

$$dM_x/dt = -M_x/T_2$$

$$dM_y/dt = -M_y/T_2$$

Changes in M_x and M_y do not alter the total Zeeman energy of the spins, whereas changes in M_z need an exchange of Zeeman energy with the lattice. The electron spin does not behave like a bar magnet in the presence of a magnetic field but instead precesses around it with a frequency, ω_o, called the Larmor frequency. Combining the effects of relaxation and Larmor precession, the spin performs a damped precession in which the rotating transverse components of M decay to zero with a characteristic time T_2, while M_z relaxes towards its equilibrium value M_o with a decay time T_1. These effects are described by the Bloch equations:

$$dM_x/dt = \omega_0 M_y - M_x/T_2$$

$$dM_y/dt = -\omega_0 M_x - M_y/T_2$$

$$dM_z/dt = -(M_z - M_o)/T_1$$

The Bloch equations provide a good description of T_1 and T_2 but they are also

very useful in providing an explanation of magnetic resonance absorption and the resultant Lorentz lineshape.

The oscillating field which provides our resonance condition must be at the Larmor frequency in order to produce a change in the magnetic moment. Our oscillating magentic moment can be broken down into three components as is done in the Bloch equations. Because the magnetic moment is oscillating, our reference frame is also rotating and our three components will have a different form. The transverse components correspond to vectors u and v which depend on T_2 as in the Bloch equations. The component of M (u) oscillates in phase with our irradiating field while v lags 90° out of phase. Bloch introduced a complex magnetic susceptibility to account for these phase relations where u and v are proportional to $\chi'(\omega)$ and $\chi''(\omega)$.

$$\chi(\omega) = \chi'(\omega) + i\chi''(\omega)$$

The true magnetic moment is the real part of this expression. By substituting in the values of u and v into the equation above, the spin susceptibilities are as follows:

$$\chi'(\omega) = 1/2\ \chi_o\omega_o\ \frac{T_2^2(\omega_o-\omega)}{1 + T_2^2(\omega_o-\omega)^2 + \gamma^2H_1^2T_1T_2}$$

$$\chi''(\omega) = 1/2\ \chi_o\omega_o\ \frac{T_2}{1 + T_2^2(\omega_o-\omega)^2 + \gamma^2H_1^2T_1T_2}$$

where γ is the magnetogyric ratio for the electron, H_1 is the magnetic component of the applied oscillating field, χ_o is the equilibrium value for the susceptibility and ω and ω_0 correspond to the angular velocity of the applied field and the Larmor frequency respectively. As the oscillating field passes through resonance, χ' changes sign so that M

is 180° out of phase with the applied field and χ'' becomes very large near resonance which produces the absorption we see. The out-of-phase signal corresponds to the dispersion of the EPR signal while the imaginary portion of the susceptibility corresponds to the absorption. These two equations account for the dependence of T_1 and T_2 upon the absorption of microwave energy. If the lifetime of the spin state (T_2) is short compared to the power (equivalent to $\gamma^2 H_1^2$), we would expect the absorption to be relatively large. This would then give an absorption with the familiar Lorentzian lineshape

$$g(\omega) = T_2/\pi \quad \frac{1}{1 + T_2^2(\omega-\omega_o)^2}$$

On the other hand, if the power is greater than the magnitude of T_1T_2 then $\gamma^2 H_1^2 T_1 T_2$ becomes significant and the amplitude of the absorption is decreased. This phenonmenon is known as power saturation. Saturation weakens the central portion of the resonance line relative to the wings and produces an apparent broadening of the spectrum.

We have seen then from Bloch's equations that the spin-lattice relaxation time T_1 determines the degree of saturation while T_2 determines the unsaturated line width. Both kinds of relaxation depend on time-dependent magnetic fields at the electron which in turn are dependent on the random thermal motions present in all substances. Time-dependent interactions with spin are an absolute requirement for relaxation. Magnetic resonance frequencies for electrons are typically 10^{10} Hz. Any interaction which changes sign faster than this will not be important, i.e., electronic motions and vibrations. However, rotation and diffusion motions are very important sources of relaxation in liquids as well as lattice vibrations in solids and collisions in gases.

2.7.7 SPIN-LATTICE INTERACTION

The effectiveness of spin-lattice interactions in inducing relaxation has already been discussed. The time necessary for the longitudinal component of the magnetic moment to decay to some equilibrium value in a magnetic field is the spin-lattice relaxation time or T_1.

In an external magnetic field, a net absorption occurs because there is an excess of up transitions (absorptions) over the number of down transitions (emissions) where both transitions are equally probable. This excess is proportional to the difference in population between the upper and lower states. During irradiation, this population difference will continuously decline until the populations become equal. In order to obtain thermodynamic equilibrium there must be some interaction between the spin system and the thermal flucuations that define the temperature of the surroundings. The temperature of the lattice is called the spin temperature. The time it takes to attain this equilibrium is the spin-lattice relaxation time, as already defined.

The phenomenon of power saturation corresponds to a rise in spin temperature such that the power absorbed from the radiation field by the spin system just balances the power fed out to the thermal bath via the spin-lattice relaxation mechanism. What is the nature of this interaction that determines the value of T_1?

The energy density of the bath which interacts directly with the spins through magnetic resonance transitions is about 10^{15} times less than the energy density of the bath of lattice vibrations. The former bath is known as the thermal electromagnetic radiation bath while the latter is called the phonon radiation bath. This discrepancy may be easily outweighed by the fact that the interactions between spins and phonons involve mechanisms which are inherently weaker than the simple magnetic resonance interaction between spins and photons. In 1932 Waller formulated two different processes where

spins can interact with the phonon radiation bath through modulation of the magnetic dipolar spin-spin interaction.

(1) *Direct process.* A phonon of the same energy as that required by the spin quantum for a resonance transition is absorbed or emitted resulting in transitions up or down, respectively.

(2) *Raman process.* Any phonon of any frequency may interact with a spin causing an up or down transition, the phonon is scattered at a different frequency.

The direct process can be regarded as a first-order (one phonon) process whereas the Raman process is a second-order (two phonon) process with a much smaller coupling of the phonons to the spin system. It is the latter process that can predominate in spin-lattice relaxation as only those phonons "on speaking terms" with the spin system can interact by the direct process whereas any phonon can participate in the Raman process. This is only true, however, when $(h\nu/kT_o) << 1$ and at lower temperatures, where the overall number of phonons has decreased sufficiently, the direct process becomes the more important of the two.

The relaxation times that Waller derived based on modulation of the spin-spin interaction are appreciably longer than those observed experimentally. Another mechanism formulated by Kronig (2.9), Van Vleck (2.10), and more recently Orbach (2.11) is based on modulation of the ligand field by lattice vibrations which are independent of the concentration of magnetic ions. This process does not involve direct interaction with the electron spins, but instead the electron feels the modulation of the orbital motion through spin-orbit coupling in much the same way as it feels the effects of the static ligand field. Spin lattice relaxation times are, therefore, greatly dependent on the quenching of the orbital moment, if present in the free ion, by the static ligand field. Therefore, one would expect

long spin-lattice relaxation times when the g-value is close to the free spin value and short spin-lattice relaxation times when g departs from this value.

Different processes contribute to the relaxation rate ($1/\tau_1$) simultaneously but to varying degrees (4). Their dependence on temperature can be written as

$$1/\tau_1 = a\coth(h\nu/2kT_o) + bT_o^n + \frac{c}{\exp(\Delta/kT_o) - 1}$$

The first term corresponds to the *direct process* involving phonons of the same energy as the magnetic resonance quantum hν. There are two limiting cases:

(i) high temperature limit where $(h\nu/kT_o) << 1$; there is an average number of quanta per phonon.

(ii) $(h\nu/kT_o) >> 1$; A constant spin-lattice relaxation rate is obtained by the spontaneous emission of phonons from the upper state when phonons of energy hν are no longer thermally excited.

The second term corresponds to the *Raman process* where all phonons take part, giving a strongly temperature dependent term. Typical values for the exponent n are:

non-Kramers doublet, n = 7

Kramers doublet, n = 9

Multiplet with small splitting, n = 5

The third term gives rise to the *Orbach process*. This involves absorption of a phonon by a direct process to excite the spin system to a much higher level at an energy Δ

above the ground doublet, followed by emission of another phonon of slightly different energy so that the magnetic ion is indirectly transferred from one level to the other of the ground doublet. The net result is to establish thermal equilibrium between the ground levels. This process is strongly temperature dependent.

How does the lifetime of a given spin state affect the linewidth in our EPR spectrum? If one considers the Heisenberg uncertainty principle where energy and time are our uncertain entities, then a small lifetime or T_2 would correspond to a larger uncertainty in energy resulting in a broadening of the EPR signal.

$$\Delta E \Delta t \geq h/2\pi$$

Other sources of line-broadening can be divided into two groups:

Inhomogeneous broadening results from each spin in a sample feeling a slightly different magnetic field due to either an inhomogeneous external magnetic field, or more commonly, random orientations of spins in a solid. Anisotropic effects in g and hyperfine interactions can further broaden the spectrum of randomly oriented solids. Unresolved hyperfine structure can also lead to inhomogeneous broadening. The characteristic lineshape is usually gaussian.

Homogeneous broadening produces lineshapes that are Lorentzian where the instantaneous magnetic field at each dipole is different instead of each dipole seeing a slightly different magnetic field. The static as well as the time-averaged magnetic field at each dipole can be considered to be the same.

The greatest contributing mechanism to line-broadening is probably the interaction between magnetic dipoles. This is usually called the spin-spin interaction or dipolar interaction. Because each spinning dipole has an electric field associated with it, the magnetic field produced can influence any nearby dipoles. If the paramagnets are identical, there are additional broadening effects due to resonance interactions between the dipoles.

The precessing components of one magnetic field set up an oscillating field at another dipole which is at just the right frequency to cause magnetic resonance transitions.

REFERENCES

2.1. Hales, B. J., Case, E. E., Morningstar, J. E., Dzeda, M. F., and Mauterer, L. A. (1986) Biochemistry **25**, 7251

2.2. Burgess, B. K., Jacobs, D. B., and Stiefel, E. I. (1980) Biochim. Biophys. Acta **614**, 196-209

2.3. Wyard, S. J. (1965) J. Sci. Instr. **42**, 769-770

2.4. Aasa, R. and Vanngard, T. (1975) J. Mag. Reson. **19**, 308-315

2.5. Carrington, A., and McLachlan, A.D. (1967) Introduction to Magnetic Resonance, Harper & Row, New York, Evanston, and London

2.6. Wertz, J.E., and Bolton, J.R. (1986) Electron Spin Resonance, Elementary Theory and Practical Applications, Chapman and Hall, New York, London

2.7. Drago, R.S. (1977) Physical Methods in Chemistry, Holt, Rinehart and Winston, Orlando, Florida

2.8. Abragam, A., and Bleaney, B. (1986) Electron Paramagnetic Resonance of Transition Ions pp. 60-74, Dover, New York

2.9. Kronig, R. De, L. (1939) Physica Grav. **6**, 33

2.10. Van Vleck, J. H. (1940) Phys. Rev. **57**, 426

2.11. Orbach, R. (1961) Proc. R. Soc. **264**, 458

THE V-NITROGENASE FROM *Azotobacter vinelandii*

Exploring the Paramagnetism of Component 1 During Enzymatic Turnover, Oxidation by Thionine, Changes in pH, and Isolation of the VFe-cofactor

3.1 INTRODUCTION

In addition to the conventional molybdenum nitrogenase, *Azotobacter vinelandii* has the ability to synthesize two different alternative nitrogenases, the V-nitrogenase and the so-called Fe-only-nitrogenase. While the presence of a V-nitrogenase has also been documented for *Azotobacter chroococcum* (3.1), only *A. vinelandii* has been shown to produce the Fe-only enzyme (3.2). The evidence leading up to the discovery of these alternative nitrogenases has been discussed previously (see Section 1.3), and, therefore, will not be discussed here. Only the V-nitrogenase of *A. vinelandii* will be discussed here, specifically, component 1 (Av1') of the V-nitrogenase.

Component 1, or Av1', can be characterized as having an $\alpha_2\beta_2\gamma_2$ polypeptide structure (3.3) possessing at least two different types of metal clusters. MCD spectroscopy has shown that, analogous to Mo-nitrogenase, Av1' contains P-clusters with a probable [4Fe-4S] structure (3.4). These clusters are EPR-silent in the as-isolated protein with a spin state of 5/2 or 7/2. There are also S = 3/2 centers similar to the M-centers of Mo-nitrogenase.

The EPR spectrum of Av1' is more complex (3.5-3.7) than that of the MoFe protein, consisting of three major paramagnetic components, S1, S2 and S3. S1 is an axial signal with spectral inflections at $g_{||} = 2.04$ and $g_{\perp} = 1.95$ and most likely arises from a reduced Fe/S cluster. S2 is comprised of two inflections at g = 5.80 and 5.40

which are only two of a possible six inflections that would be observable for an S = 3/2 spin state. Because of the temperature dependence of these two signals, and the rhombicity ($\lambda = 0.26$), these inflections have been assigned to transitions from both the ground and excited state levels. The four remaining inflections (g = 2.46, 1.69, 1.66 and 1.29) are not observed, perhaps because of g-strain broadening. The third signal (S3) of Av1' is not readily observable in the normal derivative absorption mode but can be seen easily in the dispersion mode under the conditions of rapid passage (3.7). Therefore, while the origins of each of the three signals in the spectrum of Av1' are not known, it can be stated that S1 and S2 typify spectra of metalloprotein metal clusters, while the spectrum of S3 suggests that it originates from a spin-coupled center. It should be noted here that the EPR spectrum of component 1 of the V-nitrogenase from *A. chroococcum* (3.8) is more complex than that described above, possessing at least one additional inflection at g = 3.6.

The EPR spectrum of the S = 1/2 signal in Av1' is very sensitive to the effects of temperature and incident microwave power. At temperatures above 10 K, this signal exhibits an axial structure similar to that observed in several other proteins for reduced Fe:S clusters with $g_{av} < 2$. However, at low temperatures (around 4-5 K) the spectrum in this region changes dramatically and is highly dependent on the incident power. Specifically, the spectrum loses its axial structure and demonstrates a non-uniform saturation behavior. Part of this change may be due to the increase in intensity of the recently observed third signal of Av1' (S3) as well as the introduction of passage effects at these low temperatures. Changes in the S = 1/2 signal of Av1' with temperature and power are shown in Figure 3.2. The two EPR signals, S1 and S2, of Av1' were investigated under the following conditions: [1] During enzymatic turnover, [2] extraction of the VFe-cofactor, [3] oxidation by thionine, and [4] changes in pH .

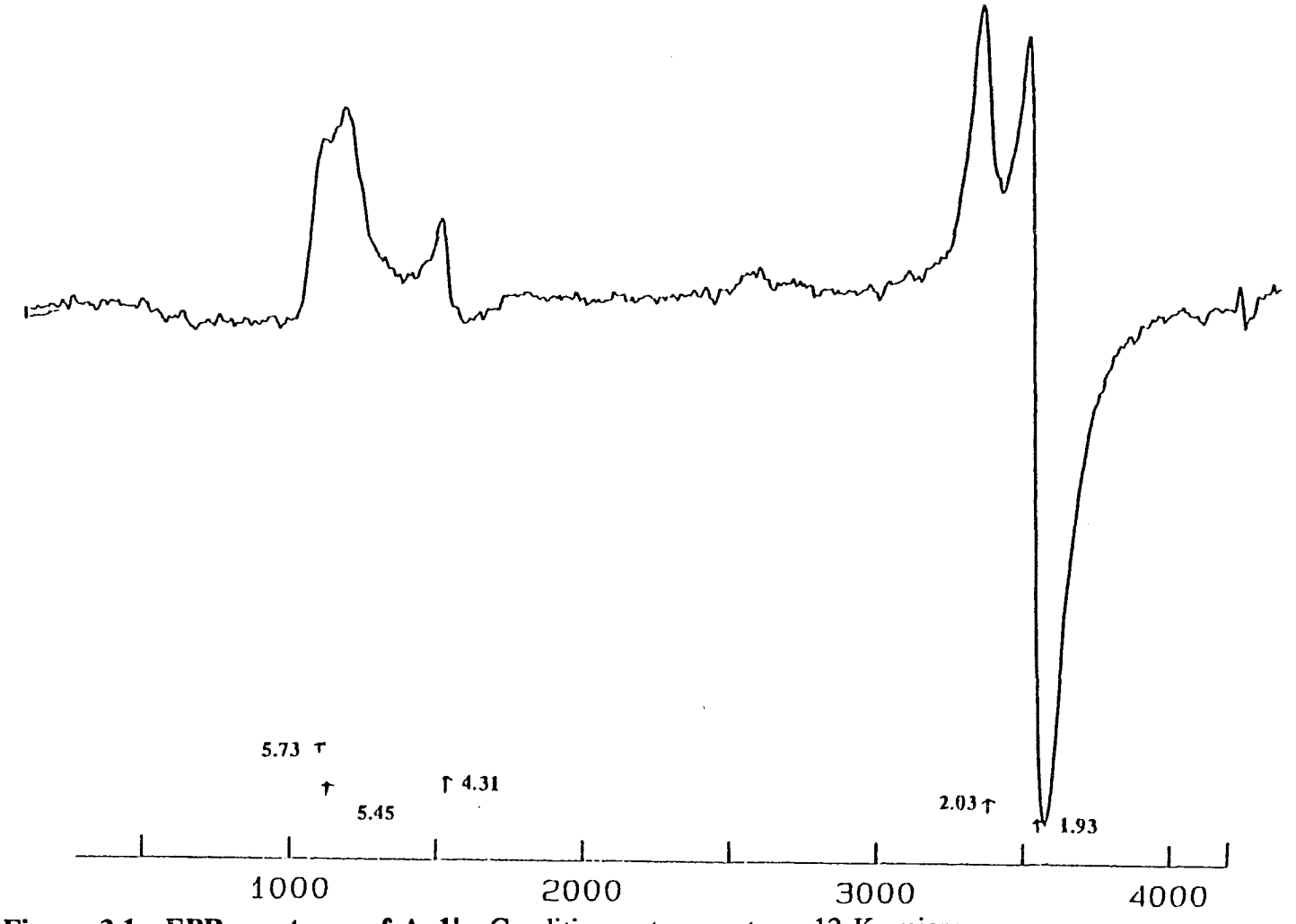

Figure 3.1. EPR spectrum of Av1'. Conditions: temperature, 12 K; microwave power, 20 mW; microwave frequency 9.30 GHz; modulation frequency, 100 kHz; modulation amplitude, 12.6 G; scan time 200 s; time constant, 0.5 s; protein concentration, 46 mg/ml.

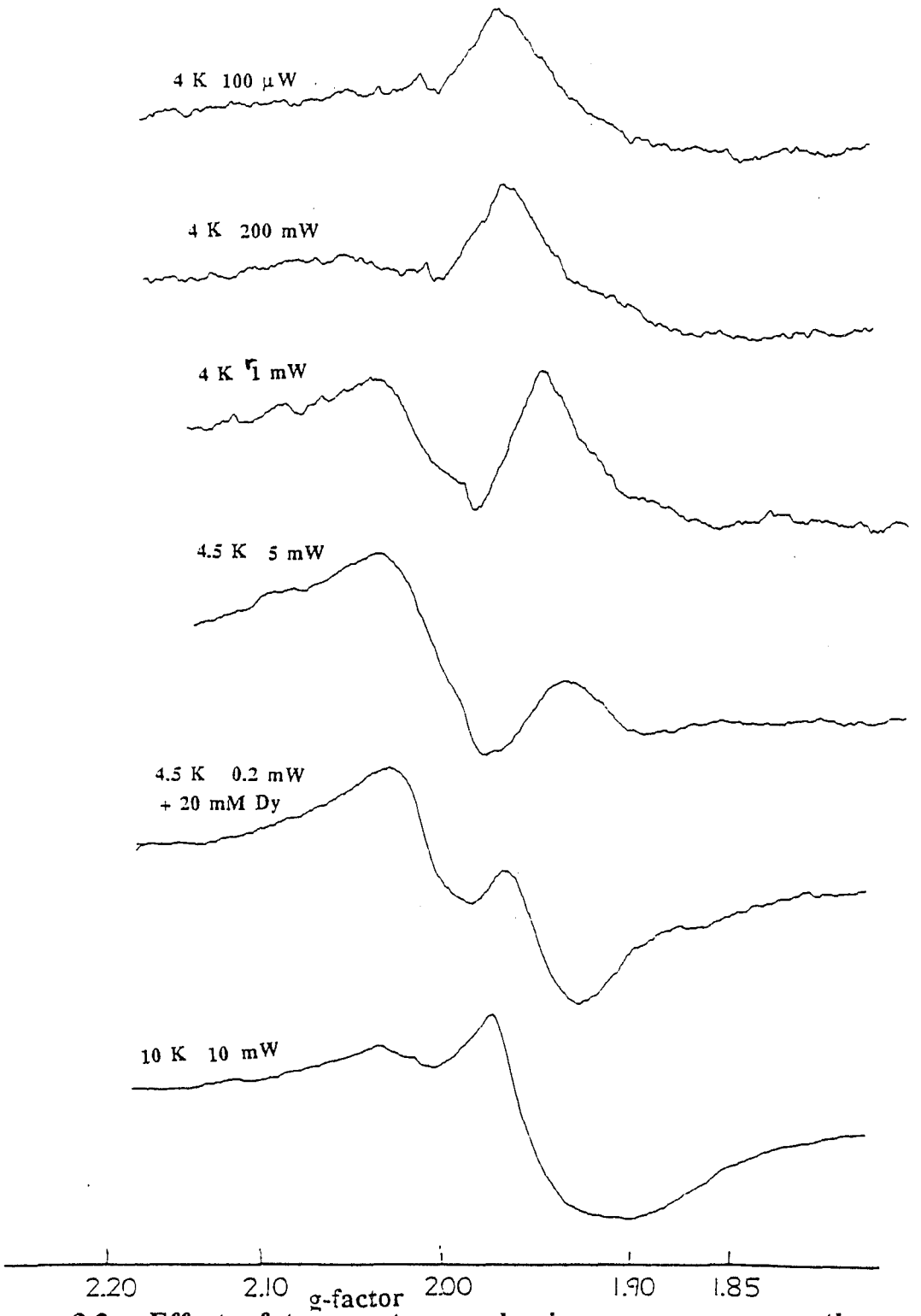

Figure 3.2. Effect of temperature and microwave power on the g = 2 region of the EPR spectrum of Av1'. Conditions: temperature and power as noted in figure; microwave frequency, 9.45 GHz; modulation amplitude, 12.6 G; modulation frequency, 100 kHz; scan time, 84 s; time constant, 2.6 s; protein concentration, 75 mg/ml;

3.2 ENZYMATIC TURNOVER

Despite intensive efforts by several research groups over the past two decades, the mechanism governing catalytic turnover is not completely understood. What is known, however, has come almost exclusively from studies on the conventional molybdenum-containing form of the enzyme. The study presented here monitored the changes in the V-nitrogenase paramagnetic spectrum that occurred during different conditions of catalytic turnover.

Studies on enzymatic turnover with Mo-nitrogenase show that one turnover cycle occurs when component 2 is reduced by an external electron source and combines with MgATP, binds to component 1, and hydrolyzes the MgATP to MgADP while it transfers an electron to component 1 (see Figure 3.3). In this mechanism, MgADP can compete with MgATP and therefore inhibits turnover. Current evidence suggests that the mechanism for turnover for V-nitrogenase is similar.

To investigate the effects of turnover on the different paramagnetic signals of V-nitrogenase, the EPR spectrum of this enzyme was recorded in the presence of an ATP regenerating system and dithionite, as a reductant. The ATP-regenerating system was used in order to eliminate the buildup of inhibiting concentrations of ADP. Within 2 minutes of initiation of turnover, a decrease is observed (Fig. 3.4) in the S = 3/2 signal of component 1 and in the S = 1/2 signals (Fig. 3.5) in the g = 2 region. It is important to remember that the spectra of the S = 1/2 signals from component 1 and component 2, in the presence of MgATP, are nearly identical in shape and g-factors and, therefore, are indistinguishable. Upon completion of turnover (40 minutes in Fig.3.4), both signals in the g = 2 region are completely bleached while the S = 3/2 signal (Fig. 3.4) decreased in intensity.

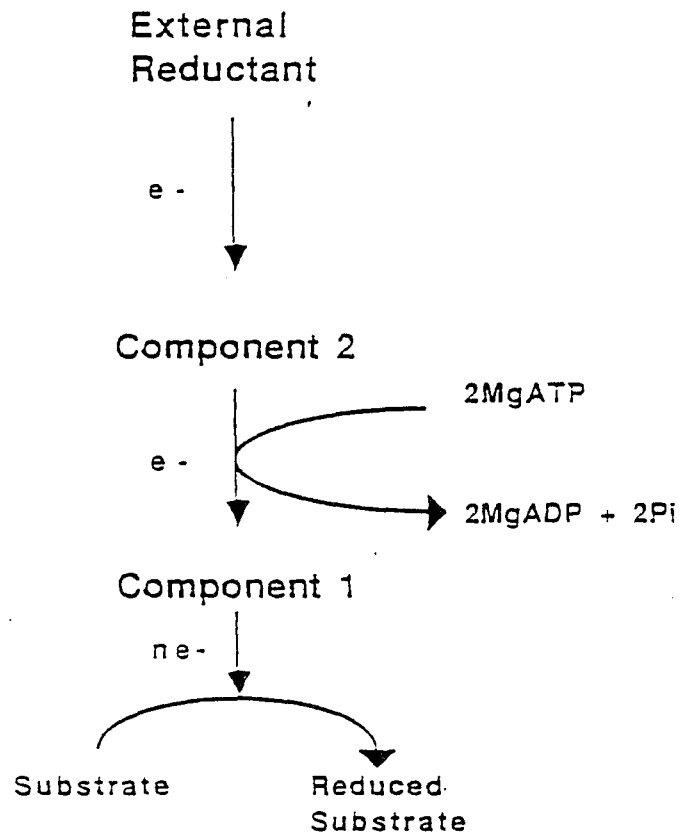

Figure 3.3. Electron flow diagram for enzymatic reduction by nitrogenase. Reductants used to reduce component 2 are ferredoxin or flavodoxin *in vivo*, or (typically) dithionite *in vitro*. Figure taken from reference 3.3.

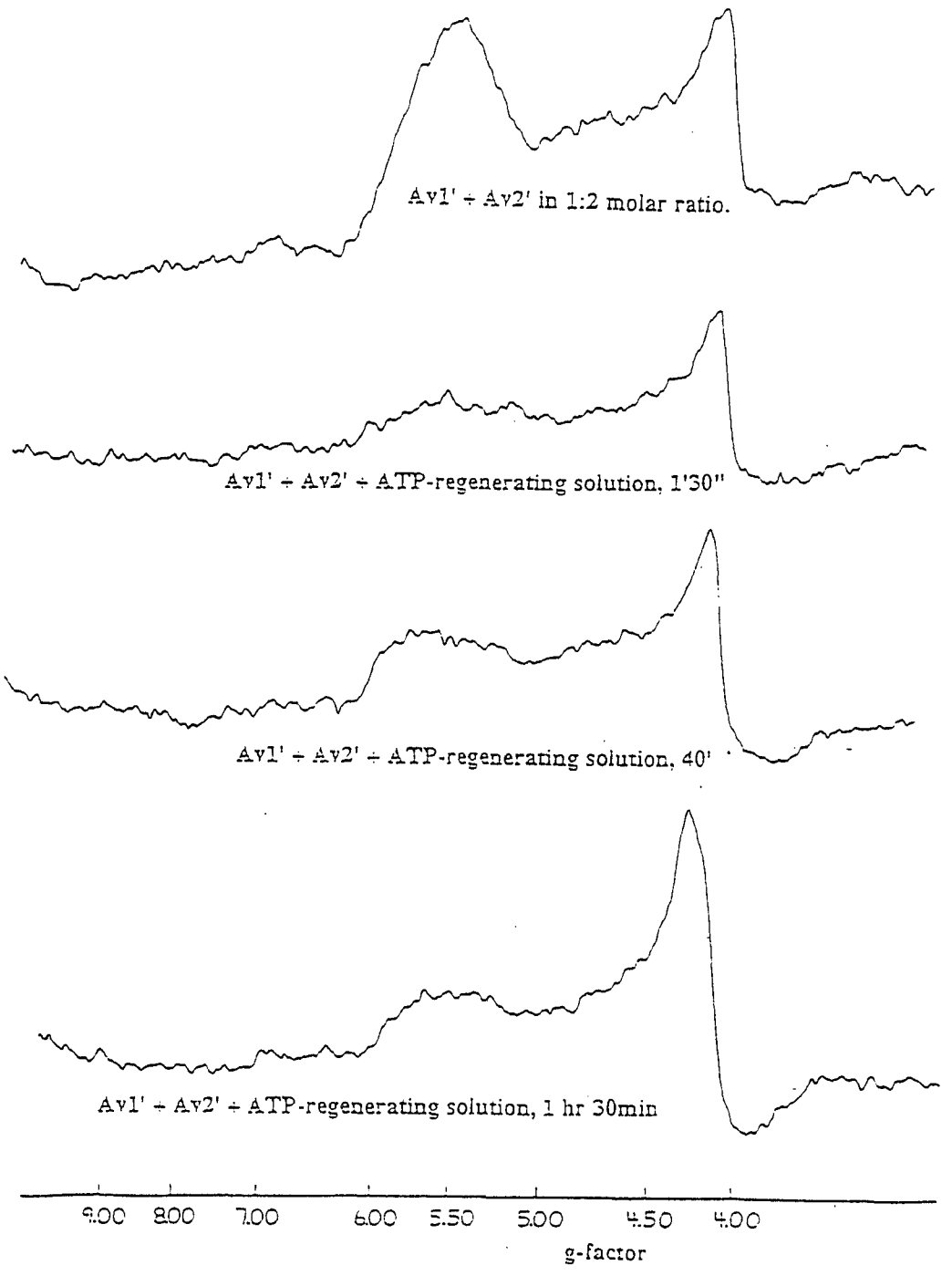

Figure 3.4. EPR spectra of Av1' + Av2' as affected by addition of ATP-regenerating solution. A. Av1' + Av2' in 1:2 molar ratio. Total volume 0.3 ml, 0.24 ml Av1' (35.4 mg/ml) and 0.060 ml Av2' (89.8 mg/ml). (B) Av1' + Av2', total volume 0.14 ml (1:2 molar ratio), combined with 0.165 ml of ATP-regenerating solution containing 1.0 mg of creatine phosphate kinase. 2.5 mmoles of ATP, 30 mmoles of creatine phosphate, and 5 mmoles of $MgCl_2$. 1'30" elapsed before freezing. All EPR tubes were approximately 20 mM in dithionite. (C) Tube in B was rapidly thawed and incubated for a total of 40 min. (D) Tube in C was thawed and incubated for a total of 1 hr. 30 min. Conditions: microwave frequency, 9.30 GHz; temperature, 10 K; modulation amplitude, 12.5 G. All spectra at same gain.

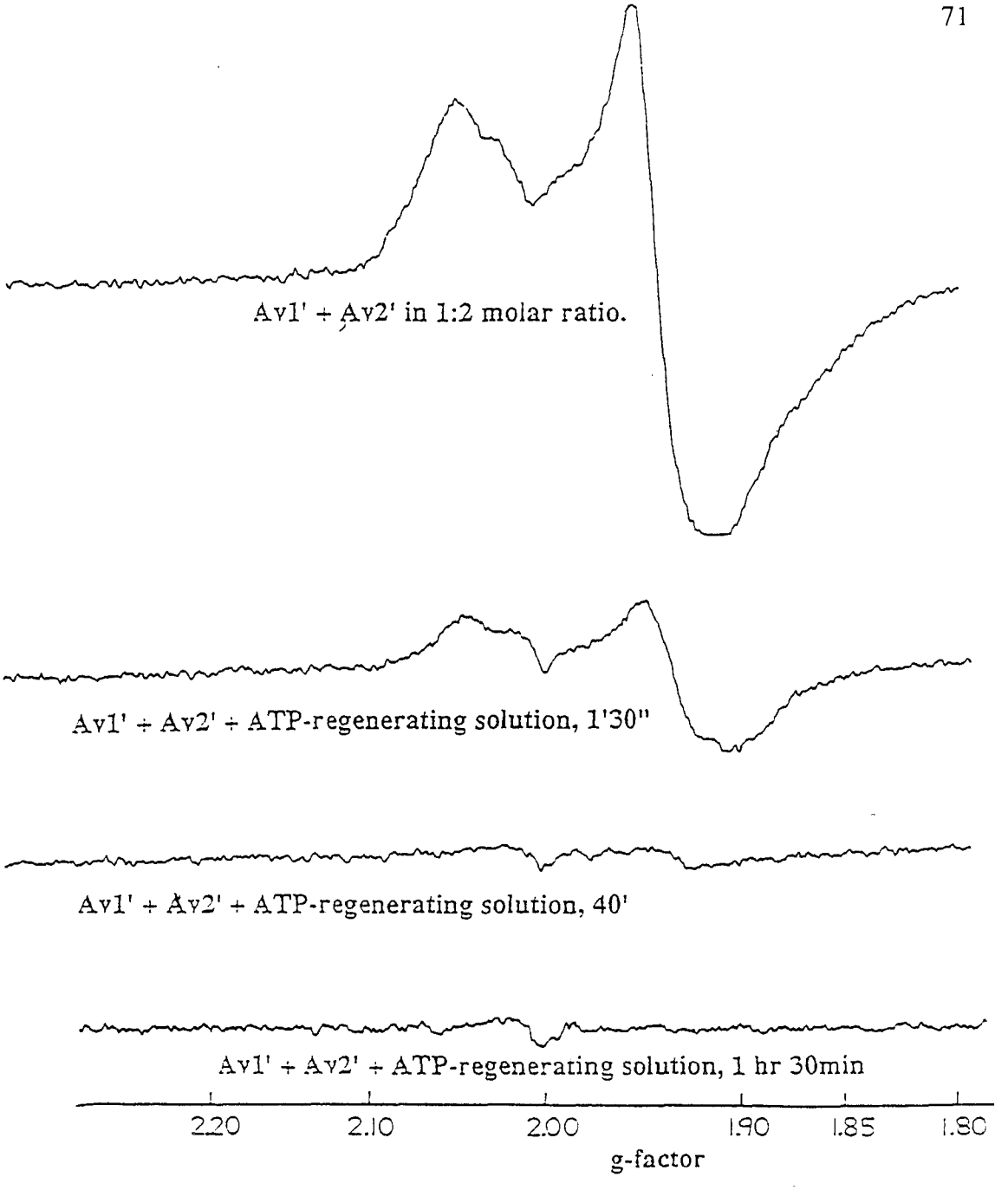

Figure 3.5. EPR spectra of Av1' + Av2' as affected by addition of ATP-regenerating solution. A. Av1' + Av2' in 1:2 molar ratio. Total volume 0.3 ml, 0.24 ml Av1' (35.4 mg/ml) and 0.060 ml Av2' (89.8 mg/ml). (B) Av1' + Av2', total volume 0.14 ml (1:2 molar ratio), combined with 0.165 ml of ATP-regenerating solution containing 1.0 mg of creatine phosphate kinase. 2.5 mmoles of ATP, 30 mmoles of creatine phosphate, and 5 mmoles of $MgCl_2$. 1'30" elapsed before freezing. All EPR tubes were approximately 20 mM in dithionite. (C) Tube in B was rapidly thawed and incubated for a total of 40 min. (D) Tube in C was thawed and incubated for a total of 1 hr. 30 min. Conditions: microwave frequency, 9.30 GHz; temperature, 10 K; modulation amplitude, 12.5 G. All spectra at same gain.

To investigate the effects of MgADP on the time course of this reaction, the spectra of V-nitrogenase were rerecorded with only MgATP and dithionite present, thus allowing the MgADP concentration to increase with time. Under this new set of conditions, the EPR spectra are very different. Specifically, the intensity of the S = 3/2 signal of component 1 (Fig. 3.6) is diminished only slightly after two minutes following initiation of turnover while the S = 1/2 signals (Fig. 3.7), arising from both component proteins, are completely bleached. After 40 minutes, when the reaction has been completely inhibited by the excess MgADP concentration, these S = 1/2 signals do not reappear. However, the fact that all signals are bleached in the g = 2 region during turnover shows that both Av1' and Av2' signals are affected. It is also important to note that after these EPR measurements were complete, dithionite was found to still be present in all the samples.

EPR spectroscopy shows that initially the paramagnetism of both Av1' and Av2' are diminished. Since component 2 reduces component 1 during catalysis, this bleaching of the EPR spectra of both proteins is interpreted to mean that component 2 has been oxidized to a diamagnetic state while the M center of component 1 has been reduced to an EPR-silent state. Upon depletion of the MgATP and the subsequent build up of MgADP, the signal of the M center of component 1 remains diminished in amplitude, as does the EPR signal for component 2 (i.e., the protein remains partially oxidized), even though reductant is still present. This suggests that some of the proteins are still present in their intermediate turnover state.

Mo-nitrogenase has also been investigated (3.9, 3.10) under similar conditions where ATP can be regenerated, thus eliminating a build up in the concentration of MgADP. Under this condition, turnover proceeded until the dithionite was depleted. During turnover, the EPR signal of component 2 did not diminish appreciably, whereas the amplitude of the S = 3/2 signal for component 1 decreases as long as the dithionite

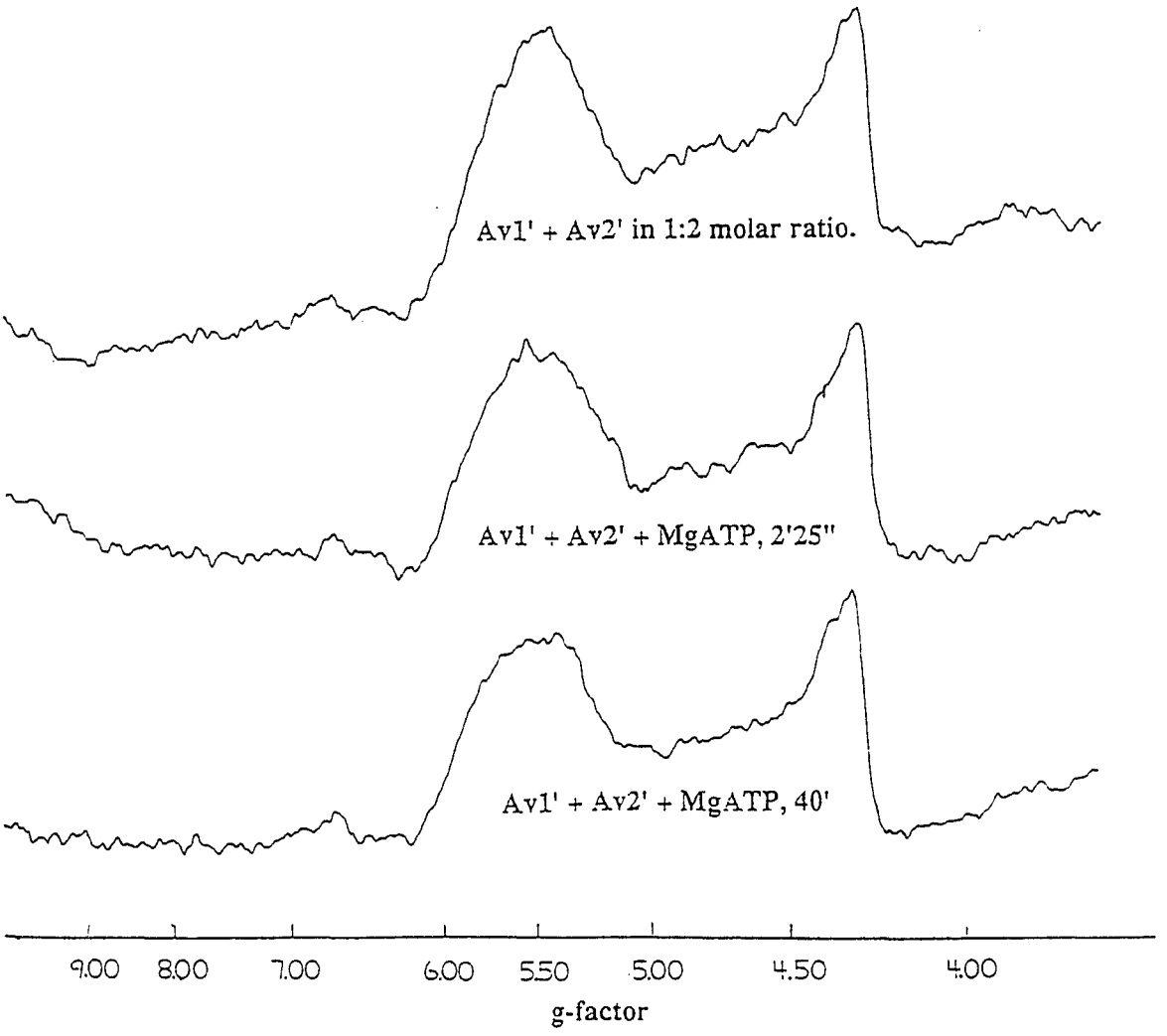

Figure 3.6. EPR spectra of Av1' + Av2' as affected by addition of MgATP. Conditions: microwave frequency, 9.45 GHz; modulation frequency, 100 KHz; modulation amplitude, 12.6 G; scan time, 168 s; time constant, 0.66 s; temperature, 4 K; power as noted in figure; protein concentration, 42 mg/ml.

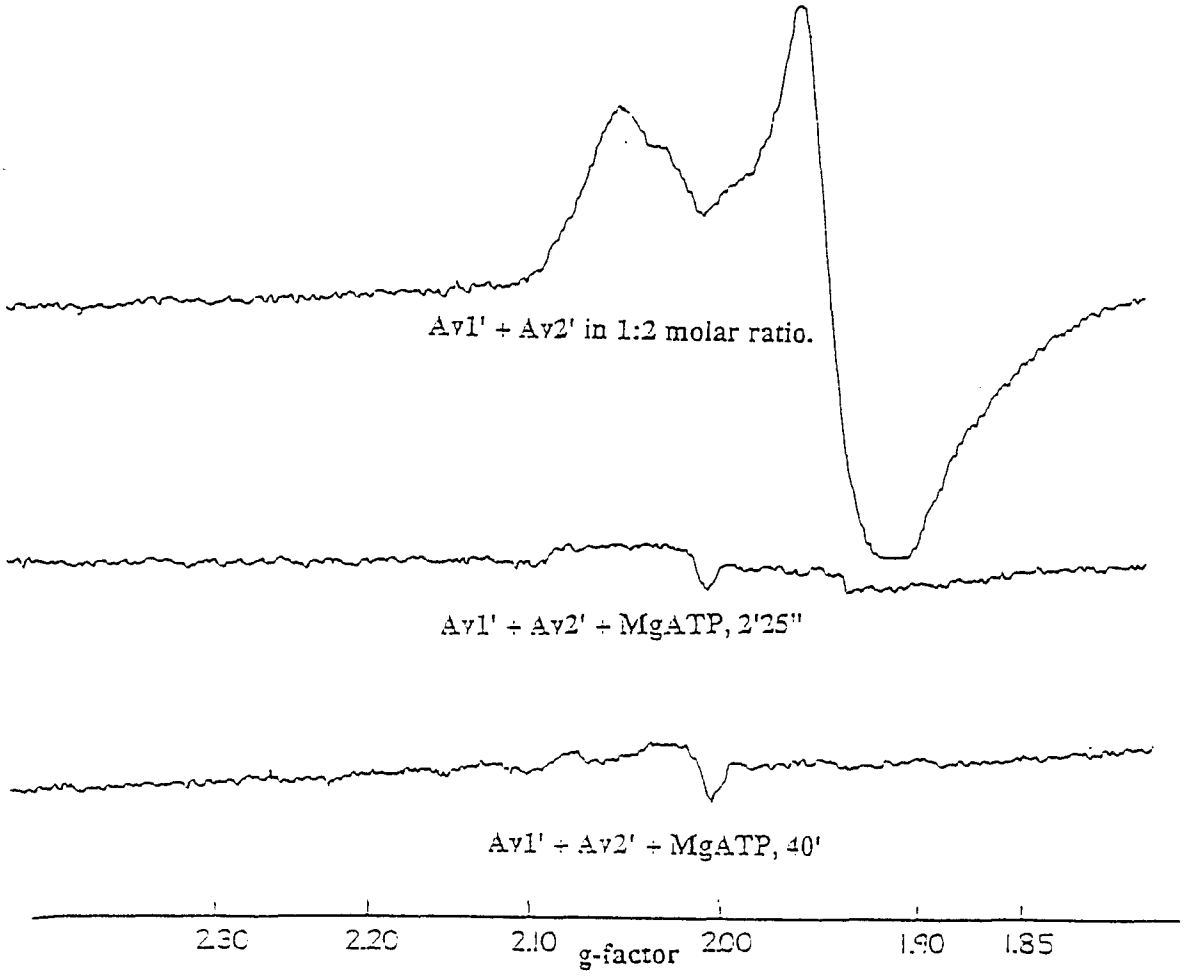

Figure 3.7. EPR spectra of Av1' + Av2' as affected by addition of MgATP. (A) Av1' + Av2' in 1:2 molar ratio. Total volume 0.3 ml, 0.24 ml Av1' (35.4 mg/ml) and 0.060 ml Av2' (89.8 mg/ml). (B) 0.010 ml of 0.3 M MgATP was added to the same amount of protein as in A, 2'25" elapsed before freezing. (C) Tube in B was rapidly thawed and incubated to 40 min. total. All EPR tubes were approximately 20 mM in dithionite. Conditions: microwave frequency, 9.30 GHz; modulation amplitude, 12.5 G; temperature, 10 K. All spectra at same gain.

source was not depleted. Upon depletion of dithionite, the S = 3/2 signal returned to full amplitude while the component 2 signal was fully diminished because this protein was now oxidized.

In our system, the S = 3/2 signal of Av1' only increased slightly in amplitude upon completion of turnover. However, since dithionite was still present in the sample, component 2 still should have been reduced. There was no signal observed in the g = 2 region implying that component 2 and the S = 1/2 center in Av1' were both oxidized to an EPR-silent state.

The differences between the Mo-nitrogenase and the V-nitrogenase as seen during enzymatic turnover may be due to a number of factors. Obviously, the unique S = 1/2 axial signal for Av1' is participating in the turnover reaction in some as of now unknown way. This may or may not be the source of some of the different spectral properties seen. Furthermore, the potentials for the analogous clusters between the two nitrogenases may not be the same, as suggested in the experimental data presented on thionine oxidation and effects of pH on Av1'. In a personal communication to us from B.H. Huynh, the Mössbauer spectrum of dithionite-reduced Av1' appears to still contain partially oxidized P clusters, which provides further evidence that the clusters in V-nitrogenase may have different redox environments from the analogous clusters in Mo-nitrogenase.

3.3 ISOLATION OF THE COFACTOR FROM NITROGENASE

3.3.1 INTRODUCTION

Early in the history of nitrogenase, many investigators searched for the active site of this enzyme as well as other molybdenum-containing enzymes. Nitrogenase seems to be unique in its molybdenum-containing center, which also contains iron and sulfur.

The molybdenum-containing active site has been called a cofactor, but it is not in the strict biochemical sense of the word. It is a nondissociable metal cluster believed to be the site of substrate reduction in nitrogenase. It is usually referred to as FeMoco (registry no. 72994-52-6) and will be here. The cofactor was first isolated by Shah and Brill from acid-treated extracts of component 1 of *A. vinelandii* (3.11). Activity was monitored by combining the acid-treated extracts with mutant strains of *A. vinelandii* and *K. pneumoniae* containing apoprotein which lacks cofactor. These mutant strains were constructed by introducing mutations in the *nif* genes that control nitrogenase regulation and production. These mutations were later found to be at a site in the *nif* B gene. Presently there are over 20 known genes contained in the *nif* cluster.

The cofactor isolation method of Shah and Brill is as follows: Crystalline component 1 was dissolved in 250 mM NaCl (containing 25 mM TRIS-HCl buffer, pH 7.4) and diluted with water. Citric acid solution was added to a final concentration of 15 mM, mixed, and allowed to stand for 3 min. Disodium hydrogen phosphate solution was added to a final concentration of 25 mM, mixed, and allowed to stand for 25 min. The protein was centrifuged at 8000x g for 10 minutes. The pellet was washed with 4 ml of N-methylformamide (NMF) three times, followed by centrifugation at 8000x g for 10 min. FeMoco was present in solution in NMF.

Since the publication of this procedure in 1977, the efficiency of cofactor recovery has been reported to be between 45% and 90% (3.11-3.13). The resulting FeMoco has a composition of $MoFe_{6-8}S_{8-9}$. Using this procedure, only NMF and, more recently, 2-pyrrolidinone (3.12-3.15), have been shown to give appreciable results in the extraction of FeMoco. Formamide gave fair results, with a yield below 60%, but dissolved the denatured protein, making separation of cofactor from protein very difficult (3.12,3.15). Although modifications to the Shah and Brill procedure have been

proposed (12,14,16,17), the solvent of choice has always been NMF. Explanations accounting for the ability of NMF to extract FeMoco have ranged from its high dielectric constant (16) to the dissociability of its amide proton (3.12, 3.13). Recently, extraction of FeMoco into DMF/Et_4NOH has been reported (3.14) but with low specific activities and variable recoveries. FTIR spectra of FeMoco in NMF, showing evidence of coordination of deprotonated solvent, were used to explain coordination of FeMoco to deprotonated peptide N-groups in the protein (3.13). Therefore, the so-called requirement for a dissociable amide proton kept FeMoco chemistry in NMF.

3.3.2 CURRENT ISOLATION OF COFACTOR

More recently a procedure that allows for the isolation of cofactor into different solvents and with better yields has greatly enhanced the study of isolated cofactor (3.18). Although the molybdenum cofactor has been isolated into such solvents as methanol and dichloromethane, crystals of the cofactor that can be used for x-ray diffraction studies are still forthcoming. Because of the enhanced yields obtainable, we decided to use a modification of this procedure to isolate the V-containing cofactor from Av1'.

Because of the extreme oxygen sensitivity of isolated cofactor as well as its sensitivity to water, a different glove box was used for this procedure from the one used for protein work. Better yields were generally obtained when pure Av1' was used, but we used crude DEAE extracts, which contain component 2, in this procedure which also gave acceptable yields. DEAE-cellulose or sepharose was used in short columns (bed volumes of 5-10 ml) equilibrated with reducing buffer (no salt) preceding application of protein. Care must be taken to dilute salty DEAE extracts, as these will not bind to the

DEAE. After application, the protein was bound to the top of the DEAE as an intense dark band. The column was then washed with several bed volumes of reducing buffer, followed by a washing with dry DMF, containing tetrabutyl-ammonium dithionite, to rid the column of water and to denature the protein. Anhydrous DMF in a nitrogen-charged cylinder was obtained from Aldrich Chemicals; no further purification was needed. Elution of the negatively charged cofactor was performed by passage of a quaternary ammonium salt in DMF. Tetrabutylammonium bromide was used, 0.25-0.5 M, in addition to the chloride salt. Because this procedure denatures the protein, all metal clusters eluted in DMF, not just FeVco. However, it has been observed that using NMF in the isolation of FeMoco by this procedure does not result in contamination with other metal clusters (3.18). However, when NMF was used in the isolation of FeVco by this procedure, no elution of the cofactor resulted. A flow diagram for this procedure used in isolation of the cofactor is shown in Figure 3.8.

In order to remove some of the excess iron, either a solution of 25 mM bipyridyl (bipy) in DMF was added while the cofactor was still attached to the first DEAE column, or a second DEAE column was used for this purpose, or application of bipy was done at both steps. However, before a second DEAE column could be run, the cofactor solution had to be desalted using a sizing column (1.5 x 20 cm) containing G25 or LH20 resin (from Sigma Chemicals). Alternatively, the cofactor solution could also be diluted with DMF before loading onto the second DEAE column in order to reduce the salt concentration.

The DMF used in all the steps was made reducing by addition of 2-5 mM tetrabutylammonium dithionite (TBD). This compound was used instead of sodium dithionite because of the poor solubility of the latter in DMF. To synthesize TBD, a concentrated solution of dithionite in buffer (1 M) was added to a small (2 cm x 5 cm)

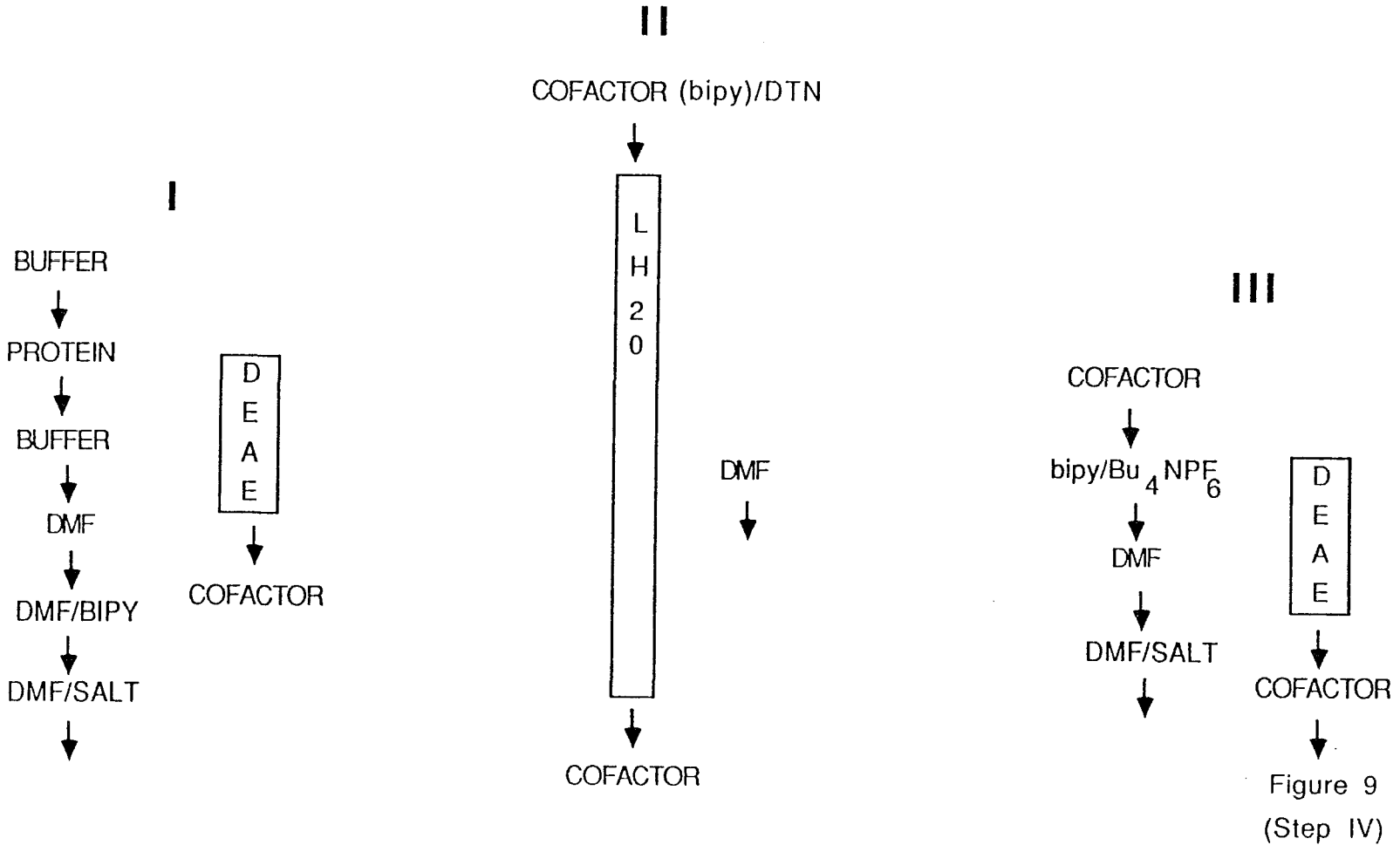

Figure 3.8. Procedure for isolation of cofactor.

DEAE column and washed with DMF (3 to 5 bed volumes) to remove the water. The column turned bright yellow at this point. Passage of 0.25 M tetrabutylammonium bromide down the column eluted the intensely yellow product, $(Bu_4N)_2S_2O_4$. TBD was added to all DMF until reducing. The absence of oxygen was tested by addition of benzyl viologen to the DMF (a dark blue solution resulted when the two were mixed).

The fourth and final step in the isolation of FeVco was a gel filtration column used for desalting. In order to completely desalt the cofactor sample, a "precolumn" was used just to rid the DMF of the TBD. These two columns were run in tandem (see Figure 3.9) where the first column contained Dowex-50 (supplied by Aldrich Chemicals). Prior to use, this column was washed with a 1 M solution of NaCl followed by a 5 % solution of methyl viologen (sodium salt). Because the Dowex is a strongly acidic cation exchange resin, methyl viologen (pQ^{2+}) binds tightly to it. Finally, the column was washed with a 1M solution of sodium dithionite, turning it blue to indicate the lack of oxygen.

The cofactor was then applied to a LH20 column and eluted with DMF that had previously been desalted with the first Dowex column. The resultant cofactor solution could be vacuum evaporated to dryness and then redissolved in other solvents if so desired.

3.3.3 RECONSTITUTION OF COFACTOR

Cofactor preparations were analyzed by adding a small amount of cofactor solution to one of three different apoproteins (see Table 3.1). Initially, apoproteins were used as crude extracts since, at that time, purification of apoprotein was not well-developed. The apoproteins become increasingly unstable during purification, suggesting the

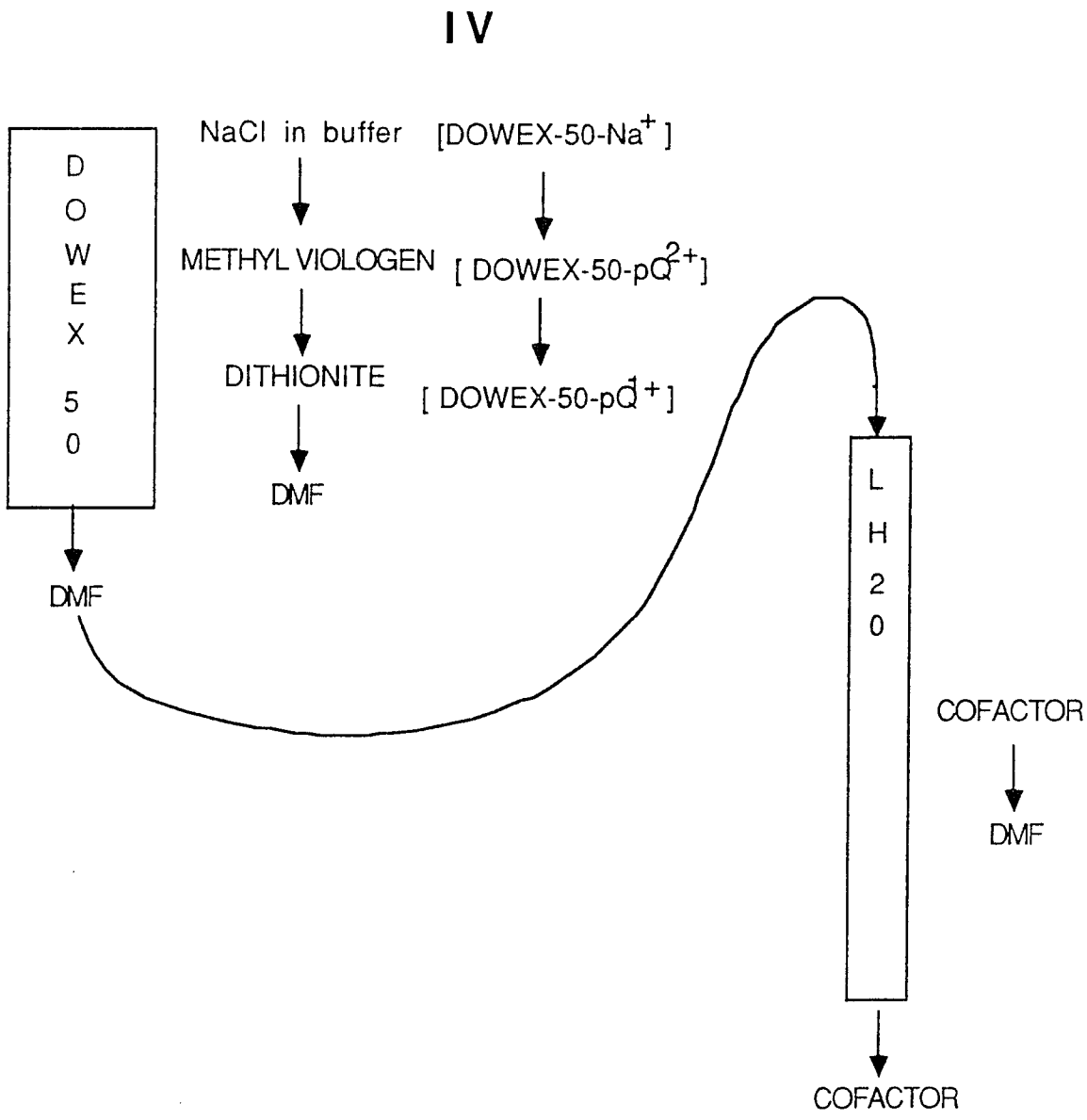

Figure 3.9. Column(s) used for desalting cofactor and DMF.

presence of an unknown factor in the crude extract that stabilizes the apoprotein. The initial activity of the apoproteins was inferred by monitoring component 2 activity in the extract, using the acetylene assay. It should be noted, however, that this assay is not an accurate indication of the condition of the apoprotein itself but only indicates that the enzyme had been expressed. In fact, it was not at all unusual for an extract to have good component 2 activity, but poor component 1 activity when active cofactor was added.

It was of interest to us to isolate both FeVco and FeMoco in order to cross-combine one cofactor into the apoprotein of the other. For instance, FeMoco was added to apoprotein of the *A. vinelandii* V-nitrogenase (strain LS25), and FeVco was added to apoprotein of the *A. vinelandii* Mo-nitrogenase (strain UW45). One other strain of apoprotein was used: the *nif*B- strain of *K. pneumoniae* which was donated by W. H. Orme-Johnson at MIT. It has been shown that mutations in *nif*B, *nif*N, or *nif*E result in formation of an apo-nitrogenase (lacking FeMoco), that can be activated *in vitro* with purified FeMoco (3.19, 3.20). Table 3.1 shows the results of all the combinations of cofactors with apoproteins.

As stated before, FeVco was isolated into DMF. This solvent denatures protein, and, in fact, this property was used as an advantage in isolation of the cofactor. Therefore, when adding cofactor solution to the crude extract, no more than 5-10% by volume could be added without degradation of proteins occurring. Another factor necessary in the reconstitution assay is the presence of component 2. There is evidence that component 2 is necessary for FeMoco synthesis both *in vivo* and *in vitro* (3.21-3.23). Component 2 may also be necessary for FeMoco insertion into the apoprotein. Therefore, the reconstitution assay was prepared as follows: ATP-regenerating solution (1 ml) was degassed and equilibrated with an atmosphere of 10% acetylene. Dithionite

was added to 20 mM, followed by the addition of crude extract (100 ml) and component 2 (2-4 mg). The assay started upon addition of cofactor (5 ml) and terminated with 0.1 ml of 33% trichloroacetic acid, followed by the analysis for the presence of ethylene in the atmosphere above the solution.

As can be seen in Table 3.1, all combinations of cofactor with apoprotein gave activity. Relative activities are ranked in Table 3.1.

TABLE 3.1

Reconstitution of Cofactor into apo-component 1

Apoprotein Strain	+FeMoco	+FeVco
UW45	++++	+++
LS25	++	+
KpB-	+++++++	+++++

The KpB- extracts were always the most active in component 1, while LS25 always gave low reconstitution activities even if component 2 activity was good. At this point, more concrete numbers are not possible due to lack of purification of apoprotein and no suitable V analysis.

Specific activities for our FeVco preparations were not calculated due to difficulties in determining the vanadium concentration in these dilute samples. Wet techniques as well as atomic absorption were tried without success at the concentration limits with which we were working: micromolar to nanomolar amounts of vanadium. However, a sample of FeVco in DMF was submitted for ICP (Inductively Coupled Plasma)

analysis, and the ratio of Fe:V was found to be 9:1, indicating that we were effectively removing most of the excess iron that existed in the DMF extractions of the cofactor.

3.3.4 EPR Spectrum of Cofactor

The EPR spectrum of isolated FeVco in DMF is shown in Fig. 3.10. There is a pronounced S = 1/2 signal with fine structure that is evident of a signal that is vanadyl-like. In the S = 3/2 region, there is a broad absorption in the g = 5 region with a pronounced radical-like signal in the g = 4.3 region that is similar to that seen at the same g-value in the thionine-oxidized EPR spectrum of Av1' (see Figure 3.11). The visible absorption spectrum of FeVco is similar to that of FeMoco in that the absorbance decreases steadily as wavelength increases (data not shown).

This procedure for FeMoco extraction, which binds protein to a DEAE column, has allowed use of solvents like DMF, methanol, benzene, THF, acetonitrile and acetone (3.18, 3.24). These solvents are more convenient for further characterization by electrochemical and crystallization techniques. These solvents also dissipate the need for a dissociable amide proton by FeMoco. Instead, it is an *organic* cation that appears to be necessary to extract the anionic cofactor from the protein while remaining bound to the DEAE column. The efficiency of this technique is between 50% and 90% using the amide solvent systems of DMF and NMF (3.18). Specific activities of FeMoco based on Mo content did not differ whether using DMF or NMF. However, there is a difference in the Fe content of the final product between DMF and NMF. When NMF is used, the Fe content of the FeMoco preparation is roughly equivalent to the stoichiometry present in the cofactor molecule: 6-8 Fe atoms per Mo atom. In the case of DMF, however, there is little color left on the column following extraction of cofactor into DMF (unlike that observed for NMF), indicating that almost all of the iron present

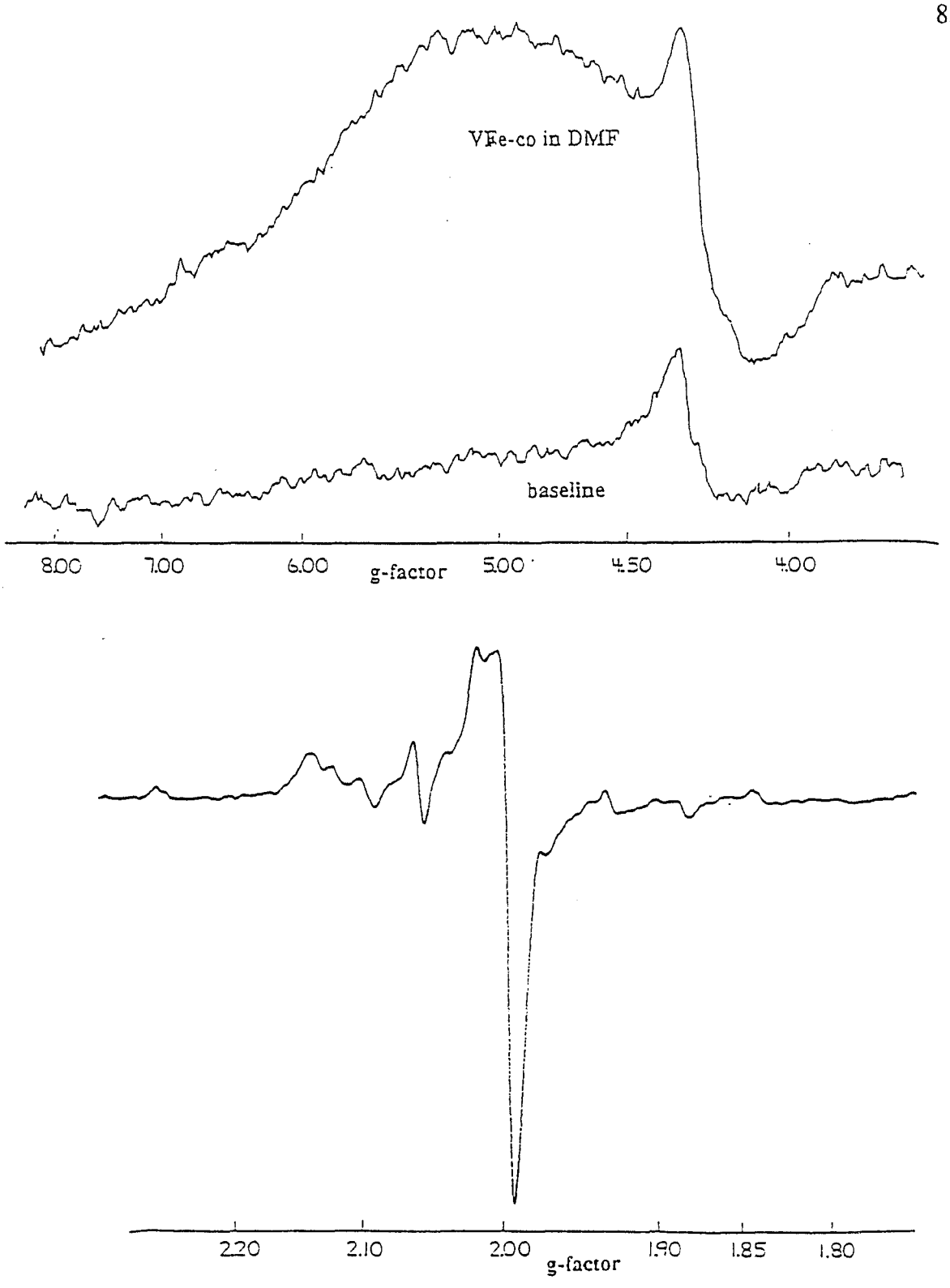

Figure 3.10. EPR spectrum of VFeco in DMF. Conditions: microwave frequency; 9.30 GHz, modulation frequency, 100 kHz; modulation amplitude, 12.5 G; scan time, 2 min.; time constant, 0.5 s; power: top, 10 mW, bottom, 2 mW; temperature, 7 K.

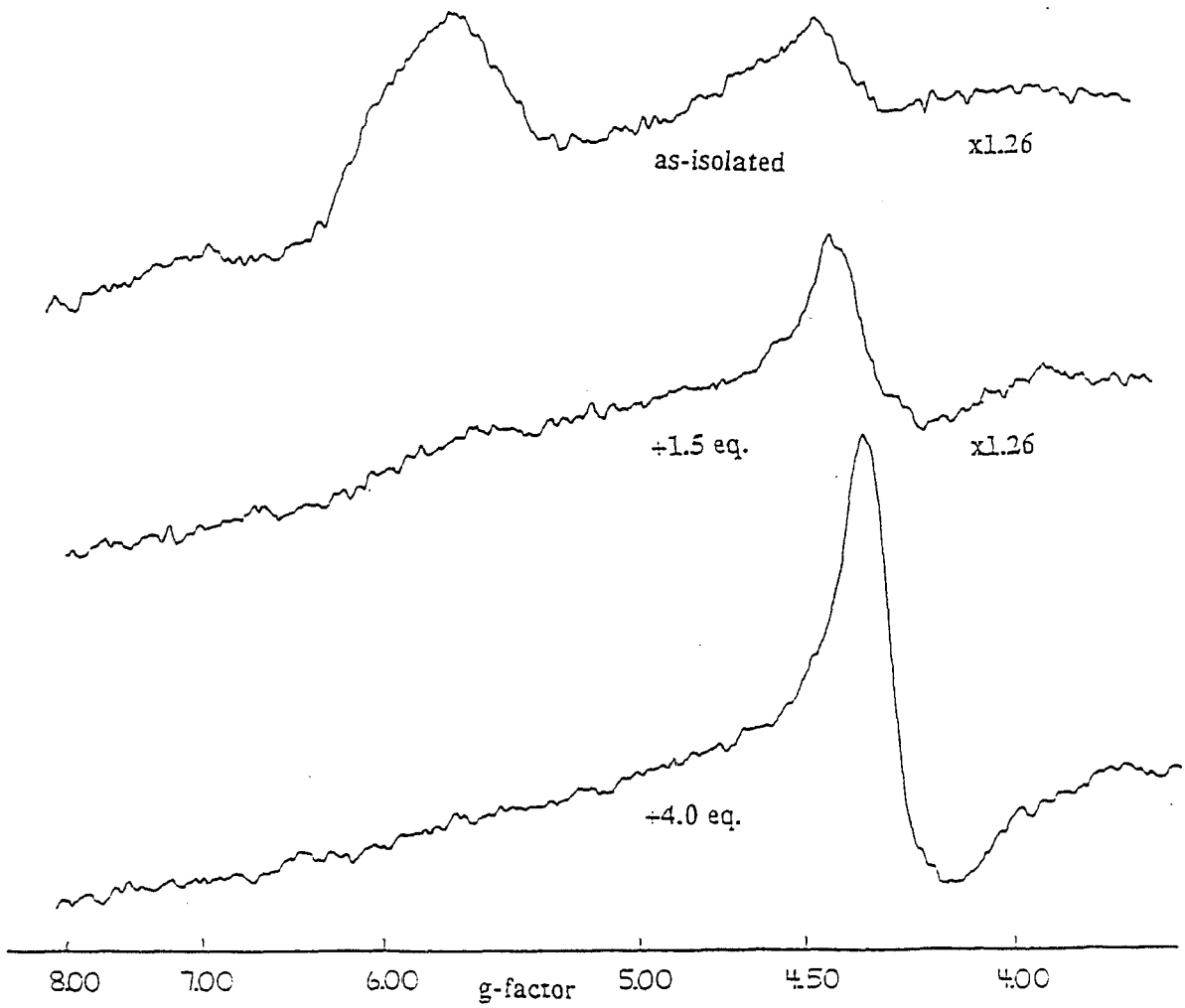

Figure 3.11. EPR spectra of thionine oxidation of Av1'. Conditions: microwave frequency; 9.30 GHz, modulation frequency, 100 kHz; modulation amplitude, 12.5 G; scan time, 2 min.; time constant, 0.5 s; power, 10 mW; temperature, 7 K; protein concentration, 45 mg/ml.

as Fe-S clusters is also extracted along with the cofactor into DMF. The extraction of all the metal clusters into DMF was also observed during FeVco isolation. This problem was remedied by using iron chelators while the protein was still bound to the column, as discussed in section 3.3.2. DMF serves two functions in the extraction procedure, removal of water and denaturation of protein. This denaturation is not complete, however, since only the noncofactor iron present in the P clusters is chelated by the bipy/DMF used (3.18). In fact, it has been observed that the DMF denaturation step leaves the cofactor protected even from aqueous solvents applied to the column after DMF (3.24). However, the cofactor can still be eluted with almost full recovery of activity if reequilibrated with DMF following the aqueous treatment. A combination of this technique and that originally developed by Shah and Brill showed that FeMoco could be extracted into DMF using the Shah procedure, as long as a soluble organic cation was present (3.24).

There is much work left to be done in isolation and purification of the cofactor. The work done with FeMoco in other solvents (3.24), as mentioned above, should also be done with FeVco. Better analysis of V is needed in order that both specific activities of cofactor preparations and quantitation of EPR spectra may be done. Many problems in the isolation of FeMoco by other groups have involved the organic cation used in extraction of the cofactor. In particular, if tetraphenylarsonium is used, arsenic tends to crystallize with the cofactor, yielding poor quality crystals as well as providing heavy atom contamination (3.24). Other salts which may prove helpful as ligands are bis-triphenyl phosphoranylidene or the chloride salt of dicyclohexyl amine.

3.4 OXIDATION BY THIONINE

The component 1 of Mo-nitrogenase (Av1) from *A. vinelandii* has been investigated during thionine oxidation by EPR, Mössbauer (3.25-3.27), and MCD studies (3.28, 3.29). Thionine reacts with Av1 to effect reversible oxidation. EPR studies have shown that this oxidation occurs in two distinct phases (3.25, 3.30, 3.31). The first equivalents of thionine oxidize Av1 without affecting the S = 3/2 signal as monitored by EPR. Further addition of thionine, however, results in the disappearance of the EPR signal. Results from Mössbauer spectroscopy (3.25) have shown that the first equivalents of thionine oxidize the EPR-silent P-clusters followed by subsequent oxidation of the M-centers. The redox potential ($E^{0'}$) of thionine at pH 7 is 0.064V, which is more positive than either the P-clusters or the M-centers for Av1. In our study of the thionine oxidation of Av1 (see Section 4.4), we also saw that the P clusters were first oxidized with the first four equivalents of thionine, followed by the oxidation of the M-centers with the next two equivalents of thionine. However, this experiment done for Av1 is not repeated here for Av1', because the S = 3/2 signal (S2) is extremely hard to saturate in Av1' even at very low temperatures. Therefore, it was our goal in the oxidation of Av1' to study the changes that were observed in the EPR signals during titration with thionine.

The oxidation of Av1' was performed sequentially, and upon addition of the first equivalent of thionine, the S = 1/2 signal in the g = 2 region was immediately bleached. This suggests that this signal has a low midpoint potential and is easily oxidized. Upon further addition of thionine, the S = 3/2 signal disappears with the simultaneous appearance of a sharp radical-like signal in the g = 2 region, a signal which continues to increase upon further oxidation. Finally, with the addition of four equivalents, an

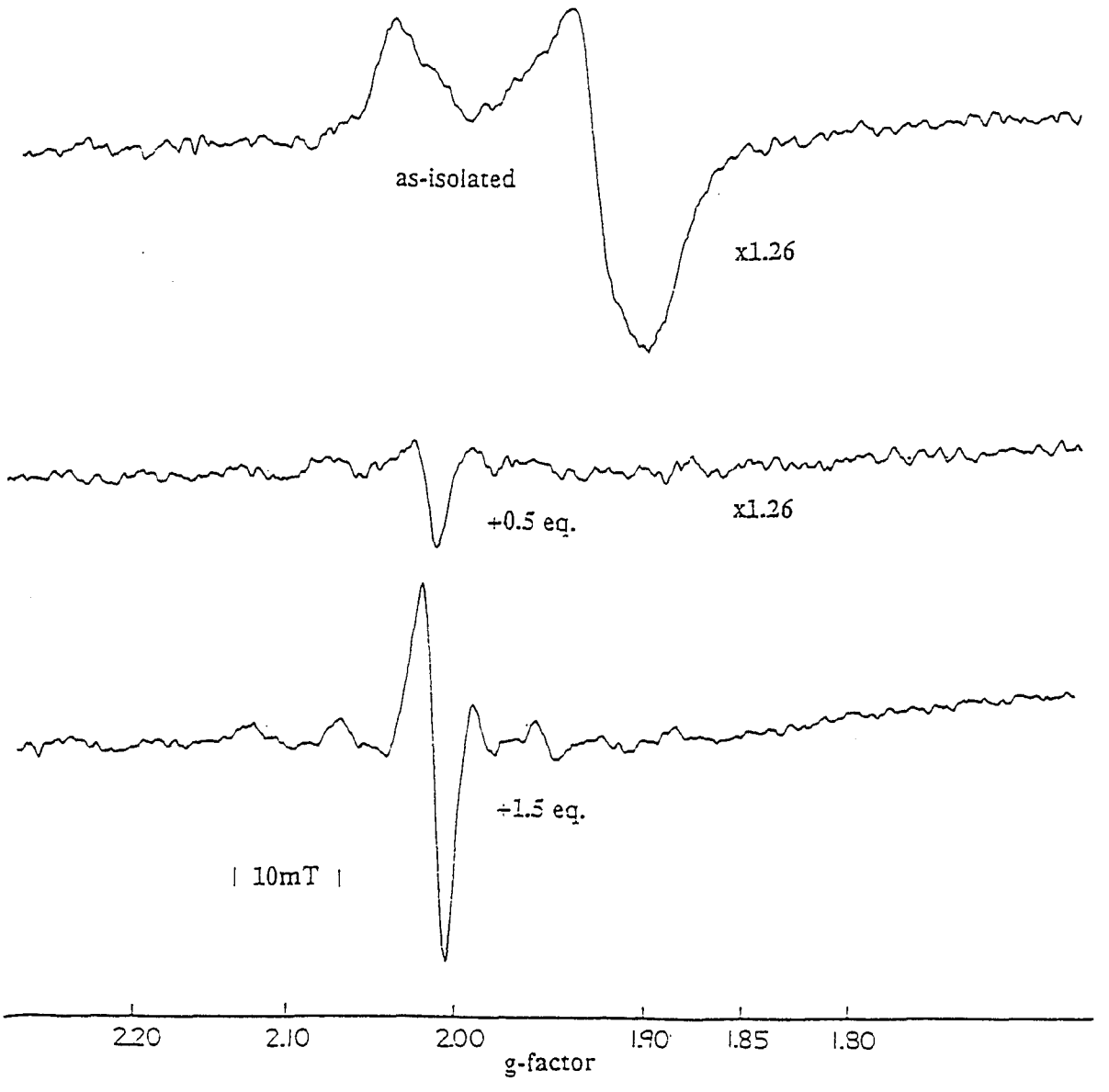

Figure 3.12. EPR spectra of thionine oxidation of Av1'. Conditions: microwave frequency; 9.30 GHz, modulation frequency, 100 kHz; modulation amplitude, 12.5 G; scan time, 2 min.; time constant, 0.5 s; power, 2 mW; temperature, 7 K; protein concentration, 45 mg/ml.

augmented signal in the g = 5 region is seen which similarly continues to increase in amplitude with oxidation. These changes are shown in Figures 3.11 and 3.12.

The EPR spectrum of thionine-oxidized Av1' in the g = 2 region (see Fig. 3.12) looks a lot like the EPR spectrum of vanadyl. This observation raises some interesting questions: Does this imply that the g = 2 signal is associated with the cofactor or some form of it, or is this signal appearing only upon oxidation and, therefore, not normally associated with whatever metal cluster normally produces the axial S = 1/2 (S1) signal in Av1'? In Av1, the M center, or cofactor, becomes oxidized with thionine after roughly six equivalents. The cofactor is, therefore, EPR-silent. If the M center in the VFe protein is an analogous cofactor, then we would expect the same to happen with Av1'. However, the appearance of a vanadyl-like EPR spectrum after the M center is supposedly oxidized would lead us to believe that this entity is not the M center, but some other form of the cofactor. These questions have not been answered fully, but a comparison of the thionine-oxidized spectrum of Av1' to that of the extracted VFeco (see Figure 3.10) shows that the EPR spectrum of the cofactor is dominated by similar-looking species in both the g = 2 region and the g = 5 region.

3.5 EFFECT OF pH ON THE PARAMAGNETISM OF Av1'

The EPR spectrum of purified Av1' was investigated under different pH conditions. It was believed that the redox potentials of the species giving rise to the S = 3/2 and the S = 1/2 signals were sufficiently different to warrant this type of investigation. It is important to remember that as the pH is raised, the effective midpoint potential of dithionite is lowered (3.32). Therefore, different pH conditions would provide a different redox environment for the protein.

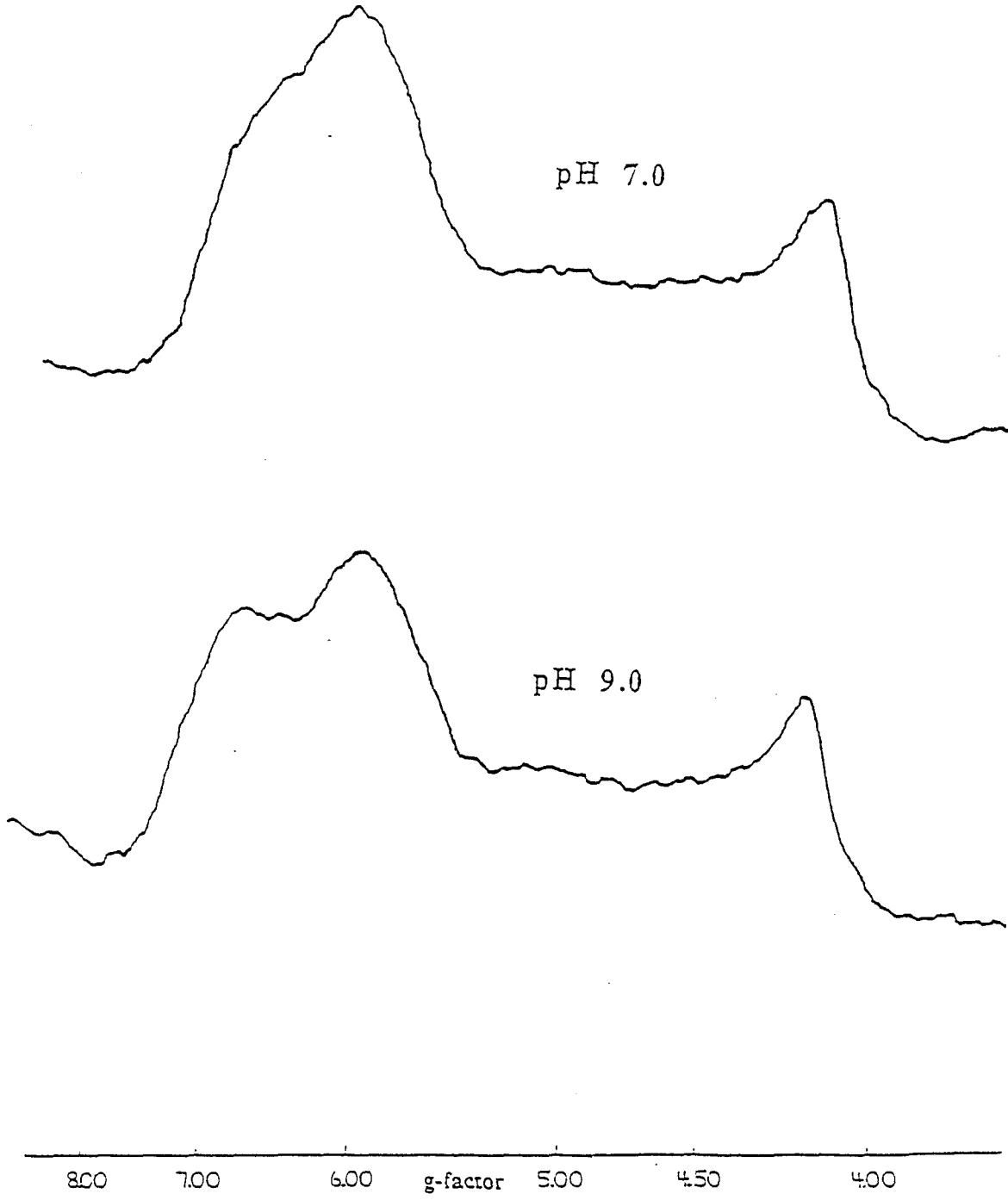

Figure 3.13. Effect of pH on S = 3/2 signal of Av1'. Conditions: microwave frequency; 9.30 GHz, modulation frequency, 100 kHz; modulation amplitude, 12.5 G; scan time, 100 s; time constant, 0.5 s; power, 10 mW; temperature, 7 K; protein concentration, 45 mg/ml.

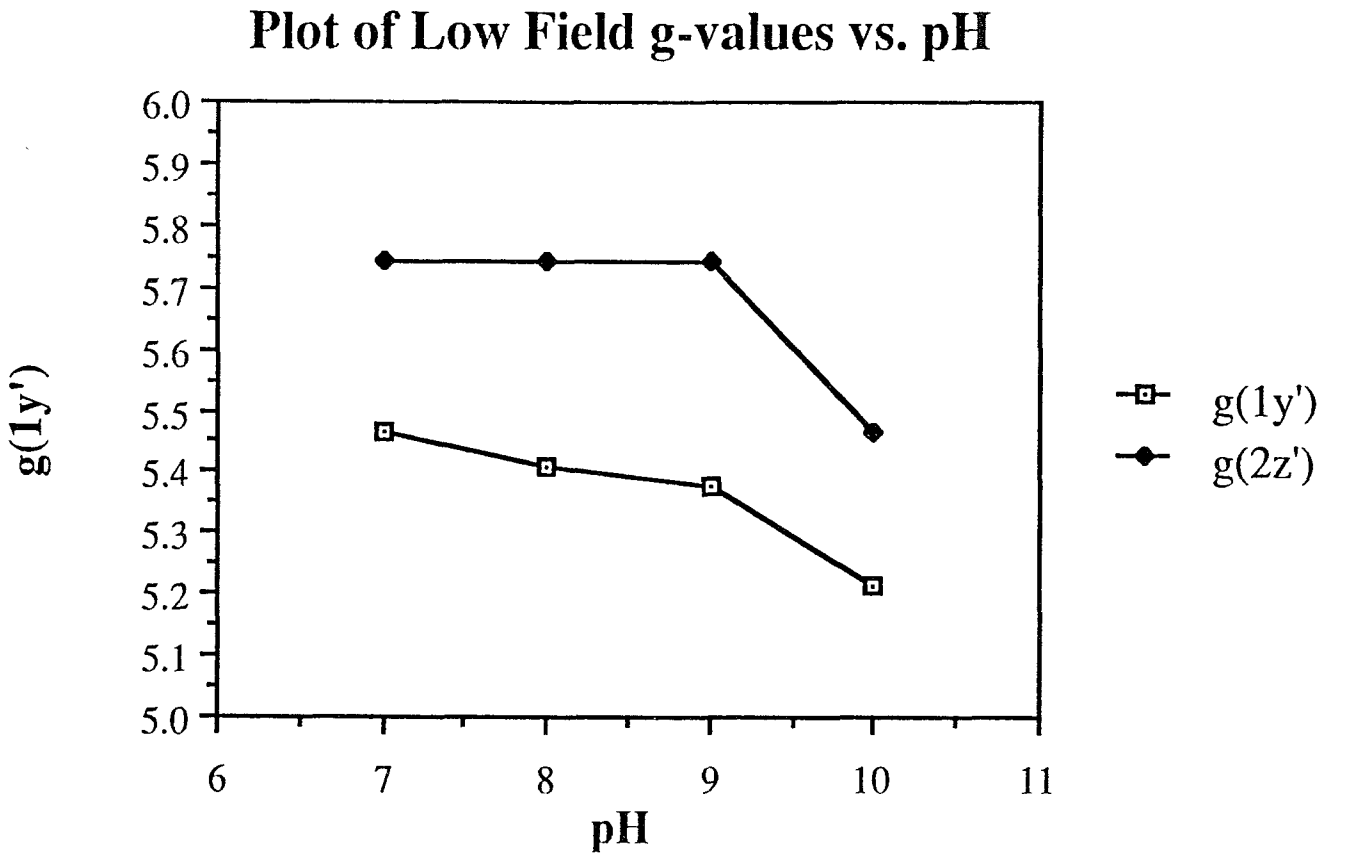

Figure 3.14. Plot of Low Field g-values vs. pH for S = 3/2 signal in Av1'.

The samples were prepared by dialyzing Av1' in different buffers at different pH. TRIS buffer was used for pH 7 and 8, while phosphate buffer was used for pH 9 and 10. In each sample, 2 mM dithionite was present.

The results of the change in pH on the S = 3/2 signal can be seen in Figures 3.13 and 3.14. Figure 3.13 shows shifts to higher field with increasing pH for Av1'. These changes in the S = 3/2 signal resulted in a general decrease in the rhombicity parameter (|E|/|D|) vs. pH. This is shown graphically in Figure 3.14. These types of changes in an EPR spectrum are indicative of a conformational change in the protein.

The changes seen in the S = 1/2 signal with pH were different. The most marked change in this signal was the increase in amplitude of this signal as the pH was raised. (see Figures 3.15 and 3.16) There was no change, however, in the g-values for this signal. It is apparent, therefore, that the S = 1/2 signal probably results from a metal cluster with a low mid-point potential. This type of change in an EPR signal could also be the result of pH-induced conformational changes in a protein. Most of the EPR studies performed on Av1' have been done at physiological conditions (pH 7). Our results suggest that the S = 1/2 signal is not fully reduced at this pH, and, therefore, would afford lower spin quantitations at pH = 7. In fact the S = 1/2 signal has been spin-quantitated to about 0.2 spins per vanadium atom at pH 7 (3.6). (Mike Johnson (personal communication, University of Georgia, Athens) has recently looked at the MCD of one of our samples at increased pH (pH 10). His observations indicated that the S = 1/2 signal arises from an atypical ferredoxin-type cluster.)

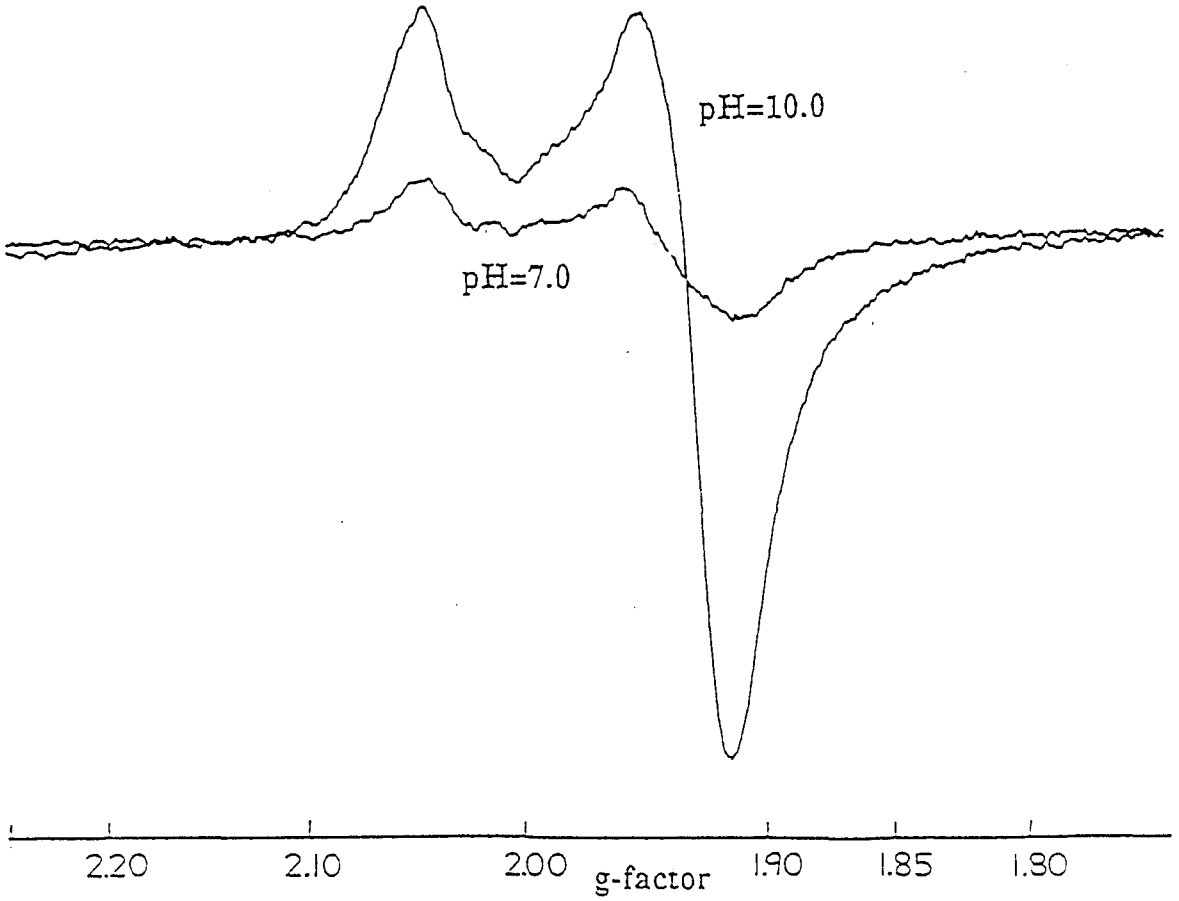

Figure 3.15. EPR spectra of g = 2 signal in Av1' at pH 7 and 10. Conditions: microwave frequency; 9.30 GHz, modulation frequency, 100 KHz; modulation amplitude, 12.5 G; scan time, 100 s; time constant, 0.2 s; power, 1 mW; temperature, 10 K; protein concentration, 37 mg/ml.

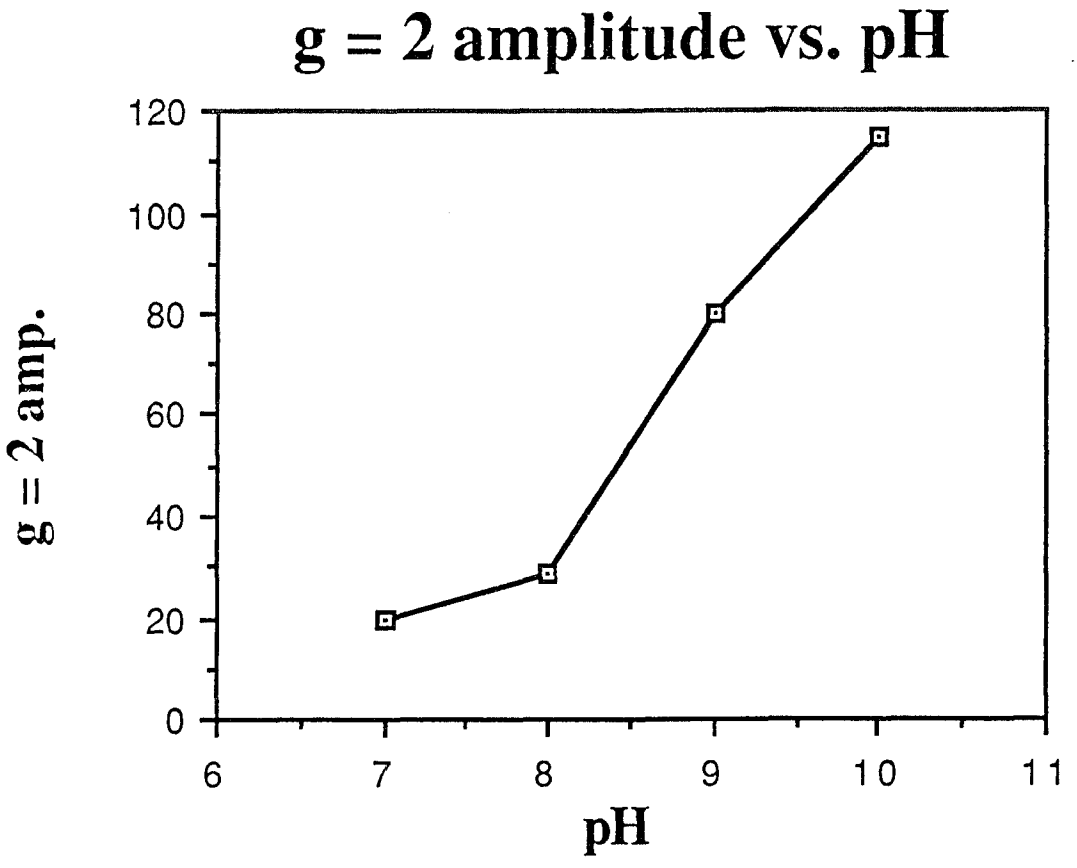

Figure 3.16. Plot of amplitude of g = 2 EPR signal in Av1' vs. pH.

REFERENCES

3.1. Robson, R. L., Eady, R. R., Richardson, T. H., Miller, R. W., Hawkins, M., and Postgate, J. R. (1986) Nature **322**, 388

3.2. Chisnell, J. R., Premakumar, R., and Bishop, P. E. (1988) J. Bacteriol. **170**, 27

3.3. Hales, B. J. (1990) in Advances in Inorganic Biochemistry **8**, pp. 165-198, (Eichhorn, G. L. and Marzilli, L. G., Eds.) Elsevier, New York

3.4. Hales, B. J., Case, E. E., Morningstar, J. E., Dzeda, M. F., and Mauterer, L. A. (1986) Biochemistry **25**, 7251

3.5. Morningstar, J. E., Johnson, M. K., Case, E. E., and Hales, B. J. (1987) Biochemistry **26**, 1795

3.6. Morningstar, J. E., and Hales, B. J. (1987) J. Am. Chem. Soc. **109**, 6854

3.7. Hales, B. J., True, A. E., and Hoffman, B. M. (1989) J. Am. Chem. Soc. **111**, 8519

3.8. Eady, R. R., Robson, R. L., Richardson, T. H., Miller, R. W., and Hawkins, M. (1987) Biochem. J. **244**, 197

3.9. Mortenson, L. E., Zumft, W. G., Palmer, G., *Biochim. Biophys. Acta*, **1973**, *292*, 422-435.

3.10. Orme-Johnson, W. H., Hamilton, W. D., Ljones, T., Tso, M.-Y. W., Burris, R. H., Shah, V. K., Brill, W. J., (1972) Proc. Natl. Acad. Sci. U. S. A. **69**, 3142-3145

3.11. Shah, V. K., and Brill, W. J. (1977) Proc. Natl. Acad. Sci. U. S. A. **74**, 3249-3253

3.12. Yang, S.-S., Pan, W.-H., Friesen, G. D., Burgess, B. K., Corbin, J. L., Stiefel, E. I., and Newton, W. E. (1982) J. Biol. Chem. **257**, 8042-8048

3.13. Walters, M. A., Chapman, S. K., and Orme-Johnson, W. H. (1986) Polyhedron **5**, 561-565

3.14. Lough, S. M., Jacobs, D. L., Lyons, D. M., Watt, G. D., and McDonald, J. W. (1986) Biochem. Biophys. Res. Commun. **139**, 740-746

3.15. Shah, V. K., Ugalde, R. A., Imperial, J., and Brill, W. J. (1984) Annu. Rev. Biochem. **53**, 231-257

3.16. Smith, B. E. (1980) in Molybdenum Chemistry of Biological Significance (Newton, W. E., and Otsuka, S., Eds.) pp. 179-190, Plenum Press, New York

3.17. Schultz, F. A., Gheller, S. F., Burgess, B. K., Lough, S., and Newton, W. E. (1985) J. Am. Chem. Soc. **107**, 5364-5368

3.18. McLean, P. A., Wink, D. A., Chapman, S. K., Hickman, A. B., McKillop, D. M., and Orme-Johnson, W. H. (1989) Biochemistry **28**, 9402-9406

3.19. Roberts, G. P., MacNeil, D., and Brill, W. J. (1978) J. Bacteriol. **136**, 267-279

3.20. Ugalde, R. A., Imperial, J., Shah, V. K., and Brill, W. J. (1984) J. Bacteriol. **159**, 888-893

3.21. Imperial, J., Shah, V. K., Hoover, T. R., and Ludden P. W. (1988) in Nitrogen Fixation: Hundred Years After (Bothe, H., deBruijn, F. J., and Newton , W. E., Eds.) p. 128 Gustav Fischer Verlag, Stuttgart, New York

3.22. Robinson, A. C., Dear, D. R., and Burgess, B. K. (1987) J. Biol. Chem. **262**, 14327-14332

3.23. Shah, V. K., Hoover, T. R., Imperial, J., Paustian, T. D., Roberts, G. P., and Ludden P. W. (1988) in Nitrogen Fixation: Hundred Years After (Bothe, H., deBruijn, F. J., and Newton , W. E., Eds.) pp. 115-120 Gustav Fischer Verlag, Stuttgart, New York

3.24. Wink, P. A., McLean, P. A., Hickman, A. B., and Orme-Johnson, W. H. (1989) Biochemistry **28**, 9407-9412

3.25. Zimmermann, R. M., Münck, E., Brill, W. J., Shah, V. K., Hentzl, M. T., Rawlings, J., and Orme-Johnson, W. H. (1978) Biochim. Biophys. Acta **537**, 185-207

3.26. Münck, E., Rhodes, H., Orme-Johnson, W. H., Davis L. C., Brill, W. J., and Shah, V. K. (1975) Biochim. Biophys. Acta **400**, 32-53

3.27. Dunham, W. R., Hagen, W. R., Braaksma, A., Grande, H. J., and Haaker, H. (1985) Eur. J. Biochem. **146**, 497-501

3.28. Johnson, M. K., Thomson, A. J., Robinson, A. E., and Smith, B. E. (1981) Biochim. Biophys. Acta **671**, 61-70

3.29. Morningstar, J. E., Johnson, M. K., Case, E. E., and Hales, B. J. (1987) Biochemistry **26**, 1795

3.30. Watt, G. D., Burns, A., Lough, S., and Tennent, D. L. (1980) Biochemistry **19**, 4926-4932

3.31. Euler, W. B., Martinsen, J., McDonald, J. W., Watt, G. D., and Wang, Z.-C. (1984) Biochemistry **23**, 3021-3024

3.32. Mayhew, S. G. (1978) Eur. J. Biochem. **85**, 535-547

THE MOLYBDENUM IRON PROTEIN OF *Azotobacter vinelandii*

Exploring the Effects of Salt, Dysprosium, and Oxidation by Thionine on the Relaxation of the S = 3/2 Center in Av1

4.1 INTRODUCTION

The structure and properties of the molybdeum iron protein (Av1) have already been discussed in the introduction (see section 1.2). Briefly, Av1 is a tetramer of $\alpha_2\beta_2$ subunits containing at least two different types of metal clusters, the EPR-silent P clusters and the M clusters, which are S = 3/2 in the dithionite-reduced, or as-isolated, state. For each tetramer there are most likely four P clusters and two M clusters. Primarily, it is the two M centers in which we will be interested; the presence of the P clusters will be addressed when we oxidize Av1 with thionine.

There have been many reports in the literature that simple salts, including NaCl, affect the catalytic and physical properties of nitrogenase. These effects include inhibition of the overall rate of catalysis (4.1-4.4) and interference with the elementary steps in the nitrogenase catalytic cycle (4.5). In addition, it has been found that Av1 can be crystallized at low ionic strength (4.6). Small reversible effects of NaCl on Av1 have been observed with EPR spectroscopy (4.7), and NaCl is known to inhibit chemical cross-linking of the two components (4.8). Furthermore, the oxidation of Av1 with organic dyes is influenced by the presence of NaCl (4.9). It has also been shown that NaCl, as well as other salts, inhibits the reduction of substrates where the pattern of inhibition is sigmoidal, and it was also found that NaCl is an inhibitor of the MgATP-dependent iron chelation of Av2 showing a hyperbolic pattern of inhibition (4.10).

Nitrogenase catalysis has been shown to be inhibited by 17 different salts where the inhibition is highly cooperative. This effect is not attributable to a simple ionic strength effect since both the anion and the cation contribute to the overall inhibition (4.10).

In the studies presented here we examined the effect of salt concentration on the power saturation of the S = 3/2 M center in Av1.

4.2 MICROWAVE SATURATION

For cases where the Bloch equations are valid (see section 2.7.6) the first derivative of the magnetic resonance absorption, A, is given by:

$$A \propto H_1 \frac{d\chi''}{dH} = \frac{N_0 \cdot H_1}{1 + 0.25\, H_1^2 \gamma^2 T_1 T_2}$$

where T_1 is the spin-lattice relaxation time, T_2 is the spin-spin relaxation time, H_1 is the microwave magnetic field at the sample, γ the gyromagnetic ratio and N_0 is the number of spins in the resonant field. In order to characterize the saturation behavior, a series of EPR spectra are recorded with the power varying from a condition of negligible saturation ($0.25\, H_1^2 \gamma^2 T_1 T_2 \ll 1$) to one of pronounced saturation ($0.25\, H_1^2 \gamma^2 T_1 T_2 \gg 1$). Under the condition $0.25\, H_1^2 \gamma^2 T_1 T_2 \ll 1$, the absorption line will be proportional to H_1.

It is possible, in principle, to calculate T_1 from saturation data and T_2 from the line width below saturation. This saturation method is based on the validity of the Bloch equations which assume homogeneous broadening, where the sample contains identical paramagnetic centers all resonating at the same magnetic field, giving rise to a Lorentzian lineshape. For inhomogeneously broadened samples, the derivative amplitude increases monotonically to a limiting value with increasing power where the overall lineshape is

normally Gaussian. The latter lineshape can be thought of as consisting of individual Lorentzian spin packets.

Sources of inhomogeneous broadening include hyperfine interactions, anisotropy due to zero-field splitting, dipolar interaction between spins with different Larmor frequencies, and 'g-strain' or heterogeneous populations of the centers. Because of the complicated relaxation behavior of most metalloproteins, including nitrogenase, saturation of the EPR line will be studied without attempting to calculate T_1 and T_2.

Relief from power saturation of an EPR line through a mechanism involving relaxation enhancement is reflected in a higher value for $P_{1/2}$, the power for half-saturation with microwave energy. The equation relating the magnetic resonance absorption, A, to microwave power for homogeneously broadened lines is $A \propto \sqrt{P}[1 + P/P_{1/2}]^{-3/2}$ and that for inhomogeneously broadened lines is $A \propto \sqrt{P}[1 + P/P_{1/2}]^{-1/2}$ (4.11). Homogeneous and inhomogeneous broadening are only extreme cases, with a whole range of intermediate cases. The degree of inhomogeneous broadening is determined by the ratio of the Lorentzian spin packet width and the Gaussian envelope width (4.12).

The most convenient way to compare power saturation data is to present it as a plot of log $(A/\sqrt{P})$ against log P which results in a line which is parallel to the abscissa while the signal is not saturated but slopes downward towards the abscissa with increasing saturation (4.13-4.16) see Figure 4.1. The power for half-saturation is given by the intersection of the extrapolated straight-line portions of the line.

Changes in electron spin relaxation for different iron-sulfur proteins have been studied using microwave power satuation (4.11). Differences in power saturation behavior between [2Fe-2S]- and [4Fe-4S]-containing proteins are best observed at low

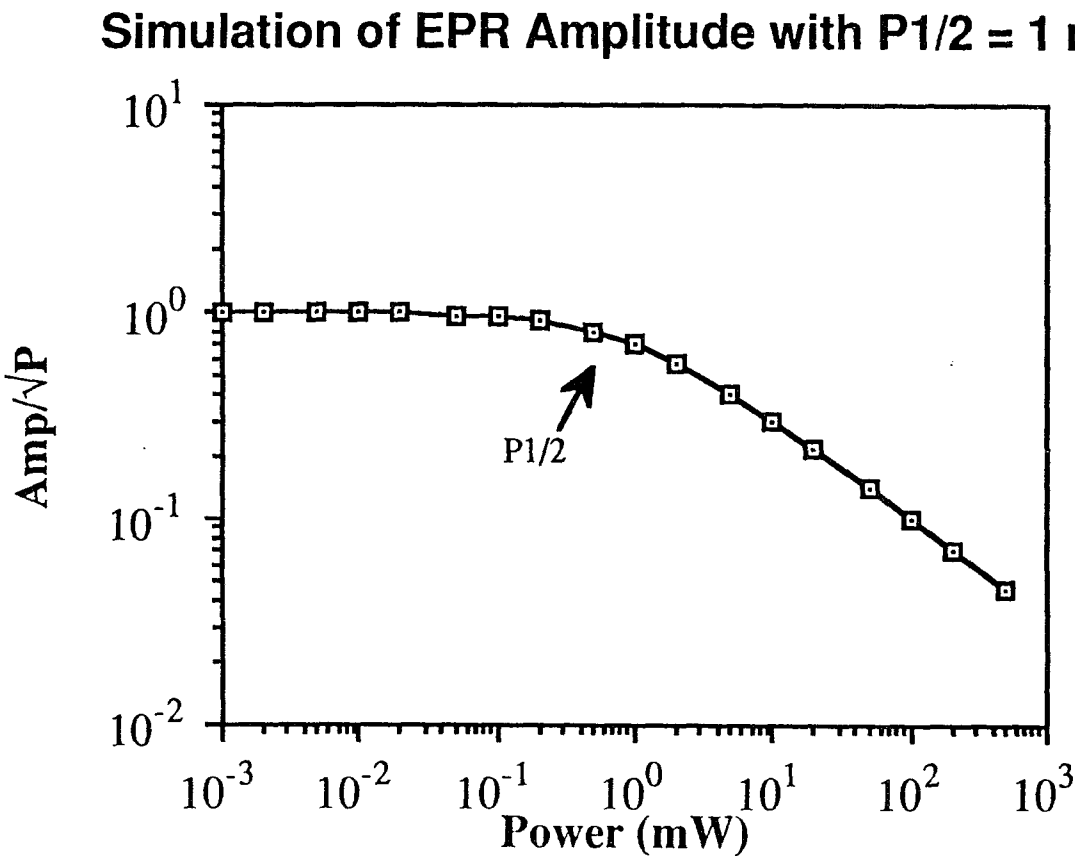

Figure 4.1. Power Saturation Plot. Double log plot of A/√P vs. Power used for power saturation data.

temperatures. The behavior of the signal intensity as a function of microwave power can be analyzed in terms of the power for half saturation $P_{1/2}$ and the degree of homogeneous/inhomogeneous broadening. In such analysis, a decrease in the electron spin relaxation rate corresponds to a decreased value of $P_{1/2}$. Spin-spin interactions between two paramagnetic centers in a protein molecule, such as a 2[4Fe-4S] ferredoxin, leads to a more rapid electron-spin relaxation. Similarly, if a paramagnetic probe, such as Ni^{2+} or gadolinium ions, is added to a protein solution, an increase in electron-spin relaxation rates may be observed. This increase occurs if the paramagnetic center in the protein is at or near the surface. This same phenomenon will be employed with the nitrogenase proteins using Dy^{3+} as an external paramagnetic probe.

4.3 THE EFFECT OF DYSPROSIUM ON POWER SATURATION

Power saturation may be relieved by adding an extrinsic relaxer. One of the advantages of such an agent is that they enable EPR spectra to be recorded for proteins at higher powers, with improved signal-to-noise ratios, where they might normally be saturated. These studies have been performed on many proteins, including cytochrome c and several iron-sulfur proteins (4.17-4.23). The probe used in most of these studies, as in ours, was dysprosium. Nickel and gadolinium ions have also been used, but are not as good relaxing agents as dysprosium. The dysprosium ion, Dy^{3+}, with J = 15/2, and a short spin-lattice relaxation time, is a very efficient agent for enhancing the electron spin relaxation of another paramagnet.

One important advantage in using a lanthanide ion as an external paramagnetic probe is that the magnetic properties of these ions are, for the most part, not affected by the ligands with which they may be associated. Furthermore, La^{3+}, which is diamagnetic, can be used as a control to separate chemical from magnetic interactions.

The interaction between the biological paramagnet and the added lanthanide has been formulated by Hyde and Rao (4.23). This dipolar interaction acts as a modulation of the C component of the dipolar Hamiltonian by spin-lattice relaxation of the metal. The result of this modulation is a line broadening and a relief from saturation of electron paramagnetic signals. Temperature effects are observed because the spin-lattice relaxation time of the perturbing ion decreases with increasing temperature. Therefore, by observing changes in either line width or power saturation when the lanthanide is added, information can be obtained relating to the distance between the perturbing ion and the radical or metal cluster being investigated, i.e., the distance of closest approach of the perturbing ion to the center of the cluster or radical. This has become an important tool for studying the paramagnetic centers in proteins or membranes where the position of the reactive center is typically not known. Experiments done with soluble iron-sulfur proteins (4.19, 4.20) show that the increase in $P_{1/2}$ ($\Delta P_{1/2}$) is proportional to r^{-6} (4.20, 4.24) (r = distance of closest approach) and is directly proportional to the concentration of relaxers, i.e., Dy^{3+}, where

$$\Delta P_{1/2}\ (\text{mW/mM}) = 4.12 \times 10^{8}\ r^{-6}\ \exp\ (-12.5/T)$$

There is evidence that Dy^{3+} as a complex, such as DyEDTA, attaches to the protein surface through both specific binding to particular amino acid residues and non-specifically to other residues and possibly through electrostatic interactions (4.20). Lanthanides also have a high affinity for oxygen. Therefore, it is possible that carboxylates of the amino acids are the target groups for specific binding. In studies where dysprosium was added to iron-sulfur proteins (4.19), changes in the nominal charge of the dysprosium complex profoundly altered the dysprosium effect. For these proteins, the negatively charged complex DyEDTA, had a large effect, whereas the nitrate (positive) and hydroxy EDTA complex (neutral) gave no effect. However, in

another study (4.24), $Dy(NO_3)_3$ was seen to give equivalent results, while in yet other studies, the nitrate was effective while the EDTA complex was ineffective or less effective in relieving saturation. This behavior argues against the possibility of the dysprosium complexes being present in a uniform dispersion (4.18, 4.23). Rather, this data is consistent with the idea that the rare earth complexes bind to the protein surface. It is also reasonable to assume that DyEDTA binds to the protein because lanthanides can attain coordination numbers greater than 6.

If the dysprosium complexes are not randomly dispersed, then one might ask whether we are seeing effects from unbound DyEDTA. As mentioned above, the increase in $P_{1/2}$ is proportional to r^{-6} and to the concentration of relaxers. Therefore, because of this distance dependence, it is highly unlikely that we are seeing a contribution from any nonbound dysprosium. In these distance calculations, 5 Å is allowed for the size of the DyEDTA complex.

4.4 CYTOCHROME c AS A MODEL FOR THE DYSPROSIUM EFFECT

Cytochrome c is a 13,000 dalton globular molecule with a diameter of 25 Å containing a low-spin heme at one side of the molecule. The EPR spectrum of cytochrome c is rhombic with principal g-values of approximately 1.25, 2.25, and 3.05 (4.27, 4.28). Because the structure of cytochrome c is known, it can be used to calibrate distance estimates.

The effect of dysprosium on the relaxation rate of cytochrome c may be summarized as follows (4.28):

$$\mathbf{P_{1/2} = A + B[DyEDTA]}$$

where A and B are temperature-dependent and [DyEDTA]-independent parameters. The effect of Dy increases as the temperature is raised because the spin-lattice relaxation time

of the Dy complex decreases. Over the temperature range 6-20 K, this effect is proportional to exp(-12.5/T). Since the intrinsic relaxation time of cyt c varies more rapidly than this, the most accurate measurements can be made at lower temperatures.

The results presented here for the nitrogenase proteins are for systems where the structure of the protein is not known and, therefore, we used a known system such as cytochrome c as a model to standarize our results. Cytochrome c with and without 5 mM DyEDTA as well as with the control LaEDTA (5 mM) was investigated by EPR using power saturations. The g = 2.25 resonance at 4.3 K was used for our saturation studies (see Figure 4.2).

As can be seen from the power saturation curves in Figure 4.2, there is a significant effect upon adding dysprosium. Table 4.1 below lists the $P_{1/2}$ values for the saturation curves. After allowing for the 5 Å dysprosium complex, the $\Delta P_{1/2}$ [mW/(mM Dy used] gave an r = 3.7 Å (at 4.3 K). This distance agrees quite well with previous studies where r = 4 Å (4.28).

TABLE 4.1

$P_{1/2}$Values for Cytochrome c with and without DyEDTA and LaEDTA

Sample	$P_{1/2}$ (mW)	$\Delta P_{1/2}$
Cyt c	11	
Cyt c + DyEDTA	270	
Cyt c - Cyt c + Dy		260
Cyt c + LaEDTA	14	

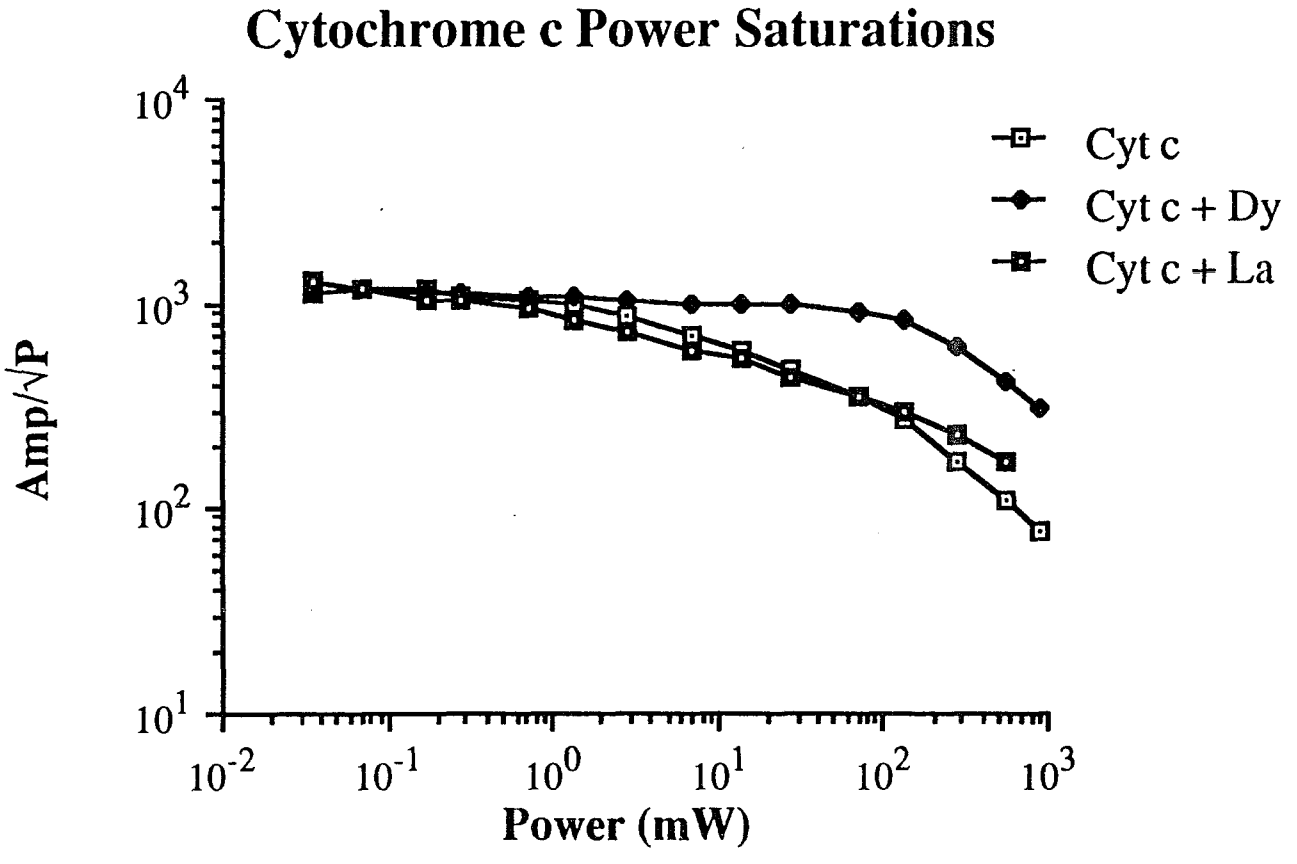

Figure 4.2. Power Saturations for Cytochrome c. Cytochrome c power saturations of g = 2.25 signal: AI: as isolated; + 5 mM DyEDTA; + 5 mM LaEDTA. Conditions: temperature, 4.4 K; microwave frequency, 9.46 GHz; modulation amplitude, 12.6 G; g value = 2.25.

4.5 ELECTRON PARAMAGNETIC RESONANCE OF Av1

The MoFe protein has been characterized extensively by EPR, Mössbauer, MCD, and ENDOR spectroscopies (4.25-4.28). The EPR spectrum of the M cluster is observable when the protein is present with a reductant such as dithionite (Figure 4.3). The three inflections in the EPR spectrum of Av1 (g = 4.32, 3.68, and 2.01 for Av1) correspond to the transitions of the ground state of an S = 3/2 spin system (4.25). The energy levels of an isolated axial S = 3/2 spin system (Figure 4.4) would be composed of four degenerate states characterized by the magnetic quantum numbers m_s = 3/2, 1/2, -1/2, and -3/2. These states are split into two levels characterized by $m_s \pm$ 3/2 and $m_s \pm$ 1/2, called Kramers doublets. The separation of these two levels is the zero-field splitting for the cluster which originates predominantly from spin-orbit coupling. Figure 4.4 represents the levels for an S = 3/2 system with a positive zero-field splitting (D) as in Av1 (D = +6.0 cm^{-1}) (4.29). If the zero-field splitting were negative, the $m_s \pm$ 3/2 doublet would be the ground state.

Application of an external magnetic field (Zeeman interaction), such as that present in an EPR spectrometer, further splits the levels in Figure 4.4. Because the zero-field splitting for nitrogenase is much larger than the Zeeman interaction (Figure 4.4), transitions will only occur within levels of the Kramers doublets and not between them. The magnitude of the Zeeman interaction depends on the orientation of the cluster in the external magnetic field, so that three possible inflections will be oberved for a cluster of rhombic electronic symmetry (two inflections are possible for axial symmetry). We would expect, then, a maximum of six possible inflections (three for each of the two different levels) to be oberved for a rhombic S = 3/2 spin system. The g factors of these inflections depend on the symmetry of the system. A convenient parameter, λ (=

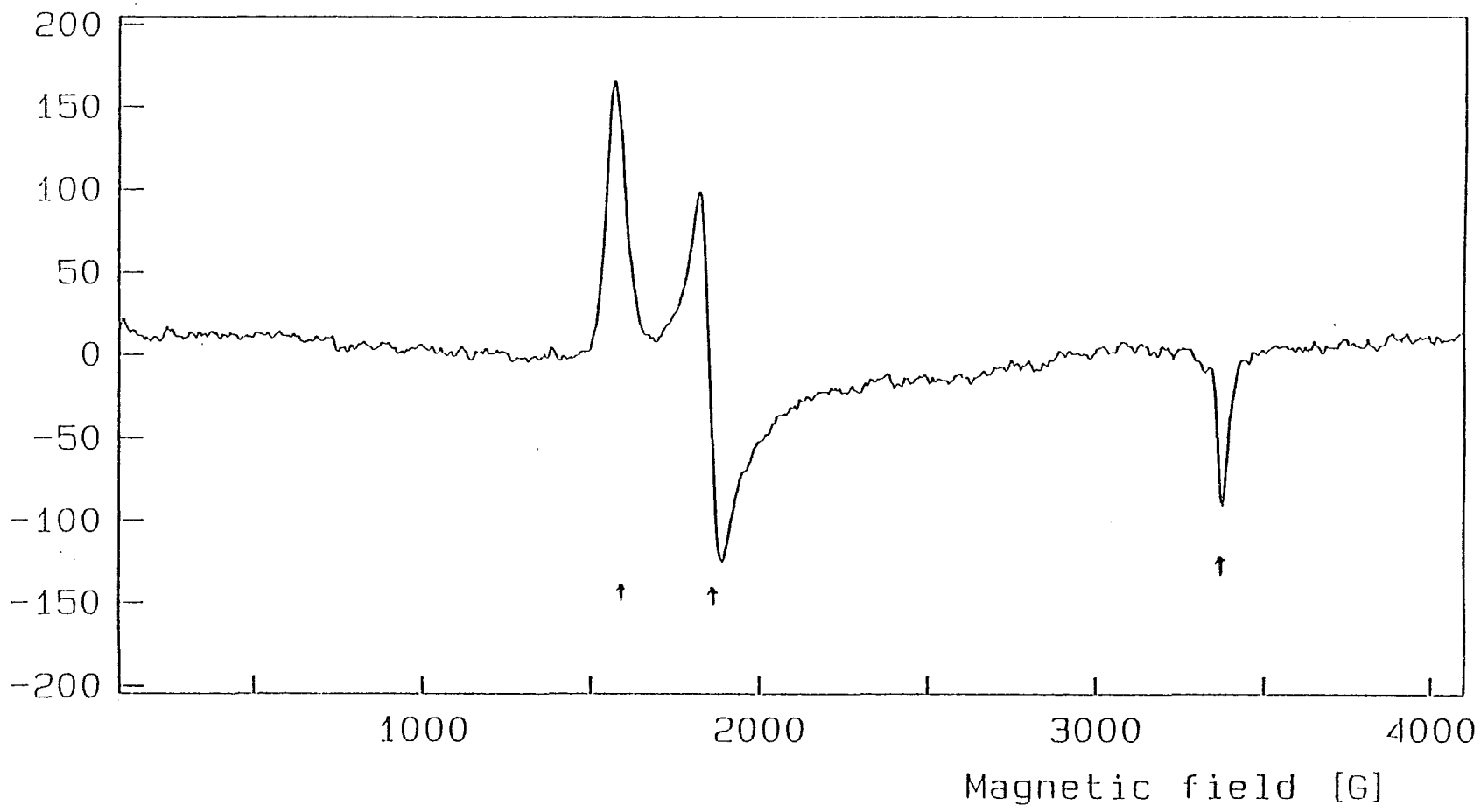

Figure 4 3. EPR spectrum of Av1. Samples in 0.025 M TRIS, pH 7.5, 1M NaCl. The principal g-values indicated by the arrows on the spectrum are g = 4.34, 3.68, and 2.01. Conditions: Microwave power, 1.0 mW; temperature, 3.8 K; modulation amplitude, 12.6 G; microwave frequency, 9.46 GHz.

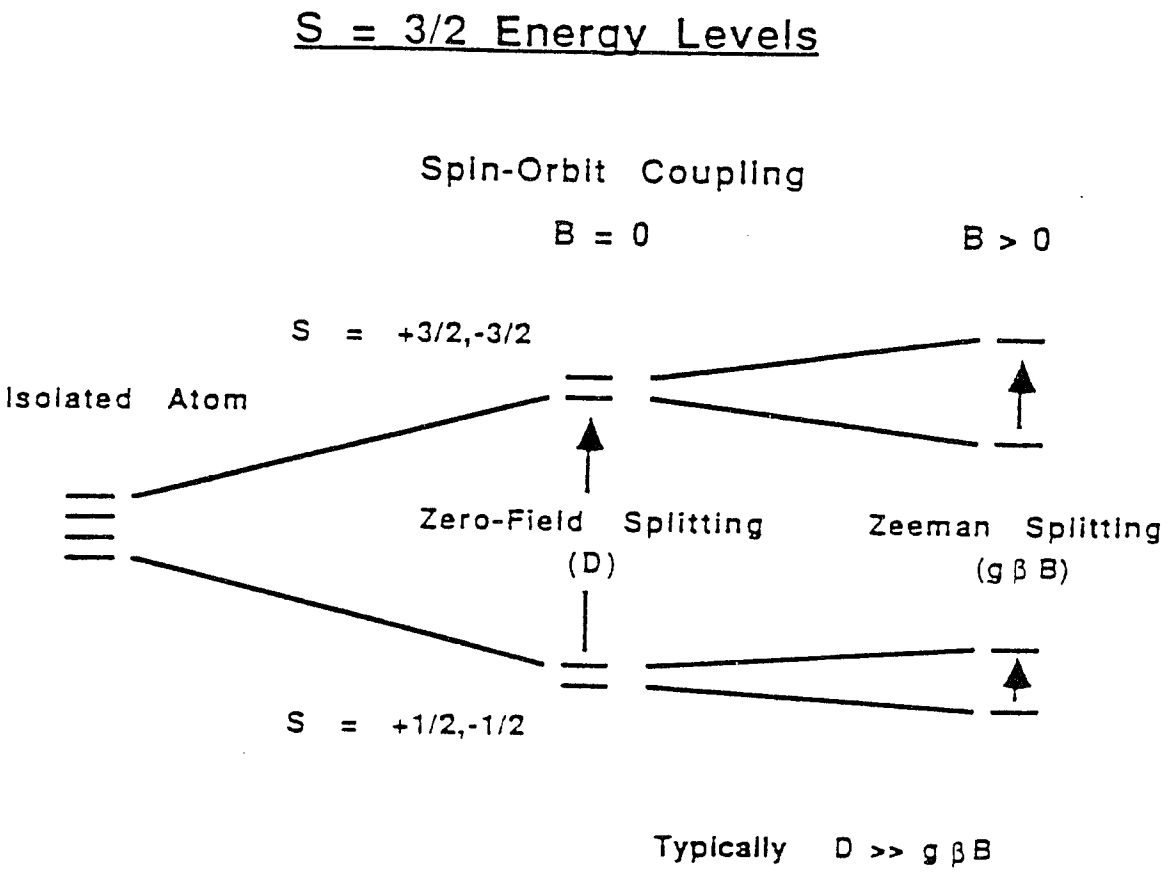

Figure 4.4. Energy Levels of an S = 3/2 spin system. The effects of zero-field splitting and the Zeeman interaction are depicted. The arrangement of the doublets is that obtained for positive zero-field splitting. If the incident microwave radiation is less then the zero-field splitting (gßB <<D), then transitions will only occur within the Kramer's doublets as shown. Figure adapted from ref. 4.29.

|E|/|D|), is used to depict the rhombic nature of a cluster with $0 \leq \lambda \leq 1/3$, where $\lambda = 0$ represents a purely axial system. Figure 4.5 shows a plot of the different inflections, in terms of apparent spectroscopic g factors (g'), for different values of λ. The spectrum for the Av1, is representative, then, of an S = 3/2 spin system with $\lambda = 0.053$. The spectrum for Av1 increases in amplitude with decreasing temperature, which corresponds to the ground state level with a positive zero-field splitting.

4.6 RESULTS

4.6.1 The Effect of Salt Concentration on the Power Saturation of Av1

We are now ready to look at how the power saturation of the EPR spectrum for Av1 changes in the presence of different amounts of NaCl. The samples were prepared by lowering the salt concentration that is already present in purified Av1. After purification, most of the component proteins contained 0.15-0.3 M salt; this is because NaCl is present in most of the buffers used in purification (see section 2.1). Care was taken in lowering the salt of Av1 solutions since Av1 will crystallize at concentrations below about 0.05 M salt, which was the lowest salt concentration used in this study. However, it has been shown (4.3) that Av1 solutions in excess of 10 mg/ml can be prepared in pure water with no loss of activity or change in spectroscopic properties. Av1 precipitates in TRIS-NaCl solutions below 0.05 M in each. The protein concentration of our samples, in 0.025 M TRIS buffer, were lower than 10 mg/ml for the more dilute salt concentrations. Higher salt concentrations were obtained using a 0.5 M NaCl stock solution. Power saturations were determined using a range of 0.02 mW to 450 mW on the EPR spectrometer at a temperature of 3.8 K. Figure 4.6 shows the

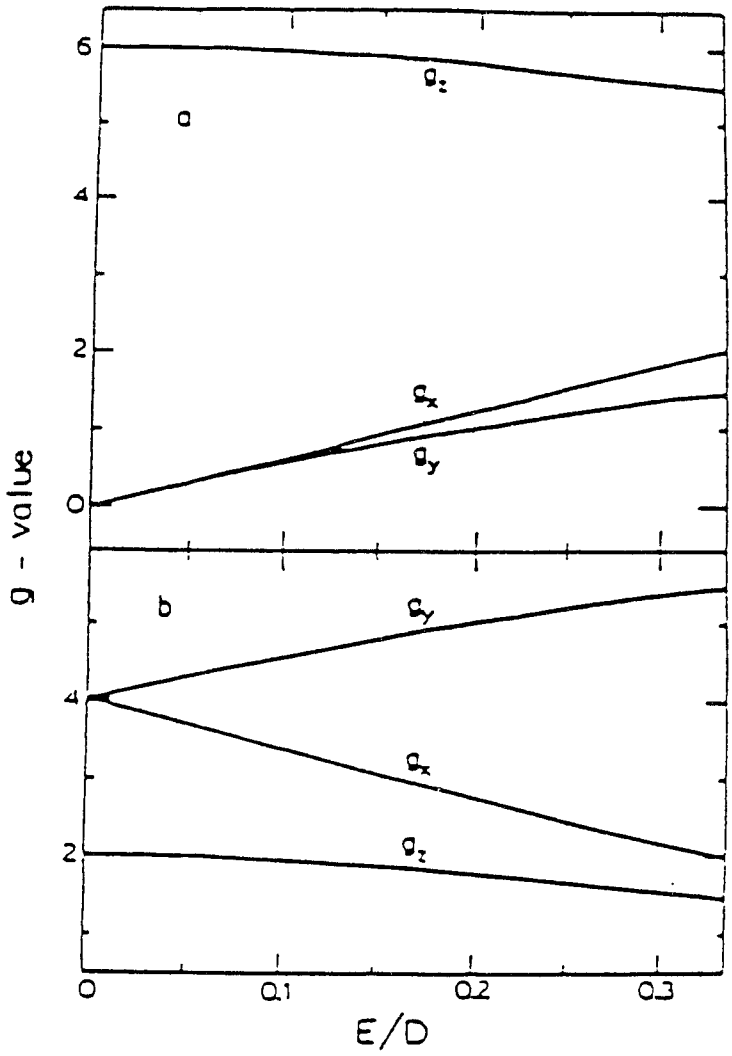

Figure 4.5. Plot of g-values for an S = 3/2 system as a function of E/D. (a) $M_s = \pm 3/2$; (b) $M_s \pm 1/2$. Figure adapted from ref. 4.29.

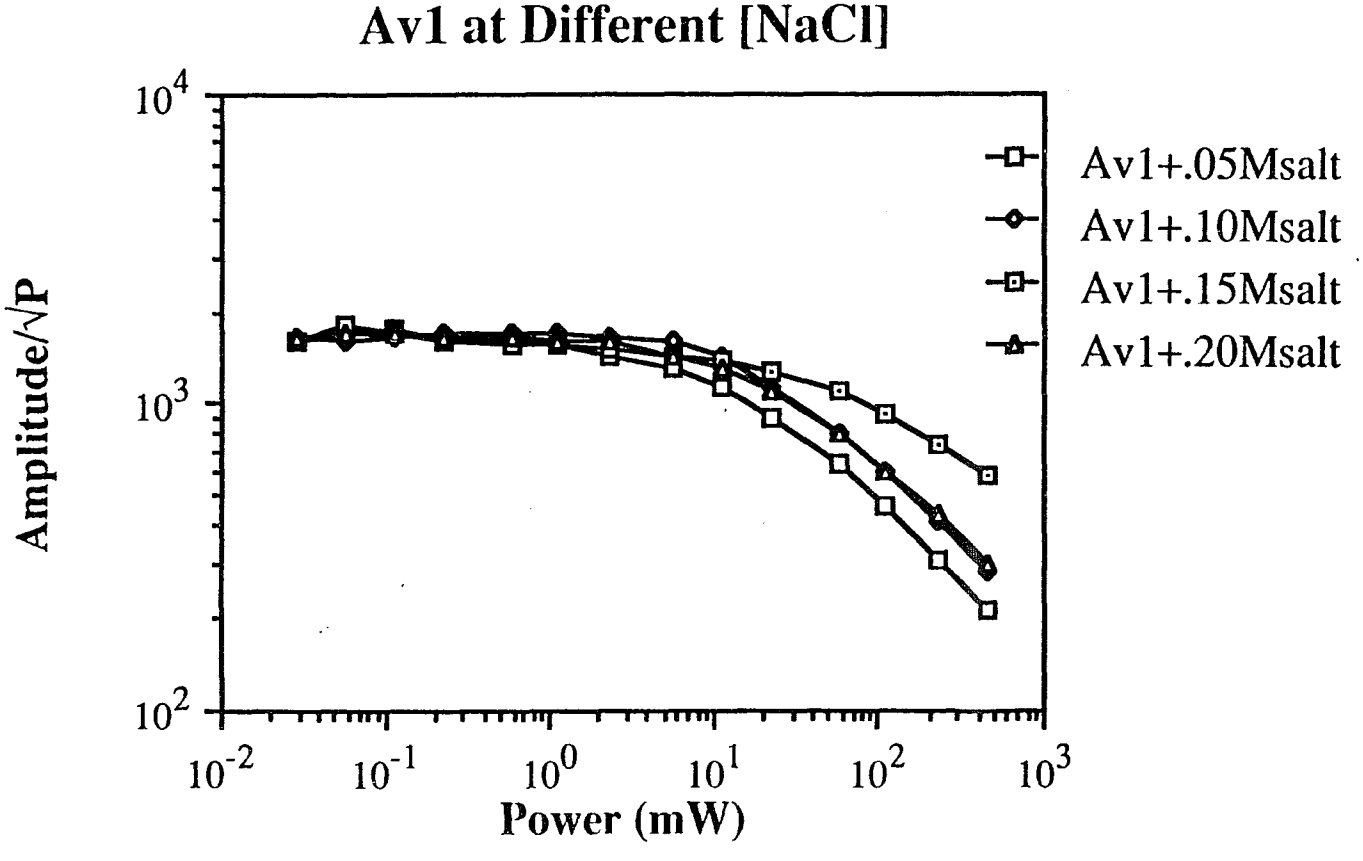

Figure 4.6. Av1 Power Saturations at Different [NaCl]. Salt concentrations: 0.05-0.20 M. Conditions: temperature, 3.8 K; microwave frequency, 9.46 GHz; modulation amplitude, 12.6 G; g value = 3.64.

power saturation curves for Av1 at different salt concentrations. Table 4.2 gives the $P_{1/2}$ for each curve vs. [NaCl].

The EPR spectrum for Av1 does not change in the presence of increased amounts of salt. This agrees (4.3) with previous results where it was also observed that the optical properties of Av1 do not change with salt concentration (4.3). However, conformational changes in other metalloproteins in the presence of perturbing agents such as salt have been monitored by studying their saturation behavior, showing how sensitive this technique can be (4.11).

TABLE 4.2

$P_{1/2}$ for Av1 Power Saturation Curves at Different [NaCl]

[NaCl] (M)	$P_{1/2}$ (mW)
0.05	33
0.10	54
0.15	150
0.20	53

The data in Table 4.2 indicates that as the salt concentration is increased, the M center in Av1 relaxes at a faster rate, leading to an increase in $P_{1/2}$ up to a salt concentration of 0.15 M. From previous studies, we do know that Av1 crystallizes at low salt concentrations and would, therefore, be expected to exist in some aggregated form at low salt concentrations. The data presented here does not refute this arguement,

but, instead, indicates that if aggregation is occurring, there is negligable spin-spin interaction between the M centers located on adjacent protein molecules at low salt. If there were noticeable interactions, the relaxation rates of the lower salt samples would be faster, leading to an increase in $P_{1/2}$ for these samples relative to the others rather than the decrease observed. This result suggests that the M centers between two adjacent protein molecules are not close enough (>2 or 3 nm) to enable such an interaction to occur.

If Av1 proteins did exist in an aggregated state at lower salt concentrations, the extrinsic paramagnet, Dy^{3+}, would not be able to efficiently enhance the relaxation rate of the M centers, because the distance between each M center and the Dy ions would be larger than if the protein molecules existed in a more isolated state. In order to test this hypothesis, DyEDTA was added in a final concentration of 1 mM to Av1 samples present in the same salt concentration range as before. Power saturations were performed for these samples under exactly the same conditions as for those samples lacking DyEDTA. The power saturation curves for these samples are shown in Figure 4.7. The $\Delta P_{1/2}$ values for these samples are shown in Table 4.3 as these values reflect the change in $P_{1/2}$ ($\Delta P_{1/2}$) at each salt concentration with and without DyEDTA.

As can be seen from the results in Table 4.3, there is clearly a relief from power saturation with added dysprosium at all salt concentrations. As the salt concentration increased, this enhancement became more marked as the values for $\Delta P_{1/2}$ increased. This would indicate that Av1 molecules were more accessible to the Dy ion as the amount of salt increased in the sample, which is in line with the hypothesis that Av1 is less aggregated at higher salt concentrations.

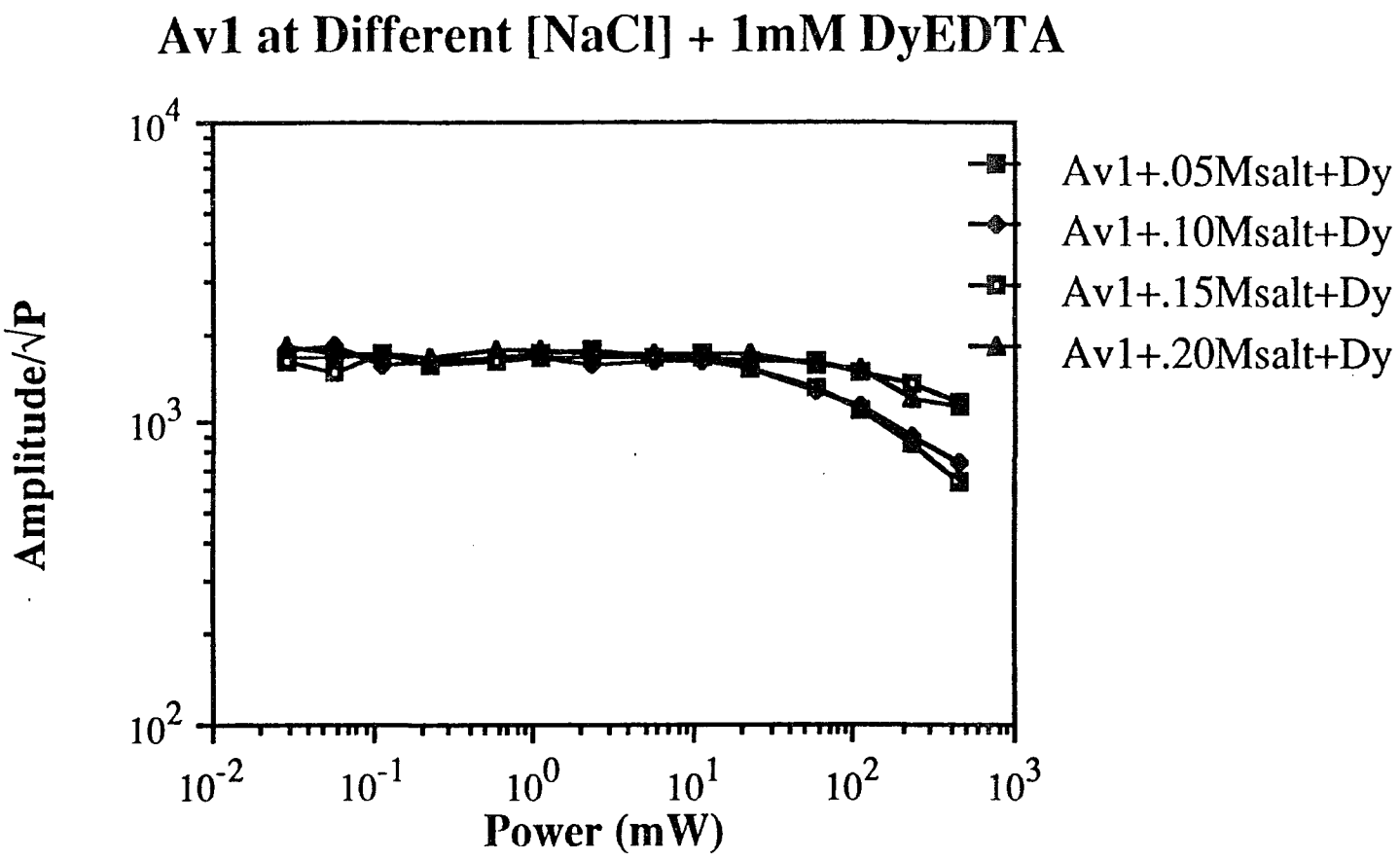

Figure 4.7. Av1 Power Saturations at Different [NaCl] + 1 mM DyEDTA. Salt concentrations: 0.05-0.20 M. Conditions: temperature, 3.8 K; microwave frequency, 9.46 GHz; modulation amplitude, 12.6 G; g value = 3.64.

TABLE 4.3

$\Delta P_{1/2}$ for Av1 Power Saturation Curves at Different [NaCl] with 1 mM DyEDTA

[NaCl] (M)	$\Delta P_{1/2}$ (with Dy-without Dy)
0.05	210
0.10	280
0.15	>300*
0.20	>400*

*$P_{1/2}$ was not calculated as the amplitude at half the maximum was off the curve.

4.6.2 THE EFFECT OF [DyEDTA] ON THE POWER SATURATION OF Av1

Before the effect of ionic strength could be measured in a quantitative way for Av1, with and without the presence of dysprosium, it was necessary to measure the optimal amount of dysprosium needed to effectively relieve the power saturation. In fact, an ionic strength effect for Av1 was originally done using 20 mM DyEDTA as a "first guess" based on the amount used in the cytochrome c studies.

Based on these results, a study of how the power saturation of Av1 changed with [DyEDTA] was done. In these samples, and in all subsequent samples, a median salt concentration of 0.1 M was used. Almost 100% activity is seen with nitrogenase at

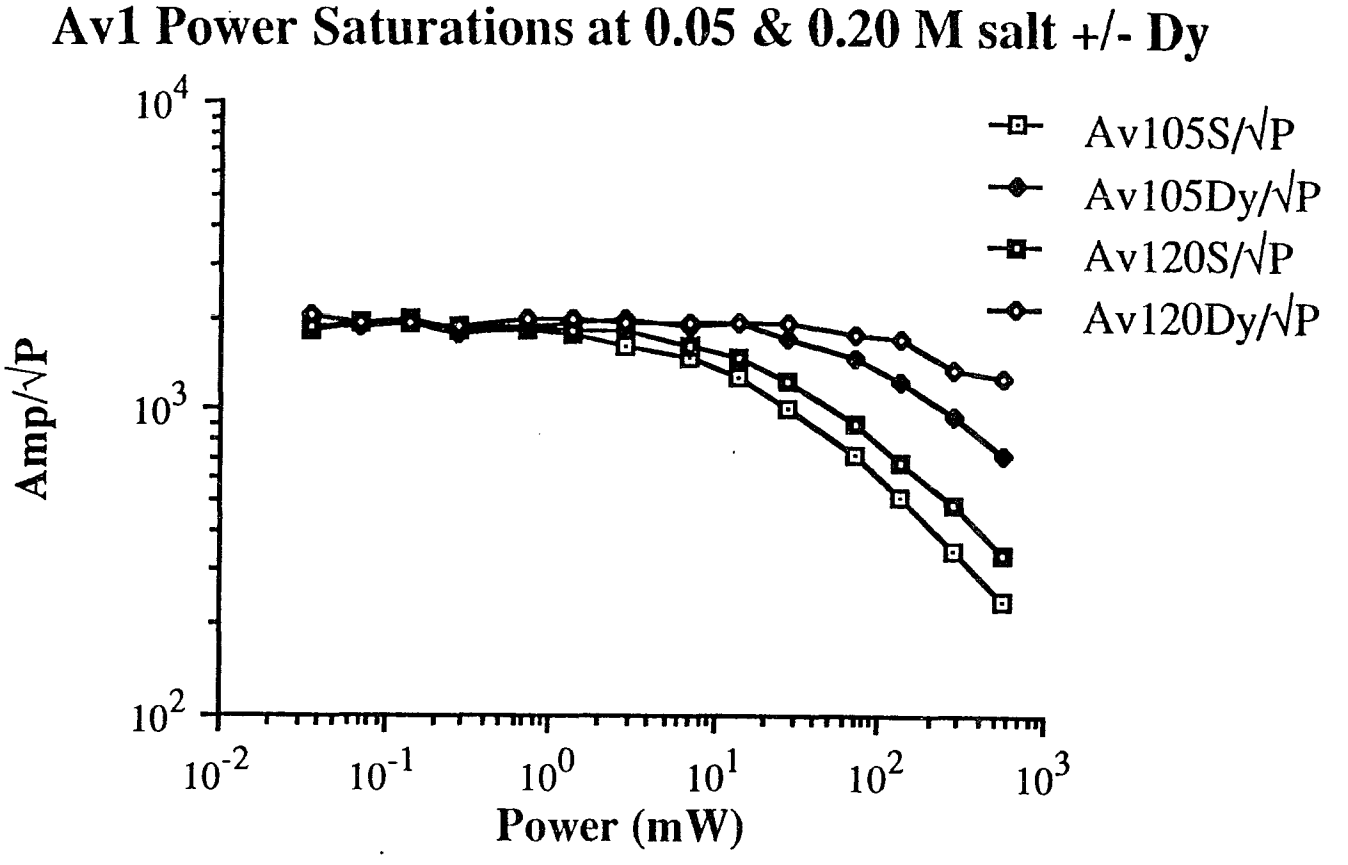

Figure 4.8. Av1 Power Saturations with and without 1 mM DyEDTA. Salt concentrations: 0.05 and 0.20 M. Conditions: temperature, 3.8 K; microwave frequency, 9.46 GHz; modulation amplitude, 12.6 G; g value = 3.64.

this salt concentration (4.10). The range of concentration for [DyEDTA] was 0.2-10 mM DyEDTA. The power saturation curves for Av1 at different [DyEDTA] are shown in Figure 4.9. We might expect that as the dysprosium concentration becomes small compared to Av1 concentration, the value of $P_{1/2}$ will fall towards the intrinsic value, but not necessarily in a simple way, since some of the specific binding sites will be occupied and others will not, as found with the cytochrome c studies (4.21, 4.22). The $P_{1/2}$ values for the saturation curves in Figure 4.9 are tabulated in Table 4.4.

A plot of $\Delta P_{1/2}$ vs. [DyEDTA] is shown in Figure 4.10. In the cytochrome c studies, $P_{1/2}$ is proportional to [DyEDTA] only at higher concentrations (5 mM) (4.22) after local specific binding sites were occupied. However, in other studies, $P_{1/2}$ is directly proportional to [DyEDTA] for all concentrations (4.19, 4.24), although a slight change in slope is observed at concentrations > 0.5 mM.

What does the slope of the curve in Figure 4.9 tell us about the distance of closest approach of the M center in Av1? The slope of this curve is very large (856 mW/mM) and corresponds to an r = 5 Å before allowing for the 5 Å DyEDTA complex. This result is unrealistically small. The M centers in the MoFe protein are believed to be located at opposite sides of the molecule (radius of Av1 = 40Å). Therefore, while we expected the M centers to be close to the surface, and indeed they are, the value we have obtained requires further thought as to what might actually be occurring for Av1.

The MoFe protein is an S = 3/2 system which relaxes much faster than an S = 1/2 spin system. The model which we have used here for the enhancement of relaxation was originally developed by Hyde and Rao (4.23) for S = 1/2 spin systems. This model for an S = 1/2 system implies that one term in the dipolar interaction predominates. This may not be the situation for an S = 3/2 system. Also, given the fact that we know little about the actual structure of Av1, we cannot improve upon the

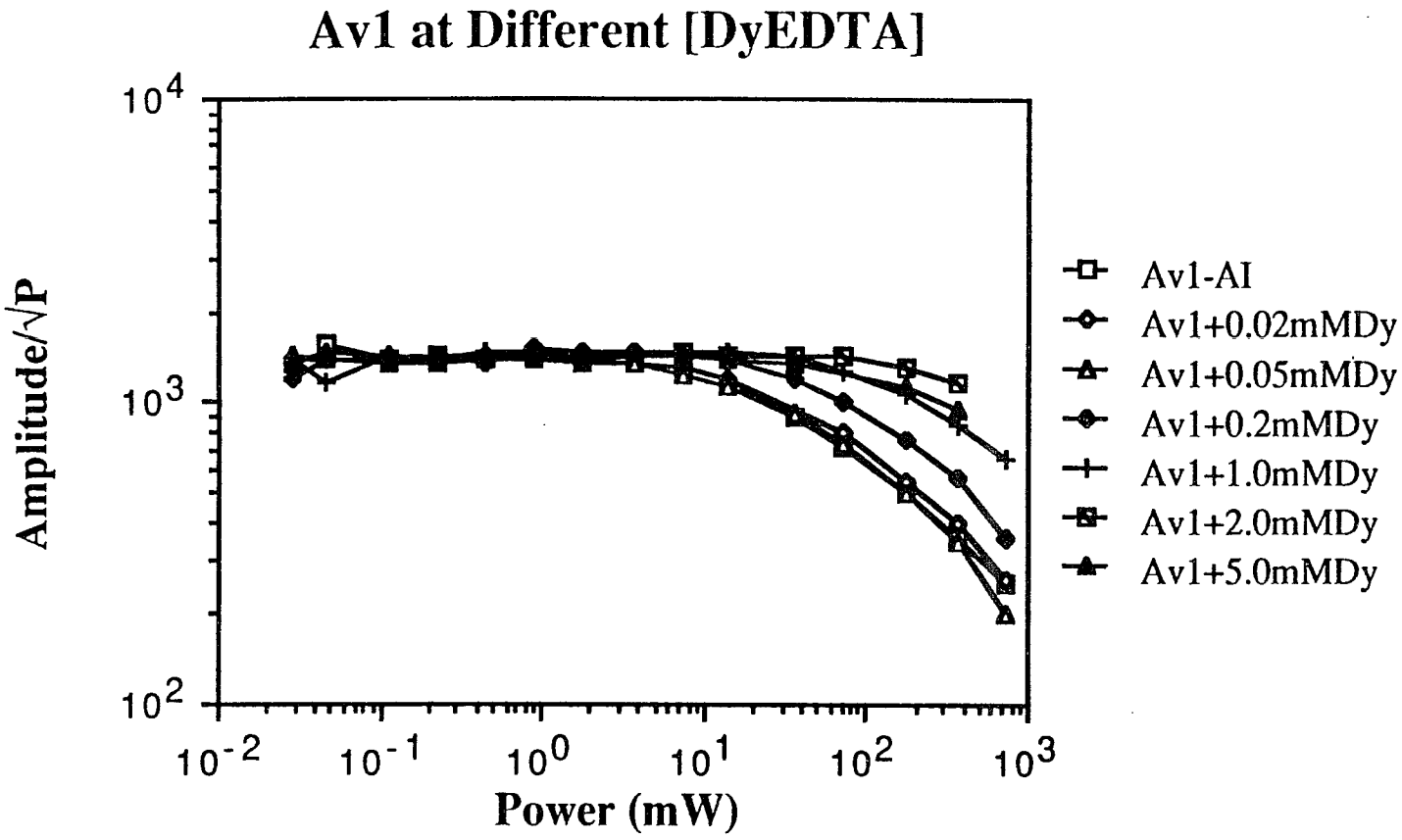

Figure 4.9. Power Saturation Curves for Av1 at Different [DyEDTA]. DyEDTA concentrations: (AI: 0), 0.02, 0.05, 0.2, 1.0, 2.0, 5.0 mM. Conditions: temperature, 3.8 K; microwave frequency, 9.46 GHz; modulation amplitude, 12.6 G; g value = 3.64.

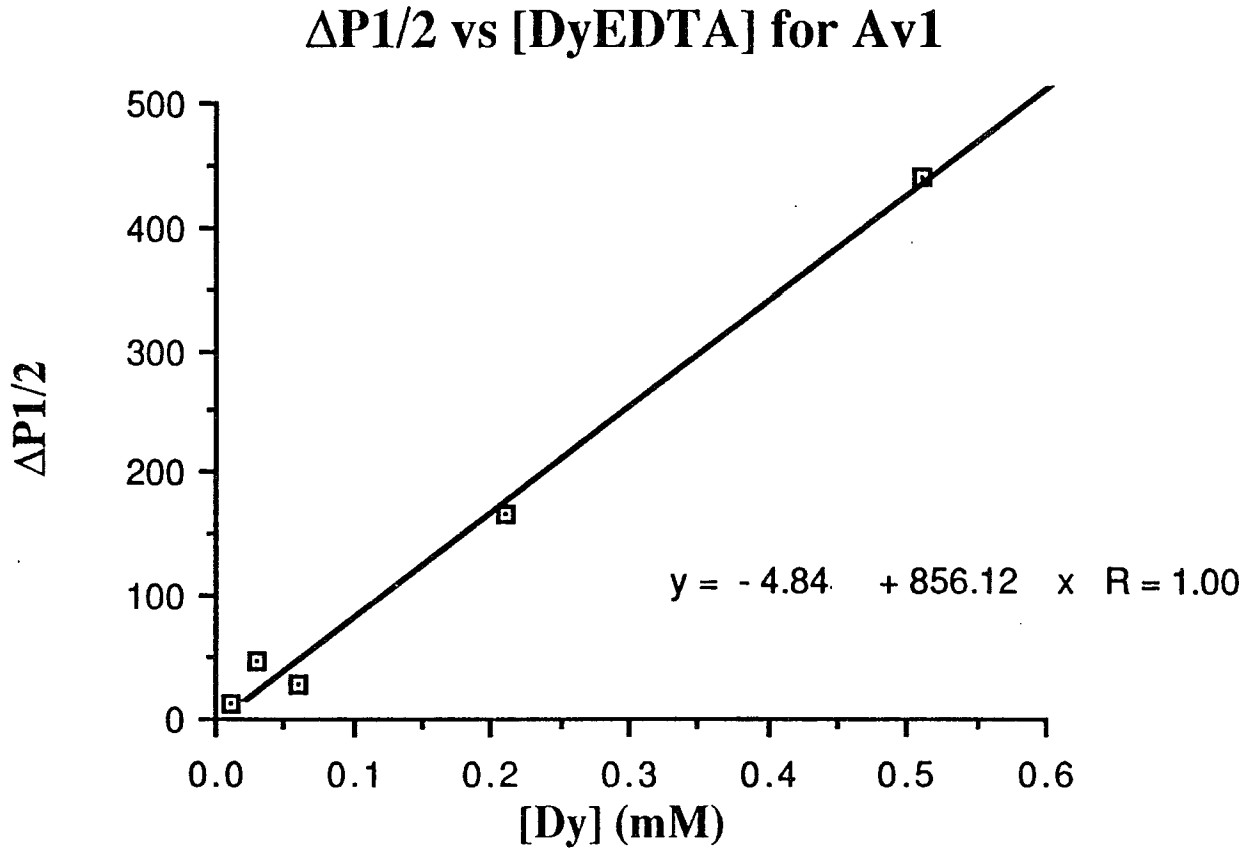

Figure 4.10. $\Delta P_{1/2}$ for Av1 Power Saturations vs. Different [DyEDTA]. [DyEDTA] ranged from 0.02 to 5.0 mM. Conditions: temperature, 3.8 K; microwave frequency, 9.46 GHz; modulation amplitude, 12.6 G.

current model in such a way as to make a large impact on our results. We propose that the current model for enhancement of relaxation of S = 1/2 spin systems by extrinsic rare earth ions be modified to take into account the faster-relaxing S = 3/2 system in Av1.

TABLE 4.4

$P_{1/2}$ Values for Power Saturation Curves of Av1 at Different [DyEDTA]

[DyEDTA] (mM)	$P_{1/2}$ (mW)
0	80
0.02	110
0.05	100
0.20	240
0.50	510
1.0	610
2.0	>720
5.0	>720

4.6.3 THIONINE OXIDATION OF Av1

Characterization of the molybdenum-iron protein by EPR, Mössbauer, MCD, and ENDOR spectroscopies has greatly enhanced our understanding of the metal clusters present in this protein. However, the number and types of P clusters present in

Av1 is still unclear. Because the P clusters are EPR-silent when the protein is dithionite-reduced, it is generally agreed that their spin is zero in this state. This is supported by Mössbauer (4.30-4.32) and MCD studies (4.33, 4.34). However, oxidation by thionine does not give rise to an observable EPR for the P clusters even though they have been assigned spins of 5/2-7/2 by magnetic susceptibiltiy (4.35), MCD (4.33), and Mössbauer (4.30-4.32) studies. The P clusters have been identified as [4Fe-4S]-like by core extrusion (4.36) and Mössbauer studies (4.30-4.32) although they are certainly a novel form of Fe-S cluster. It is generally believed that there are four P clusters per Av1 molecule. Mössbauer studies (4.30-4.32) have labeled the P clusters as the only paramagnetic species in thionine-oxidized Av1. The MCD spectra for thionine-oxidized Av1 (4.34) are in agreement with thionine-oxidized Kp1 (4.33) and with studies from component 1 from *nif* B- from Kp1 (4.37) indicating that the P clusters in the Mo-containing conventional nitrogenases are conserved from diverse nitrogen-fixing organisms.

The Av1 protein has been oxidized with thionine in repeated studies in order to better understand the relationship between the two types of metal cluster. Oxidation by thionine occurs in two phases: first P clusters and then the M centers are oxidized with subsequent loss of their characteristic S = 3/2 EPR spectrum. Five or six electrons seem to be removed in oxidizing these centers; however, there is general disagreement over how these electrons are distributed about the clusters. Values range from 3-4 electrons for P cluster oxidation and 2-3 electrons for oxidation of the M centers (4.38). There have been 9- and 12-electron oxidized species of Av1 reported as well (4.39). During oxidation of Kp1 by $Fe(CN)_6^{3-}$ (4.44), it appeared that at low $Fe(CN)_6^{3-}$ concentrations, electrons were only removed from the P clusters; at high $Fe(CN)_6^{3-}$ concentrations, electrons were also removed from the M centers. The EPR-active M

centers have been quantitated to one electron per molybdenum atom (4.31, 4.41) and when extracted from the protein, these centers act as one-electron acceptors (4.42). We can, therefore, be reasonably certain that the M centers are one-electron redox centers.

Oxidation with solid thionine has yielded some rather unusual EPR spectra, with g values of 10.4, 5.8, and 5.5 (4.43). In this study, it was proposed that there are either two P clusters which are like 8Fe ions or that there are four P clusters with 4 Fe atoms (the latter hypothesis is more conventional). The authors propose that with either model oxidation takes place by eight electrons and not the usual six, yielding P clusters with S = 7/2. Their EPR quantitations indicate that there are two paramagnetic P clusters per two M centers.

Discrepancies in electron counting may be due to the fact that these numbers have been based on protein concentrations, which are notoriously inaccurate for taking into consideration such things as amount of apoprotein present. The method we used in this study of the thionine-oxidation of Av1 was different in that we did not base the amount of added thionine on the protein concentration, but we titrated thionine in until the faintest blue remained in the protein sample for longer than 5-10 min. The study mentioned above, where the P clusters are assigned an S = 7/2, uses excess thionine and bases its electron counting on the fact that it would require eight electrons to oxidize the M centers to S = 0 and the P clusters all the way to S = 7/2.

There may, in fact, be two classes of P clusters, as suggested by Mössbauer spectroscopy of thionine-oxidized protein, P_a and P_b. The rapid-freeze EPR study of the oxidation of Kp1 (4.40) and titration of Av1 (4.44, 4.45) suggest that the first four electrons are removed from the P clusters, leaving them all in the P^{1+} oxidation level. At this level, they transiently exhibit the $g_{av} = 1.93$ EPR signal observed in the $[Fe(CN)_6^{3-}]$ oxidations and then subsequently relax into a higher spin state thought to be S = 5/2

(4.33). It was observed that the rate of decay of the transient $g_{av} = 1.93$ EPR signal was more rapid at intermediate ratios of oxidant/Av1. It was postulated that there could be interactions between pairs of P^{1+} clusters (4.40). If further electrons were removed (the M centers are oxidized) from the system to form a $P^{1+}P^{2+}$ pair, then there could be an S = 7/2 system (4.43). Questions regarding intermediate levels of oxidation of the P clusters as well as their final oxidation state are not answered in the current study. In all the studies done thus far, there is still no idea as to where the P clusters are relative to the M centers.

It is probably a good assumption that the P clusters are close enough for intramolecular electron transfer to the M centers (< 20 Å). Our question is are they close enough for magnetic interaction during oxidation? By one-electron oxidizing Av1 and looking at the saturation of the S = 3/2 EPR signal of the M center at each electron, we hoped to see changes in the saturation behavior of the M centers as each P cluster was oxidized. Changes observed in the M center relaxation with P cluster oxidation would imply that there is a magnetic interaction between the two types of metal clusters in Av1.

The samples were prepared in the following way. Dithionite-reduced Av1 was combined with methyl viologen to ensure complete reduction of all the clusters and then passed down an anaerobic dithionite-free G-25 column to rid the protein of dithionite and methyl viologen. A sample of thionine which had been prepared anaerobically and its concentration determined optically at 602 nm (ε_{602} = 56,300 $cm^{-1}M^{-1}$) was titrated into the protein sample until a faint blue color persisted for 5-10 min. The amount of thionine added was then assumed to be that required for six electrons and one-sixth of the volume was taken as the amount necessary for one electron. An EPR tube was prepared for 0-6 electrons and the power saturations performed as for the other Av1 samples, with great care taken to insure as low a temperature as possible (<3.8K).

The amplitude of the g = 3.640 EPR signal was monitored to insure complete oxidation of Av1 at six electrons added. Figure 4.11 is a plot of the amplitude of the g = 3.640 peak vs. the number of electrons taken away by thionine. As can be seen from this plot, the amplitude is fairly constant for up to four electrons. The fifth electron brings the amplitude of this signal to about one-half of the maximum that would be expected if one-half of the M centers in each Av1 molecule had been oxidized. The sixth electron then quenched the M center EPR signal entirely. These results insured us that we were indeed oxidizing Av1 in a manner that was representative of previous results.

The $P_{1/2}$ values for the power saturation curves for the thionine oxidation of Av1 were calculated for four separate trials. The data in Table 4.5 was obtained by normalizing the $P_{1/2}$ for each saturation curve to the "as is" sample. In each trial, the same general trend was observed.

This trend is shown graphically in Fiqure 4.12 where the $\Delta P_{1/2}$ vs. electrons oxidized are plotted. Our question is: what does this data say about the arrangement of the P clusters and the M centers? It is pretty clear that there are indeed magnetic interactions occurring between the P clusters and the M centers, although it is rather small, suggesting that the clusters are not close to one another. Upon oxidation by one electron, we see that the power saturation of the M center is relieved, and the increase in $P_{1/2}$ is indicative of this relief. The relief from power saturation does not really change in magnitude until the fourth electron. In this sample we see that the M center saturates at a power ($P_{1/2}$) similar to that of the "as-isolated" sample. Upon addition of the fifth electron, we observe that the M center power saturation is again relieved with a $\Delta P_{1/2}$ comparable in magnitude to the values observed for electrons 1-3. Note, however, that in the case of the sample with 5 electrons oxidized, we observed a decrease in the amplitude of the g = 3.640 EPR signal for Av1 (see Fig. 4.11) to about one-half of the

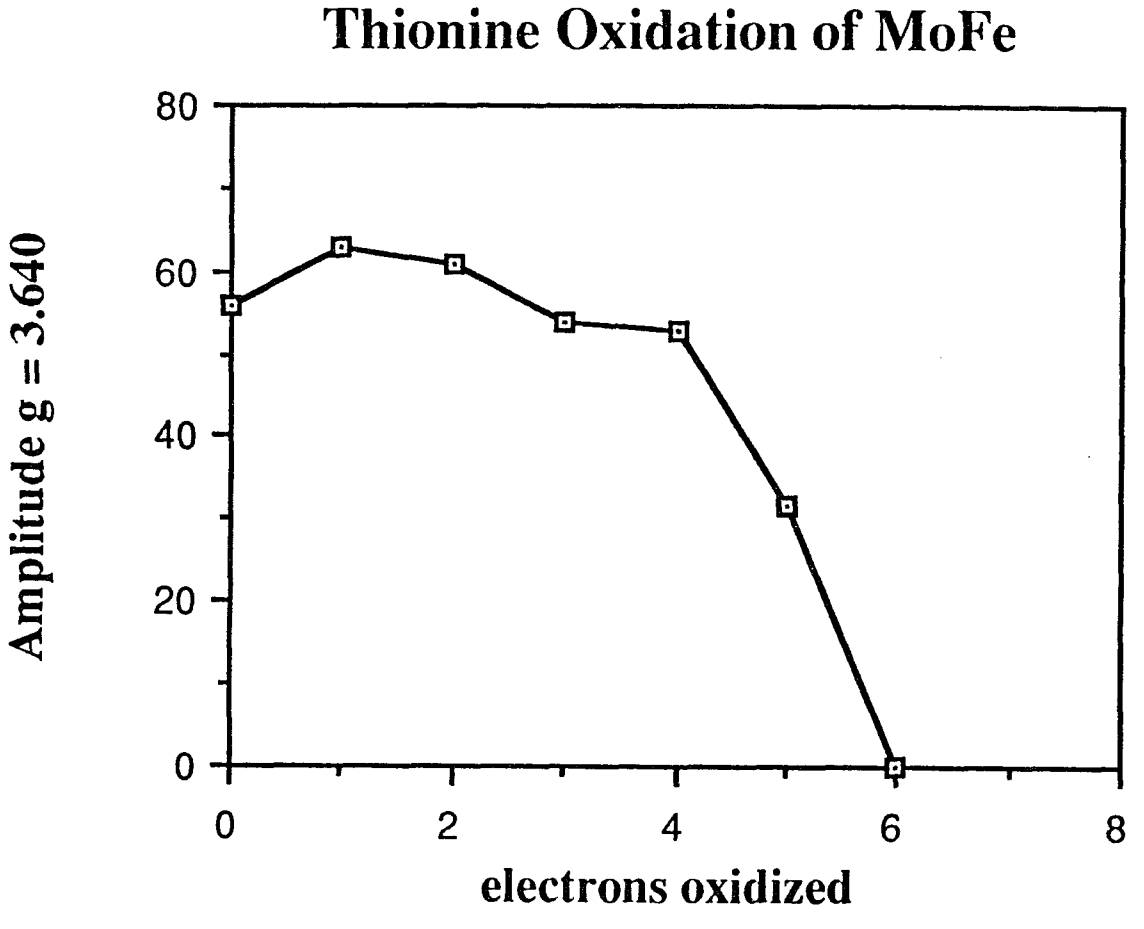

Figure 4.11. Amplitude of g = 3.640 EPR Signal of Av1 During Thionine Oxidation vs. Electrons Oxidized. The amplitude was measured from peak to trough at g = 3.640. Conditions: Microwave power, 1.0 mW; temperature, 3.8 K; modulation amplitude, 12.6 G; microwave frequency, 9.46 GHz.

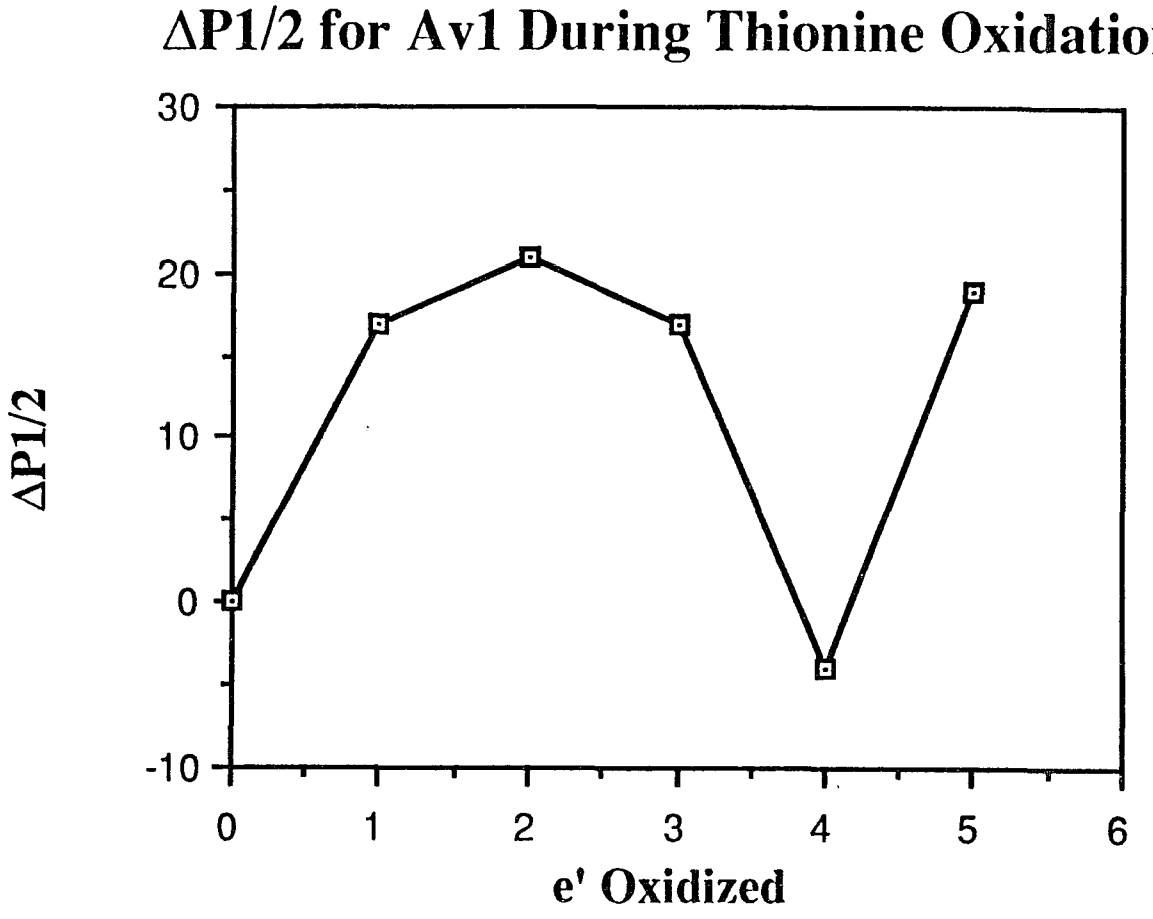

Figure 4.12. $\Delta P_{1/2}$ for Av1 Power Saturations During Thionine Oxidation vs. electrons oxidized. Conditions: temperature, 3.8 K; microwave frequency, 9.46 GHz; modulation amplitude, 12.6 G; g value = 3.64.

TABLE 4.5

$\Delta P_{1/2}$ for the Thionine Oxidation of Av1

Sample	$\Delta P_{1/2}$ (mW)
As is	0
-1 e-	17
-2 e-	21
-3 e-	17
-4 e-	-4
-5 e-	19

original maximum. This is indicative that half the M centers in Av1 have been oxidized to S = 0 and are, therefore, EPR-silent. However, we see a $\Delta P_{1/2,}$ for the sample with 5 electrons oxidized, comparable in magnitude to the samples with 1-3 electrons oxidized where there are two S = 3/2 M centers present. What does this say about the number and position of the P clusters relative to the M centers?

As discussed previously, there are two current models for the P clusters based on EPR, MCD, and Mössbauer results. The final spin state of the P clusters after oxidation by thionine has been shown to be between 5/2 and 7/2. However, in this study, we will make no predictions as to the final spin state of the P clusters. It is probably a good assumption that it is 5/2, as this has been observed most frequently by both MCD and Mössbauer spectroscopies. The biggest difference between the current models lies in the number of P clusters. There is a general disagreement as to whether

there are four distinct clusters with a [4Fe-4S]-type of arrangement, or two larger clusters with a 8Fe nuclearity. It is unclear, at this time whether the 8Fe cluster arrangement is not two [4Fe-4S]-types oriented very close together.

Based on the results presented in Figure 4.11, we can safely say that the first four electrons most probably go to the P clusters, because the g = 3.640 signal amplitude for the M centers does not fall until the fifth electron has been oxidized. Figure 4.12 shows the relationship between $\Delta P_{1/2}$ and electrons oxidized. This trend should enable us to make some predictions as to the arrangement of the P clusters relative to the M centers. Figure 4.13 shows some possible models for the arrangement of metal clusters based on our data.

The models shown in Figure 4.13 differ from one another based on the degree of interaction between the two M centers and the P clusters. Model 1 is a noninteracting model where each P cluster acts independently of the others (for the sake of argument, we assume that each M center "sees" only two of the four P clusters; as it turns out, this assumption is not necessary). Model 2 represents a semi-interacting model where the P clusters are grouped in pairs such that, when oxidized by two equivalents, the pairs of P clusters look diamagnetic to the M center. Finally, model 3 is a fully-interacting model where all the P clusters are grouped such that on even numbered oxidations the whole group appears diamagnetic.

The paramagnetic environment seen by the M centers during oxidation would, then, depend on the degree of interaction between the P clusters. This "paramagnetism" seen by the M centers can be represented by the following notation: (a) diamagnetic, 0; (b) P oxidized by one equivalent, 1, and, therefore, paramagnetic; (c) P oxidized by two equivalents, 2, also paramagnetic. The expected paramagnetic environment seen by the M centers during thionine oxidation is shown in Table 4.6.

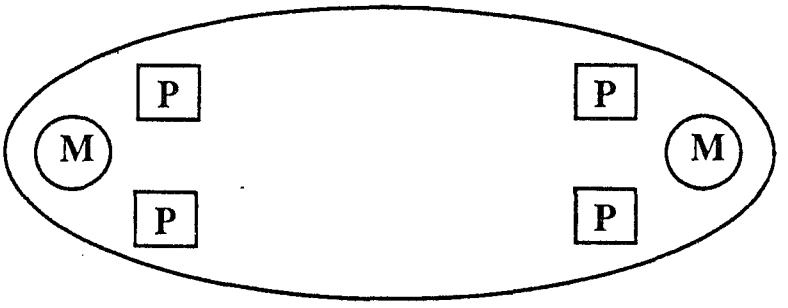

MODEL 1

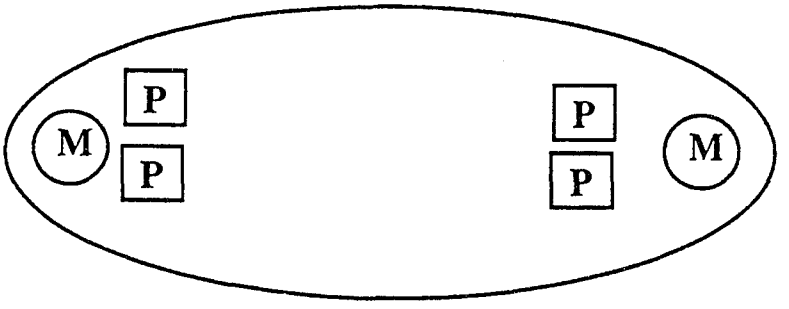

MODEL 2

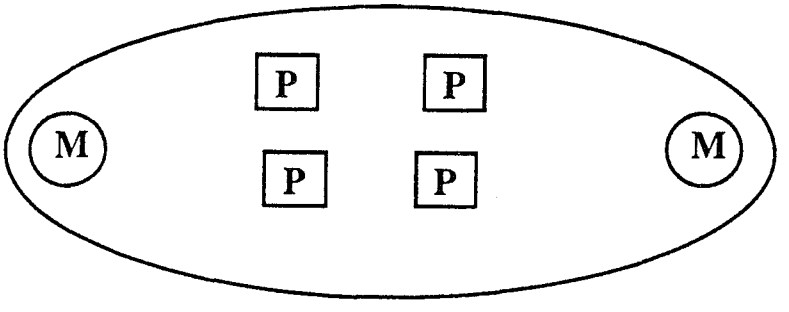

MODEL 3

Figure 4.13. Models for P Cluster and M Center Arrangement in Av1. Model 1, Noninteracting Model; Model 2, Semi-Interacting Model; Model 3, Fully Interacting Model.

TABLE 4.6

Paramagnetic Environment "Seen" by Each M Center During Thionine Oxidation

#Oxidizing Eq.	Model 1	Model 2	Model 3
0	0 & 0	0 & 0	0 & 0
1	1 & 0	1 & 0	1 & 1
2*	2 & 0 or 1 & 1	0 & 0 or 1 & 1	0 & 0
3	2 & 1	1 & 0	1 & 1
4	2 & 2	0 & 0	0 & 0

*For this situation there are two possibilities for configurations for models 1 and 2.

For model 1, both oxidizing equivalents could be with the P clusters associated with one of the M centers while the other M center sees oxidized P clusters (2 & 0), or each M sees one P cluster oxidized in its pair by one equivalent (1 & 1). In model 2, the same situation exists except that the M center associated with two oxidized P clusters sees a diamagnetic environment (0 & 0).

Based on the interactions in Table 4.6, and on the models represented in Figure 4.13, what changes might we expect for $\Delta P_{1/2}$ during thionine oxidation? The graphs in Figure 4.14 theoretically represent the results we would expect from the power saturation experiments. A comparison of Figure 4.12 with Figure 4.14 shows that our experimental data is indicative of the type of interactions represented by model 2. Therefore, based on these results, we would expect the orientation of the P clusters relative to the M centers to be representative of model 2 as shown in Figure 4.13.

4.7 CONCLUSIONS

In the studies presented here, we have examined the effects of salt, dysprosium, and oxidation by thionine on the relaxation of the M centers in Av1. The effect of ionic strength on the relaxation of the M center appears to be quite complex in nature. The effect seen in the absence of dyprosium indicates that a change is occurring in the overall structure of the protein that serves to increase the relaxation rate of the M center. A decrease in this trend was observed at the highest salt concentration used, which may also indicate a gross change in conformation. A larger range of salt concentration may serve to further investigate this effect. However, the salt range used is one in which large changes in substrate reduction are seen (4.10).

When the extrinsic relaxer, DyEDTA, is added to an identical set of samples, the same effect is observed albeit with a large relief from relaxation via the added DyEDTA. The fact that there is no apparent difficulty in DyEDTA's access to the MoFe protein would lead us to assume that salt ions are not binding to the protein.

The effect of the Dy^{3+} concentration on the change in relaxation of the M center allowed us to find the optimal amount of DyEDTA to use in the ionic strength study, and to calculate the distance of closest approach of DyEDTA to the M center. If 5 Å is allowed for the size of the dysprosium complex, we find that this distance is an unreasonable 0.1 Å. The M center is, therefore, very close to the surface of the protein. However, we are reasonably sure that it is not located right on the surface of the protein. Because Av1 is an S = 3/2 spin system, the current model for enhancement of relaxation of S = 1/2 spin systems by rare earth ions may need to be modified to take into account the much faster relaxing S = 3/2 system in Av1. Based on preliminary x-ray results, though, it is probably located at either end of an oval shape as depicted in Figure 4.13, and we believe that the M center is probably 4-5 Å below the surface of the protein.

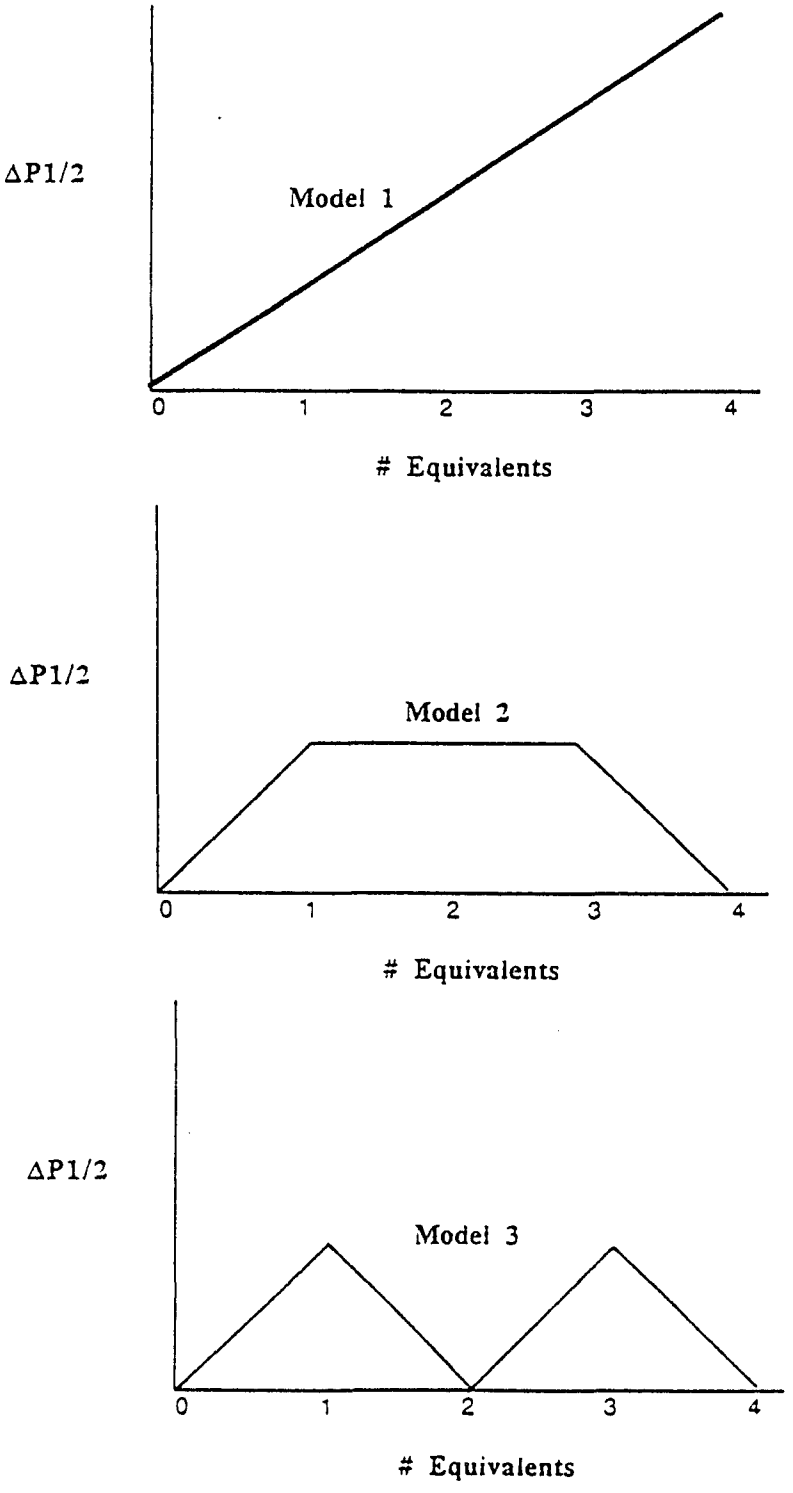

Figure 4.14. Projected $\Delta P_{1/2}$ Values For Thionine Oxidation of Av1 Based on Models 1, 2, and 3. See Figure 4.13.

The investigation of the thionine oxidation of the MoFe protein enables us to confirm results already present in the literature concerning the stoichiometry of thionine equivalents needed for oxidation and to make an educated guess as to the distribution and degree of interaction between the EPR-silent P clusters. Further investigation of the thionine oxidized samples at different temperatures may reveal some otherwise hidden resonances which may be attributable to the P clusters.

REFERENCES

4.1. Bulen, W. A., and LeCompte, J. R. (1966) Proc. Natl. Acad. Sci. U. S. A. **56**, 979-986

4.2. Shah, V. K., Davis, L. C., and Brill, W. J. (1972) Biochim. Biophys. Acta **256**, 498-511

4.3. Burns, A., Watt, G. D., and Wang, Z. C. (1985) Biochemistry **24**, 3932-3936

4.4. Guth, J. H., and Burris, R. H. (1983) Biochem. J. **213**, 741-749

4.5. Thorneley, R. N. F., and Lowe, D. J. (1983) Biochem. J. **215**, 393-401

4.6. Eady, R. R. (1980) Methods Enzymol. **69**, 753-778

4.7. Lindahl, P., Goerlick, N. J., Munck, E., and Orme-Johnson, W. H. (1987) J. Biol. Chem. **262**, 14945-14953

4.8. Willing, A. H., Georgiadis, M. M., Rees, D. C., and Howard, J. B. (1989) J. Biol. Chem. **264**, 8499-8503

4.9. Watt, G. D., Burns, A., and Lough, S. (1980) in Nitrogen Fixation (Newton, W. E. and Orme-Johnson, W. H., Eds.) Vol I, p 159, University Park Press, Baltimore, MD.

4.10. Deits, T. L., and Howard, J. B. (1990) J. Biol. Chem. **265**, 3859-3867

4.11. Rupp, H., Rao, K. K., Hall, D. O., and Cammack, R. (1978) Biochim. Biopys. Acta **537**, 255

4.12. Castner, T. G., Jr., (1959) Phys. Rev. **115**, 1506

4.13. Beinert, H., and Orme-Johnson, W. H. (1967) in Magnetic Resonance in Biological Systems (Ehrenberg, A., Malström, B. G., and Vänngard, T., Eds.), pp221-247, Pergamon Press, Oxford

4.14. Rajagopalan, K. V., Handler, P., Palmer, G., and Beinert, H. (1968) J. Biol. Chem. **243**, 3784-3796

4.15. Rajagopalan, K. V., Handler, P., Palmer, G., and Beinert, H. (1968) J. Biol. Chem. **243**, 3797-3806

4.16. Beinert, H. (1972) in Biological Applications of Electron Spin Resonance (Swartz, H. M., Bolton, J. R., and Borg, D. C., Eds.) pp. 351-410, Wiley-Interscience, New York

4.17. Suma, T., Hyde, J. S., and Swartz, H. M. (1976) Science **192**, 1132

4.18. Antholine, W. E., Hyde, J. S., and Swartz, H. M. (1978) J. Mag. Res. **29**, 517-522

4.19. Blum, H., Cusanovich, M. A., Sweeney, W. V., and Ohnishi, T. (1981) J. Biol. Chem. **256**, 2199-2206

4.20. Blum, H., Bowyer, J. R., Cusanovich, M. A., Waring, A. J., and Ohnishi, T. (1983) Biochem. Biophys. Acta **748**, 418-428

4.21. Blum, H., and Ohnishi, T. (1980) Biochem. Biophys. Acta **621**, 9-18

4.22. Blum, H. Leigh, J. S., and Ohnishi, T. (1980) Biochem. Biophys. Acta **626**, 31-40

4.23. Hyde, J. S., and Rao, K. V. S. (1978), J. Mag. Res. **29**, 509-516

4.24. Ohnishi, T., Blum, H., Harmon, H. J., and Hompo, T. (1980) in Interaction between Iron and Proteins in Oxygen and Electron Transport (Ho, C., Ed.) Elsevier/North Holland, New York

4.25. Münck, E., Rhodes, H., Orme-Johnson, W. H., Davis, L. C., Brill, W. J., and Shah, V. K. (1975) Biochim. Biophys. Acta **400**, 32

4.26. Zimmermann, R., Münck, E., Brill, W. J., Shah, V. K., Henzl, M. T., Rawlings, J., and Orme-Johnson, W. H. (1978) Biochim. Biophys. Acta **537**, 185

4.27. Kurtz, D. M., McMillan, R. S., Burgess, B. K., Mortenson, L. E., and Holm, R. H. (1979) Proc. Natl. Acad. Sci. U. S. A. **76**, 4986

4.28. McLean, P. A., Papaefthymiou, V., Orme-Johnson, W. H., and Münck, E. (1987) J. Biol. Chem. **262**, 12900

4.29. Lindahl, P. A., Day, E. P., Kent, R. A., Orme-Johnson, W. H., and Münck, E. (1985) J. Biol. Chem. **260**, 11160-11173

4.30. Zimmermann, R., Münck, E., Brill, W. J., Shah, V. K., Hentzl, M. T., Rawlings, J., and Orme-Johnson, W. H. (1978) Biochim. Biophys. Acta **537**, 185-207.

4.31. Münck, E., Rhodes, H., Orme-Johnson, W. H., Davis, L. C., Brill, W. J., and Shah, V. K. (1975) Biochim. Biophys. Acta **400**, 32-53

4.32. Dunham, W. R., Hagen, W. R., Braaksma, A., Grande, H. J., and Haaker, H. (1985) Eur. J. Biochem. **146**, 497-501

4.33. Johnson, M. K., Thomson, A. J., Robinson, A. E., and Smith, B. E. (1981) Biochim. Biophys. Acta **671**, 61-70

4.34. Morningstar, J. E., Johnson, M. K., Case, E. E., and Hales, B. J. (1987) Biochemistry **26**, 1795

4.35. Smith, J. P., Emptage, M. H., and Orme-Johnson, W. H. (1982) J. Biol. Chem. **257**, 2310-2313

4.36. Kurtz, D. M., McMillan, R. S., Burgess, B. K., Mortenson, L. E., and Holm, R. H. (1979) Proc. Natl. Acad. Sci. U. S. A. **76**, 4986-4989

4.37. Robinson, A. E., Richards, A. J. M., Thomson, A. J., Hawkes, T. R., and Smith, B. E. (1984) Biochem. J. **219**, 495-503

4.38. Stephens, P. J. (1985) in Molybdenum Enzymes (Spiro, T. G., Ed.) pp.117-159, Wiley, New York

4.39. Watt, G. D. (1985) in Nitrogen Fixation Research Progress (Evans, H. J., Bottomley, P. J., and Newton, W. E., Eds.) pp. 585-590, Nijhoff, Dordrecht

4.40. Smith, B. E., Lowe, B. J., Chen, G. X., O'Donnell, M. J., and Hawkes, T. R. (1983) Biochem. J. **209**, 207-213

4.41. Euler, W. B., Martinsen, W. J., McDonald, J. W., Watt, G. D., and Wang, Z. C. (1984) Biochemistry **23**, 3021-3024

4.42. Schultz, F. A., Gheller, S. F., Burgess, B. K., Lough, S., and Newton, W. E. (1985) J. Am. Chem. Soc. **107**, 5364-5368

4.43. Hagen, W. R., Wassink, H., Eady, R. R., Smith, B. E., and Haaker, H. (1987) Eur. J. Biochem. **169**, 457-465

4.44. Orme-Johnson, W. H., Lindahl, P., Meade, J., Warren, W., Nelson, M., Grog, S., Orme-Johnson, N. R., Münck, E., Huyhn, B. H., Emptage, M., Rawlings, J., Smith, J., Roberts, J., Hoffmann, B., and Mims, W. B. (1981) in Current Perspectives in Nitrogen Fixation (Gibson, A. H., and Newton, W. E., Eds.) pp. 79-83, Australian Academy Of Science, Canberra

4.45. Morgan, T. V., Mortenson, L. E., McDonald, J. W., and Watt, G. D. (1988) J. Inorg. Biochem. **33**, 111-120

THE IRON PROTEIN OF *Azotobacter vinelandii*

Exploring the Effects of Temperature, Salt, MgATP, and Dysprosium on the Relaxation of the S = 1/2 EPR Signal of the Fe Protein

5.1 INTRODUCTION

The structure and properties of the iron (Fe) protein have already been discussed in the introduction (see section 1.2). Briefly, the Fe protein (60 - 65 kDa) is a γ_2 dimer protein consisting of two identical subunits (5.1) each having a MW ~ 30,000 (5.2, 5.3). The dimeric nature of the protein was determined by gel filtration chromatography and ultracentrifugation measurements (5.4-5.7). The Fe protein is generally accepted as being the electron donor to the MoFe protein during turnover of the enzyme (5.8-5.12) as well as the site of ATP binding (5.13, 5.14).

The Fe protein of any nitrogenase complex possesses one [4Fe-4S] cluster (5.12, 5.15, 5.16). This composition was first based on iron and sulfide determinations from various Fe proteins isolated from different bacteria, such as *Clostridium pasteurianum* (5.4, 5.7, 5.17, 5.18), *Azotobacter chroococcum* (5.19), *Klebsiella pneumoniae* (5.5), and *Azotobacter vinelandii* (5.20). In general, there is an average of 3.7 iron atoms and 3.3 sulfur atoms per protein molecule. Evidence that these iron atoms were present in one [4Fe-4S] center came from cluster extrusion studies from *C. pasteurianum* component 2 (5.21-5.24).

The homology in the Fe protein sequences is quite high: Av2 and Kp2 are 90% homologous, while other species show about 60% homology (5.25-5.28). There are five completely conserved cysteines in all known Fe protein sequences (5.29). These cysteines, numbered according to the Av2 sequence, are located at residues 38, 85, 97, 132, and 184 (5.30). Cysteines 97 and 132 were identified, through labeling, as the four ligands (two per subunit) necessary for ligation of the [4Fe-4S] where the cluster is bound with twofold symmetry between the identical subunits (5.30). At this time, cysteines 38 and 85 had been proposed as associated with the ATP-binding sites (5.30, 5.31). Furthermore, these labeling studies also showed that Av2 contains no disulfides, hyperactive thiols, or surface thiols (5.30). However, Av2 does not contain the usual pattern of conserved cysteines found in iron-sulfur ferredoxins: CysxxCysxxCys.

Mutant strains of *A.vinelandii* Fe protein were recently constructed by substituting serine for each of the five conserved cysteines (5.32). At least moderate activity (>10% of wild type enzyme) was found for substitutions at cysteines 38, 85, and 134; whereas no activity was found for component 1 or 2 when serines substitued for cysteines at residues 97 and 132. This is consistent with 97 and 132 being the ligands to the [4Fe-4S] cluster in the Fe protein. Furthermore, if either cysteine 97 or 132 is replaced, it appears that a functional Fe:S cluster cannot be incorporated into apo-Fe-protein (5.32). The surprising result is the loss of component 1 activity when these substitutions are made. It had been known that the Fe protein is required for biosynthesis of the FeMo-cofactor (5.33-5.39). It appears that wild type apo-Av2 cannot support cofactor synthesis without containing an active Fe:S cluster. Burgess has also shown that component 2 may be necessary for cofactor incorporation (5.34, 5.36). Finally, substitutions made at cysteines 38, 85, and 132, which result in at least some level of

activity, indicates that earlier predictions (5.30) concerning cysteines 38 and 85 as components of the MgATP binding site are incorrect (5.32).

The Fe protein binds two MgATP (or MgADP) molecules (5.40, 5.41). There are at least two regions, from residues 1-30 and 85-110 (5.30, 5.42), which may be involved in the binding of the adenylate portion of ATP and/or ADP since the residues in these regions are somewhat homologous to the nucleotide binding residues of adenylate kinase. An ongoing determination of the crystal structure of Av2 (5.43) addresses the probable site of nucleotide binding and finds a site where molybdate binds 20 Å from the Fe:S cluster. Molybdate is believed to be acting as a phosphate analog, and this site may be the position at which the terminal phosphate of the nucleotide binds.

5.2 ELECTRON PARAMAGNETIC RESONANCE SPECTRUM OF THE Fe PROTEIN

EPR studies of reduced Fe protein show the presence of a signal with resonances at $g_z = 2.06$, $g_y = 1.94$, and $g_x = 1.87$ (5.44, 5.45). This signal is similar to the g = 1.94 spectra of reduced $[2Fe\text{-}2S]^{1+}$ and $[4Fe\text{-}4S]^{1+}$ clusters in simple Fe:S proteins. This signal cannot be seen at temperatures higher than about 35 K due to relaxation broadening, which is characteristic of $[4Fe\text{-}4S]^{1+}$ signals of the ferredoxin type (5.5, 5.46). There are two features of this EPR signal that are unusual (5.23, 5.47). First, the g-value anisotropy and broadness of the signal is somewhat atypical for ferredoxin-type $[4Fe\text{-}4S]^{1+}$ centers; second, the double integration of the g = 1.94 signal gives low values for the spin quantitation. These spin quantitations consistently yield about 0.3-0.4 spins/molecule (5.23, 5.44, 5.45, 5.48-5.52) rather than the expected 1 spin/molecule (5.53), as suggested by a report on potentiometric studies of Av2 (5.3) that shows a transfer of one electron per molecule.

Explanations for the unusual EPR behavior of the [4Fe-4S] cluster in the Fe protein ranged from there being another EPR-silent metal cluster also present in the Fe protein (5.54), which would broaden some of the signal beyond detection, to the low spin quantitations being the result of samples with low specific activity (5.11). The former explanation was not supported by metal analyses of the protein (5.5, 5.52) or by room temperature absorption, CD, and MCD studies (5.55). Spin quantitations were reported of 1 spin/molecule which could be achieved if the protein were present in 50% ethylene glycol (5.52). It was also shown that in the presence of 0.5 M urea, the EPR signal disappears (5.50). These effects of urea and ethylene glycol were further characterized by EPR and Mössbauer spectroscopies, and magnetic susceptibility (5.56-5.58). The "EPR-silent" urea state showed low-field EPR resonances with g-values of 5.8 and 5.15 which are attributable to a cluster with an S = 3/2 ground state. Mössbauer spectra supported the evidence of an ethylene glycol state which quantitated by EPR to 1 spin/molecule and originates from a standard S = 1/2 $[4Fe\text{-}4S]^{1+}$--type cluster. The native Av2 Mössbauer spectrum can be simulated by summing a 40% contribution from the ethylene glycol spectrum and a 60% contribution from the urea spectrum. Therefore, the low spin integrations observed in the Fe protein can be attributed to a mixture of spin states for the $[4Fe\text{-}4S]^{1+}$ cluster, with 40% in the S = 1/2 form that exhibits the g = 1.94 signal and 60% in the S = 3/2 form that exhibits the g = 5 signal (5.56). It should be noted here that all of the studies on the distribution of spin state in the Fe protein were done on frozen solutions at cryogenic temperatures. A recently published NMR study done on room-temperature Fe protein from *C. pasteurianum* suggests that the magnetic properties of the [4Fe-4S] center assumed a spin-state ladder similar to those occurring in proteins that display a single S = 1/2 ground spin state at

low temperature (5.59). Furthermore, these properties do not change when nucleotide is bound to the Fe protein.

5.3 NUCLEOTIDE BINDING TO THE Fe PROTEIN

There are several studies involving the effects of nucleotide binding to the Fe protein. It is known that MgATP binds to the Fe protein at two possible sites (5.60). It has also been shown that MgADP binds to the Fe protein more tightly than MgATP and that the former competes for at least one of the two binding sites (5.60). Because MgATP binds tighter in the presence of the MoFe protein, the presence of the nucleotide appears to affect the association of the two components of nitrogenase. It has been suggested that the nucleotide may, in fact, bridge the Fe protein and the MoFe protein during catalysis (5.61, 5.62).

Six physical changes occur in the Fe protein upon MgATP binding. The redox potential of the Fe-S cluster is lowered from -290 to -400 mV (5.63). The EPR spectrum changes from rhombic to more axial symmetry (5.44, 5.49, 5.50), presumably as a result of a conformational change in the vicinity of the $[4Fe\text{-}4S]^{1+}$ cluster (5.61, 5.63). (The nucleotide-bound Fe protein has been shown to exist in an S = 1/2 and S = 3/2 mixture, with the latter exhibiting a broad EPR signal at g = 5-6) (5.58, 5.64). The CD and MCD spectra of the Fe protein are altered (5.65). Chelation of the iron present in the Fe:S cluster occurs (5.9, 5.48). The ^{57}Fe quadrupole splittings in the Mössbauer spectra for the Fe protein decrease (5.56). The crystals of the protein are destabilized (5.66). The latter effect is not observed when MgADP is added to the Fe protein (5.66). The redox properties of both states have been found to be identical (5.67) in the presence and absence of ATP or ADP, and no noticable changes were seen in the EXAFS of the MgATP-bound protein (5.68), indicating that the conformational

change probably causes very little structural change in the cluster. This is further supported by NMR data which show that shifted proton resonances associated with ligation of the cluster are insensitive, for the most part, to the presence of MgATP, indicating that there is not a drastic structural change in the vicinity of the active site (5.59). However, MgADP was shown to induce major shifts in proton resonances.

The crystal structure of Av2 (5.43) at 3 Å resolution shows that the Fe:S cluster is set between the two identical subunits as a "gem" in a setting. The twofold symmetric ligation seen in Av2 is consistent with the results of chemical modification (5.30), genetic data (5.32), and NMR studies (5.59).

The NMR studies (5.59) found that nucleotide binding only affected a few of the proton resonances thought to be associated with the cysteines ligating the cluster. This would indicate that the presence of the nucleotide is only affecting one part of the cluster. In fact, the most remarkable effect of MgATP on the spectra was the grouping of the shifted proton resonances into sets of two or four having identical chemical shifts and temperature dependencies. These results further support the twofold symmetrical ligation of the metal cluster.

In a recent paper published on the pulsed EPR spectrum of the Fe protein and its interactions with MgATP and D_2O (5.69), it was found that the "solvent accessibility" of the [4Fe-4S] cluster is very different from that seen in other [4Fe-4S]-containing proteins. In the latter, changes in the deuterium modulations of the echo envelope only took place after incubations of as long as 24 hours. The Fe protein, however, showed that deuterium exchange was essentially complete in 15 seconds. This apparent solvent accessibility is not changed by the presence of MgATP. This result is supported somewhat by the crystal structure of the Fe protein in that the cluster is close to the surface of the protein structure. However, this result is in contrast to the iron chelation

studies which require MgATP in order for chelators to get to the cluster. It could be that the so-called conformational change evoked by MgATP only changes the cluster environment in such a way that the iron chelators are able to get to the cluster. This may or may not be supported by the existence of two conformers upon MgATP binding (5.70). It is exactly this type of question that we hoped to be able to answer with the studies presented here involving MgATP and Dy.

The Electron Paramagnetic Resonance studies presented here for Av2 are much like those for Av1 in that we were concerned with the relaxation of the metal cluster and how it is affected by temperature, salt, and dysprosium. We also examined the effect of MgATP on the relaxation of the S = 1/2 signal in Av2 with and without the presence of the extrinsic relaxer Dy. Although there have been a number of studies investigating the mixture of spin states that exists for component 2, we will only be concerned with the S = 1/2 EPR signal in these studies.

5.4 RESULTS

5.4.1 THE EFFECT OF TEMPERATURE ON THE POWER SATURATION OF Av2

Our samples of component 2 as purified in our laboratory contain what we believe to be a small amount of contaminating flavoprotein, which also exhibits an EPR signal in the g = 2 region. Figure 5.1 shows an example of this mixture of signals that we see along with a component 2 spectrum which lacks this signal. The flavoprotein signal is similar to a free radical in its shape, g-value, and relaxation properties. Because the spectrum of the flavoprotein is much narrower than that of component 2, its presence can still be observed at low concentration. Furthermore, it saturates a lot easier than the

S = 1/2 signal of Av2 does and is, therefore, smaller in amplitude as the power is increased.

Because of the impurity mentioned above and the apparent complexity of the Av2 signal, we first investigated the effect of temperature on the saturation of the S = 1/2 signal of Av2. This signal is already saturated at low powers at the temperature needed for the component 1 studies, 4K. Figure 5.2 shows the effects of temperature on the power saturation of Av2. Therefore, in order to study saturation of Av2, it was necessary to obtain a temperature that showed the best classical saturation curve (i.e., such as those seen in Figure 4.1). As can be seen from Figure 5.2, there is really no such thing as a classical saturation curve for Av2 at any temperature such as those seen in Chapter 4. However, 8K gives the best saturation profile obtainable for Av2.

Temperatures were controlled in these experiments by adjusting the flow of liquid helium via a needle control valve located on the helium transfer line. The temperature was monitored by a digital readout on an Oxford Instruments ITC4 model Temperature Controller. Because of the dynamics involved in the design of the cryostat, without a separate thermocouple which may be inserted into the sample holder, the temperature displayed by the digital readout is not as accurate as we would like.

In a previous study (5.71) on the temperature dependence of Av2, it was found that the signal at g = 1.94 was saturated even at 9 K at a power of 20 mW. They observed a power saturation range between 13 and 20 K. This range is indicative of isolated [4Fe-4S] clusters. At 12 K we observed power saturation behaviour closer to previously published data taken at 20K. It should be noted that the shape of their power saturation curves are more "classical" at 13 K than any curve we obtained at any temperature. The reason for this difference in saturation behavior is not known. It is unlikely that there is a temperature difference large enough such that our 8 K data looks more like the

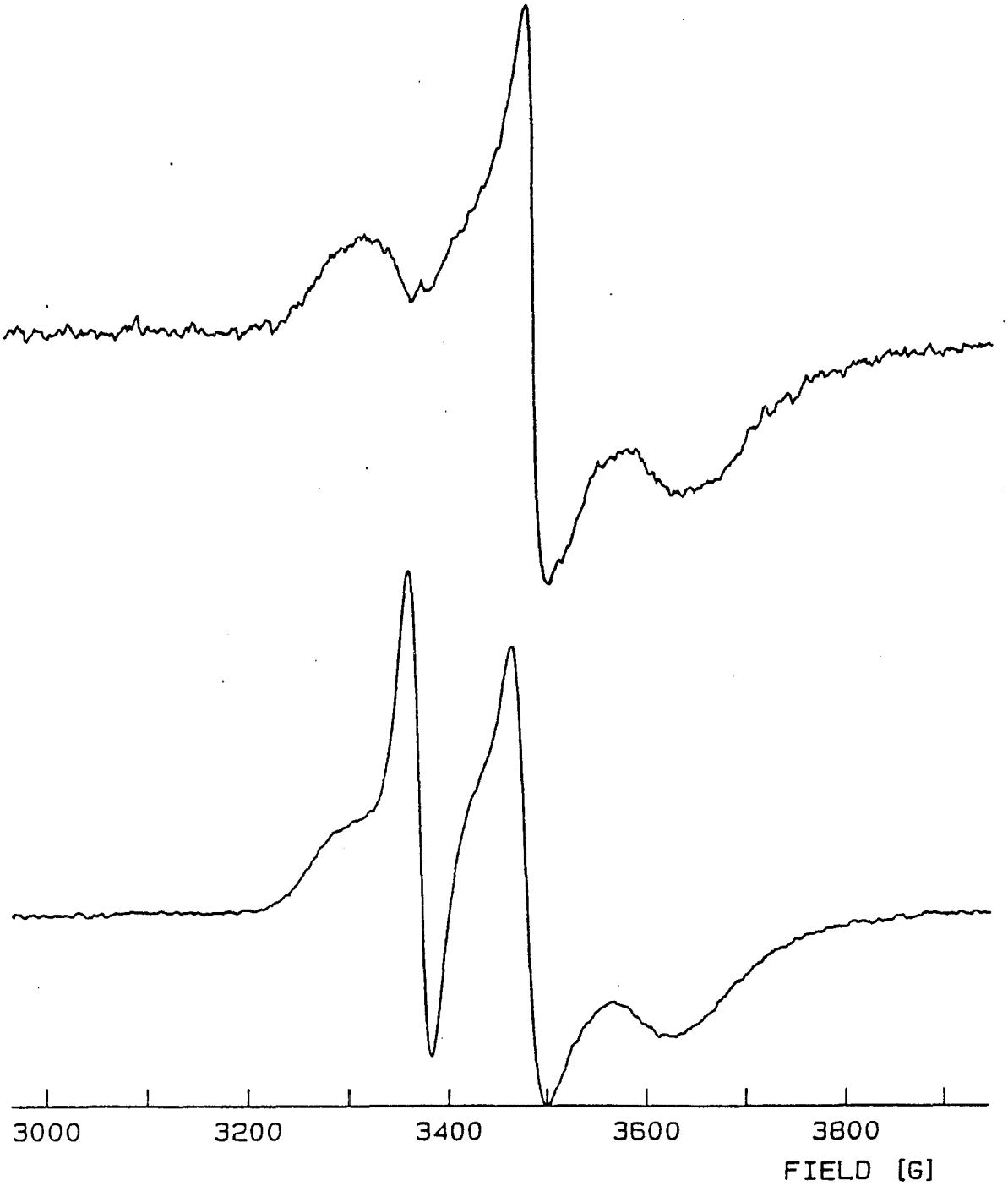

Figure 5.1 EPR spectra of Av2 with and without Flavoprotein Contaminant Conditions: microwave frequency, 9.46 GHz; modulation frequency, 100 kHz; modulation amplitude, 12.6 G; scan time, 84 s; time constant, 0.33 s; power, top, bottom,; temperature, 8K; protein concentration, top, 38 mg/ml, bottom, 42 mg/ml; g values for Av2: 2.05, 1.94, and 1.86, for flavoprotein signal g = 2.000.

published 13 K data. What is more puzzling is the shape of our power saturation curves. However, it is not likely that this "unclassical" shape is due to the flavoprotein impurity or to rapid passage effects.

5.4.2 THE EFFECT OF SALT ON THE SATURATION OF AV2

Azotobacter vinelandii nitrogenase activity is strongly inhibited by the presence of electrolytes as discussed in Chapter 4 (see section 4.6.1) (5.72). It is thought that this inhibition is mainly due to prevention of the component proteins from interacting during the catalytic cycle and, therefore, a decrease in activity is seen with increasing salt. As was observed for the MoFe protein, there are minimal effects by NaCl on the spectral features of the Fe:S cluster of Av2 as seen by EPR (5.64), visible, and NMR spectroscopy.

Recently, a study on nitrogenase inhibition by salt (5.73) showed that NaCl had a large inhibitory effect on the Fe protein Fe:S cluster reactivity to chelators. The apparent association constant for MgATP increases as the salt concentration increases, and even high [MgATP] cannot completely overcome NaCl inhibition. Therefore, NaCl is affecting both substrate reduction and the apparent association constant for MgATP (5.73).

When MgATP is added to the Fe protein, the Fe:S cluster becomes accessible to iron chelators as mentioned before. It has been suggested that this chelation may involve two conformers of the Fe protein (5.70), and salt may affect the ratio between them. However, the primary effect of salt seems to be inhibition of iron chelation and not redistribution of the conformers (5.73).

Salt acts to inhibit nitrogenase in two ways: by affecting the affinity of Av2 for MgATP, and by preventing the Av2Av1 complex from forming (5.73). In this way

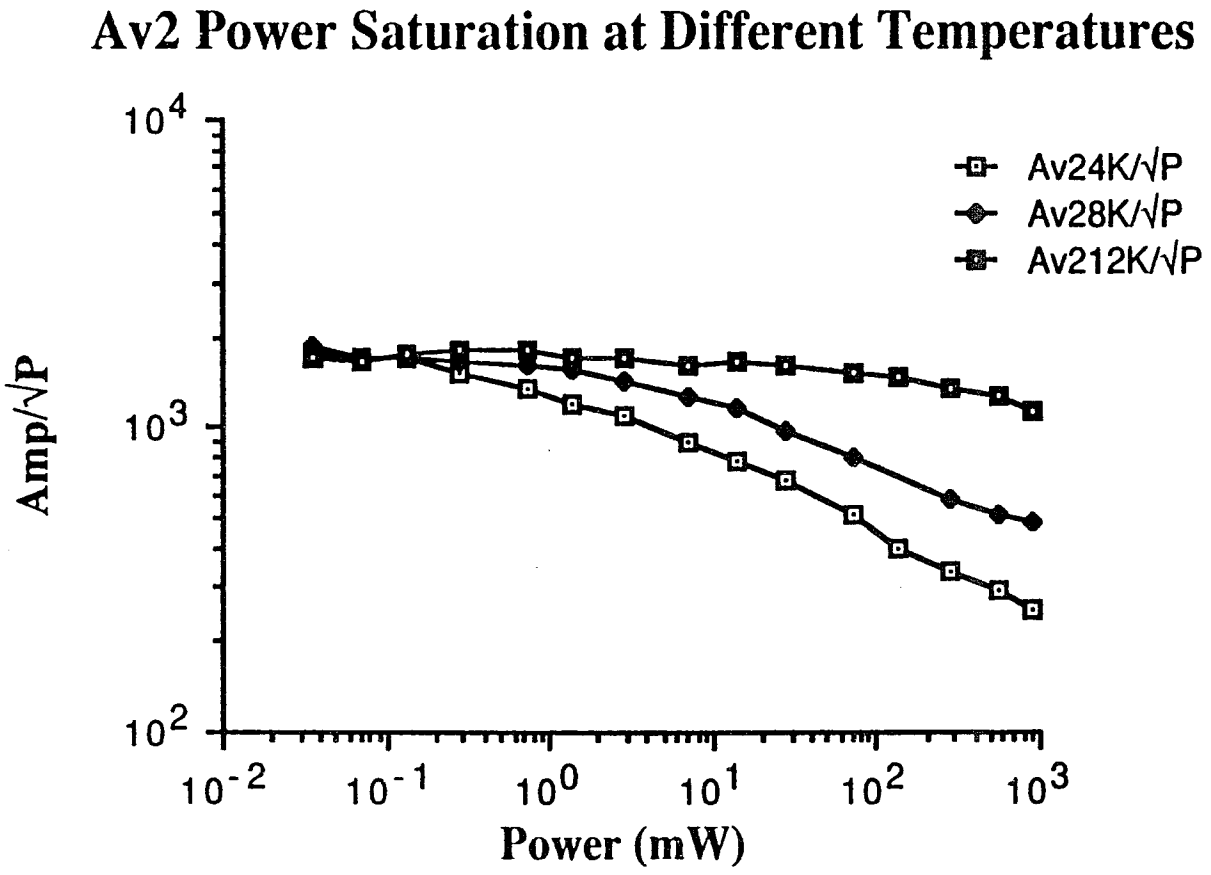

Figure 5.2 Power Saturation Curves for Av2 at Different Temperatures Conditions: microwave frequency, 9.46 GHz; modulation frequency, 100 kHz; modulation amplitude, 12.6 G; power: .029-700 mW; temperature, 8 K; protein concentration, 35 mg/ml; g value = 1.94.

NaCl is acting as a competitive inhibitor by removing one of the component proteins. The apparent K_I changes only twofold over a 40-fold increase in component ratio. This implies that the association of Av1 for salt-free Av2 is more favorable than the association of the individual protein components and salt.

In the studies presented here we did not look at how salt affected MgATP binding, but instead we were interested in how salt affected the saturation of the S = 1/2 center of Av2. If there is a correlation between a binding site for salt and that for MgATP, it was not addressed here.

The samples were prepared using the procedure outlined for Av1 samples in chapter 4. The NaCl concentration ranged from 0.05 to 0.20 M salt. Matched samples were also prepared with and without dysprosium. Initially, the optimum dysprosium concentration was determined for Av2 saturation. Based on the temperature dependent results described above, the power saturation studies were performed at 8K.

The results of the power saturations for the samples containing different concentrations of salt are shown in Figure 5.3. The $P_{1/2}$ values were determined for these saturation curves and are listed in Table 5.1.

Unlike Av1, Av2 does not crystallize at low salt concentrations. The effect of salt on Av2, however, seems to be similar to that for Av1. In Av1, the $P_{1/2}$ values for the power saturations at different salt concentrations increased up to a salt concentration of 0.15 M salt. The $P_{1/2}$ values for Av2 only increased up to a salt concentration of 0.10 M salt and then decreased at 0.20 M salt.

The studies performed on the inhibition of catalytic activity by salt showed that at a salt concentration of 0.1 M, there was almost 100% activity. However, as the salt concentration increased to 0.2 M, the inhibition of activity became dramatic. The results

TABLE 5.1

$P_{1/2}$ Values for the Power Saturation of Av2 in the Presence of Different [NaCl]

[NaCl] (M)	$P_{1/2}$ (mW)
0.05	52
0.10	76
0.20	57

presented in Table 5.1 show a change in the saturation behavior after 0.10 M salt. The dynamics of the salt inhibition may involve changes in conformation which may affect the saturation behavior of the [4Fe-4S] cluster in Av2. It is believed that these interactions are quite complex, and from what we have seen here, we agree.

The results seen in Table 5.2 and in Fig. 5.4 provide further evidence of the complex saturation effects seen in the salt concentration range of 0.1 to 0.2 M. There has been no direct evidence of aggregation of Av2 molecules occurring at low salt. It is tempting to invoke this argument to explain the data seen in both Tables 5.1 and 5.2, but there is not enough evidence to do so. Further studies on this system should include a larger range of salt concentration, to about 0.6 M salt.

5.4.3 THE EFFECT OF [DyEDTA] ON THE SATURATION OF Av2

The interaction of DyEDTA with the [4Fe-4S] center of Av2 was investigated in the same way as was done with Av1 in Chapter 4. Samples of Av2 were prepared at a

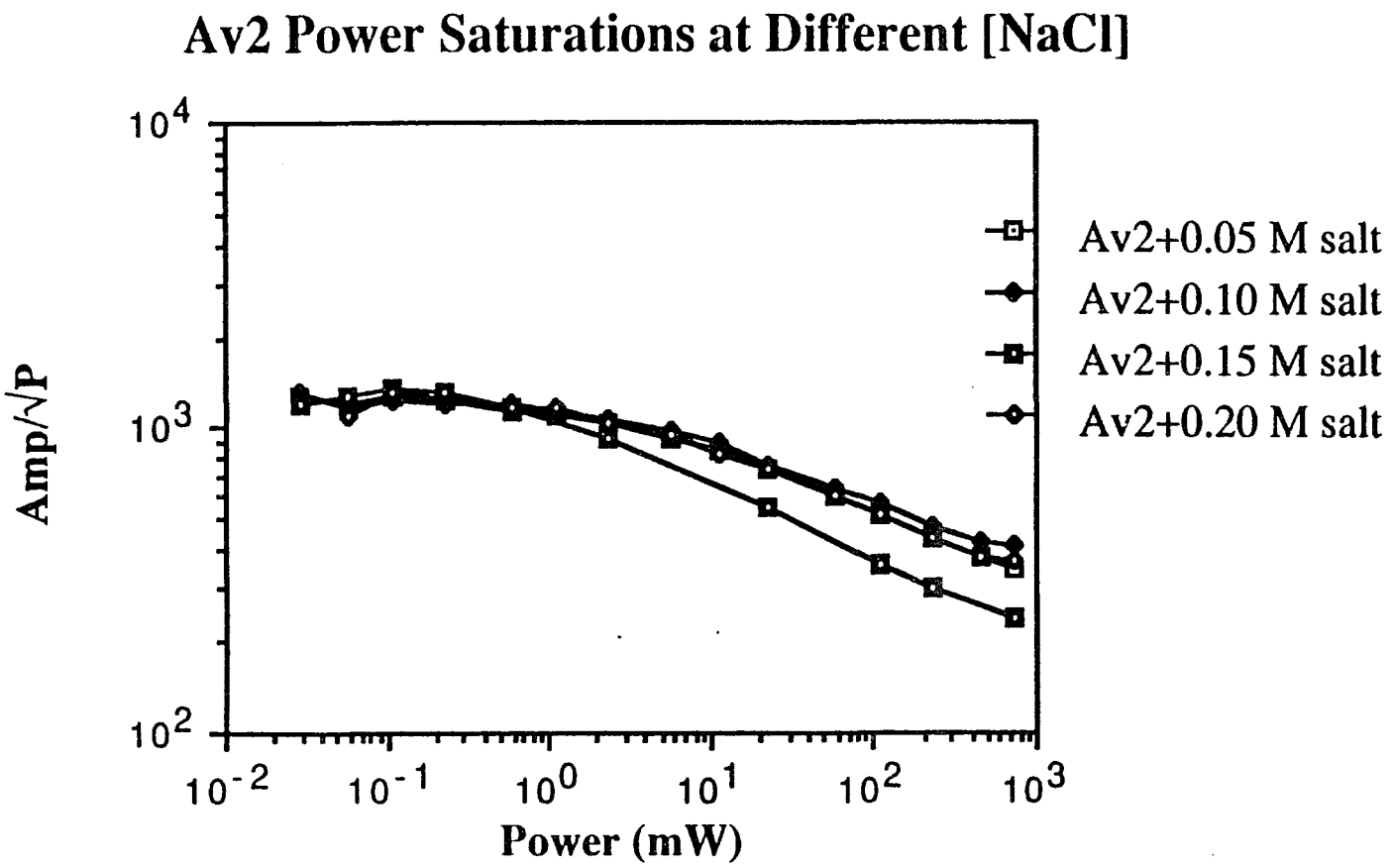

Figure 5.3 Power Saturation Curves for Av2 at Different Salt Concentrations Conditions: microwave frequency, 9.46 GHz; modulation frequency, 100 kHz; modulation amplitude, 12.6 G; power: .029-700 mW; temperature, 8 K; protein concentration, 35 mg/ml; g value = 1.94.

median salt concentration of 0.1 M, and DyEDTA was added in increasingly larger concentrations. The power saturations were performed at 8 K as for the salt samples. The power saturation curves for Av2 at different [DyEDTA] are plotted in Figure 5.5.

TABLE 5.2

$P_{1/2}$ Values for the Power Saturation of Av2 in the Presence of Different [NaCl] and 0.2 mM DyEDTA

[NaCl]	$P_{1/2}$	$\Delta P_{1/2}$ (with Dy-without Dy)
0.10	20	-50
0.20	55	-2

The $P_{1/2}$ values for the power saturation curves of Av2 at different [DyEDTA] are listed in Table 5.3. The data presented in Table 5.3 has been normalized with respect to the as-isolated sample, and the corresponding $\Delta P_{1/2}$ values are listed for each sample. The plot of $\Delta P_{1/2}$ vs. [DyEDTA] is shown in Figure 5.6.

The distance between the DyEDTA complex and the metal cluster can be quantitatively calculated based on how $P_{1/2}$ changes with the Dy concentration. As presented in Chapter 4, the relief of saturation ($\Delta P_{1/2}$) is dependent on the distance between two paramagnets by r^{-6} as seen below:

$$\Delta P_{1/2}\ (\text{mW/mM}) = 4.12 \times 10^{8}\ r^{-6} \exp(-12.5/T)$$

TABLE 5.3

$P_{1/2}$ Values for the Power Saturation Curves of Av2 at Different [DyEDTA]

[DyEDTA]	$P_{1/2}$	$\Delta P_{1/2}$
0	0.6	0
0.2	17	16
0.5	30	30
1.0	95	95
2.0	149	148
5.0	356	355

Figure 5.6 is a plot of how $\Delta P_{1/2}$ changes with [DyEDTA] for Av2 at 8 K. The plot is linear with DyEDTA and, therefore, the slope of this region is representative of $\Delta P_{1/2}/\Delta$[Dy]. The slope of this line corresponds to 71 mW/mM and would yield r equal to 5 Å after allowing for 5 Å for the DyEDTA complex. Therefore the distance of closest approach between the DyEDTA complex and that of the [4Fe-4S] center in Av2 is 5 Å. This result agrees qualitatively with the recently published crystal structure of Av2 which puts the Fe:S cluster close to the surface of the protein (5.43).

5.4.4 THE EFFECT OF MgATP ON THE SATURATION OF Av2

The effect of MgATP on the Fe protein has been discussed already. Our objective was to link the Dy effect with the effect of MgATP. If the [4Fe-4S] cluster is more

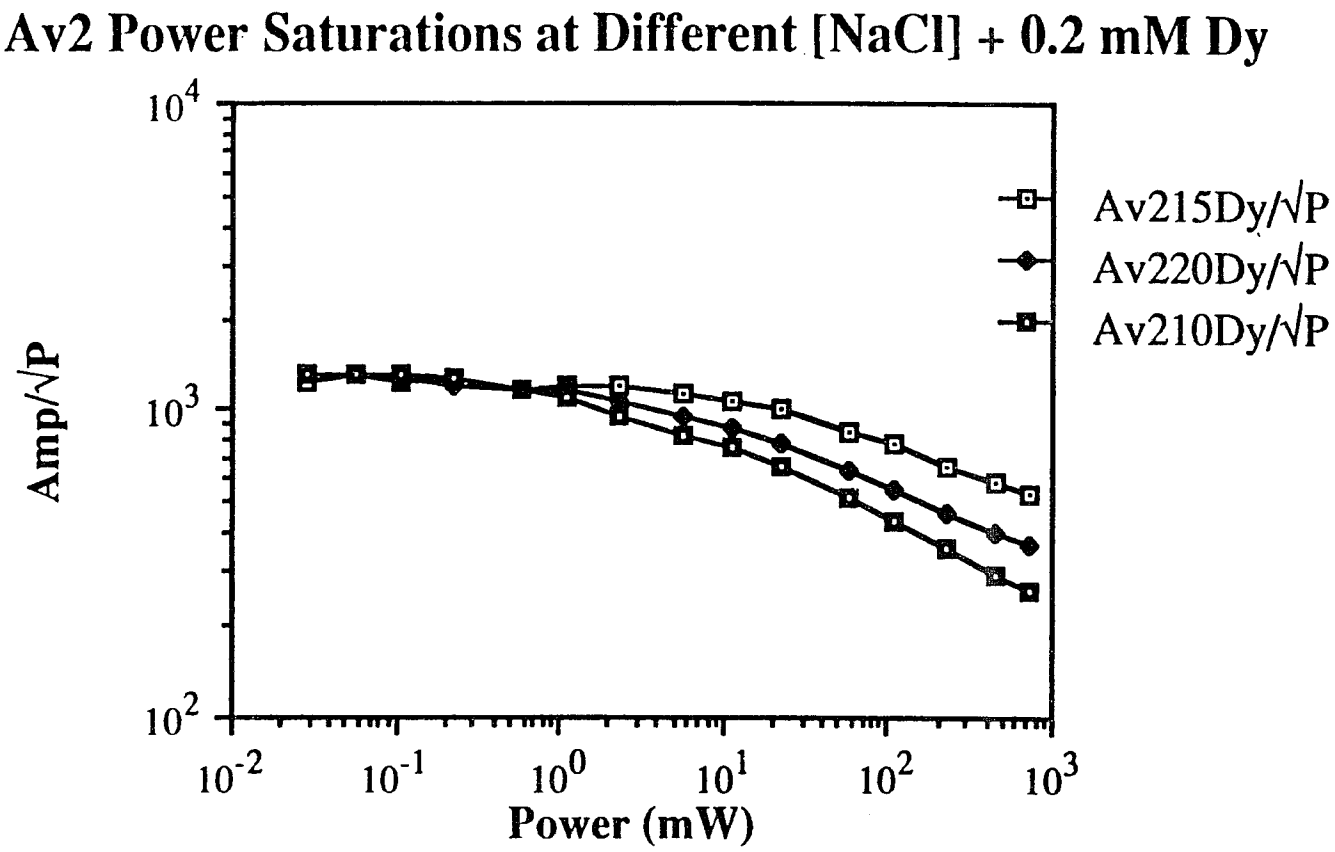

Figure 5.4 Power Saturation Curves for Av2 at Different Salt Concentrations and 0.2 mM DyEDTA. Conditions: microwave frequency, 9.46 GHz; modulation frequency, 100 kHz; modulation amplitude, 12.6 G; power: .029-700 mW; temperature, 8 K; protein concentration, 35 mg/ml; g value = 1.94.

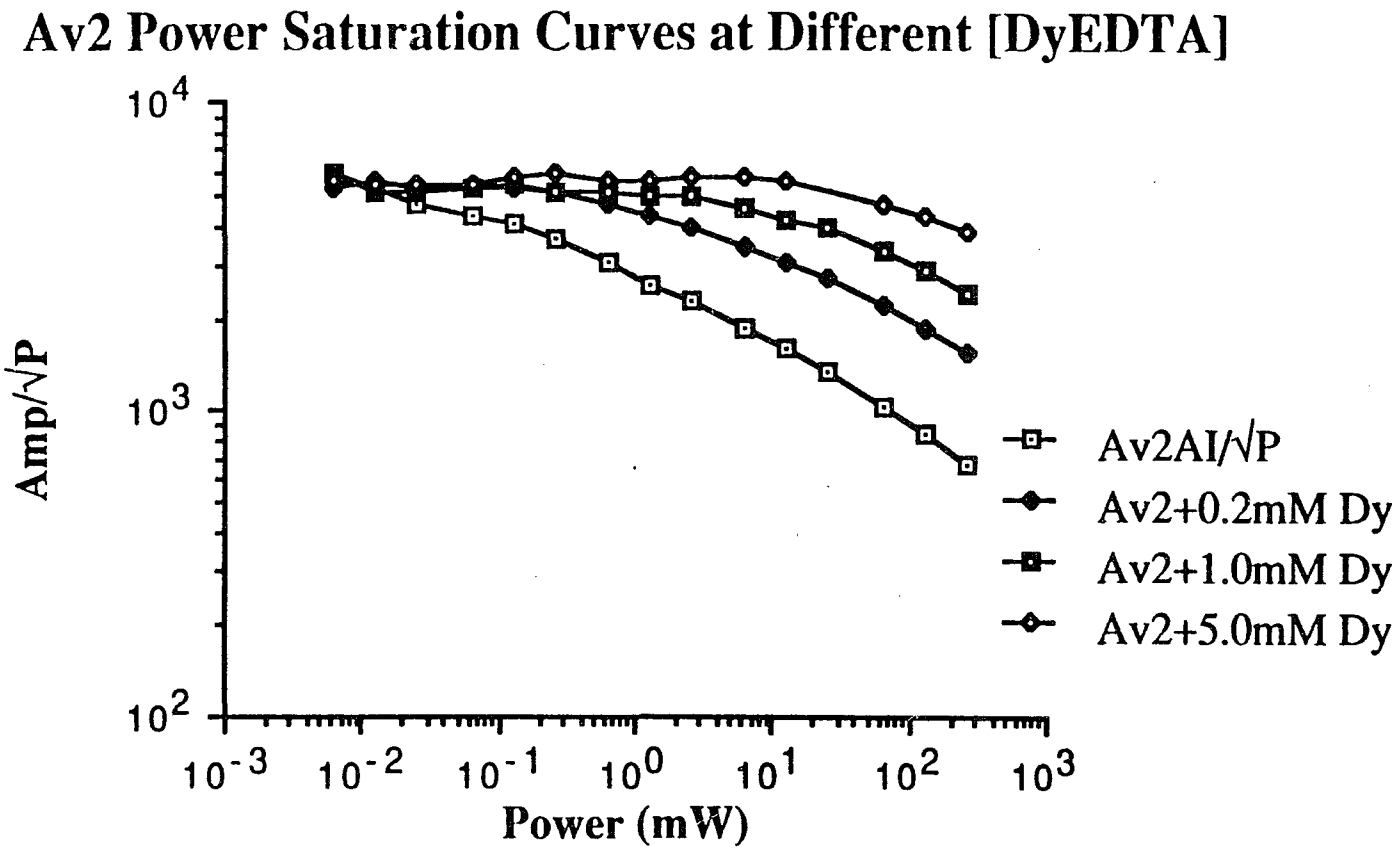

Figure 5.5 Power Saturation Curves for Av2 at Different [DyEDTA] Conditions: microwave frequency, 9.46 GHz; modulation frequency, 100 kHz; modulation amplitude, 12.6 G; power: .029-700 mW; temperature, 8 K; protein concentration, 35 mg/ml; g value = 1.94.

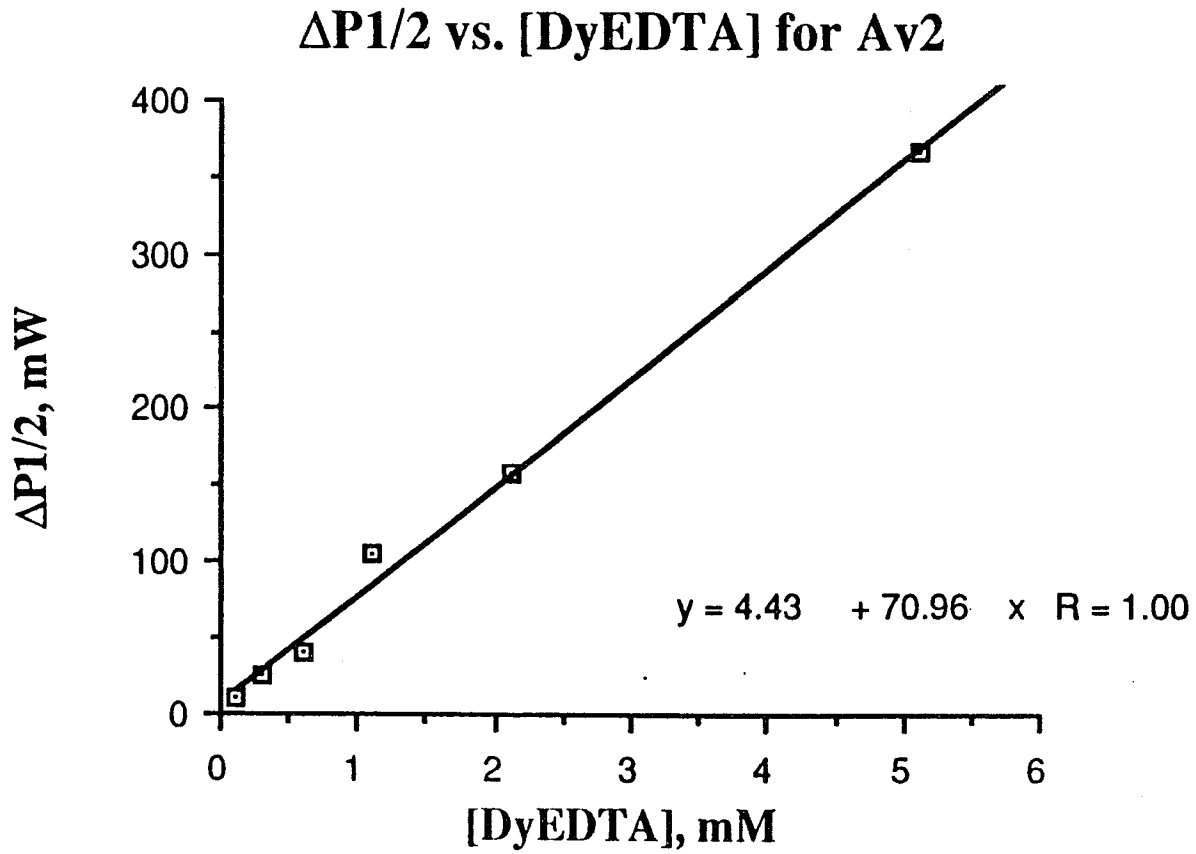

Figure 5.6 Plot of $\Delta P_{1/2}$ vs. [DyEDTA] for Av2

exposed after MgATP binding, then we would expect to see an enhancement of the Dy effect after MgATP had been added. The samples were prepared as follows: MgATP was added to $MgCl_2$ in a 1:1.5 molar ratio in 50 mM HEPES. The resulting pH was very acidic and was adjusted with KOH to pH 7.5. The resulting solution was made anaerobic and then added to Av2 in a final concentration of 15 mM in MgATP. This represents about a tenfold excess over the protein concentration. Evidence for MgATP binding to the Fe protein was taken from the appearance of the EPR spectrum, as reported earlier (5.58, 5.64). The spectra in Figure 5.7 show the effect of MgATP on the Av2 S = 1/2 EPR signal. Parallel samples were prepared containing 1 mM DyEDTA with and without MgATP. The samples, all frozen after 15 minutes, were prepared at the median NaCl concentration of 0.1 M.

The power saturations were performed, as before, at 8K; the results of these power saturations can be seen in Figure 5.8. The $P_{1/2}$ values for the curves in Fig. 5.8 are shown in Table 5.4 below.

From the data presented in Table 5.4 we can make the following obervations: we certainly see a dramatic Dy effect in the sample containing 1 mM DyEDTA as expected; the presence of MgATP is relieving the saturation of the Fe:S cluster in Av2; we are not seeing an enhancement of the Dy effect in the sample containing both MgATP and DyEDTA. This latter result is in contrast to what we might have expected based on the iron chelation studies done on Av2. Apparently, the Fe:S cluster is not accessible to DyEDTA in the presence of MgATP. One possible explanation is that the presence of MgATP is affecting the interaction between DyEDTA and the protein itself. It is possible that the only DyEDTA the protein "sees" once MgATP is bound is that which is randomly dispersed in solution.

TABLE 5.4

$P_{1/2}$ Values for Power Saturations of Av2

Bound to MgATP with and without DyEDTA

Sample	$P_{1/2}$ (mW)
as-isolated	40
+ 1 mM Dy	350
+ 15 mM MgATP	100
+ 1 mM Dy and 15 mM MgATP	50

5.5 CONCLUSIONS

We have examined the effects of temperature, salt, DyEDTA, and MgATP on the relaxation of the S = 1/2 signal of Av2. Temperature seems to affect our Av2 slightly differently from what has been reported previously. We observed that the optimal temperature for power saturations was 8 K instead of about 20 K as reported previously.

As with Av1, salt affects the relaxation behavior of Av2 in a very complex manner. Given the concentration range we chose, we might have expected to see abrupt changes in relaxation, and we did. The salt concentration range of 0.1 to 0.2 M is the same range where inhibition of substrate reduction becomes dramatic (5.73). The addition of 0.2 mM DyEDTA to the same samples also resulted in complex saturation behavior.

As has been observed with other proteins, it is possible to obtain information about the distance from the surface of a protein to a paramagnetic center upon addition of the

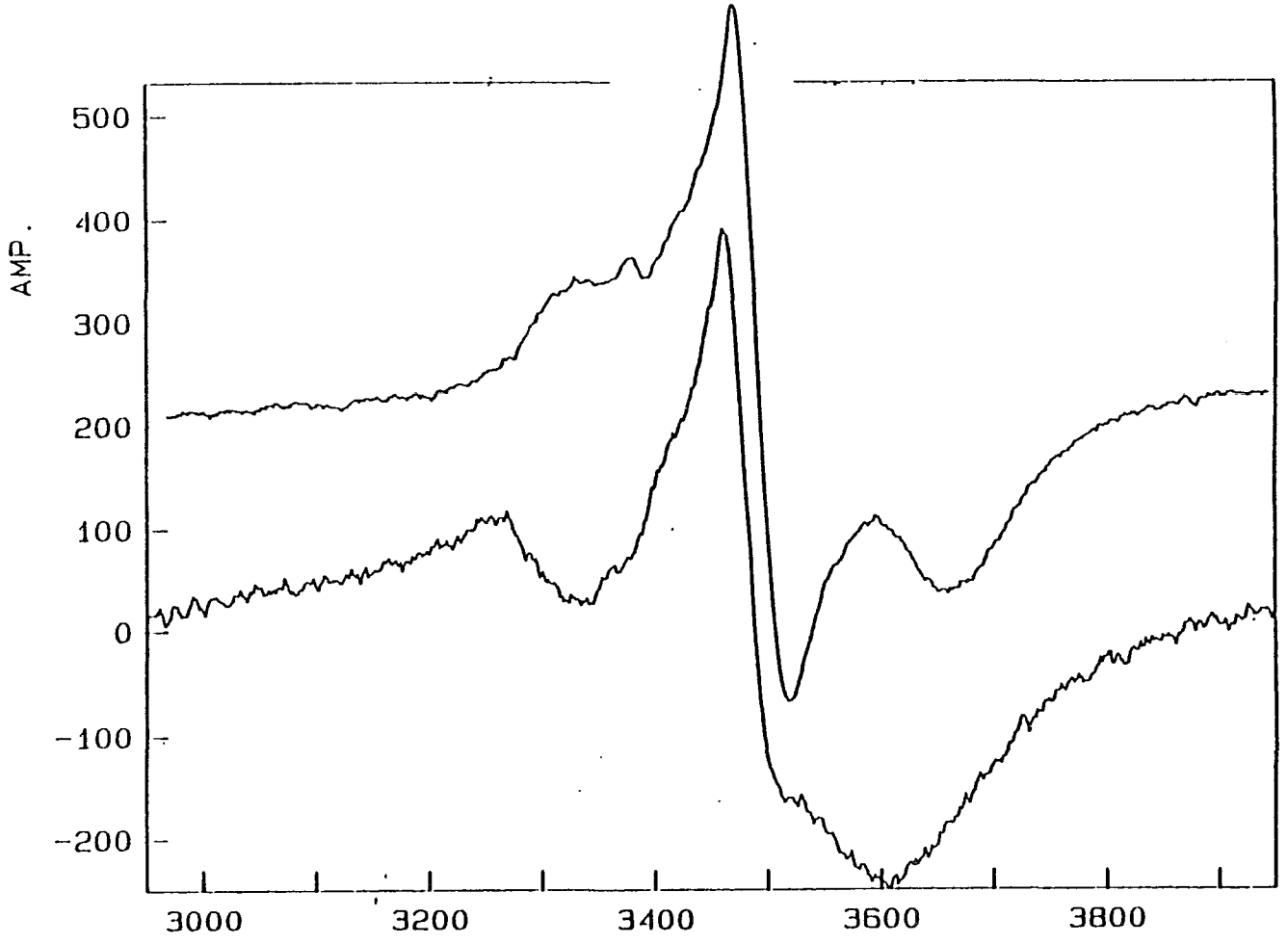

Figure 5.7 EPR spectra of Av2 with and without MgATP Conditions: microwave frequency, 9.46 GHz; modulation frequency, 100 kHz; modulation amplitude, 12.6 G; scan time, 84 s; time constant, 0.33 s; temperature, 8K; g values: top, 2.05, 1.94, 1.86, bottom, 2.06, 1.94, and 1.87.

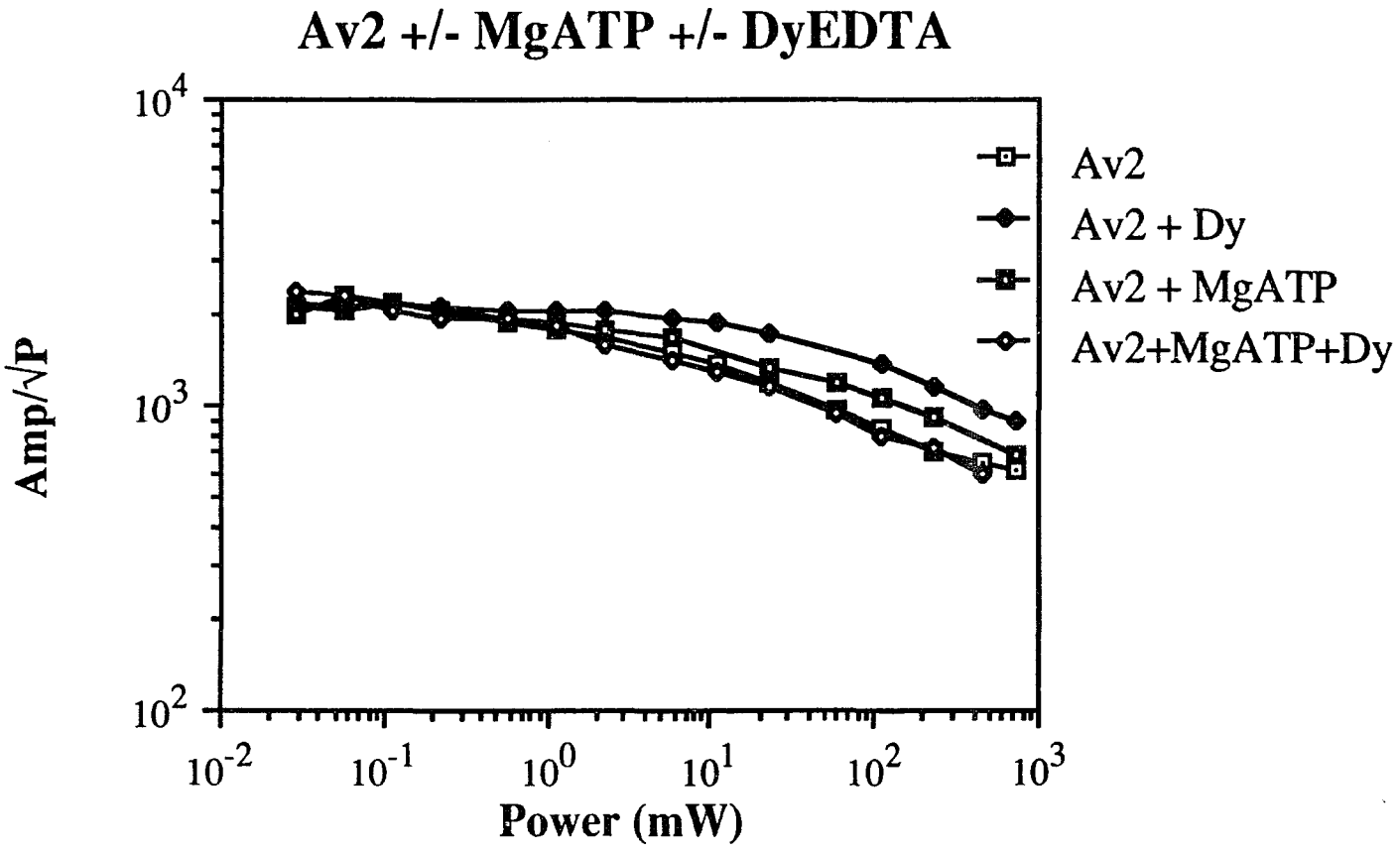

Figure 5.8 Power Saturation Curves for Av2 with and without DyEDTA and MgATP Conditions: microwave frequency, 9.46 GHz; modulation frequency, 100 kHz; modulation amplitude, 12.6 G; power: .029-700 mW; temperature, 8 K; protein concentration, 35 mg/ml; g value = 1.94.

extrinsic relaxer, DyEDTA. Based upon how the $P_{1/2}$ changes with DyEDTA concentration, this distance can be easily calculated. After allowing for the size of the DyEDTA complex, 5Å, we calculated that the distance of closest approach to the [4Fe-4S] cluster in Av2 was 5Å. This result agrees with the ongoing x-ray structure of Av2 which locates the [4Fe-4S] cluster near the surface of the molecule.

There has been intensive study concerning the effects of nucleotide binding on the structure and function of the Fe:S cluster in component 2. The most dramatic effect has been that iron chelators cannot reach the Fe:S cluster until MgATP is bound. In addition, the shape of the EPR spectrum of component 2 changes upon nucleotide binding. Other studies such as Mössbauer, pulsed EPR, NMR, and EXAFS do not show a dramatic change in the Fe:S cluster with MgATP binding. Likewise, we do not see an enhancement of the dysprosium effect when MgATP is bound to Av2.

REFERENCES

5.1. Emerich, D. W., and Burris, R. H. (1978) J. Bacteriol. **134**, 936-943

5.2. Swisher, R. H., Landt, M., and Reithel, F. J. (1975) Biochem. Biophys. Res. Commun. **163**, 1476-1482

5.3. Burgess, B. K. (1984) in Advances in Nitrogen Fixation Research (Veeger, C. and Newton, W. E., Eds.) pp. 103-113, Nijhoff/Junk Publishers, The Hague, Netherlands

5.4. Nakos, G., and Mortenson, L. E. (1971) Biochemistry **10**, 455-458

5.5. Eady, R. R., Smith, B. E., Cook, K. A., and Postgate, J. R. (1972) Biochem. J., **128**, 655-675

5.6. Kleiner, D., and Chen, C. H. (1974) Arch. Microbiol. **98**, 93-100

5.7. Tso, M-Y. W. (1974) Arch. Microbiol. **99**, 71-80

5.8. Hageman, E. V., and Burris, R. H. (1978) Biochemistry **17**, 4117-4124

5.9. Ljones, T., and Burris, R. H. (1978) Biochem. Biophys. Res. Commun. **80**, 22-25

5.10. Ljones, T., and Burris, R. H. (1978) Biochemistry **17**, 1866-1872

5.11. Braaksma, A., Haaker, H., Grande, H. J., and Veeger, C. (1982) Eur. J. Biochem. **121**, 483-491

5.12. Mortenson, L. E., and Thorneley, R. N. F. (1979) Annu. Rev. Biochem. **48**, 387-418

5.13. Orme-Johnson, W. E. (1985) Annu. Rev. Biophys. Chem. **14**, 419-459

5.14. Burgess, B. K. (1984) in Advances in Nitrogen Fixation Research (Veeger, C., and Newton, W. E. Eds.) pp. 103-114, Martinus Nijhoff Publishing, Norwell, MA

5.15. Eady, R. R. (1980) Methods in Enzymol. **69**, 753-792

5.16. Orme-Johnson, W. H., and Münck, E. (1980) in Molybdenum and Molybdenum-Containing Enzymes (Coughlan, M. P., Ed.) pp. 427-438, Pergamon Press, Oxford

5.17. Walker, G. A., and Mortenson, L. E. (1974) Biochemistry **13**, 2382-2388

5.18. Walker. G. A., and Mortenson, L. E. (1973) Biochem. Biophys. Res. Commun. **53**, 904-999

5.19. Yates, M. G., and Planqué, K. (1975) Eur. J. Biochem. **60**, 467-476

5.20. Burgess, B. K., Jacobs, D. B., and Stiefel, E. I. (1980) Biochim. Biophys. Acta **614**, 196-209

5.21. Orme-Johnson, W. H., and Davis, L. C. (1977) in Iron-Sulfur Proteins (Lovenberg, W., Ed.) Vol III, pp. 15-60, Academic Press, New York

5.22. Gillum, W. O., Mortenson, L. E., Chen, J. S., and Holm, R. H. (1977) J. Am. Chem. Soc. **99**, 584-595

5.23. Orme-Johnson, W. H., Davis, L. C., Henzl, M. T., Averill, B. A., Orme-Johnson, N. R., Münck, E., and Zimmermann, R. (1977) in Recent Developments in Nitrogen Fixation (Newton, W., Postgate, J. R., and Rodriquez-Barrueco, C., Eds.) pp. 131-178, Academic, New York

5.24. Averill, B., Bale, J. R., and Orme-Johnson, W. H. (1978) J. Am. Chem. Soc. **100**, 3034-3043

5.25. Sundaresan, V., and Ausuble, F. M. (1981) J. Biol. Chem. **256**, 2808-2812

5.26. Hausinger, R. P., and Howard, J. B. (1982) J. Biol. Chem. **257**, 2483-2490

5.27. Hausinger, R. P., and Howard, J. B. (1980) Proc. Natl. Acad. Sci. U. S. A. **77**, 3826-3830

5.28. Tanaka, M., Haniu, M., Yasunobu, K. T., and Mortenson, L., E. (1977) J. Biol. Chem. **252**, 7093-7100

5.29. Pretorius, I-M., Rawlings, D. E., O'Neill, E. G., Jones, W. A., Kirby, R., and Woods, D. R. (1987) J. Bacteriol. **169**, 367-370

5.30. Hausinger, R. P., and Howard, J. B. (1983) J. Biol. Chem. **258**, 13486-13492

5.31. Howard, D. B., Deits, T. L., Anserson, G. L., Maroney, M., Que, L., and Hausinger, R. P. (1985) in Nitrogen Fixation and CO_2 Metabolism (ludden, P. W, and Burris, J. E., Eds.) pp. 153-162, Elsevier Science Publishing Co., New York

5.32. Howard, J. B., Davis, R., Noldenhauer, Cash, V. L., and Dean, D. (1989) J. Biol. Chem. **264**, 1-5

5.33. Filler, W. A., Kemp, R. M., Ng, J. C., Hawkes, T. R., Dixon, R. A., and Smith, B. E. (1986) Eur. J. Biochem. **160**, 371-377

5.34. Robinson, A. C., Burgess, B. K., and Dean, D. R. (1986) J. Bacteriol. **166**, 180

5.35. Robinson, A. C., Chun, T. W., Li, J-G., and Burgess, B. K. (1989) J. Biol. Chem. **264**, 10088-10095

5.36. Robinson, A. C., Dean, D. R., and Burgess, B. K. (1987) J. Biol. Chem. **262**, 14327-4332

5.37. Tal, S., Li, J., Chun, T., Robinson, A., and Burgess, B. (1990) in Nitrogen Fixation: Achievements and Objectives (Gresshoff, P. M., Roth, L. E., Stacey, G., and Newton, W. E., Eds.) pp. 79-86, Chapman and Hall, New York

5.38. Shah, V. K., Hoover, T. R., Imperial, J., Paustian, T. D., Roberts, G. P., and Ludden, P. W. (1988) in Nitrogen Fixation: Hundred Years After (Bothe, H., De Bruijn, F. J., and Newton, W. E., Eds.) pp. 115-120, VCH Publishers, Florida

5.39. Shah, V. K., Madden, M. S., and Ludden, P. W. (1990) in Nitrogen Fixation: Achievements and Objectives (Gresshoff, P. M., Roth, L. E., Stacey, G., and Newton, W. E., Eds.) pp. 87-93, Chapman and Hall, New York

5.40. Hageman, R. V., Orme-Johnson, W. H., and Burris, R. H. (1980) Biochemistry **19**, 2333-2342

5.41. Cordewener, J., Haaker, H., and Veeger, C. (1983) Eur. J. Biochem. **132**, 47-54

5.42. Robson, R. L. (1984) FEBS Lett. **173**, 394-398

5.43. Georgiadis, M. M., Chakrabarti, P., and Rees, D. C. (1990) in Nitrogen Fixation: Achievements and Objectives (Gresshoff, P. M., Roth, L. E., Stacey, G., and Newton, W. E., Eds.) pp. 111-116, Chapman and Hall, New York

5.44. Orme-Johnson, W. H., Hamilton, W. D., Ljones, T., Tso, M-Y. W., Burris, R. H., Shah, V. K., and Brill, W. J. (1972) Proc. Natl. Acad. Sci., U. S. A. **69**, 3142-3145

5.45. Palmer, G., Multani, J. S., Cretney, W. C., Zumft, W. G., and Mortenson, L. E. (1972) Arch. Biochem. Biophys. **153**, 325-332

5.46. Orme-Johnson, W. H., and Orme-Johnson, N. R. (1982) in Iron-Sulfur Proteins (Spiro, T. G., Ed.) pp. 67-96, Wiley Interscience, New York

5.47. Lowe, D. J., Smith, B. E., and Eady, R. R. (1979) in Recent Advances in Biological Nitrogen Fixation (Subba Rao, N. S. Ed.) pp. 34-87, Oxford and IBH Publishing Co., New Delhi

5.48. Anderson, G. L., and Howard, J. B. (1984) Biochemistry **23**, 2118-2122

5.49. Smith, B. E., Lowe, D. J., and Bray, R. C. (1973) Biochem. J. **135**, 331-341

5.50. Zumft, W. G., Palmer, G., and Mortenson, L. E. (1973) Biochim. Biophys. Acta **292**, 413-421

5.51. Yates, M. G., Thorneley, R. N. F., and Lowe, D. J. (1975) FEBS Lett. **60**, 89-93

5.52. Haaker, H., Braaksma, A., Cordewener, J., Klugkist, J., Wassink, H., Grande, H., Eady, R. R., and Veeger, C. (1984) in Advances in Nitrogen Fixation Research (Veeger, C., and Newton, W. E., Eds.) pp. 123-331, Nijhoff?Junk Publishers, The Hague, Netherlands

5.53. Stombaugh, N. A., Burris, R. H., and Orme-Johnson, W. H. (1973) J. Biol. Chem. **248**, 7951-7956

5.54. Lowe, D. J. (1978) Biochem. J. **175**, 955-957

5.55. Stephens, P. J., McKenna, C. E., Smith, B. E., Nguyen, H. T., McKenna, M. C., Thomson, A. J., Devlin, F., and Jones, J. B. (1979) Proc. Natl. Acad. Sci. U. S. A. **76**, 2585-2589

5.56. Lindahl, P. A., Day, E. P., Kent, T. A., Orme-Johnson, W. H., and Münck, E. (1985) J. Biol. Chem. **260**, 11160-11173

5.57. Watt, G. D., and McDonald, J. W. (1985) Biochemistry **24**, 7226-7231

5.58. Hagen, W. R., Eady, R. R., Dunham, W. R., and Haaker, H. (1985) FEBS Lett. **189**, 250-254

5.59. Meyer, J., Gaillard, J., and Moulis, J.-M. (1988) Biochemistry **27**, 6150-6156

5.60. Tso, M-Y. W., and Burris, R. H. (1973) Biochim. Biophys. Acta **309**, 263-270

5.61. Thorneley, R. N. F., and Eady, R. R. (1973) Biochem. J. **133**, 405-408

5.62. Kimber, S. J., Bishop, E. O., and Smith, B. E. (1982) Biochim. Biophys. Acta **705**, 385-395

5.63. Zumft, W. G., Mortenson, L. E., and Palmer, G. (1974) Eur. J. Biochem. **46**, 525-535

5.64. Lindahl, P. A., Gorelick, N. J., Münck, E., and Orme-Johnson, W. H. (1987) J. Biol. Chem. **262**, 14945-14953

5.65. Rees, D.C., and Howard, J.B. (1983) J. Biol. Chem. **258**, 12733-12734

5.66. Stephens, P. J., McKenna, C. E., Smith, B. E., Nguyen, H. T., McKenna, M.-C., Thomson, A. J., Devlin, F., and Jones, J. B. (1979) Proc. Natl. Acad. Sci. U. S. A. **76**, 2585-2589

5.67. Morgan, T. V., Prince, R. C., and Mortenson, L. E. (1986) FEBS Lett. **206**, 4-8

5.68. Lindahl, P. A., Teo, B-K., and Orme-Johnson, W. H. (1987) Inorg. Chem. **26**, 3912-3916

5.69. Morgan, T.V., McCracken, J., Orme-Johnson, W.H., Mims, W.B., Mortenson, L.E., and Peisach, J. (1990) Biochemistry **29**, 3077-3082

5.70. Deits, T. L., and Howard, J. B. (1989) J. Biol. Chem. **264**, 6619-6628

5.71. Hagen, W. R., Dunham, W. R., Braaksma, A., and Haaker, H. (1985) FEBS Lett. **187**, 146-150

5.72. Burns, A., Watt, G. D., and Wang, Z. C. (1985) Biochemistry **24**, 3932-3936

5.73. Deits, T. L., and Howard, J. B. (1990) J. Biol. Chem. **265**, 3859-3867

COMPLEX FORMATION BETWEEN COMPONENT PROTEINS OF NITROGENASE

Exploring the Paramagnetism of Active and Inactive Complexes of Nitrogenase

6.1 INTRODUCTION

This chapter will explore the effects of complex formation on the paramagnetism of the nitrogenase component proteins from *A. vinelandii*. In any study concerning the function of nitrogenase, it is important to keep in mind the interaction between the Fe protein and the MoFe protein. This interaction affects the enzyme's efficiency and relative reactivity toward alternative substrates (6.1-6.3). The physical and chemical properties of the Fe and MoFe proteins are highly conserved among all N_2-fixing bacteria, but some significant differences also exist, especially between nitrogenase from *Clostridium pasteurianum* (Cp) compared to other species. Specifically, nitrogenase components (the MoFe protein, in particular) of *C. pasteurianum* have a distinctly low capacity to form an active hybrid enzyme with complementary components from other organisms (6.3-6.7). In a comprehensive study using highly purified proteins, crosses between eight different organisms were done (6.4). Of the 55 crosses done, 45 produced measurable amounts of activity. When no activity was recorded, a cross with one of the proteins of *C. pasteurianum* was always involved. *C. pasteurianum* nitrogenase is also less sensitive to H_2 as an inhibitor (6.8), and it shows a higher specificity for nucleotides (6.9). Recently, a difference between *C. pasteurianum* and *A. vinelandii* MoFe proteins was observed in both the relative reduction sequence of the redox centers and their measured midpoint potentials when redox titrations were

monitored by EPR (6.10). These observations show contrasts between the highly conbserved subunit and metal compositions of nitrogenase from these organisms.

In the present study we combined both the component proteins from *C. pasteurianum* with those from *A. vinelandii* and examined the saturation behavior of both Av1 and Av2. We also looked at the effect of adding the extrinsic relaxer dysprosium to these systems. In addition to these studies, we also looked at the saturation behavior of Av1 and Av2 when "complexed" together as well as when the two proteins were chemically cross-linked via the cross-linking reagent, 1-ethyl-3-(3-dimethylaminopropyl)-carbodiimide (EDC). The *A. vinelandii* cross-linking reaction has been studied (6.11), and the cross-linking site has been determined on both component proteins (6.12). Dysprosium was also added in these studies in order to ascertain the effect that complex formation would have on accessibilty of the metal clusters to the dysprosium compared to the dyprosium effect seen when the component proteins were separated.

6.2 THE CATALYTICALLY INACTIVE COMPLEX BETWEEN *C. pasteurianum* and *A. vinelandii.*

The catalytically inactive complex generated by the combination of Av1 and Cp2 inhibits N_2 reduction, C_2H_2 reduction, H^+ reduction and ATP hydrolysis catalyzed by the homologous nitrogenases (6.3-6.7). Kinetic data indicates that the inactive complex consists of two molecules of Cp2 to one molecule of Av1, with values for the inhibitor constant in the range of 1-10 nM (6.6). Inhibition of *C. pasteurianum* nitrogenase by Av1 produces a lag phase in acetylene reduction that increases with increasing Av1. The lag phase is found only at levels of Av1 sufficient to keep the ratio of Cp2:Cp1 lower than 2. The inhibition is specific for Av1, as Av2 has no effect. In comparison, Cp2

inhibits *A. vinelandii* nitrogenase activity, but Cp1 does not. Inhibition of nitrogenase activity occurs only when Av1 and Cp2 are two of the three nitrogenase components present in the reaction mixture (6.7). Gel filtration of a mixture of Av1 and Cp2 provides evidence for complex formation and indicates that each Av1 molecule binds more than one Cp2 molecule. One mole of Cp2 per mole of Av1 does not affect substrate reduction appreciably. It is the second mole of Cp2 per mole of Av1 that causes drastic inhibition. If one of the two binding sites on Av1 for Av2 is blocked by Cp2, substrate reduction is not inhibited, implying that only one binding site on Av1 for Av2 is required for a normal rate of substrate reduction and ATP hydrolysis (6.6).

Although MgATP is not required for complex formation, the MgATP-Cp2 dissociation constant is lowered approximately threefold by complex formation (6.6). In fact, the Av1-Cp2 complex can be isolated by gel-filtration, indicating the low dissociation constant for the complex. Furthermore, Av1 completely protects the iron-sulfur center in Cp2 against the MgATP-induced reaction with chelators, indicating that Av1 bound to Cp2 covers the iron-sulfur site of Cp2. However, MgATP can still bind to Cp2 when complexed to Av1, and in fact the EPR spectrum of Cp2-Av1 exhibits the same conformational change upon MgATP-binding as seen in free Cp2 (6.13).

Because of the nature of the inhibition seen in kinetic experiments and the strong interaction of the heterologous components relative to the homologous components, it is assumed that Cp2 binds to the same site(s) as Av2. The inhibition exhibited by Cp2 is noncooperative in nature and the dissociation constant for the Av1-Cp2 complex is finite. The slope of 1/v vs. [I] curves is linear and finite in value (6.7).

The effects of substrate reduction, MgATP-binding and dissociation, and MgATP-dependent iron chelation have been studied for the Av1-Cp2 complex. Most of the studies done thus far have focused on Cp2, whereas no studies to date have been done which examine the effect of complex formation on the paramagnetism of Av1. Does

complex formation hide the M-center in the same way that the Fe:S center in Cp2 is believed to be hidden? If the M-center is "hidden" we should see little or no effect when the extrinsic relaxer, dysprosium, is added to the complex. Furthermore, how does the saturation behavior of the M-center in free Av1 compare to that for the Av1-Cp2 complex? Are the metal clusters on the adjacent complexed proteins close enough for there to be an observable dipolar interaction? How do the results compare to recent information available about the site of interaction between component proteins? These are the questions addressed in the present study.

In this study Av1 and Cp2 were combined in a 1:2 molar ratio in the absence of MgATP. (Both the Cp1 and the Cp2 were the generous gift of Dr. Rick Bare of Exxon, Annandale, New Jersey.) Another sample was also prepared in which 1 mM DyEDTA was also added. Both samples were 2 mM in dithionite. The Av1 power saturations were performed at 3.8 K and the resulting curves are shown in Figure 6.1. The $P_{1/2}$ values for these curves as well as for free Av1 (Av1AI) and Av1 + 1mM DyEDTA are shown in Table 6.1.

TABLE 6.1

$P_{1/2}$ Values for the Av1-Cp2 Complex in the Presence and Absence of DyEDTA Compared to Free Av1

Sample	$P_{1/2}$
Av1-Cp2	190 mW
Av1-Cp2 + Dy	190
Av1AI	160
Av1 + Dy	300

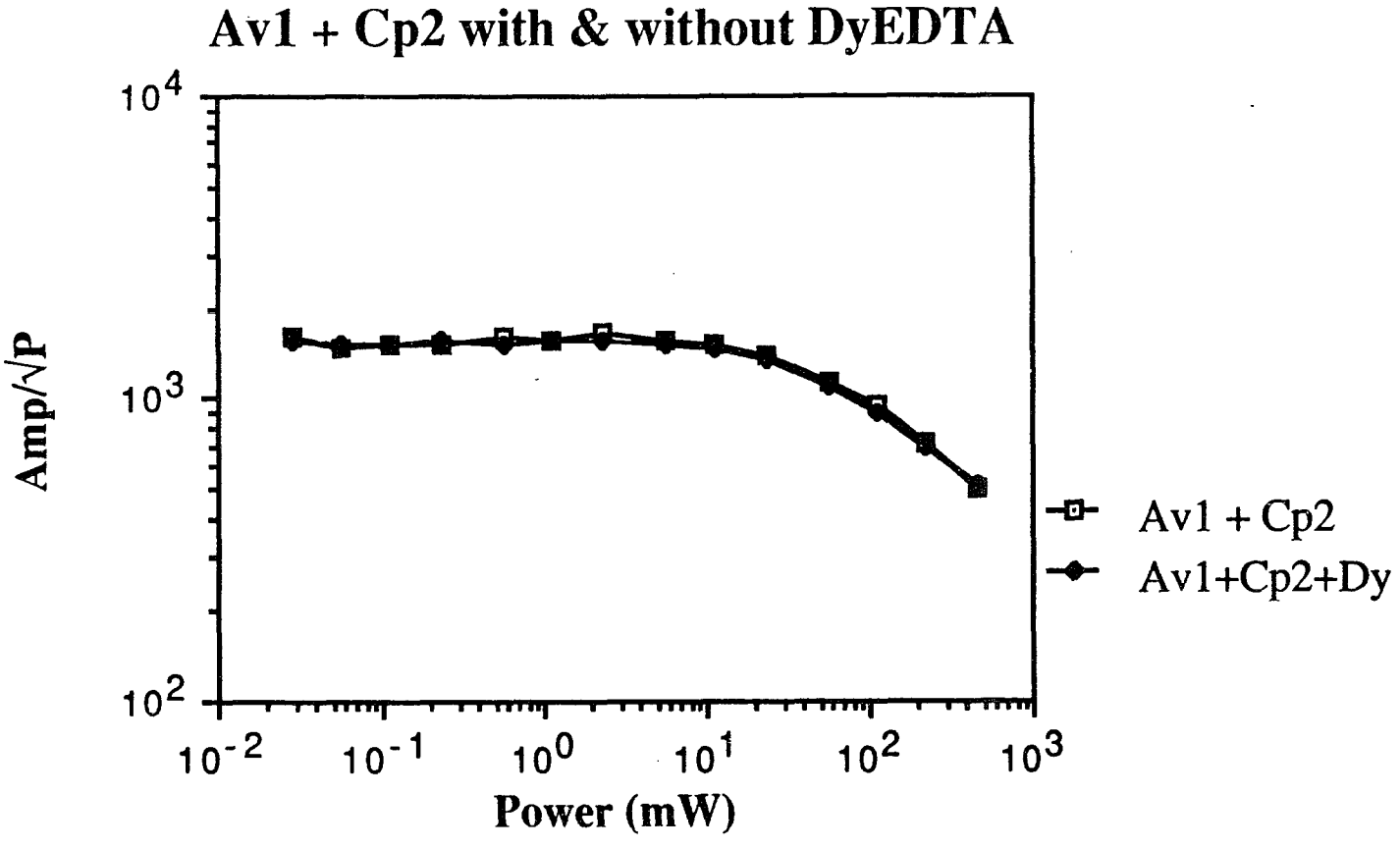

Figure 6.1. Power Saturation Curves for Av1 Complexed with Cp2 with and without DyEDTA. Av1 and Cp2 combined in a 1:2 molar ratio. 1 mM DyEDTA added to identical sample. Conditions: temperature, 3.8 K, microwave frequency, 9.46 GHz; modulation amplitude, 12.6 G; g = 3.640

The Av1-Cp2 complex does not exhibit a dysprosium effect. Therefore, we would expect the M center to be "hidden" within the Av1-Cp2 complex in such a way that the dysprosium cannot get close enough to relieve the saturation of the M center. However, there is a small relief from power saturation if the $P_{1/2}$ for free Av1 is compared to that of the complex. This might certainly be expected if one considers the tight binding of Av1 and Cp2. The respective metal clusters are close enough, then, for a dipolar interaction to occur. In fact, the metal clusters are probably held in a fixed orientation to one another. If this is true, there would exist an orientation dependence to the dipolar interaction, but this aspect was not explored. Also, the possibility of a small complex-induced change in the relaxation of Av1 cannot be ruled out.

In the study where heterologous crosses were made between nitrogenase components from different organisms (6.4), the cross between Av2 and Cp1 yielded no activity as seen by acetylene reduction, nitrogen fixation, or H_2 evolution. In the study of inhibition using *C. pasteurianum* components to inhibit *A. vinelandii* nitrogenase activity, Cp1 did not inhibit *A. vinelandii* nitrogenase activity, but Cp2 did (6.7). It was established that Av1 and Cp2 are both needed in a reaction mixture in order for inhibition of substrate reduction to occur. Therefore, while the cross between Av2 and Cp1 yields no activity, there is no inhibition by Cp1 of Av1 activity if Av2 is present. This would imply that Av2 and Cp1 are inactive but do not form the tight complex that Av1 and Cp2 do. Because we wanted to look at both component proteins of *A. vinelandii* we looked at both heterologous crosses of *C. pasteurianum* and *A. vinelandii*.

The same set of experiments that were done for Av2-Cp1 were performed with Av1 and Cp2. The ratio of Av2 to Cp1 was 2:1. DyEDTA (1 mM) was added to an identical sample of Av2 and Cp1. The power saturations for Av2 were done at 8 K as for other Av2 samples. The power saturation curves for these samples are shown in

Figure 6.2. The $P_{1/2}$ values for these curves are shown in Table 6.2 as well as the $P_{1/2}$ values for free Av2 with and without dysprosium.

TABLE 6.2

The $P_{1/2}$ Values for the Av2 Saturation in the Av2-Cp1 "Complex" with and without DyEDTA

Sample	$P_{1/2}$
Av2AI	10 mW
Av2 + Dy	90
Av2-Cp1	20
Av2-Cp1 + Dy	430

A comparison of the $P_{1/2}$ value for free Av2 and for the "complexed" Av2 shows that there is a small difference in these values, but not enough to warrant there being any appreciable dipolar interaction in the complex. This would again imply that there is not a tight nondissociable complex associated with Av2-Cp1. The $\Delta P_{1/2}$ between free Av2 and Av2 with dysprosium is 84 mW; the same change in $P_{1/2}$ for the complex is 415 mW.

Unique structural comparisons are expected to be present in both the Fe protein and the MoFe protein of *C. pasteurianum* to account for their distinct specificity for a compatible complement. Structural comparisons of nitrogenase from *C. pasteurianum* with the highly cross-reactive nitrogenases, such as the enzymes from *A. vinelandii* and *Rhizobium japonicum*, could reveal structural features distinguishing Cp nitrogenase

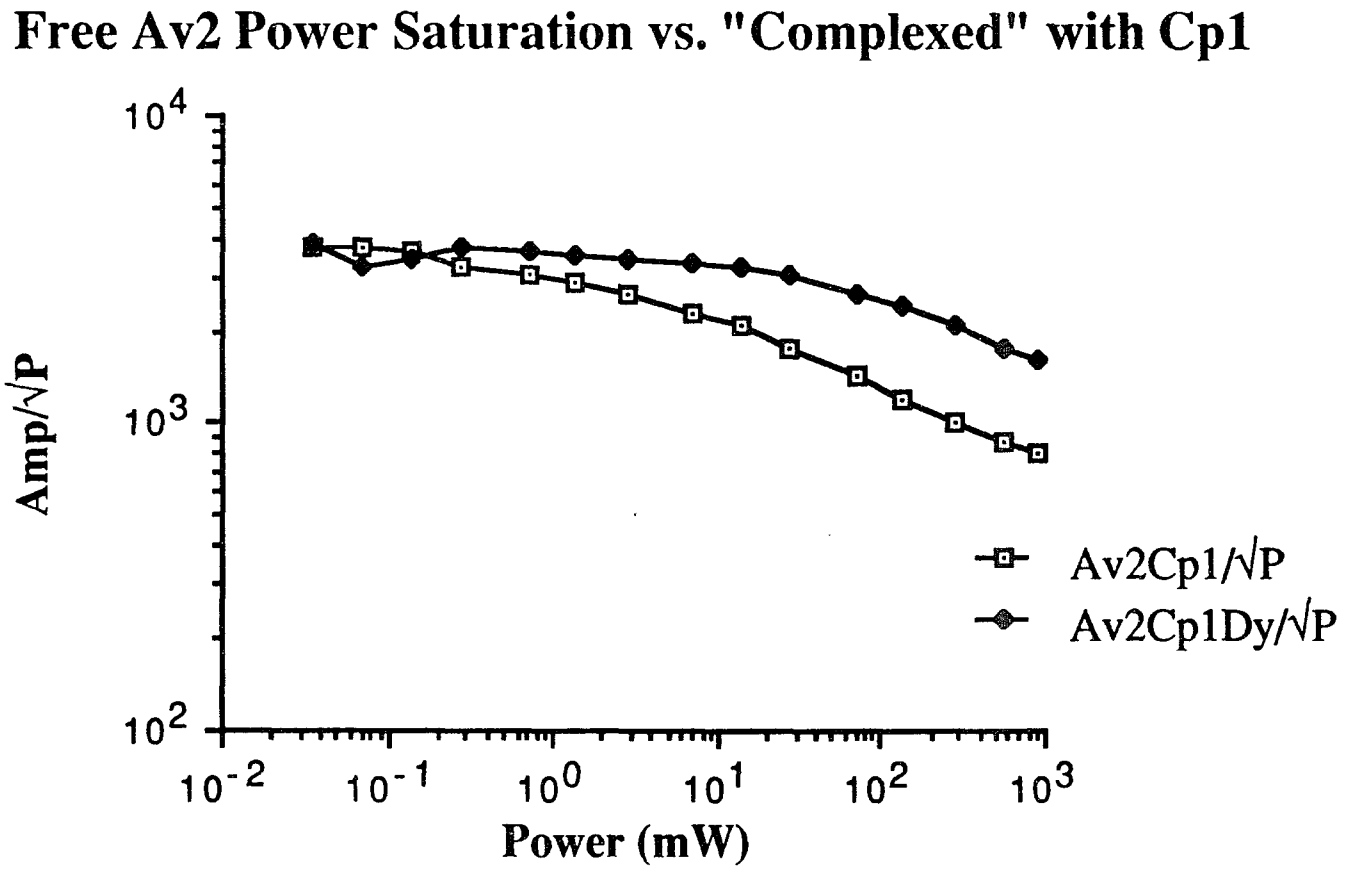

Figure 6.2. Power Saturation Curves for Av2 "Complexed" with Cp1 with and without DyEDTA. Av2 and Cp1 combined in a 1:2 molar ratio. 1 mM DyEDTA added to identical sample. Conditions: temperature, 8 K, microwave frequency, 9.46 GHz; modulation amplitude, 12.6 G; g = 1.942

from the others and indicate regions potentially involved in interaction between component proteins (6.14). The amino acid sequences of three polypeptides of nitrogenase are available for two highly cross-reactive organisms, *A. vinelandii* (6.15, 6.16) and *R. japonicum* (6.17-6.19). Complete amino acid sequences of the Cp Fe protein and the α subunit of Cp MoFe protein are also available (6.20-6.23). A comparison of amino acid sequences from six organisms for the α subunit and five organisms for the β subunit of MoFe proteins was done for nitrogenases from *C pasteurianum, A. vinelandii,* and *R. japonicum* (6.14). The MoFe subunits of *A. vinelandii* and *R. japonicum* were chosen for a detailed comparison with the Cp subunits because the Av and Rj proteins are highly active in reciprocal heterologous reconstitutions (6.4). The regions not conserved in the α and β subunits of *A. vinelandii* and *R. japonicum* are presumed not critical to component interaction, i.e., where significant differences do not prevent effective component interactions.

The distinct features of the nitrogenase MoFe protein of *C. pasteurianum* include size, charge (especially a sensitivity to pH above 7 and the occurrence of unique histidine residues near the conserved cysteine residues), and other differences in the primary and predicted secondary structures. The Cp α subunit is the largest (larger by 18-41 residues), whereas the Cp β subunit is the smallest (smaller by 54-65 residues). In other organisms, the α subunit is smaller than the β subunit by 3-31 residues, whereas in Cp the α subunit is larger than the β subunit by 75 residues. Despite the variations in size of the respective subunits in the organisms compared, the combined size of the two subunits is a fairly constant 1009-1033 residues, whereas in Cp there are

991 residues in the combined subunits. Therefore, since both Cp2 (6.21) and Cp1 (6.14) are smaller than in the other organisms, it might be postulated that in Cp1, the Fe protein binding site(s) is(are) a smaller domain that can only accomodate the smaller Cp2. Therefore, the smaller Cp2 protein could fit into the conceivably larger Av1 protein domain, but the interaction could be such (e.g., too strong) that the normal reactions could not occur. Likewise, the larger Av2 simply cannot fit into the smaller domain of the Cp1 (6.14).

In addition to differences in size between Cp and other nitrogenases, there is also a difference in overall charge, and a larger number of histidines located near conserved cysteines in Cp1. The pI's for the subunits of Cp1 are relatively acidic (5.9-6.1) relative to Av1 (6.3-6.6) and Rj1 (6.3-7.2). Cp nitrogenase shows a 50% reduction in activity at pH 7.4; its optimal pH range is 6.6-6.8 (6.24). Therefore, Cp1 is sensitive to pH above 7, and the decreased activity could result from decreased binding between nitrogenase components because of a change in the net charge of group(s) at the binding site (6.7).

Both the α and β subunits of Cp MoFe protein have a number of unique histidine (His) residues which occur near conserved cysteines (Cys). Between pH 6.5 and 7.5, His is responsible for changes in the charge properties of proteins. Some of the MoFe His residues and their positive charges could be an important determinant for compatibility between Cp MoFe protein and Fe proteins. The location of these His residues probably encompasses the Fe protein binding region(s) of Cp MoFe protein (6.14).

When the Fe proteins of *A. vinelandii* and *C. pasteurianum* are compared, there is an overall 65% conservation in sequence identity between these proteins which is distributed throughout the length of the polypeptides (6.25). Particularly strong

sequence conservation is located in the amino-terminal region of the polypeptides which may contain a proposed ATP-binding domain (6.26), and also in the regions surrounding the two conserved cysteines (residues 97 and 132 using Av2 sequence as a reference). The most striking difference between the proteins is that Av2 is elongated by 13 residues compared to Cp2. These 13 amino acids include 5 negatively charged residues (4 glutamates and 1 aspartate) and one positively charged residue (lysine). It has been suggested that these differences in size and charge density located at the carboxyl ends of the respective Fe protein sequences could account for the formation of the tight, ineffective complex in heterologous Av1-Cp2 (6.21, 6.27). This hypothesis was tested by removing the carboxyl-coding 18 codons from the Av2-encoding gene and replacing them with the analogous five codons from the Cp2 sequence (6.25). When the activity of the hybrid Fe protein is compared to wild type, almost maximal activity is seen when Av1/Av2 is less than one. Once the concentration of Av1 becomes limiting (high Av1/Av2 ratios) there is an apparent defect in the hybrid Fe protein as its specific activty decreases under these conditions. If the Av1-Av2 complex were tight and slower to dissociate, one would expect a reduced hybrid Fe protein activity even at low Av1/Av2 ratios. Therefore, the tight complex formed between Av1-Cp2 *in vitro* cannot be accounted for completely based on differences found in the carboxyl ends of the respective polypeptides (6.25).

6.3 THE CATALYTICALLY ACTIVE HOMOLOGOUS COMPLEX OF *A. vinelandii*

Having addressed inactive heterologous complexes of nitrogenase, we now turn our attention to the active homologous complex of *A. vinelandii*. The nature of the active complex is manifest in the association-dissociation of components 1 and 2. The rate of association between component proteins is rapid, less than 10 msec (6.28-6.30).

There have been conflicting reports on the lifetime of the complex. The complex between components from *K. pneumoniae* has been reported to be tight (6.29), while the complex for the components of *A. vinelandii* has been reported to be transient (6.31, 6.32). There has been some evidence for complex formation between components under conditions that did not support substrate reduction (6.33, 6.34). Sedimentation measurments by ultracentrifugation have revealed sedimentation coefficients larger than those of either protein alone. Thorneley has measured the association (6.35) rate constant to be $10^8\ M^{-1}\ s^{-1}$, while the dissociation rate constant has been calculated to be $10\ s^{-1}$ (6.36).

It is the tight binding between heterologous components, such as between Av1 and Cp2, that has helped yield information about the active complex. From the kinetic, titration, and gel filtration experiments done with this system, the stoichiometry of Av1 to Cp2 was established. It was also established that MgATP was not required for complex formation (6.6). The Fe:S center on Cp2 is protected from chelators in the complex, even though MgATP can still bind. The characterization of the Av1-Cp2 complex had direct implications for the interactions between Av1 and Av2.

In a study of nitrogenase from *A. vinelandii* with protons as substrate, there is a lag phase in H_2 evolution but not in the rate of ATP hydrolysis. The lag in H_2 evolution exists for approximately as long as the average turnover time of nitrogenase (6.31). This result has been interpreted to mean that components 1 and 2 associate and dissociate with every electron transferred. The fact that ATP hydrolysis occurs without a lag indicates that electron transfer occurs during the lag in H_2 evolution, and that ATP hydrolysis is coupled to electron transfer but not to substrate reduction. Therefore, there must be a random distribution of electrons among component 1 molecules. This situation would not exist if the two proteins formed an active complex that lasted

through many electron transfers. Therefore, the lifetime of the complex between the proteins should be no longer than the turnover time for transfer of one electron (~6.4 sec^{-1}) (6.31).

Given the above information, it is not evident beforehand that Av1 and Av2 will form a complex in the absence of MgATP. From the observed saturation behavior of the two proteins together, could we see evidence of such a complex? By comparing the homologous "complex" saturation behavior to that of the heterologous Av-Cp complex, would we see similarities? Would there be a difference in both the Av1 and the Av2 saturation behavior compared to the respective free proteins?

The samples containing Av1 and Av2 were prepared as for the Av-Cp samples: a 2:1 ratio of Av2:Av1 was used, and another identical sample was prepared with 1 mM DyEDTA added. The Av2 power saturations were determined at 8 K, and those for Av1 at 3.8 K. The Av2 power saturation curves are shown in Figure 6.3 while the Av1 curves are shown in Figure 6.4. The $P_{1/2}$ values for the curves in both Figures 6.3 and 6.4 are shown in Table 6.3.

An examination of the Av1 $P_{1/2}$ values reveals that there is the expected dysprosium effect with free Av1 as well as an effect with "complexed" Av1. It is not known why the $P_{1/2}$ for the "complexed" Av1 in the absence of dysprosium is lower than that of free Av1. However, the $P_{1/2}$ for both samples containing dysprosium is essentially the same. None of these results indicate that there is an Av1-Av2 complex. It should be noted that there may, in fact, be a distribution of free Av1 and Av2 as well as complexed Av1-Av2.

The $P_{1/2}$ values for the Av2 power saturations yield about the same conclusions as for Av1. Although there is a relief from saturation in the "complexed" Av2 compared to free Av2, it is not appreciable. There is a two-fold difference, though, in the $P_{1/2}$ values

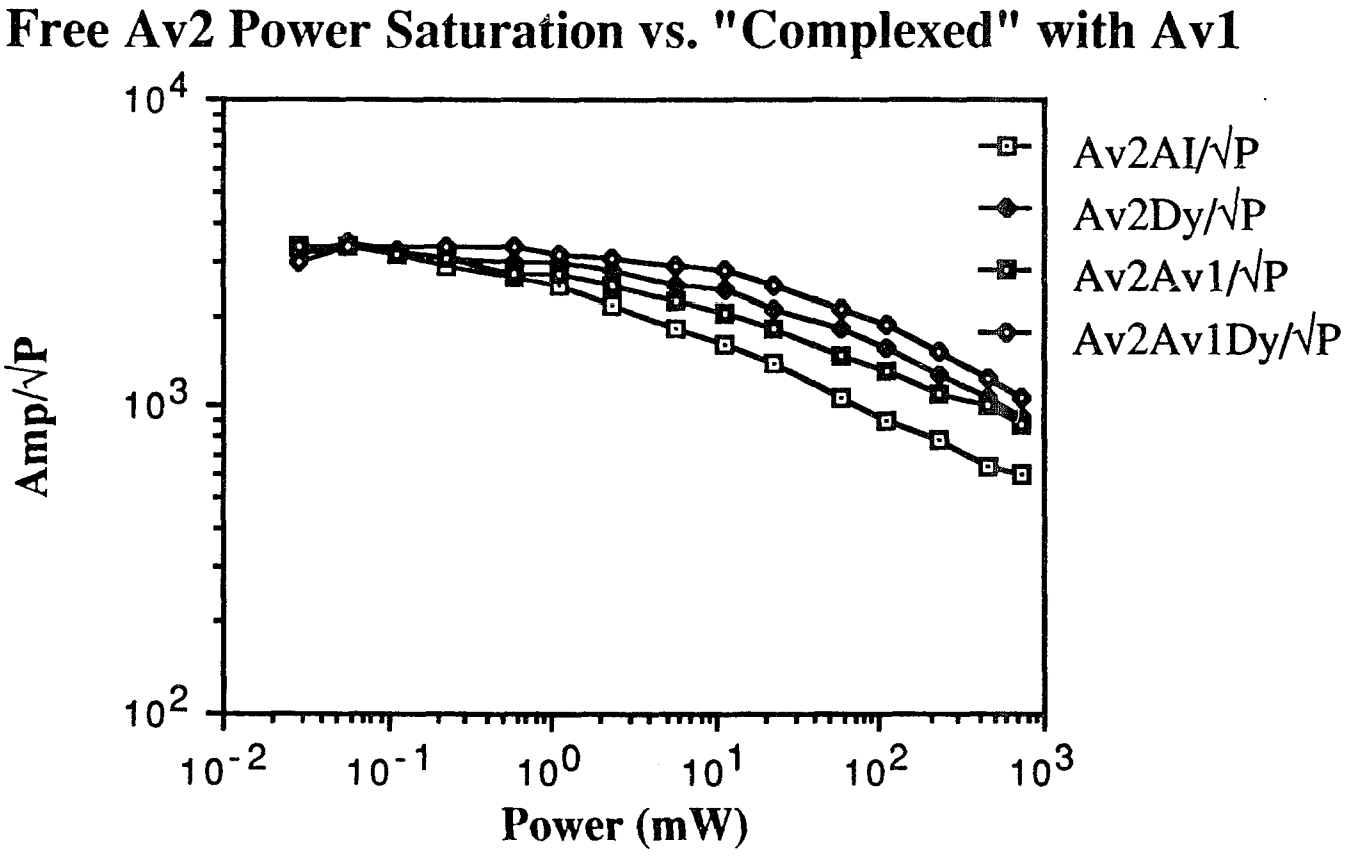

Figure 6.3. Power Saturation Curves for Av2 "Complexed" with Av1 with and without DyEDTA. Av2 and Av1 combined in a 1:2 molar ratio. 1 mM DyEDTA added to identical sample. Conditions: temperature, 8 K, microwave frequency, 9.46 GHz; modulation amplitude, 12.6 G; g = 1.942

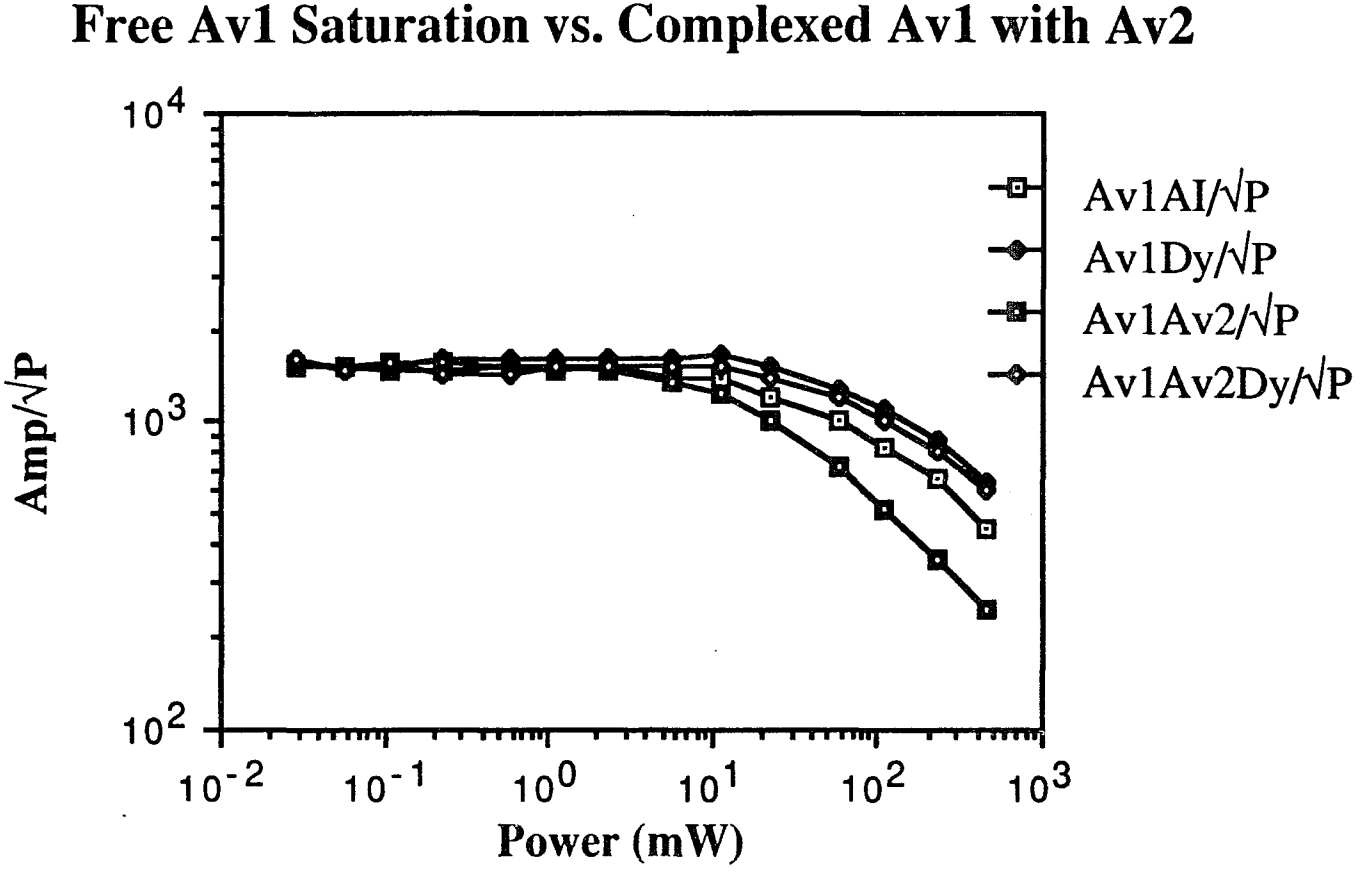

Figure 6.4. Power Saturation Curves for Av1 "Complexed" with Cp2 with and without DyEDTA. Av1 and Cp2 combined in a 1:2 molar ratio. 1 mM DyEDTA added to identical sample. Conditions: temperature, 3.8 K, microwave frequency, 9.46 GHz; modulation amplitude, 12.6 G; g = 3.640

for the samples containing DyEDTA. This profile of Av2 saturation is very similar to that for the Av2-Cp1 samples (see Table 6.2). In both sets of data there is a larger dysprosium effect for the "complexed" Av2. This would imply that the Av2 is more accessible to the dysprosium in these systems, which is in contrast to what has been observed for Cp2 in the nondissociable Av1-Cp2 complex where it has been shown that, the Fe:S cluster in Cp2 is inert to chelation (6.7). The $\Delta P_{1/2}$ for complexed Av1 is 228, while that for Av2 is 168. We will again see this larger dysprosium effect for complexed Av1 vs. complexed Av2. The above data indicates that there is not a definite observable complex for Av1 combined with Av2.

TABLE 6.3

$P_{1/2}$ Values for the Saturation of both Component Proteins of *A. vinelandii* with and without DyEDTA

	Av1 (@4 K)	Av2 (@8 K)
AI	160 mW	10 mW
+Dy	300	90
+Av1	___	40
+Av2	50	___
+Avx + Dy	280	190

What is the nature of the complex during electron transfer? Because of the salt inhibition seen in studies done on the catalytic properties of nitrogenase, and on the chemical cross-linking reaction, it is highly likely that the complex is electrostatic in

nature. We can look to examples of other native protein complexes involved in electron transfer between proteins. Many of these complexes are electrostatic in nature, and rates of electron transfer are highly dependent on the ionic strength of the environment (6.37, 6.38). If a complex is electrostatically stabilized in order for electron transfer to occur, it is the electrostatic interactions that are responsible for bringing the two proteins together in such a manner that the prosthetic groups have a favorable distance and orientation for electron transfer from one protein to another. It is reasonable to assume that association of the complex and the rate of electron transfer should be inversely proportional to the ionic strength of the solution. In one study, however, where cytochrome c was covalently linked to cytochrome c peroxidase and then compared to the native electrostatic complex, the rate of electron transfer for the covalent complex was independent of ionic strength, while that of the native electrostatic complex was highly dependent on ionic strength (6.37). In fact, better rates were obtained in the electrostatic complex with higher ionic strengths, as this environment allowed for the optimal distance and orientation between the proteins for effective electron transfer. The covalently linked complex prevented the subtle rearrangements apparently necessary for effective association. However, this is not the case for nitrogenase because salt is highly inhibitory to catalytic activity (6.39). Low ionic strengths are necessary for optimal activity; therefore, optimal protein association is probably not as ionic in nature as in the example above, but electrostatic interactions most surely affect the complex formed during catalytic turnover.

6.4 AN INACTIVE CROSS-LINKED COMPLEX IN *A. vinelandii*

The water-soluble cross-linker 1-ethyl-3-(3-Dimethylaminopropyl)carbodiimide (EDC) was used to cross-link Av1 to Av2 (6.11). EDC allows a linkage to be made between an amine and a carboxylic acid group (6.40-6.42). The EDC coupling reaction

is shown in Figure 6.5. If both nitrogenase components are present in the cross-linking reaction mixture, a new band, M_r = 97,000, was observed by gel electrophoresis (6.11). Formation of this new band requires active protein components, because O_2-damaged, inactive components exhibit higher molecular weight cross-linked material. This is evidence that the linkage involved was that of a catalytically significant complex. However, the complex seen upon cross-linking was not active no matter what the component ratio was. The amount of cross-linked material observed via the 97,000 molecular weight band increased with an increase in Av1:Av2. This indicates that cross-linking occured until Av1 was used up. Likewise, as the ratio of Av2:Av1 increased, cross-linking increased until Av2 was depleted by only 50-60%. This indicates that only one subunit in Av2 was reacting, whereas in Av1 both β subunits were being depleted. (The 97,000 molecular weight band was indicative, by position on the gel, of the β subunit of Av1 and not the α subunit.) Just as in the complex formed between Av1 and Cp2, nucleotides did not affect the cross-linking reaction, nor was the binding of MgATP prevented by the cross-linking of Av1 and Av2.

The effect of salt on substrate reduction by nitrogenase, and, therefore, complex formation, has been discussed previously (see Section 4.6.1) (6.39, 6.43). The formation of the cross-linked complex Av1-Av2 is similarly inhibited by salt (6.11). The same pattern of inhibition on activity was also seen with the active complex.

What is the composition of the complex produced in the cross-linking? An analysis of the 97,000 MW band excluded any participation of the α subunit from Av1. One subunit of the γ_2 Av2 molecule was shown to interact. The combined molecular weights of one β subunit with one γ subunit is 89,000. Therefore, it was proposed that

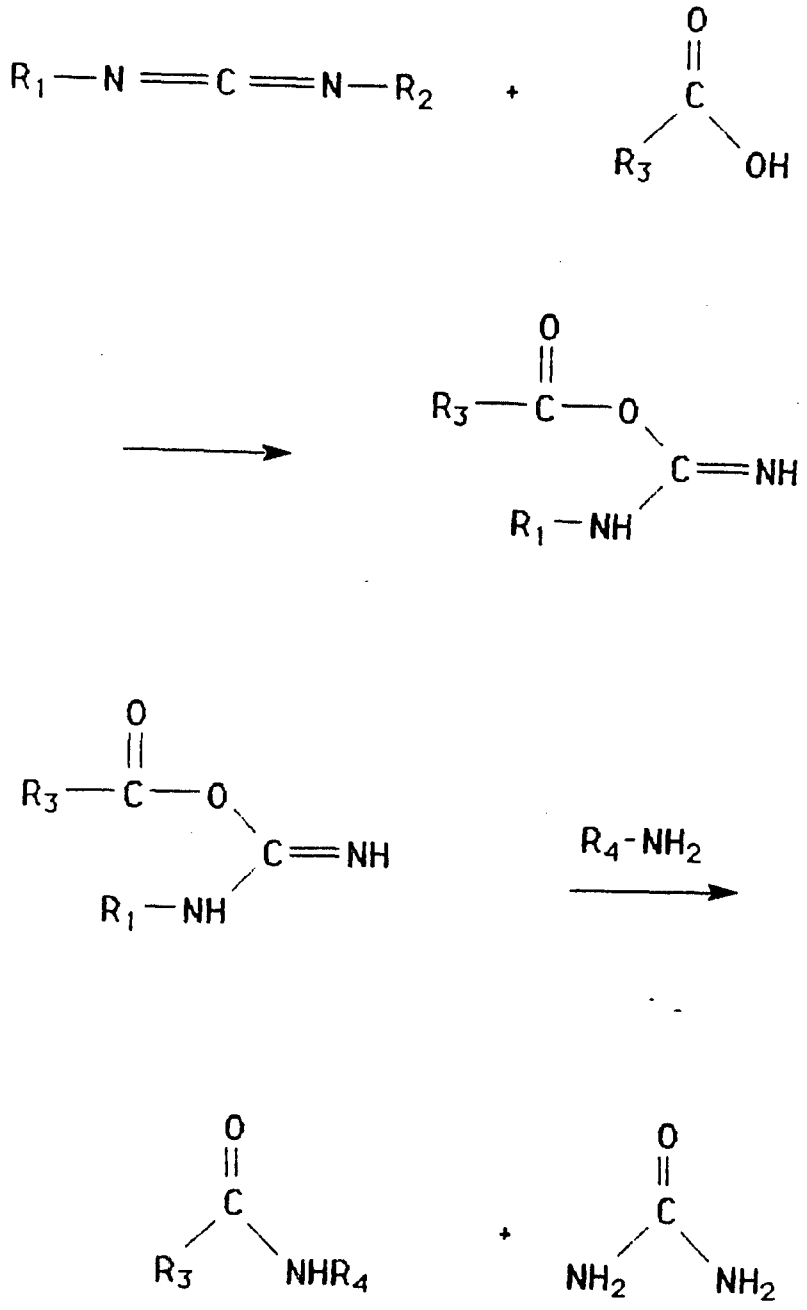

Figure 6.5. Mechanism of the EDC Coupling Reaction (1) EDC reacts with carboxylic acid group and activates the carboxyl group, allowing it to be coupled to the amino group (R_4NH_2) in the reaction mixture. (2) EDC is released as a soluble urea derivative after displacement by the nucleophile, R_4NH_2.

a 1:1 complex was being observed. Five conclusions about the proposed Av1-Av2 docking site were made from this study: [1] at least part of the docking site for the Fe protein on the MoFe protein is on the β subunit, although a docking between the two MoFe subunits cannot be ruled out. A twofold symmetry of the MoFe protein (6.44) would provide two separate sites for interaction, [2] the docking site is somewhat asymmetric in that only one of the identical Fe protein subunits is being linked, [3] the primary recognition for docking comes from ionic interactions at least some of which are from amino and carboxylic acid functions. In addition, no cross-linking occurred between individual components, which further supports ionic recognition as being primary in complex formation, [4] the cross-linked complex is inactive, which further supports the earlier idea that the components must dissociate after each electron transferred, and [5] individual components were neither inactivated nor cross-linked, whereas the complex was rapidly cross-linked and inactivated.

In order to resolve questions such as whether both Av2 subunits were involved in the cross-linking of Av1 and Av2, mixed peptide maps were prepared which included 2-^{3}H-carboxylmethylated complex and either 2-^{14}C-carboxymethylated Av2, α-Av1, or β-Av1 subunits. The radioactive amino acids were analyzed by doing Edman degradations. The results are consistent with a primary site of cross-linking between Av1 and Av2 at residues Glu-112 on Av2 and Lys-399 on the β subunit of Av1. One surprising result is that neither residue is invariant among the known sequences of nitrogenase components (6.14, 6.45, 6.46). Glu-112 is conserved in only half of the species, but it is located in one of the most conserved sequences in the Fe protein. In contrast, Lys-399 is not conserved at all in the five MoFe sequences analyzed (6.14). Therefore, it could be that the cross-linking reaction is restricted to the *Azotobacter*

system and the fortuitous location of Lys-399. It is interesting to note that this residue is also a Lys residue in the highly cross-reactive MoFe protein from *R. japonicum*. The corresponding residue in *C. pasteurianum* is a methionine residue (6.14).

Glutamine 112 is located C-terminal from the Fe:S cluster helix (25 Å away) as observed in the ongoing crystal structure of the Fe protein (6.47). This would put the cross-linking site for Av2 on "top" of the molecule. Glu-112 is located almost midway between the putative Cys ligands for the Fe:S cluster in Av2 (residues 97 and 132). It is interesting that MgATP had no effect on cross-linking; it might have been expected that, with Glu-112 being located between the Fe:S cluster ligands, any conformational change upon binding of MgATP would affect cross-linking in some way.

The study presented here hoped to answer some of the following questions: Is the saturation of the cross-linked complex different from the catalytically active complex? How does the saturation of the individual components, Av1 and Av2, compare to that of the free component? Would we see the same type of result in this inactive complex as compared to that between Av1 and Cp2? As in the other studies presented above, how would the extrinsic relaxer affect the relaxation of the cross-linked complex? The saturation of each individual component was measured at the optimal conditions for that protein. The power saturations for Av1 were run at 3.8 K and those for Av2 at 8 K. As with the other studies presented here, these power saturations were run for each series of samples on different days. While we cannot statistically compare one day's data to another, we ran each series until definite trends were repeatable. The saturation behavior of each component in the different complexes will be presented separately.

The samples were prepared as follows: Av1 and Av2 were combined in a 1:2 ratio. Two identical tubes contained a fresh solution of 12 mM EDC, which was prepared just before freezing the sample. To one sample, DyEDTA was added to a final

concentration of 1 mM. The power saturation curves for free Av1 (Av1AI), Av1Av2, and cross-linked Av1Av2 (symbolized as Av1-Av2) are shown in Figure 6.6. Figure 6.7 shows the power saturation curves for Av1 in both the homologous complexes with and without DyEDTA. The $P_{1/2}$ values for these curves are presented in Table 6.4 along with the values for the samples also containing DyEDTA.

The saturation behavior of Av1 in each of the complexes is slightly different. We are concerned with major changes, however, and these changes are best observed by examining the $\Delta P_{1/2}$ for each complex. Doing so, we see that the $\Delta P_{1/2}$ for both

TABLE 6.4

$P_{1/2}$ Values for the Saturation of Av1 in Different Complexes with and without DyEDTA

Sample	without Dy	with Dy	$\Delta P_{1/2}$
Av1AI	160 mW	300 mW	140
Av1Av2	50	280	230
Av1-Av2	110	360	250
Av1-Cp2	190	190	0

homologous complexes are very similar in value, and are very different from the $\Delta P_{1/2}$ for the inactive heterologous complex. The differences in size and charge of the respective proteins from *A. vinelandii* and *C. pasteurianum* have affected the saturation behavior of the heterologous Av1-Cp2 complex significantly.

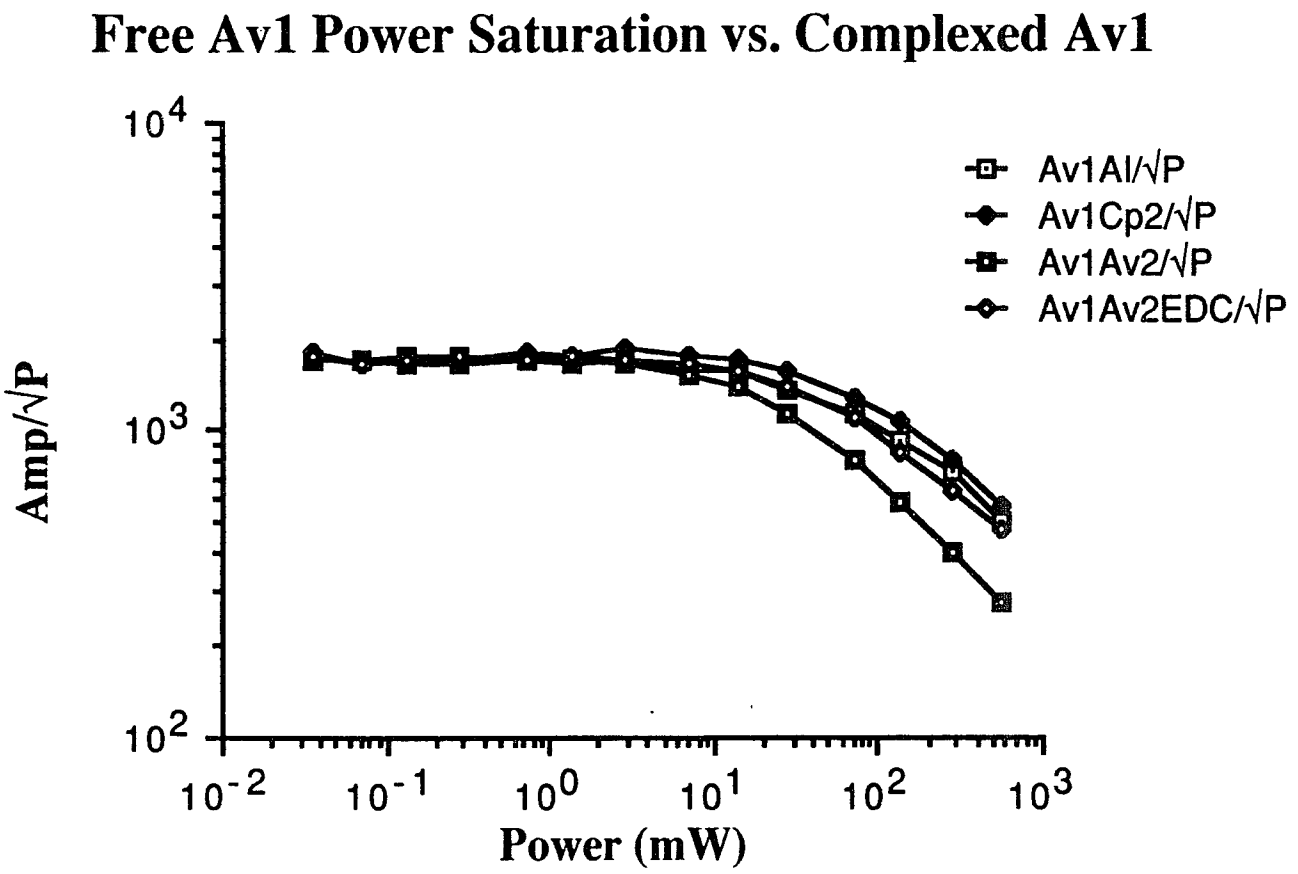

Figure 6.6. A Comparison of the Power Saturations of Free Av1 vs. Complexed Av1. Conditions: temperature, 3.8 K, microwave frequency, 9.46 GHz; modulation amplitude, 12.6 G; g = 3.640

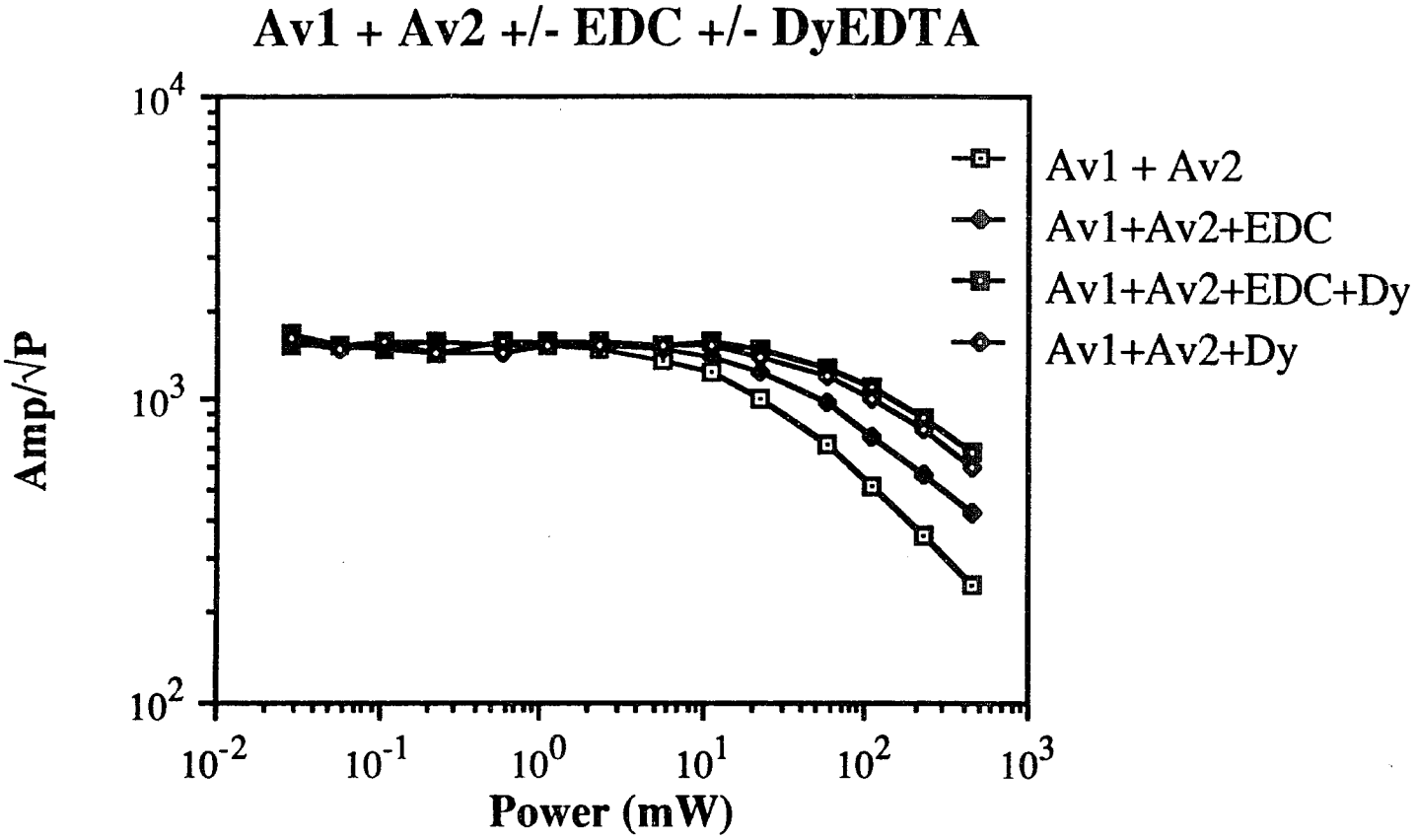

Figure 6.7. Av1 Power Saturation in the Presence of Av2 +/- EDC +/- DyEDTA. Conditions: temperature, 3.8 K, microwave frequency, 9.46 GHz; modulation amplitude, 12.6 G; g = 3.640

The fundamental question remains, however, as to whether the inactive complexes represent catalytically significant complexes. In the case of the Av1-Cp2 complex, previous results have indicated that this complex is representative of the type of complex formed between active homologous components. However, there are significant differences between the nitrogenase proteins from *C. pasteurianum* and those from other organisms. These differences manifested themselves in our examination of the saturation of Av1. Of all the systems in Table 6.4, however, only Av1-Cp2 shows a relief from saturation over free Av1 in the absence of dysprosium. Another result worth noting is that the $\Delta P_{1/2}$ values for both homologous complexes are very similar. We are reasonably sure from this and other results (specificity of cross-linking and stoichiometry) that the inactive cross-linked complex is catalytically significant in its interaction.

One of major differences between Cp2 and other iron proteins lies in the C-terminal region of Cp2. It is shorter by 16 to 26 residues and lacks charged residues towards the end of this region that are present in other Fe proteins. However, the recent hybrid Fe protein formed by replacing the C-terminal "tail" in Av2 with the C-terminus from Cp2 was active with Av1 both *in vivo* and *in vitro* (6.25). Therefore, it is improbable that this region is the sole reason for the incompatibility (or, perhaps, over-compatibility) of Cp2 with Av1.

The activity of purple photosynthetic bacterium *Rhodospirilium rubrum* component 2 is regulated by ADP-ribosylation of a specific arginine residue (6.48, 6.49). This regulation is accomplished via two enzymes that bind ADP-ribose, 'dinitrogenase reductase ADP-ribosyltransferase' (DRAT), and remove the ADP-ribose moiety, 'dinitrogenase-reductase-activating glycohydrolase' (DRAG). Component 2 from *R. rubrum* and also from *Rhodobacter capsulatus* (6.50) is covalently regulated by this ADP-ribosylation where the enzyme is inactive to complex formation when the ADP-

ribose moiety is bound. The ADP-ribosylated form of component 2 will bind MgATP. It can be oxidized and reduced, and it exhibits a normal EPR spectrum. However, it is incompetent with respect to electron transfer to component 1. The ADP-ribosylated form does not inhibit the unmodified form of component 2 (6.51). A reasonable hypothesis, therefore, is that the ADP-ribosylated form of component 2 is unable to bind to component 1. In these organisms, it is Arg 101 that is covalently regulated by DRAT and DRAG. It has also been shown that only one subunit in component 2 can be ADP-ribosylated (6.52).

DRAT has been shown to be extremely specific with respect to acceptor substrate. The only acceptor which has been identified is component 2 of nitrogenase (6.53). DRAT catalyzes the ADP-ribosylation of component 2 from other species besides *R. rubrum*, including Av2, Kp2 (6.53), and Cp2 (6.54). However, ADP-ribosylation via DRAT did not occur in any other substrates normally used by arginine-specific ADP-ribosyltransferases such as lysozyme, bovine serum albumin, polyarginine, or arginine itself (6.53).

Cp2 is known to have an arginine residue at the position analogous to the site of modification of the *R. rubrum* enzyme (6.55). Therefore, the effect of ADP-ribosylation on Cp2 was examined (6.54) in order to test the hypothesis that ADP-ribosylation prevents binding between nitrogenase components. Cp2 was shown to be a substrate for DRAT where nitrogenase activity was lost when Cp2 was pretreated with DRAT. Cp2 activity could be re-activated by treatment with DRAG (6.54). When Cp2 was added to Av1 and Av2 in the presence of DRAT, inhibition ceased. The characteristic Cp2 inhibition on Av nitrogenase could be recovered by treatment with DRAG. It was also shown that Av1 greatly inhibited the modification of Cp2. However, Av1 did not affect modification of Av2, nor did Cp1 affect the modification of Cp2. These results suggest that the site of modification on Cp2 is buried within the complex between Av1

and Cp2. This is in contrast with the result obtained for ATP-binding (6.6), where neither the affinity nor the stoichiometry of ATP-binding to Cp2 was affected by Av1. It should be noted that Cp2 is not known to exhibit modification of component 2 *in vivo*, yet Cp2 serves as a substrate for DRAT and DRAG.

There is extensive homology in the amino acid sequence in the region of the DRAT-target arginine of Kp2, Av2, Cp2, and Rr2 (6.45). A conserved Cys residue (three residues to the amino terminal side of the target arginine) is believed to be a ligand to the Fe:S cluster in Av2. The proximity of the target arginine to the 4Fe-4S cluster is consistent with the idea that this region of component 2 may interact with component 1 during electron transfer. This arginine residue (#101) was changed to a His in Kp2, and the mutant (UN1041) was purified and characterized (6.56). The mutant was able to bind MgATP and undergo the characteristic conformational change even when oxidized. Therefore, Kp2 (UN1041) has a redox-active 4Fe-4S cluster but is unable to support any proton or acetylene reduction in the presence of Kp1. The fact that UN1041 can undergo ATP-hydrolysis uncoupled from electron transfer implies that some sort of "complex" is being formed between the two components. However, it is not known whether the interaction between component 2 and 1 during reductant-independent ATP hydrolysis is the same as that during electron transfer between the two proteins; these results suggest that it is not. The ADP-ribosylated Kp2 (UN900) and UN1041 both hydrolyze ATP in the presence of Kp1, but neither are able to transfer electrons. It is highly possible that different forms of component 2 interact differently with the same Fe protein-binding site on component 1.

Both UN1041 and ADP-ribosylated Kp2 can support FeMoco biosynthesis *in vitro* (6.56). Therefore, Arg-101 is not necessary for this function of Kp2. There is a slower rate of chelation, though, for the UN1041 mutant, implying that the substitution of His for arginine results in a decreased accessibility of the 4Fe-4S cluster to chelators.

We saw a difference in the saturation of Av1 when complexed to Cp2. We are now reasonably sure that there are differences in Cp2 that may very well warrant a difference in saturation behavior. Will the same be true of Av2 in a complex with Cp1? How does cross-linking affect the saturation of Av2? The cross-linking site on Av2 is at Glu-112, reasonably close to Arg-101 which is very likely to be involved in complex formation. Figure 6.8 shows the saturation curves for free Av2 (Av2AI), the active homologous "complex" Av2Av1, the cross-linked complex Av2-Av1, and Av2Cp1. Table 6.5 lists the $P_{1/2}$ values for these curves in addition to those curves where DyEDTA was added to these samples.

The data presented in Table 6.5 shows that the relaxation of Av2 is affected by its cross-linking with Av1, i.e., there is a marked change in the saturation behavior between free Av2 and cross-linked Av2 in the absence of DyEDTA. What is even more remarkable is that it is <u>easier</u> to saturate the cross-linked complex when DyEDTA is added. This reversal of the dysprosium effect was seen in three separate trials for these samples. The cross-linking site in Av2 is 25 Å away from the cluster (6.44). Why there is a reversal is not understood but tends to imply that Av1 is shielding the 4Fe-4S cluster from the DyEDTA. We saw a substantial dysprosium effect with Av1 in the cross-linked complex (see Table 6.4). We also see a substantial relief from saturation in cross-linked Av2. One possibility is that there is a dipolar, or spin-spin, interaction between the 4Fe-4S cluster in Av2 and a nearby metal cluster in Av1. When DyEDTA is added to the complex, whatever dipolar interaction we see in Av2 must be interrupted by the interaction of Av1 with the DyEDTA, not of Av2 with DyEDTA.

Examination of the other complexes would indicate that, for Av2, there is no appreciable relief from saturation in the absence of DyEDTA. In the homologous complex, Av2Av1, there is a small deviation from the free Av2 $P_{1/2}$ value, and a similar dysprosium effect is seen. The fact that we do not see the reversal of the dysprosium

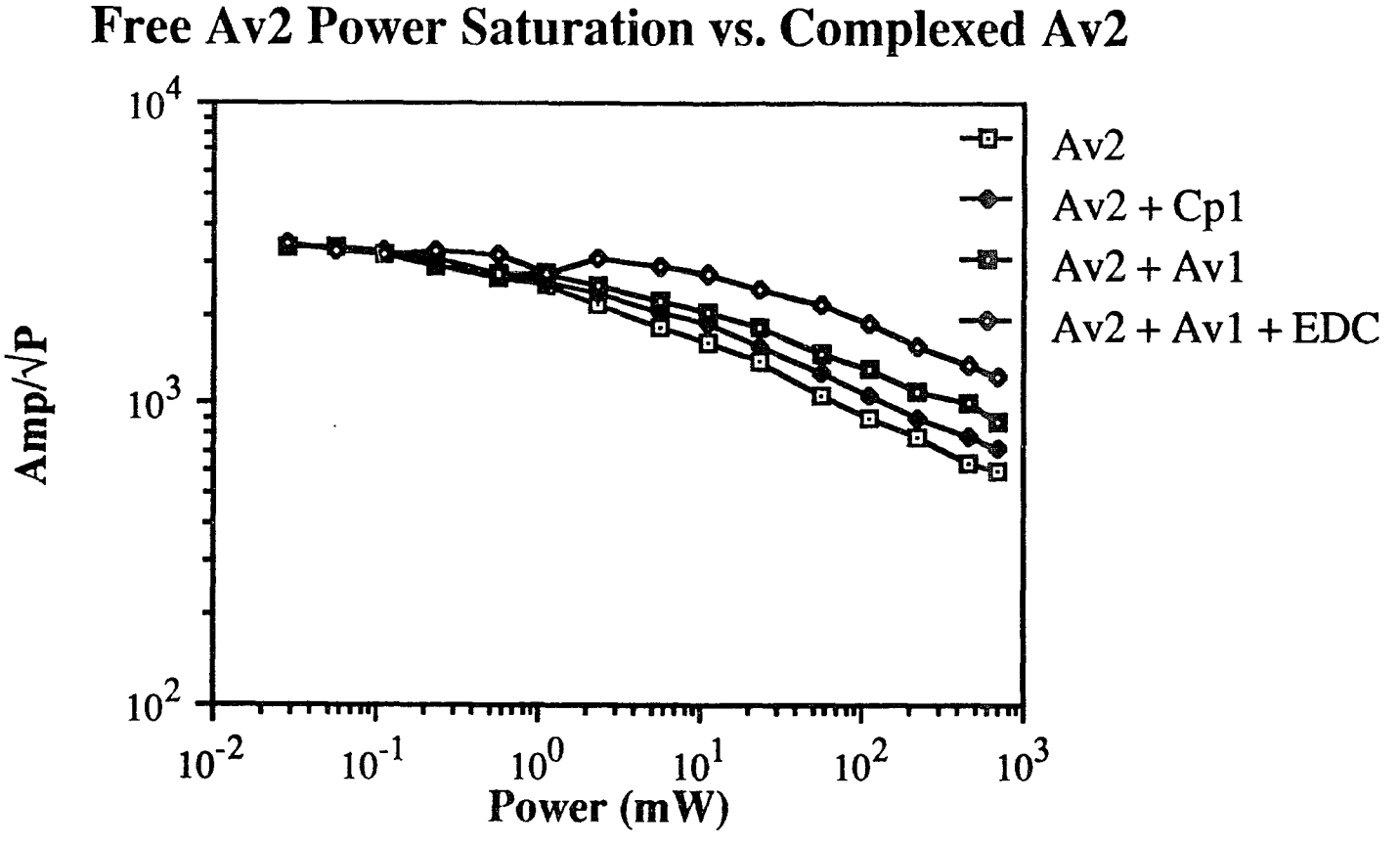

Figure 6.8. A Comparison of the Power Saturations of Free Av2 vs. Complexed Av2. Conditions: temperature, 8 K, microwave frequency, 9.46 GHz; modulation amplitude, 12.6 G; g = 1.942

TABLE 6.5

$P_{1/2}$ Values for the Saturation of Av2 in Different Systems with and without DyEDTA

Sample	without Dy	with Dy	$\Delta P_{1/2}$
Av2AI	9.3 mW	94 mW	90 mW
Av2Av1	40	190	150
Av2-Av1	210	100	-110
Av2Cp1	20	430	410

effect for this "complex" would imply that the same tight interaction is not occurring for the Av2Av1 as in Av2-Av1. This is not at all surprising; there have been no results, to date, that indicate a real complex forms under these conditions. The large dysprosium effect seen in the Av2Cp1 "complex" should be regarded with some suspicion; this is a rather large difference, one that was not repeated. In other trials, the $\Delta P_{1/2}$ for these samples was more in line with free Av2 with and without dysprosium. This would indicate that there is no complex formed between the larger Av2 (as compared to Cp2) with the smaller Cp1 (as compared to Av1).

If we compare the $\Delta P_{1/2}$ values for Av1 and Av2 in the free proteins and in the complexes, we see that there is a larger dysprosium effect with Av1 in all cases except with the Av1-Cp2 complex. This is somewhat surprising at first, as Av2 requires less DyEDTA for relief from saturation than Av1. But, given the larger and more definitive

information available concerning the structure of Av2, it is probable that the Fe:S cluster in Av2 is being hidden somewhat even in the complexes that are not covalent in nature.

6.5 POSSIBLE METAL CLUSTER LIGANDS IN Av1

In order to better understand the implications of these results, let's look at what's known about the metal clusters in component 1. There are five conserved cysteine residues present in the α subunit of the MoFe protein at positions 63, 89, 155, 183, and 275 (using the *A. vinelandii* sequence), and three conserved cysteines in the β subunit at positions 70, 95, and 153. Significant sequence homology is also found surrounding α subunit cysteine residues 63, 89, and 155 when they are respectively compared to β subunit cysteine residues 70, 95, and 153. Using site-directed mutagenesis, all the conserved cysteines in both subunits of component 1 were changed individually to alanine. The mutations made in the α subunit at positions 63, 89, 155, and 275 and in the β subunit at positions 70, 95, and 153 all resulted in a loss of diazotrophic growth, and component 1 activity, as well as a loss of the normal EPR signal of the component 1 protein (6.57). Replacement of Cys-184 with alanine in the α subunit greatly diminished growth and component 1 activity. When serine was substituted for Cys at β-153, active component 1 was produced, but not when alanine was substituted for this Cys. This may be indicative that a thiol ligand can be substituted by oxygen. Furthermore, there is an inequivalence between α-154 and β-153. Extracts of alanine-substituted α-275 complemented extracts from a mutant which was unable to

synthesize cofactor. Furthermore, the EPR signal for the alanine-275 mutant resembled that of isolated cofactor. This is evidence that Cys-275 serves as a ligand for the M center (6.57).

The results presented above are representative of many studies in which the environment of the metal cluters in component 1 has been probed. How does one know which amino acids to target for substitution or deletion? A working model has been developed where major polypeptide environments are tentatively assigned for each of the metallocluster types (6.58). This model (Figure 6.9) was based largely on primary sequence comparisons and metallocluster extrusion requirements. Three domains within the MoFe protein α and β subunits provide nearly equivalent P-cluster environments (these are labeled I, II, and III in Figure 6.9). Within the α subunit there are also two other domains, IV and V, which may provide ligation for FeMoco. The basis for this model has been presented previously (6.59-6.61). This model provides a basis for placing particular substitutions within the MoFe α subunit which result in alteration of the functional properties of the FeMoco environment. Where substitutions of alanine were made for all the conserved cysteines in the MoFe protein, the results indicated that conserved cysteines within Fe:S proteins are most probably ligands for the metal clusters.

This model (6.58) uses the concept of "domain switching", where comparisons are made between the primary structure of nitrogenase MoFe and structurally similar domains from related proteins. Domain switching provides a means of identifying important residues which may then be substituted for other amino acids.

Domain V contains the conserved cysteine α-275 which has already been identified as a possible ligand to FeMoco (6.57). Domain V from both *A. vinelandii* and

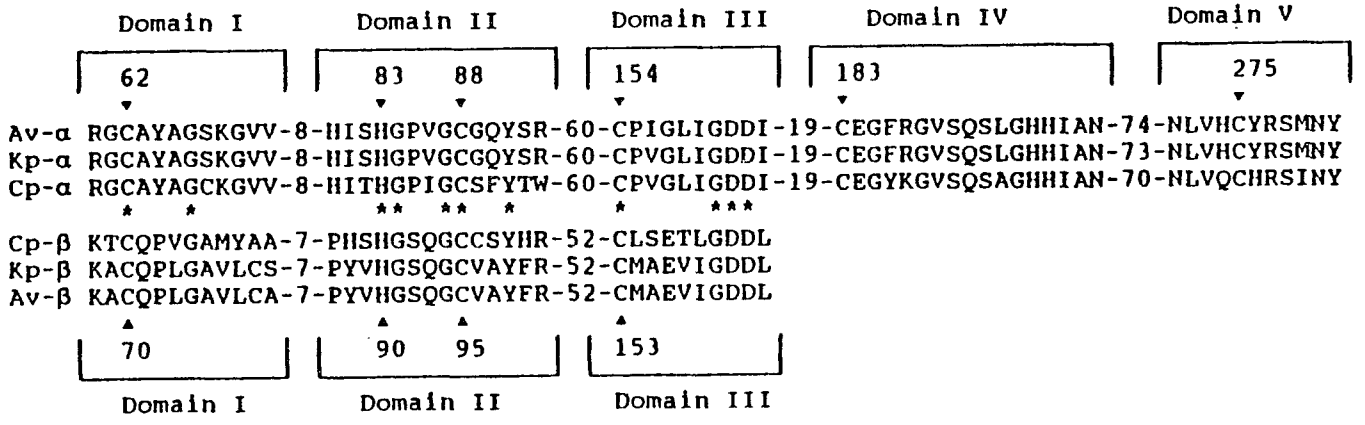

Figure 6.9. Alignment of Interspecifically Conserved Cysteine Residues From the MoFe Protein α– and β-Subunits from *A. vinelandii* (Av), *K. pneumoniae* (Kp), and *C. pasteurianum* (Cp). Residues which are conserved in both subunits are marked by asteriks. Numbers refer to the Av sequence. The Av MoFe protein α- and β-subunits have 492 and 523 residues, respectively. Domains I, II, and II are targeted as potential P cluster environments and domains IV and V are targeted as FeMoCo environments. Figure taken from ref. 58.

C. pasteurianum were compared, especially with respect to the immediate environment of residue 275. In Cp1, this sequence is Gln-Cys-His, while in Av1 it is His-Cys-Tyr. If Gln is substituted for His-274 and His for Tyr-276 in Av1 (strain DJ386), there is no real change in growth, but there is a shift in the EPR spectrum of Av1. These results do not indicate that the altered residues are involved in a direct interaction with FeMoco but do demonstrate that domain V within the MoFe protein α subunit does provide a FeMoco environment (6.58).

The same type of approach could not be used with domain IV, however, as an examination of Figure 6.9 will reveal that there are no significant differences in the sequences between Av1 and Cp1 in this domain. One fact that is known, though, about FeMoco biosynthesis helped in their approach. The gene products from *nif*E and *nif*N are thought to provide a scaffold on which FeMoco is assembled before its association with apo-MoFe protein (6.59). These gene products are absolutely required for FeMoco biosynthesis, and there is considereable sequence homology between the *nif*E product and the α subunit, and between the *nif*N product and the β subunit. Residues within domain IV of the α subunit which may provide ligation to FeMoco include Cys-183, His-195, and His-196. These residues are not found in the *nif*E product. Where α-Gln-191 is substituted for the corresponding residue in the *nif*E product, Lys, many changes were observed (strain DJ255). Diazotrophic growth was eliminated, but the overall structure of MoFe was not severly altered. There were changes in the g-values and lineshape of the EPR spectrum of the MoFe protein as well as changes in the catalytic properties. These results indicate a change in the environment of FeMoco in this mutant.

The results presented in the study discussed above clearly indicate that this approach to probing metal cluster environments is feasible. The functional properties of the metallocluster-binding regions have been analyzed without compromising their structural integrity (6.58).

6.6 CONCLUSIONS

How does the available genetic information coincide with the results from the study presented here? The identification of the ADP-ribosylation site in Av2, as well as identification of the cross-linking site, has enabled us to discover where binding with Av1 occurs on Av2. The results from the saturation studies indicate that the 4Fe-4S center is not exactly hidden in the cross-linked complex, but there is a reversal of the dysprosium effect seen with Av2 in this complex. The fact that it is harder to saturate Av2 in the cross-linked complex in the absence of dysprosium implies that the DyEDTA, when added, cannot get close to the Fe:S cluster in Av2. Instead, DyEDTA seems to effect a change in an apparent dipolar interaction between the 4Fe-4S cluster in Av2 and a metal cluster in Av1. In contrast, we see a larger dysprosium effect in the other complexes over free Av2. However, there is not a relief from saturation in Av2Av1 or in Av2Cp1 in the absence of dysprosium as compared to free Av2. These results suggest that there is no tight complex forms between Av2 and Av1 (in the absence of EDC) or between Av2 and Cp1.

Component 1 of *A. vinelandii*, however, is another story. Sequence homologies, and comparisons thereof, are useful for identifying potential ligands to metal clusters. Armed with data from mutagenesis experiments, some of the potential ligands to the metal clusters in Av1 have been identified. However, there is no information available concerning the secondary structure of MoFe. The identification of the cross-linking site

at β-Lys-399 provides little help in identifying the possible complex binding domain. This residue is far from any of the residues believed to ligate the metal clusters. More information on the folding of the protein is necessary. Our saturation studies indicate that in the Av1-Cp2 complex, the M-center is hidden; we see no dysprosium effect in this complex. In cross-linked Av1, a relief from power saturation with added dysprosium is seen, indicating that the heterologous Av1Cp2 complex is different in nature from the homologous cross-linked complex or the native "complex." This difference most surely arises from the charge and size differences seen in Cp2.

6.7 FUTURE WORK

Even though Av2 has been shown to be a substrate for DRAT (53), and is therefore, ADP-ribosylated, studies concerning the effect of ADP-ribosylated Av2 on complex formation with Av1 have not been done. This type of study should also be done with the cross-linked complex. Does ADP-ribosylated Av2 prevent the cross-linked complex from forming between Av1 and Av2?

Because it is easier to probe changes in the environment of FeMoco, more work has been done to elicit information concerning its binding region. The P clusters are usually best studied by Mössbauer or MCD spectroscopies. This researcher would like to see more work done with mutagenesis in the P cluster environments, namely domains I, II, and III in MoFe. How would these changes affect the oxidation profile of MoFe? Some information would surely be obtainable through EPR, which does not require the expensive and arduous task of growing bacteria on ^{57}Fe. For instance, after site-directed mutagenesis on potential P-cluster ligating residues, the same thionine oxidation experiments as presented in this work could be done which results may point to

ineffective P-clusters. In fact, if it is possible, one P-cluster at a time should be the target of the geneticist. We might then finally solve the P-cluster number argument.

REFERENCES

6.1. Wherland, S., Burgess, B.K., Stiefel, E.I., and Newton, W.E. (1981) Biochemistry **20**, 5132-5140

6.2. Emerich, D.W., Hageman, R.V., and Burris, R.H. (1981) Adv. Enzymol. Relat. Areas Mol. Biol. **52**, 1-22

6.3. Smith, B.E., Thorneley, R.N.F., Eady. R.R., and Mortenson, L.E. (1976) Biochem. J. **157**, 439-447

6.4. Emerich, D.W., and Burris, R.H. (1978) J. Bacteriol. **134**, 936-943

6.5. Tsai, L.B., and Mortenson, L.E. (1978) Biochem. Biophys. Res. Commun. **81**, 280-287

6.6. Emerich, D.W., Ljones, T., and Burris, R.H. (1978) Biochim. Biophys. Acta **527**, 359-369

6.7. Emerich, D.W., and Burris, R.H. (1976) Proc. Natl. Acad. Sci. U.S.A. **73**, 4369-4373

6.8. Guth, J.H., and Burris, R.H. (1983) Biochemistry **22**, 5111-5122

6.9. Weston, M.F., Kotake, S., and Davis, L.C. (1983) Arch. Biochem. Biophys. **225**, 809-817

6.10. Morgan, T.V., Mortenson, L.E., MCDonald, J.W., and Watt, G.D. (1988) J. Inorg. Biochem. **33**, 111-120

6.11. Willing, A.H., Georgiadis, M.M., Rees, D.C., and Howard, J.B. (1989) J. Biol. Chem. **264**, 8499-8503

6.12. Willing, A., and Howard, J.B. (1990) J. Biol. Chem. **265**, 6596-6599

6.13. Orme-Johnson. W.H., Hamilton, W.D., Ljones, T., Tso, M.-Y. W., Burris, R.H., and Brill, W.J. (1972) Proc. Natl. Acad. Sci. U.S.A. **69**, 3142-3145

6.14. Wang, S.-Z., Chen, J.-S., and Johnson, J.L. (1988) Biochemistry **27**, 2800-2810

6.15. Hausinger, R.P., and Howard, J.B. (1983) J. Biol. Chem. **258**, 13486-13492

6.16. Brigle, K.E., Newton, W.E., and Dean, D.R. (1985) Gene **37**, 37-44

6.17. Fuhrmann, M., and Hennecke, H. (1984) J. Bacteriol. **158**, 1005-1011

6.18. Kaluza, K., and Hennecke, H. (1984) MGG, Mol. Gen. Genet. **196**, 35-42

6.19. Thony, B., Kaluza, K., and Hennecke, H. (1985) MGG, Mol. Gen. Genet. **198**, 441-448

6.20. Tanaka, M., Haniu, M., Yasunobu, K.T., and Mortenson, L.E. (1977) J. Biol. Chem. **252**, 7093-7100

6.21. Chen, K. C.-K., Chen, J.-S., and Johnson, J.L. (1986) J. Bacteriol. **166**, 162-172

6.22. Hase, T., Wakabayashi, S., Nakano, T., Zumft, W.G., and Matsubara, H. (1984) FEBS Lett. **166**, 39-43

6.23. Wang, S.-Z., Chen, J.-S., and Johnson, J.L. (1987) Nucleic Acid Res. **15**, 3935

6.24. Riebeling, V., Thauer, R.K., and Jungermann, K. (1975) Eur. J. Biochem. **55**, 445-453

6.25. Jacobson, M.R., Cantwell, J.S., and Dean, D.R. (1990) J. Biol. Chem. **265**, 19429-19433

6.26. Robson, R.L. (1984) FEBS Lett. **173**, 394-398

6.27. Sundaresan, V., and Ausubel, F.M. (1981) J. Biol. Chem. **256**, 2808-2812

6.28. Smith, B.E., Lowe, D.J., and Bray, R.C. (1973) Biochem. J. **135**, 331

6.29. Thorneley, R.N.F. (1975) Biochem. J. **145**, 391

6.30. Zumft, W.G., Mortenson, L.E., and Palmer, G. (1974) Eur. J. Biochem. **46**, 525

6.31. Hageman, R.V., and Burris, R.H. (1978) Proc. Natl. Acad. Sci. U.S.A. **75**, 2699

6.32. Hageman, R.V., and Burris, R.H. (1978) Biochemistry **17**, 4117

6.33. Thorneley, R.N.F., Eady, R.R., and Yates, M.G. (1975) Biochim. Biophys. Acta **403**, 269

6.34. Eady, R.R. (1973) Biochem. J. **135**, 531

6.35. Thorneley, R.N.F. (1975) Biochem. J. **145**, 391-396

6.36. Thorneley, R.N.F., Eady, R.R., and Yates, M.G. (1975) Biochem. Biophys. Acta **403**, 269-284

6.37. Hazzard, J. T., Moench, S.J., Erman, J.E., Satterlee, J.D., and Tollin, G. (1988) Biochemistry **27**, 2002-2008

6.38. Peerey, L., and Kostic, N.M. (1989) Biochemistry **28**, 1861-1868

6.39. Deits, T.L., and Howard, J.B. (1990) J. Biol. Chem. **265**, 3859-3867

6.40. Sweet, F., and Adair, N.K. (1975) Biochem. Biophys. Res. Commun. **63**, 99

6.41. Newman, M.S., and Boden, H. (1979) FEBS Lett. **108**, 243

6.42. Packer, L., Tristham, S., Herz, J.M., Russell, C., and Borders, C.L. (1961) J. Org. Chem. **26**, 2525

6.43. Burns, A., Watt, G.D., and Wang, Z.C. (1985) Biochemistry **24**, 3932-3936

6.44 Yamane, T., Weininger, M.S., Mortenson, L.E., and Rossmann, M.G. (1982) J. Biol. Chem. **257**, 1221-1223

6.45. Pretorius, I.-M., Rawlings, D.E., O'Neill, E.G., Jones, W.A., Kirby, R., and Woods, D.R. (1987) J. Bacteriol. **169**, 367-370

6.46. Holland, D., Zilberstein, A., Zamir, A., and Sussman, J.L. (1987) Biochem. J. **247**, 277-285

6.47. Pope, M.R., Murrell, S.A., and Ludden, P.W. (1984) Proc. Natl. Acad. Sci. U.S.A. **82**, 3173-3177

6.48. Georgiadis, M.M., Chakrabarti, P., and Rees, D.C. (1990) in Nitrogen Fixation: Achievements and Objectives (Gresshoff, P.M., Roth, L.E., Stacey, G., and Newton, W.E., Eds.) pp. 111-116, Chapman and Hall, New York

6.49. Lowery, R.G., and Ludden, P.W. (1986) J. Bacteriol. **186**, 513-518

6.50. Jouanneau, Y., Roby, C., Meyer, C.M., and Vignais, P.M. (1989) Biochemistry **28**, 6524-6530

6.51. Ludden, P.W., Hageman, R.V., Orme-Johnson, W.H., and Burris, R.H. (1982) Biochim. Biophys. Acta **700**, 213-216

6.52. Roberts, G.P., Ludden, P.W., Burris, R.H., Fitzmaurice, W.P., Fu, H.-A., Nielson, G., Liang, J.-H., Lehman, L., Woehle, D., Lies, D., Wirt, H., Montgomery, S., Davis, R., and Bao, Y. (1990) in Nitrogen Fixation: Achievements and Objectives (Gresshoff, P.M., Roth, L.E., Stacey, G., and Newton, W.E., Eds.) pp. 475-481, Chapman and Hall, New York

6.53. Lowery, R.G., and Ludden P.W. (1988) J. Biol. Chem. **263**, 16714-16719

6.54. Murrell, S.A., Lowery, R.G., and Ludden, P.W. (1988) Biochem. J. **251**, 609-612

6.55. Tanaka, M., Hania, M., Yasunobo, K.T., and Mortenson, L.E. (1977) J. Biol. Chem. **252**, 7093-7100

6.56. Murrell, S.A., Lowery, R.G., and Ludden, P.W. (1988) Biochem. J. **251**, 609-612

6.57. Kent, H.M., Ioannidis, I., Gormal, C., Smith, B.E., and Buck, M. (1989) Biochem. J. **264**, 257-264

6.58. Dean, D.R., Scott, D.J., and Newton, W.E. (1990) in Nitrogen Fixation: Achievements and Objectives (Gresshoff, P.M., Roth, L.E., Stacey, G., and Newton, W.E., Eds.) pp. 95-102, Chapman and Hall, New York

6.59. Brigle, K.E., Weiss M.C., Newton, W.E., and Dean, D.R. (1987) J. Bacteriol. **169**, 1547-1553

6.60. Dean, D.R., Brigle, K.E., May, H.D., and Newton, W.E. (1988) in Nitrogen Fixation: Hundred Years After, Bothe, de Bruijn and Newton, Eds., pp. 107-113, Gustav Fischer, Stuttgart, New York

6.61. Scott, D.J., May, H.D., Newton, W.E., Brigle, K.E., and Dean, D.R. (1990) Nature **343**, 188-190

Vitae

Melinda Grace Ehrlich was born in New Orleans, LA. on October 8, 1959, the daughter of Robert H. Ehrlich and Amelia Vining. She attended schools in the New Orleans area until she recieved her high school diploma from Warren Easton Senior High in May, 1977.

Melinda attended Louisiana State University in Baton Rouge, LA. from September, 1977 until December, 1982 when she recieved her Bachelor of Science in Chemistry. She then taught high school in New York City for two years before returning back to Baton Rouge. Upon returning, she entered Louisiana State University in August, 1985 as a graduate student in chemistry.

Melinda married Michael Allen Oliver on April 23, 1983. Their daughter, Lauren Amelia Oliver was born on September 27, 1989.

DOCTORAL EXAMINATION AND DISSERTATION REPORT

Candidate: Melinda E. Oliver

Major Field: Chemistry

Title of Dissertation: A Study of the Metal Clusters in the Nitrogenase Proteins of Azotobacter vinelandii

Approved:

Major Professor and Chairman

Dean of the Graduate School

EXAMINING COMMITTEE:

Date of Examination:

April 5, 1991